Investigations of pit thermal energy storages in district heating systems

Sifnaios, Ioannis

Link to article, DOI:
10.11581/DTU.00000291

Publication date:
2023

Document Version
Publisher's PDF, also known as Version of record

DTU

Technical University of Denmark

Investigations of pit thermal energy storages in district heating systems

Ioannis Sifnaios

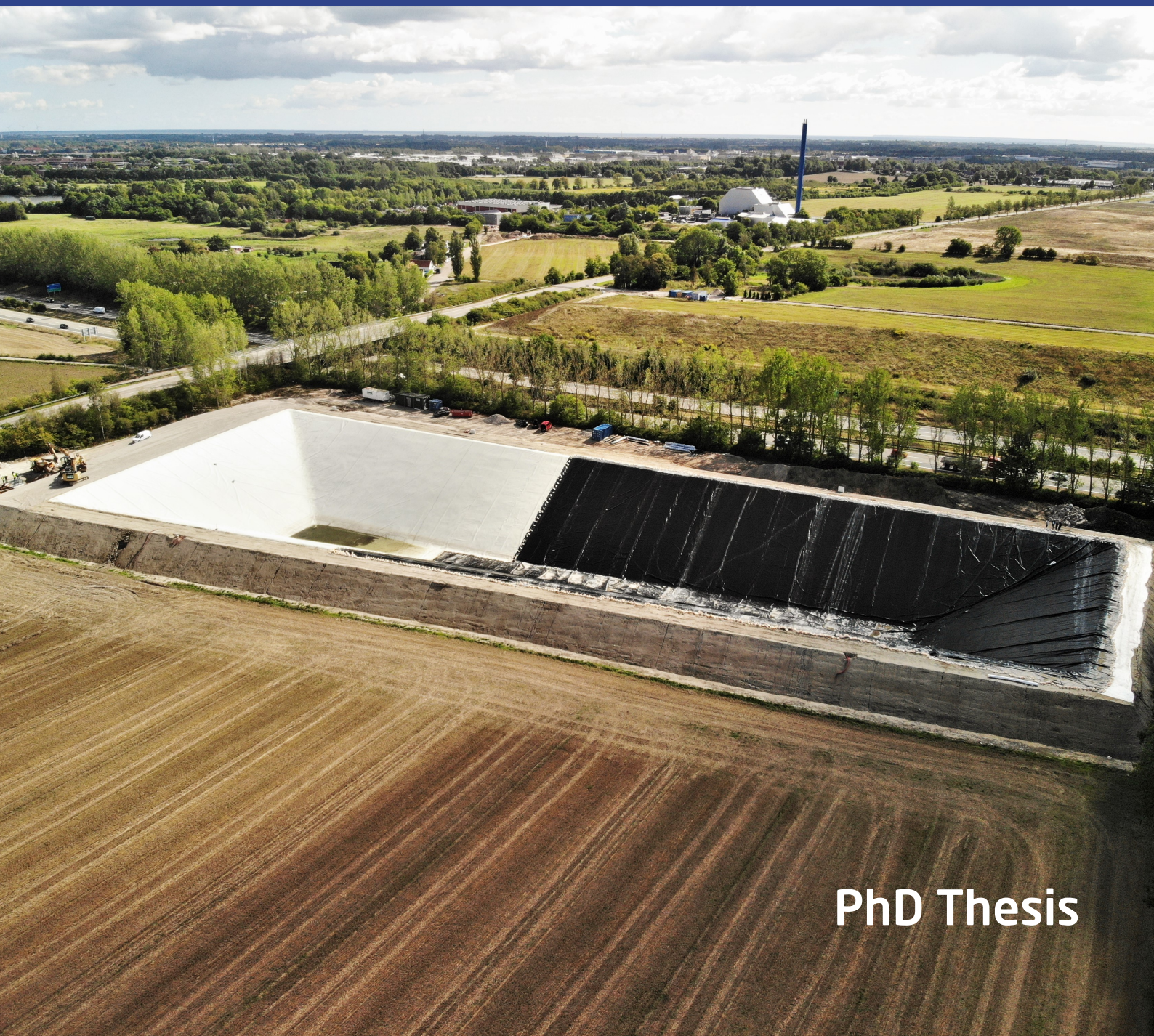

PhD Thesis

Investigations of pit thermal energy storages in district heating systems

PhD thesis
August, 2023

Author
Ioannis Sifnaios
iosif@dtu.dk

Cover photo: Ioannis Sifnaios
Published by: Department of Civil and Mechanical Engineering,
Technical University of Denmark, Kgs. Lyngby, Denmark
www.construct.dtu.dk
DOI: https://doi.org/10.11581/dtu.00000291

Preface

This thesis has been submitted as a partial fulfillment of the requirements for the degree of Doctor of Philosophy (PhD) from the Technical University of Denmark (DTU). The work presented was carried out between September 2020 and August 2023 at the Section of Energy and Services at the Department of Civil and Mechanical Engineering, DTU. The study has been supervised by associate professors Jianhua Fan and Simon Furbo and by researcher Adam R. Jensen from DTU. It was also co-supervised by professor Zhifeng Wang from the University of Chinese Academy of Sciences (UCAS).

This work has been financially supported by the Danish Energy Agency's Energy Technology Development and Demonstration Program (EUDP) under the grant number 64018-0134 and by the Sino-Danish Center for Education and Research (SDC) PhD program.

What motivated me to carry out this study was my desire to increase my knowledge and expertise by pushing the boundaries of a specific topic. Although I had never heard of pit thermal energy storages (PTES) before starting my PhD, after three years of research, I believe they can play a major role in future district heating systems, enabling a larger use of renewables and reducing fossil fuel dependency.

I feel privileged to have carried out my PhD in Denmark, which is the frontrunner in PTES systems, and thus I had the chance to visit all but one of the operational PTES in the world. Additionally, my external stay at AEE Intec in Austria and my participation in the International Energy Agency's Task 39 gave me the opportunity to meet experts in my field of research, resulting in many fruitful discussions.

Apart from research, this PhD also gave me the opportunity to acquire many experiences, including teaching university lectures, supervising the thesis of an MSc student, becoming a certified drone pilot, making field trips to district heating plants in Denmark, and attending conferences and task meetings. Overall, it has been a great experience where I had the chance to meet and interact with many wonderful people, and for that, I will be forever grateful.

Ioannis Sifnaios

Kgs. Lyngby, 31 August 2023

Abstract

In recent years, there has been a growing interest in the use of pit thermal energy storages (PTES), which is mainly attributable to their low cost and high efficiencies. However, the existing knowledge derives primarily from short-term performance monitoring of seasonal storages and a small number of scientific studies. Specifically, the effect of storage geometry, soil conditions, and storage operation remains largely uninvestigated, although they potentially have a large impact on performance. Thus, this thesis aimed to investigate methods for assessing storage performance, determining the effect of storage design and soil conditions, and quantifying the economic impact of PTES.

In order to assess the performance of PTES systems, a thorough review of key performance indicators regarding efficiency and stratification was conducted. Initially, the most common energy efficiency expressions were compared, and a recommendation for handling the internal energy change was provided. Moreover, exergy efficiency was found to be the only efficiency indicator that accounted for heat losses and mixing in the storage. Regarding stratification, exergy destruction was recommended as an indicator that can evaluate stratification without being biased by differences in heat losses.

The performance of PTES was further investigated by assessing the impact of the geometry in terms of the slope of the storage sides and the aspect ratio of the lid. It was found that, due to a smaller surface area, changing the slope of the side walls from 26° (typical PTES side-wall slope) to 44° could reduce the total heat losses by 20%. Additionally, a square-shaped PTES had 9% less heat loss compared to a rectangular one.

Moreover, the impact of groundwater on PTES performance was investigated by simulating the heat transfer in the soil domain. It was found that groundwater could increase heat losses toward the ground by up to 60%, compared to a case without groundwater. Furthermore, the increase in groundwater temperature was investigated since it is subject to regulation in many countries. It was found that if the groundwater table was at a depth of at least 25 m, the groundwater temperature could be maintained below 20 °C for a seasonal PTES. However, this was not feasible for the short-term PTES operation.

The economic impact of PTES was investigated using the Danish city of Viborg as a case study. Since it has become common practice to install electricity-based generation technologies in distinct heating grids, a system using an air-to-water heat pump, an electric boiler, and a PTES was compared to a system without a PTES. It was found that the PTES could reduce the levelized cost of heat by 10%, with a payback period of 5.1 years. Furthermore, if the PTES charge temperature was reduced from 90 °C to 80 °C, the cost of heat could be decreased by an additional 4%.

Furthermore, the impact of thermal energy storage (particularly PTES) was investigated at a country level, with a focus on Denmark. It was found that heat storage enabled higher installation of renewable technologies (i.e., 35% higher PV capacity and 10% higher wind capacity) compared to scenarios without heat storage. In parallel, heat storages allowed for utilizing excess electricity (through power-to-heat technologies), leading to 53% lower curtailment levels and ultimately to a 2.4 €/MWh lower average heat price. Last, it was demonstrated that only by utilizing heat storage systems could carbon neutrality be achieved for the energy system by 2050.

Resumé

I de senere år har der været en stigende interesse for anvendelsen af damvarmelagre (pit thermal energy storage (PTES)), hvilket primært kan tilskrives deres lave anlægsomkostninger og høje effektivitet. Den eksisterende viden om PTES stammer primært fra kortvarige måleperioder for sæsonvarmelagre og et mindre antal videnskabelige studier. Der er derfor flere aspekter, som ikke er tilstrækkeligt undersøgt, fx effekten af lagergeometri, jordbundsforhold samt driftsstrategier, selvom disse forhold potentielt kan have stor indflydelse på ydeevnen. Denne afhandling har derfor til formål at undersøge metoder til vurdering af damvarmelagres ydeevne, kvantificere effekten af lagergeometri og jordbundsforhold, samt økonomien ved integrering af damvarmelagre i fjernvarmesystemer.

For at vurdere ydeevnen af damvarmelagre blev der foretaget en undersøgelse af key performance indikatorer (KPIs) for effektivitet og temperaturlagdeling. Først blev de mest almindelige energieffektivitetsudtryk sammenlignet, og der blev formuleret en anbefaling til beregningen af effektiviteten. Desuden blev exergi-effektiviteten fundet til at være den eneste effektivitetsindikator, der tager højde for varmetab og opblanding i lageret.

Ydeevnen af damvarmelagre blev yderligere undersøgt ved at vurdere indvirkningen af geometrien i form af hældningen af lagerets sider og forholdet mellem lågets længde og bredde. Simuleringer viste at en ændring af hældningen på siderne fra 26° til 44° kunne reducere det samlede varmetab med 20% på grund af et mindre overfladeareal. Derudover havde et kvadratisk damvarmelager 9% mindre varmetab sammenlignet med et rektangulært lager.

Desuden blev påvirkningen af grundvand undersøgt ved at simulere varmestrømmene i den omkringliggende jord. Undersøgelsen viste at grundvand kan øge varmetabet til jorden med op til 60%. Derudover blev forøgelsen af grundvandstemperaturen undersøgt, da den er underlagt regulering i mange lande. Resultaterne viste, at hvis grundvandsmagasinet var placeret dybere end 25 m, kunne grundvandstemperaturen holdes under 20 °C for et sæsonvarmelager. Dette var dog ikke muligt for et kort-tids varmelager.

Økonomien af damvarmelagre blev undersøgt ved at analysere et casestudie med udgangspunkt i byen Viborg. Casestudiet var baseret på luft-til-vand varmepumper og elkedler, da disse teknologier bliver mere og mere udbredte og Viborg har ambitioner om at udfase naturgas. Ved at integrere et damvarmelager kunne varmeomkostningerne reduceres med 10%, med en tilbagebetalingstid af lageret på 5.1 år. Derudover kunne varmeomkostningen yderlige sænkes med 4%, hvis opladningstemperaturen af lageret blev reduceret fra 90 °C til 80 °C.

Til sidst blev effekten af termisk energilagring (især damvarmelagre) undersøgt på landeniveau med fokus på Danmark. Det blev fundet, at varmelagring muliggjorde større installation af vedvarende energiteknologier (35% højere solcelleeffekt og 10% højere vindeffekt) sammenlignet med scenarier uden varmelagring. Samtidig tillod varmelagring at udnytte overskudsstrøm, hvilket førte til 53% mindre spildenergi og en 2.4 €/MWh lavere gennemsnitlig varmepris. Endelig blev det vist, at CO2-neutralitet i det danske energisystem kun kan opnås inden 2050 ved at udnytte varmelagringssystemer.

List of papers

The PhD thesis is based on the following papers, which constitute the second part of this thesis:

I. **Sifnaios**, **I.**, Jensen, A. R., Furbo, S., & Fan, J. (2022c). Performance comparison of two water pit thermal energy storage (PTES) systems using energy, exergy, and stratification indicators. *Journal of Energy Storage*, *52*, 104947. https://doi.org/10.1016/j.est.2022.104947

II. **Sifnaios**, **I.**, Jensen, A. R., Furbo, S., & Fan, J. (2022b). Evaluation of stratification in thermal energy storages. *Renewable Energy Systems in Smart Grid*, 57–69. https://doi.org/10.1007/978-981-19-4360-7_6

III. **Sifnaios**, **I.**, Gauthier, G., Trier, D., Fan, J., & Jensen, A. R. (2023a). Dronninglund water pit thermal energy storage dataset. *Solar Energy*, *251*, 68–76. https://doi.org/10.1016/j.solener.2022.12.046

IV. **Sifnaios**, **I.**, Dragsted, J., & Jensen, A. R. (2021). Thermal inspection of water pit heat storages using drones. *Proceedings - ISES Solar World Congress 2021*, 925–931. https://doi.org/10.18086/swc.2021.35.02

V. **Sifnaios**, **I.**, Jensen, A. R., Furbo, S., & Fan, J. (2022a). Effect of Design Characteristics on Pit Thermal Energy Storage Performance. *Proceedings - EuroSun 2022*

VI. **Sifnaios**, **I.**, Jensen, A. R., Furbo, S., & Fan, J. (2023b). Heat losses in water pit thermal energy storage systems in the presence of groundwater. *Applied Thermal Engineering*, *235*, 121382. https://doi.org/10.1016/j.applthermaleng.2023.121382

VII. **Sifnaios**, **I.** (2023). Integration of a pit thermal energy storage in a district heating network [Draft]

VIII. **Sifnaios**, **I.**, Sneum, D. M., Jensen, A. R., Fan, J., & Bramstoft, R. (2023c). The impact of large-scale thermal energy storage in the energy system. *Applied Energy*, *349*, 121663. https://doi.org/10.1016/j.apenergy.2023.121663

Apart from the previously mentioned papers, the following papers were also published during the present PhD study. However, their topic is not relevant to this thesis; thus, they are only mentioned in this section and not included in the thesis.

a. Jensen, A. R., **Sifnaios**, **I.**, & Anderson, K. (2022a). twoaxistracking – a python package for simulating self-shading of two-axis tracking solar collectors. *MethodsX*, *9*, 101876. https://doi.org/10.1016/j.mex.2022.101876

b. Jensen, A. R., **Sifnaios**, **I.**, Caringal, G. P., Furbo, S., & Dragsted, J. (2022b). Thermal performance assessment of the world's first solar thermal Fresnel lens collector field. *Solar Energy*, *237*, 447–455. https://doi.org/10.1016/j.solener.2022.01.067

c. Jensen, A. R., **Sifnaios**, **I.**, Furbo, S., & Dragsted, J. (2022c). Self-shading of two-axis tracking solar collectors: Impact of field layout, latitude, and aperture shape. *Solar Energy*, *236*, 215–224. https://doi.org/10.1016/j.solener.2022.02.023

d. Jensen, A. R., **Sifnaios**, **I.**, Perers, B., Rothmann, J. H., Mørch, S. D., Jensen, P. V., Dragsted, J., & Furbo, S. (2022d). Demonstration of a concentrated solar power and biomass plant for combined heat and power. *Energy Conversion and Management*, *271*, 116207. https://doi.org/10.1016/j.enconman.2022.116207

e. Jensen, A. R., & **Sifnaios**, **I.** (2022). Modeling, validation, and analysis of a concentrating solar collector field integrated with a district heating network. *Solar*, *2(2)*, 234–250. https://doi.org/10.3390/solar2020013

Acknowledgements

This thesis would never have materialized without the support of many colleagues and friends, whom I would like to thank in this section. First, I wish to thank my supervisors, Jianhua Fan and Simon Furbo, for introducing me to the world of academia and for giving me the opportunity to pursue a PhD. During these three years, they have always been supportive and had confidence in my abilities. This journey would also not have been the same if I did not have Adam R. Jensen as my office mate (and as a co-supervisor toward the end of my PhD). Adam has been a fantastic colleague and a joy to work with and has become a good friend.

Additionally, I was fortunate to collaborate with many people from academia and industry during my PhD. I would like to express my gratitude to Rasmus Bramstoft and Daniel Sneum from DTU Management, who have dedicated much of their time to support my research, provided me with many insights, and co-authored a publication on PTES integration. Additionally, Michele Tunzi from DTU Construct, for providing me with insights and operation data for the Viborg district heating system. Moreover, Geoffroy Gauthier and Daniel Trier from PlanEnergi for their help in obtaining PTES data and co-authoring a publication on the PTES in Dronninglund. Also, Johan Frey from PlanEnergi for answering the many questions I had regarding the Dronninglund PTES. Further, Lasse Kjærgaard Larsen from Marstal Fjernvarme for allowing me access to data for the PTES in Marstal and a very informative tour of the facilities.

During my PhD, I spent four months in AEE Intec in Austria as part of my external stay. I would like to thank Michael Reisenbichler and Wim van Helden for arranging all the paperwork and making me feel welcome. Also, special thanks to Lorenz, Marie, Keith, Octavio, Marnoch, Maria, and Judith for making my stay in Austria enjoyable.

Furthermore, I had the pleasure of being part of the Solar Thermal Research Group at the Department of Civil and Mechanical Engineering, DTU. Specifically, I would like to mention the late Bengt Perers, who, although we interacted very little in person, was always very kind and supportive during my first years at DTU. Moreover, special thanks to many current and former colleagues from the Section of Energy and Services: Janne, Gerald, Martin, Kevin, Dorte, Donya, Marie, and Lucile, for their support and all the fun times. I would also like to thank the department's technical staff for their assistance with experimental work. Special thanks to Lars Andersen and Brian Rasmussen for always being willing to answer questions and help me with my project.

Moreover, I will always be extremely grateful to my family for their endless encouragement and love. Although they are still not 100% sure what I am working on, they have always believed in me and wanted the best for me, enabling me to pursue my dreams. Finally, words cannot express my gratitude to my better half, Stella Strouvali, for her complete support and understanding during this journey.

Contents

List of acronyms

ATES Aquifer Thermal Energy Storage
BTES Borehole Thermal Energy Storage
CAPEX Capital Expenditures
CFD Computational Fluid Dynamics
CHP Combined Heat and Power
COP Coefficient Of Performance
DH District Heating
DRY Design Reference Year
FPC Flat Plate Collector
FVM Finite Volume Method
GDP Gross Domestic Product
HDPE High-Density Polyethylene
IEA International Energy Agency
IR Infrared
KPI Key Performance Indicator
LECA Light Expanded Clay Aggregate
OM Operation and Maintenance
OPEX Operational Expenditures
PE Polyethylene
PP Polypropylene
PPd Payback Period
PTES Pit Thermal Energy Storage
TES Thermal Energy Storage
TTES Tank Thermal Energy Storage
XPS Extruded polystyrene insulation

List of symbols

$\eta_{E,S}$	Seasonal energy efficiency [%]
η_E	Energy efficiency [%]
η_X	Exergy efficiency [%]
ρ	Density [kg m^{-3}]
C_p	Specific heat [J kg^{-1} K^{-1}]
E	Energy [J]
E_{PTES}	Storage energy content [MW h]
El_{price}	Electricity price [€/MW h]
Ex	Exergy [J]
H	Enthalpy [J]
I_0	Investment cost [€]
m	Mass [kg]
M_E	Moment of energy [J m]
OM	Operation and maintenance cost [€/MW h]
Q_H	Produced heat [MW h]
Q_{Boiler}	Heat generated by the electric boiler [MW]
Q_{HP}	Heat generated by the heat pump [MW]
Q_{load}	Heat load [MW]
Q_{PTES}	Heat charged (negative) or discharged (positive) from the PTES [MW]
S	Entropy [J K^{-1}]
T	Temperature [K]
t	Timestep [year]
V	Volume [m^3]
z	Vertical distance [m]

Part I

Summary

1 Introduction

The increase in availability and accessibility of energy has transformed the course of human civilization over the last few centuries (Ritchie et al., 2022). In modern-day society, access to adequate and reliable energy resources is crucial for economic prosperity and for maintaining a high quality of life. In most countries, a high gross domestic product (GDP) per capita is matched by high energy consumption per capita. With the increase in population and living standards, global energy consumption continues to rise. In fact, energy demand has tripled in the past 50 years and might triple again within the next 30 years (Texas Education Agency, 2023).

The world's energy consumption can be divided into three main sectors, namely thermal, transport, and power. As seen in Figure 1.1, the thermal sector constitutes slightly more than half of the total energy consumption. However, the power sector is usually in the spotlight in discussions regarding climate change and energy savings despite its relatively small share of the overall consumption and high renewable energy fraction. What is alarming concerning the thermal sector is the large consumption combined with a low percentage of renewable energy (approximately 11% as of 2019). It is thus clear that there is a large need for thermal technologies that can increase the utilization of renewable energy.

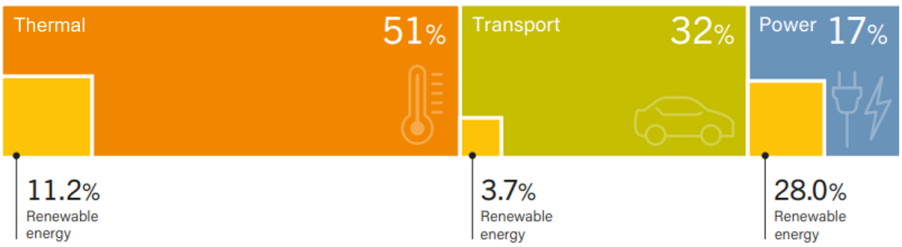

Figure 1.1: Global final energy consumption by sector and the fraction of renewable energy for 2019 (Adapted from REN21, 2022).

1.1 District heating

An efficient way to cover the heat demand in residential and commercial buildings is through district heating (DH). District heating refers to a system where heat is generated at a central location and distributed to the consumers through a network of insulated pipes. Such systems are used mainly in countries with cold climates and high space heating demand, e.g., Eastern and Northern Europe and China. However, there is a large variation in the use of DH among countries. For example, 65% of the total heat demand in Denmark is covered by DH, whereas only 4% in Norway (W.E District, 2023).

The origin of DH can be traced back to the Roman Empire, where hot water was used to heat baths and greenhouses. The first generation of modern-day DH was introduced

in the USA in 1880, using steam as the heat carrier (Lund et al., 2014). The main drawback of using steam as a transfer fluid was the high heat losses; thus, later generations of DH featured lower supply temperatures and increased efficiencies (see Figure 1.2). Additionally, higher efficiencies were achieved due to the usage of combined heat and power (CHP) plants in the DH systems. Typical CHP plants use a combustion or steam turbine that generates electricity and utilize the waste heat of this process for DH. That way, the losses of the CHP plant can be minimized, and efficiencies higher than 80% can be achieved (United States Environmental Protection Agency, 2023). In parallel, using lower supply temperatures has also made it possible to use lower-temperature heat sources, e.g., heat pumps.

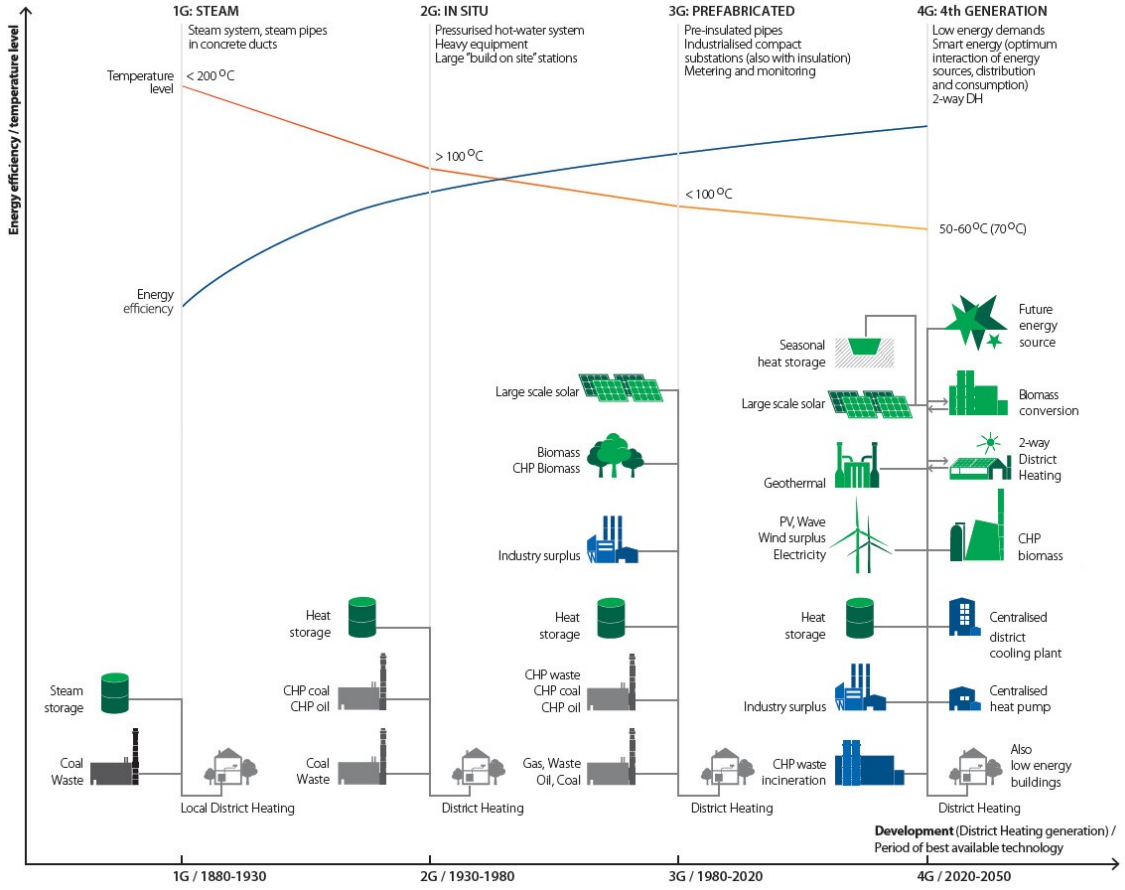

Figure 1.2: Evolution of district heating (adapted from Lund et al. (2014)).

Starting in 1980, solar district heating was introduced in Sweden, where solar thermal collectors were used for generating heat (Perez-Mora et al., 2018). The integration of solar heat is typically facilitated using thermal energy storage (TES) systems in order to cover the mismatch between solar heat production and heat demand. Additionally, TES systems can be used for peak shaving, arbitrage, and covering demand in case of plant outages. Usually, short-term TES systems have a storage duration of 1-3 days, enabling a solar thermal fraction of up to 20% (Tschopp et al., 2020). In order to increase the solar thermal fraction of DH systems, large-scale, seasonal TES systems have been installed,

allowing for heat produced in summer to be stored and used during the fall and winter. This way, solar thermal fractions of 30%-60% have been achieved (Sveinbjörnsson et al., 2017). A visual representation of the seasonal TES operation is shown in Figure 1.3.

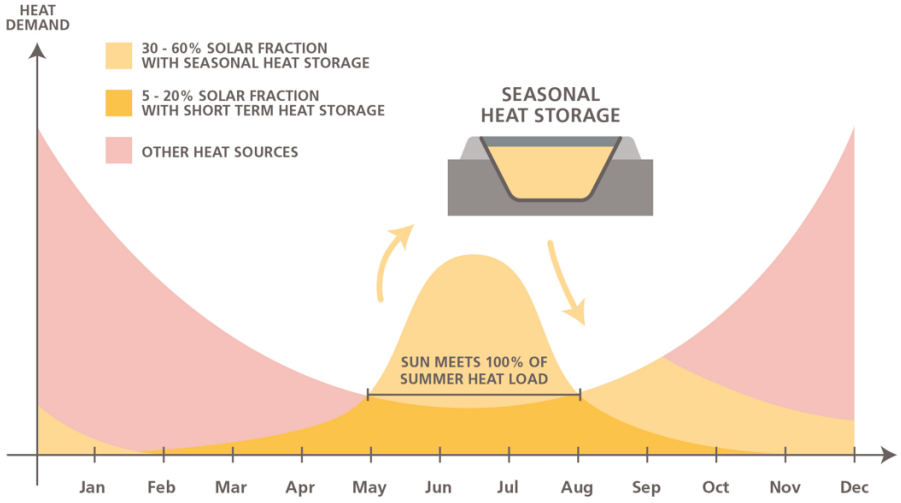

Figure 1.3: The role of seasonal heat storage (International Energy Agency (IEA), 2021).

In general, TES systems can decouple the production from the demand, which is essential for DH systems that utilize non-dispatchable heat sources. For example, systems with high shares of intermittent renewable energy (e.g., wind and solar) or industrial surplus heat. In short, TES systems increase the flexibility of the DH system to meet the demand profile by utilizing potentially any available heat source.

1.2 Overview of thermal energy storage technologies

Thermal energy storage (TES) systems store surplus thermal energy (heat or cold) for later use (Cabeza, 2012). The most common classification of TES systems is based on the physical phenomenon used for storing thermal energy. From this perspective, TES systems can be categorized as sensible, latent, or thermochemical (Guelpa & Verda, 2019).

Sensible TES is the most mature storage technology, where energy is stored by changing the temperature of a storage medium (e.g., water, oil, or rocks). The amount of stored energy depends on the temperature change and the mass and heat capacity of the storage medium (Cabeza, 2012). Sensible TES systems are described in more detail in Section 1.2.1 since they were the main focus of this thesis.

Latent TES store energy using phase-change materials (e.g., hydrocarbons or salt hydrates) and utilize the latent heat of the phase change. For example, a solid can be melted isothermally by adding heat, and the heat can then be released when the liquid solidifies (Clifford & Ambrosini, 2020).

Thermochemical TES is based on the principle that chemical reactions absorb or release

heat. Thus, heat is converted into chemical bonds using a reactive medium (charge phase), and heat is released when the reaction is reversed (discharge phase). Thermochemical TES systems store energy using a high-energy chemical process (Kumi, 2023).

1.2.1 Sensible thermal energy storage

So far, sensible TES systems are the only technology to have been used on a large scale in connection to DH systems. The four main types of sensible thermal energy storage systems are tanks (TTES), aquifers (ATES), boreholes (BTES), and pit thermal energy storages (PTES) (see Figure 1.4) (Pauschinger et al., 2018). While TTES and PTES typically use water as the storage medium, BTES systems use the soil itself (Reuss, 2020), and ATES use natural underground aquifers as the storage medium (Gao et al., 2019).

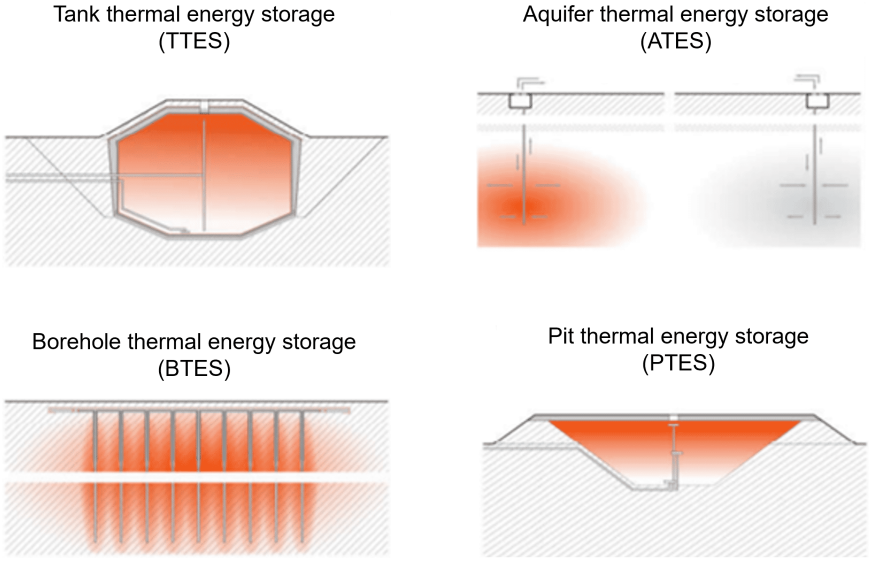

Figure 1.4: Most common types of large-scale sensible TES (Pauschinger et al., 2018).

1.2.1.1 Tank thermal energy storage (TTES)

Tank thermal energy storage systems (TTES) are the most common and mature sensible TES technology and have been used extensively in connection with DH systems. TTES are usually made of steel or concrete and use an insulation layer to minimize heat losses (Dahash et al., 2019). TTES systems are usually placed above ground; however, there are cases where large-volume TTES are placed partially or entirely underground (e.g., as in Narula et al. (2020)). The main drawback of TTES systems is that they have a higher specific cost than other heat storage technologies. However, there are no specific requirements for ground conditions for their installations, and they can also store higher temperatures compared to other TES (>100 °C when pressurized).

1.2.1.2 Aquifer thermal energy storage (ATES)

Aquifer thermal energy storage (ATES) requires the presence of an aquifer, which is an underground layer of permeable rock or saturated sediment (gravel, sand, or silt) containing groundwater. ATES systems consist of at least two wells located in one (or more) aquifer

layers. In the summer, the ATES can be used for cooling by extracting cold groundwater from the cold well while injecting heated warmer water into the hot well. In the winter, the process is reversed. This way, ATES systems are capable of delivering both heating and cooling. The global extent of aquifers is both limited and site-specific; nevertheless, they are commonly situated in proximity to populated areas and river deltas (e.g., like the Netherlands) (Schmidt et al., 2018). ATES systems require suitable hydrogeological conditions such as a low groundwater flow and high layer permeability, as well as specific geochemical conditions to prevent clogging and corrosion of wells (Fleuchaus et al., 2018).

1.2.1.3 Borehole thermal energy storage (BTES)

Boreholes store heat utilizing the thermal capacity of soil and/or rocks (Sibbitt et al., 2012). Multiple vertical boreholes are usually connected (in series and parallel) for efficient heat storage, and water is used as the heat carrier (Rad & Fung, 2016). In principle, there are no limitations regarding the location where a BTES system can be installed. However, it is preferred that the ground is easily drillable, with a high heat capacity, and that there is low natural groundwater flow (or no groundwater) (Suárez et al., 2019). Typically, an insulation layer is placed on top of the boreholes; otherwise, there is no insulation between the boreholes and the soil.

1.2.1.4 Pit thermal energy storage systems (PTES)

A PTES is, in principle, a large underground water reservoir. First, a pit is excavated in the ground that is later lined with a watertight liner (M. V. Jensen & Nielsen, 2020). In order to minimize the cost of soil handling and transportation, the excavated soil is used to form embankments around the pit. After the liner installation, the storage is filled with treated water and covered with an insulated floating lid. The PTES is connected to the DH grid through insulated pipes and a heat exchanger. In order to establish thermal stratification in the storage, diffusers are installed at the inlets/outlets of the PTES. All existing PTES systems utilize three diffusers. During charge operation, hot water is added to the PTES through the top diffuser, while cold water exits the PTES through the bottom diffuser. Similarly, during discharge operation, hot water exits the PTES through the top diffuser, while cold water is added to the PTES through the bottom diffuser. The use of the middle diffuser depends on the PTES temperature and its operation (e.g., if the PTES is used as a heat source for a heat pump). Figure 1.5 shows different stages of PTES construction along with a schematic of a PTES.

Since PTES is an underground storage technology, its performance and construction cost depend on the geological conditions at the site. High groundwater levels and poor soil conditions can increase construction costs. It is thus important that PTES systems are built in areas with suitable ground conditions. Considering that a relatively large space is required for the PTES construction, it can prove challenging to find suitable ground conditions close to urban areas (Kallesøe & Vangkilde-Pedersen, 2019). For that reason, there have been cases where PTES systems have been constructed inside or very close to a groundwater layer. Nevertheless, the effect of the soil domain characteristics on the

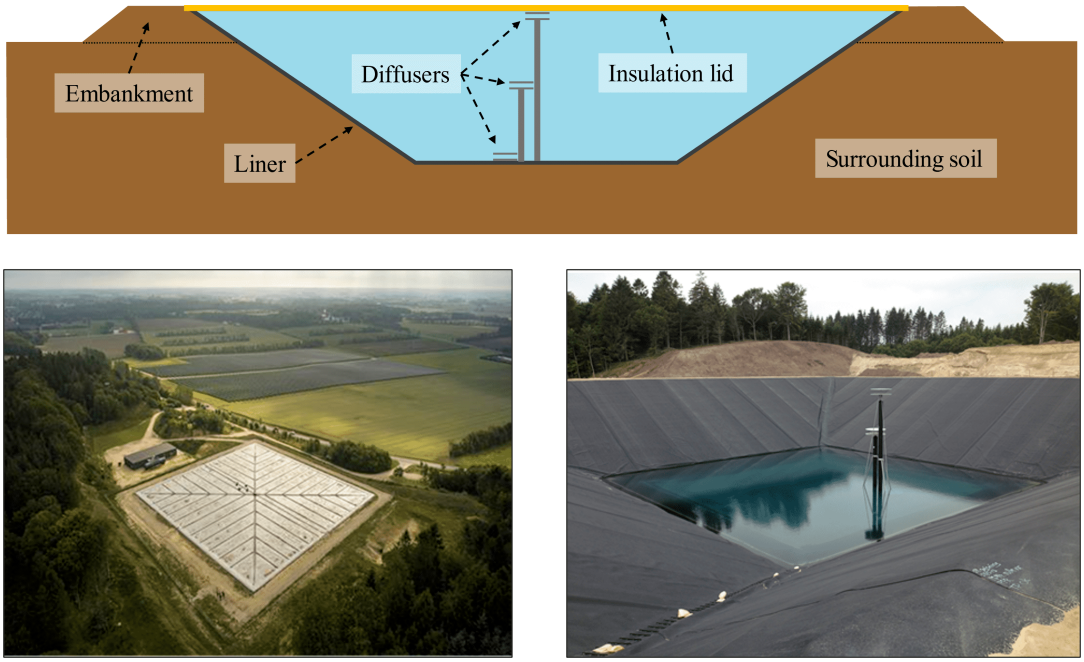

Figure 1.5: PTES design and construction (photo credit: PlanEnergi).

PTES performance has not been investigated.

Last, PTES remains a relatively new technology with only a few existing systems. Consequently, there is still a large uncertainty about the impact of design decisions and the potential impact of integrating PTES in DH grids. For this reason, PTES has been chosen to be the focus of this thesis, and a review of the PTES development is provided in the following section.

1.3 Review of PTES systems

The present study focused on pit thermal energy storage (PTES) systems. PTES have been successfully demonstrated as seasonal heat storage in combination with large solar collector fields (Soerensen & From, 2011). Compared to other storage technologies, the main advantage of PTES systems is their low construction cost and high storage efficiency. Additionally, a big advantage of PTES systems is their high charge/discharge and storage capacity since they use water as a storage medium and heat transfer fluid.

It should be noted that, in this study, the term PTES was used to describe only water-based systems. PTES that use a mix of gravel and water as a storage medium (e.g., the PTES in Chemnitz, Germany) were not investigated.

1.3.0.1 History of PTES

The PTES technology was first demonstrated on a small scale (640 m^3) at Studsvik, Sweden, in 1978, followed by a larger system (10 000 m^3) in Lambohov, Sweden. Both these systems were experimental and featured a non-floating lid construction, which is only suitable for small-scale systems. Due to their small size and insulation issues, these PTES had high heat losses and very low efficiency; thus, their operation stopped after a few

years, and the technology was abandoned in Sweden (Heller, 1994).

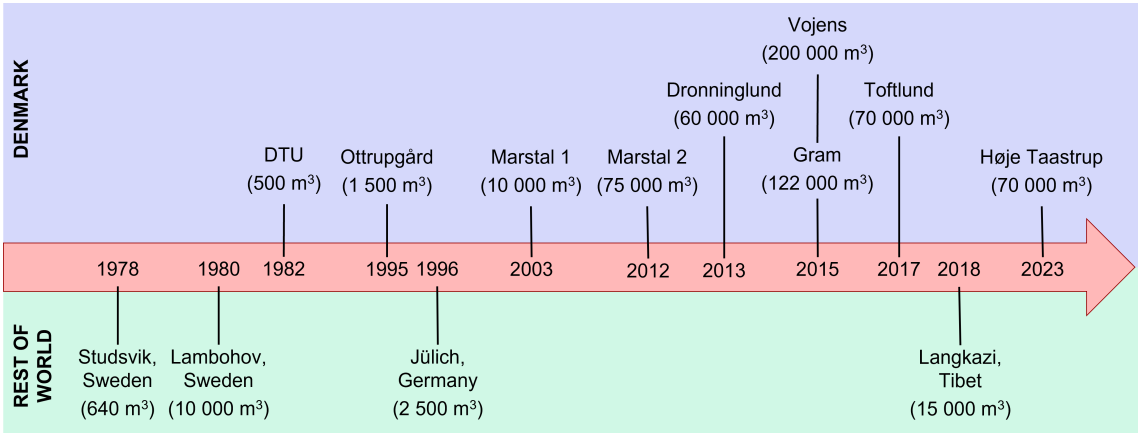

Figure 1.6: Timeline of constructed PTES systems.

The first PTES with a floating lid (500 m^3) was conceptualized and demonstrated under laboratory conditions at the Technical University of Denmark (DTU) in 1982 (Korsgaard, 1979), followed by a pilot system in Ottrupgård, Denmark, in 1995. However, the first commercial PTES was built in Jülich (Germany) in 1996 with a volume of 2 500 m^3 and connected to a 1 200 m^2 solar collector field.

The first commercial PTES in Denmark was built in Marstal in 2003, with a storage capacity of 10 000 m^3 as part of the SUNSTORE-2 project. SUNSTORE-2 aimed to cover 30% of the yearly heat demand of the town using the storage and charge it using heat generated from a solar collector field. Marstal-1 successfully demonstrated the possibility of using large-scale PTES for seasonal heat storage. However, numerous issues were discovered during operation, particularly with the lid and the liner; thus, the storage is no longer in operation. Additionally, it was realized that the storage capacity was rather small to be used for seasonal heat storage.

Subsequently, a second PTES was constructed in Marstal in 2012, having a volume of 75 000 m^3. The storage was constructed as part of the SUNSTORE-4 project and featured an improved lid design and a heat pump that could supply heat to the DH grid using the PTES as a heat source. That way, the PTES capacity was increased since it could be discharged to temperatures lower than the supply temperature of the DH grid.

Four more PTES systems were constructed in Denmark in the following years, having improved liners (i.e., Dronninglund as part of the SUNSTORE-4 project) or different lid technologies (i.e., Vojens, Gram, and Toftlund) compared to the PTES in Marstal. Until 2017, the PTES technology was limited to Europe; however, in 2018, the first PTES was constructed outside of Europe in Langkazi, Tibet. Last, the first PTES used as a short-term TES system was built in 2023 in Denmark. A timeline with the constructed PTES is presented in Figure 1.6.

It should be noted that the number of PTES systems continues to increase, with a new

system expected to start operation in late 2023 in Meldorf, Germany (50 000 m^3). Additionally, detailed plans have been made for two storages in Odense, Denmark (700 000 + 300 000 m^3).

1.3.0.2 Existing PTES systems

The efficiency of the existing PTES varies greatly, ranging from approximately 60% to more than 90%. Specifically, Gram has been reported having an efficiency of 60% (PlanEnergi, 2020), Marstal 66% (Schmidt, 2019), Toftlund 70% (Rambøll, 2020), and Dronninglund greater than 90% (Winterscheid & Schmidt, 2017). The difference in efficiencies is mainly due to the poor performance and durability of older lid constructions (**Sifnaios** et al., 2023a).

However, it should be noted that the performance of most existing PTES is usually documented only for the first 1-3 years of operation. Thus, there is no long-term monitoring and evaluation of the performance of the existing PTES systems. Additionally, apart from the difference in the components (e.g., the lid), there has never been a detailed comparison of the characteristics and performance of existing PTES systems in an effort to identify the reasons for their efficiency differences (e.g., the effect of diffuser designs, surrounding soil conditions, or presence of groundwater). In general, data can be obtained only for the PTES in Dronninglund and Marstal since they were part of former Danish research projects.

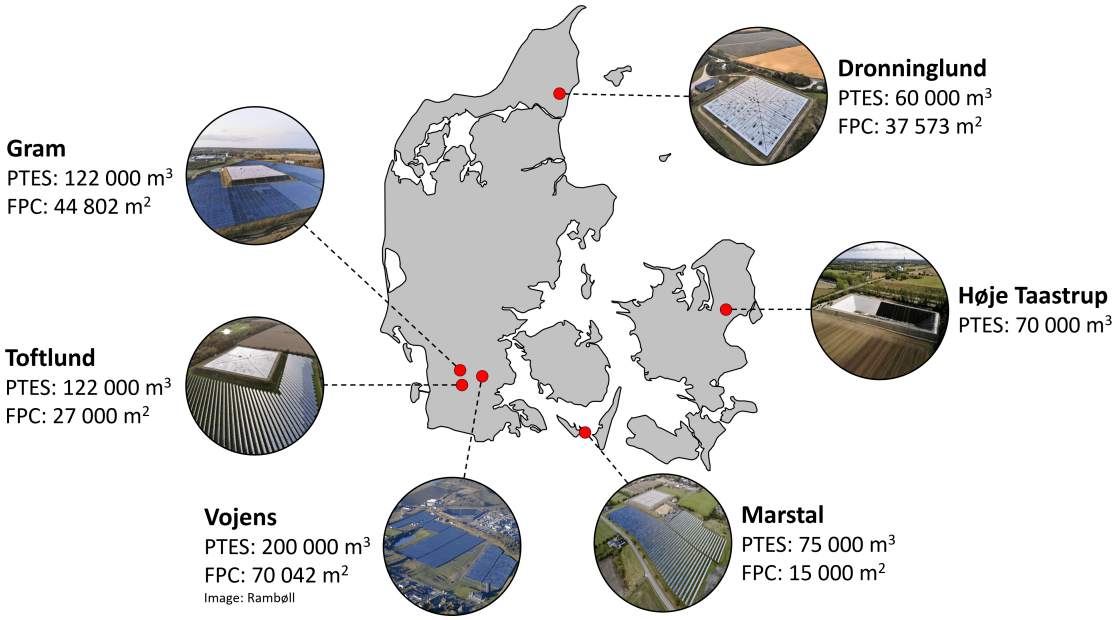

Figure 1.7: Existing PTES systems in Denmark as of 2023. The PTES storage volume and flat-plate solar collector (FPC) area are listed next to each storage.

A map of the existing PTES systems in Denmark is shown in Figure 1.7. Apart from the PTES in Høje Taastrup, all the existing systems were developed for seasonal heat storage and charged using heat from a solar collector field. Additionally, most of the storages are also connected to a heat pump. The heat pump is able to use the storage as a heat

source whenever the storage temperature is too low to be supplied directly to the district heating grid. In general, heat pump operation starts in late autumn and is able to cool the storage down to 10 - 25 °C. The heat pump operation has two main benefits for the system: (1) it increases the utilization of stored heat from the PTES, and (2) it benefits the solar collector field operation since lower inlet temperatures lead to higher collector efficiency. The only seasonal PTES system in Denmark without a heat pump is Vojens. Details on the characteristics of the existing PTES systems are summarized in Table 1.1.

Nevertheless, PTES can also be used as short-term heat storage systems for large DH grids. The PTES in Høje Taastrup started operating in 2023 and is the first PTES used for short-term heat storage. Unlike seasonal PTES, the Høje Taastrup PTES is not charged by a solar collector field but is charged directly from the Copenhagen DH grid. That way, it is possible for the PTES to store energy produced using a wide range of heat sources (e.g., heat from waste incineration, biomass CHP plants, and heat pumps operating using renewable electricity), increasing the DH system's flexibility.

1.3.0.3 Economy of PTES

In general, the primary motivation behind the development of the PTES technology was to achieve a low-cost storage solution. For example, the investment cost of existing water PTES ranges from 20 – 50 €/m^3 while the investment cost of conventional storage tanks is between 150 – 320 €/m^3 (Kallesøe & Vangkilde-Pedersen, 2019).

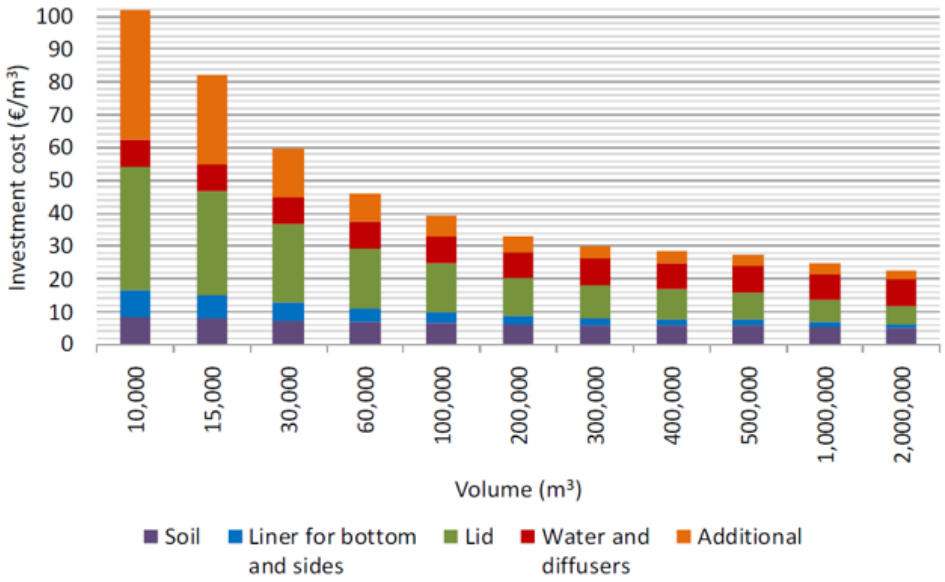

Figure 1.8: Specific investment cost of PTES for various sizes (Sveinbjörnsson et al., 2020).

The specific investment cost of PTES per volume is shown in Figure 1.8. It may be observed that the specific investment cost decreases strongly with increasing storage size (economy of scale). The main reason is the non-linear relationship between surface area and volume; specifically, as the storage size increases, the relative increase in surface area and material usage decreases. Additionally, several costs do not strongly depend on

Table 1.1: Characteristics of existing and historical PTES systems.

Location	Start year	DH load [GWh/yr]	Heat source	Volume [m^3]	Storage capacity [MWh] [a]	Price [€/m^3]	Operating temperatures [°C]	Charge/ discharge capacity [MW]	Reference
Studsvik, Sweden	1978	-	Solar thermal	640	22	-	30 – 60	-	Heller (1994)
Lambohov, Sweden	1980	-	Solar thermal	10 000	398	-	30 – 65	-	Heller (1994)
DTU, Denmark	1982	-	Solar thermal	500	17	-	30 – 60	0.035	Hansen et al. (1983)
Ottrupgård, Denmark	1995	-	Solar thermal	1 500	43	150	35 – 60	0.4	M. V. Jensen and Nielsen (2020)
Jülich, Germany	1996	0.6	Solar thermal	2 500	-	566	-	-	Meliß and Späte (2000)
Marstal-1, Denmark	2004	32	Solar thermal	10 000	626	67	35 – 90	7	Holm (2009)
Marstal-2, Denmark	2012	32	Solar thermal & heat pump	75 000	6 145	36	18 – 90	11	PlanEnergi (2013)
Dronninglund, Denmark	2014	36.4	Solar thermal & heat pump	60 000	5 462	38	10 – 90	26	PlanEnergi (2016)
Vojens, Denmark	2015	54.7	Solar thermal	200 000	12 517	24	35 – 90	39	Rambøll (2015)
Gram, Denmark	2015	55.6	Solar thermal & heat pump	122 000	9 023	35	25 – 90	30	PlanEnergi (2015a)
Toftlund, Denmark	2017	22.5	Solar thermal & heat pump	70 000	5 177	48	25 – 90	22	Rambøll (2016)
Langkazi, Tibet	2018	17.3	Solar thermal	15 000	683	-	35 – 75	18	Aalborg CSP (2019)
Høje Taastrup, Denmark	2023	-	DH grid	70 000	3 584	40	45 – 90	30	Aalborg CSP (2022)

[a] The storage capacity was calculated using a density of 980 kg/m^3, a specific heat of 4.18 kJ/(kg K), and the reported operating temperatures.

storage size, for example, planning, pumps, and diffusers. From Figure 1.8, it can also be noted that the lid is the most expensive part of the PTES, corresponding to approximately 1/2 to 1/3 of the total cost (depending on the PTES size).

However, although it is clear that PTES systems have a lower cost than TTES, their impact on the cost of heat has not been investigated. Especially when PTES systems are used for short-term storage operations, they can benefit DH grids that depend on the electricity market by shifting heat production to periods when the electricity price is low. Nevertheless, this potential financial benefit has not been quantified in the literature.

1.3.0.4 PTES design and characteristics

In principle, PTES can be designed having any shape as long as soil stability is ensured. Nevertheless, the most common PTES shapes are the reversed truncated pyramid (Dronninglund, Gram, and Toftlund) and reversed truncated obelisk (Marstal). However, there are also irregularly shaped PTES, e.g., Vojens and Høje Taastrup. Most of the existing PTES have a side-wall slope of 1:2 since this ratio ensures soil stability for clay-based soils without using any retaining walls (M. V. Jensen & Nielsen, 2020).

However, it should be noted that the shape and slope of the PTES sides are usually chosen based on the shape of the available plot of land and the soil stability. It is not yet clear, though, if the choice of the PTES shape has an impact on its performance.

Liner materials

The liner is an essential part of the PTES since it prevents water from leaking into the ground. Additionally, a liner is installed between the water surface and the floating insulation lid to prevent water from entering the lid. So far, the following materials have been identified as being applicable for PTES: polymer (i.e., polypropylene (PP) and polyethylene (PE)), elastomer, and metal (e.g., stainless steel) (M. V. Jensen & Nielsen, 2020).

Only polymer liners have been used in commercial PTES systems, mainly due to their low material price and installation cost. The main drawback of polymer liners is that they degrade when exposed to high temperatures. Additionally, polymer liners are not water-tight; thus, some water diffuses into the ground and lid construction. Most existing storages have used a PE liner, which is durable up to 90°C and features low water permeability. However, a PP liner was developed for the most recent storage in Høje Taastrup, which has a higher temperature resistance (up to 95°C) than PE liners. Nevertheless, it should be noted that the PP liner has approximately four times higher water permeability.

Elastomer liners have higher temperature resistance compared to polymer liners. Still, they have a higher installation price (they cannot be welded like polymer liners), and they have a higher water permeability compared to polymer liners. For these reasons, they have not been used in large-scale PTES installations.

Metal liners are very temperature resistant, have a long lifetime, and are water-tight. However, the material and installation cost is very high. Additionally, corrosion can be a prob-

lem when metal liners are in contact with the soil (since treated water is used, there is no problem when in contact with the PTES water).

Overall, the PTES lifetime is very much dependent on the lifetime of the liner. It is thus important to select a liner material that provides a good trade-off between price, thermal resistance, lifetime, and water permeability.

Lid constructions

So far, in all the existing PTES, only the lid has been insulated, whereas the sides and bottom have had no insulation. The three main drivers for this decision were that (1) it was difficult and expensive to find an insulation material that would not collapse under the weight of the water, (2) the soil offers natural insulation, and (3) most of the heat losses occur through the top of the PTES.

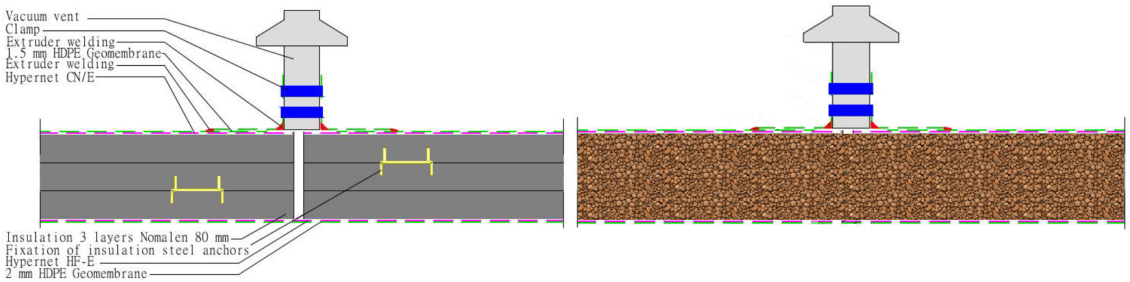

Figure 1.9: PTES lid based on Nomalén (left) and based on LECA (right) (PlanEnergi, 2015b).

For this reason, the floating insulating lid is the only component that minimizes heat losses to the ambient air and is the most expensive component of the PTES. Flexible insulation materials are usually used in lid constructions for the lid to be able to bend due to the water's thermal expansion.

Table 1.2: Lid areas and insulation materials for the PTES in Denmark. The lid area was estimated using drone photos. Multiple insulation types are provided for some storages due to the replacement or modifications of the original lid solutions.

Location	Lid area (m^2)	Lid operation	Insulation type
Marstal	10 900	2012 - 2018	Nomalén
		2019 -	Nomalén + XPS
Dronninglund	8 300	2014 - 2020	Nomalén
		2021 -	Nomalén + XPS
Høje Taastrup	11 000	2023 -	Nomalén + XPS
Vojens	22 500	2015 -	LECA
Gram	14 500	2015 - 2021	LECA
		2022 -	LECA + XPS
Toftlund	11 500	2017 -	LECA

In general, two different insulation materials have been used, namely Nomalén (NMC Termonova, 2011) and Light Expanded Clay Aggregate (LECA). Nomalén insulation is sold as mats made of cross-linked polyethylene foam with a closed-cell structure, while LECA is small, expanded clay pebbles. Table 1.2 presents the lid insulation materials and the corresponding areas for the PTES systems in Denmark.

The performance of both insulation technologies degrades with exposure to moisture and high temperatures for long periods of time. However, since polymer liners are not water-tight, some water vapor inevitably enters the lid construction. For this reason, natural (or mechanical) ventilation systems are usually installed in the lids in order to dry out the insulation material, as seen in Figure 1.9.

Furthermore, since the lid is a large, flat surface, rainwater can easily accumulate, which has to be removed to maintain the structural integrity of the lid. To remove the rainwater, some lid designs feature weight pipes that are placed on the lid surface to guide it to a single (or multiple) location from where it can be removed using a pump.

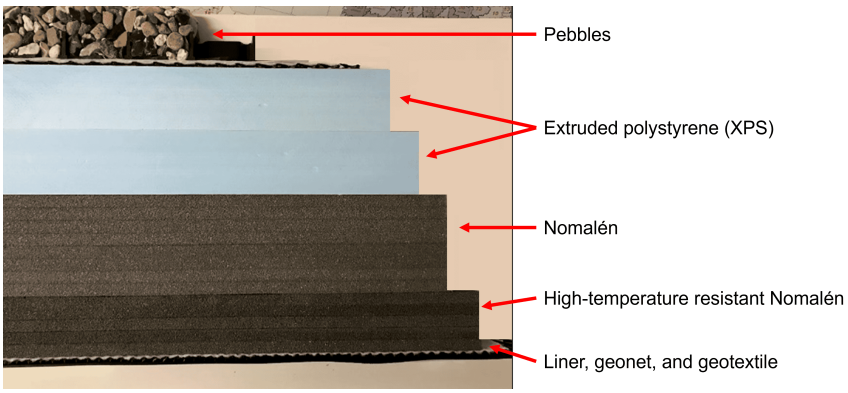

Figure 1.10: The new version of Nomalén lid used in Dronninglund, Marstal, and Høje Taastrup, constructed by the company Aalborg CSP.

The first version of a Nomalén-based lid was installed in Marstal in 2012 and in Dronninglund in 2014. Unfortunately, in both storages, this lid construction was irreparably damaged after approximately six years of operation (i.e., in 2018 in Marstal and at the end of 2020 in Dronninglund). For both PTES systems, the reason was that water had entered the lid, causing the bottom lid liner to tear. To overcome the challenges of previous lid designs, the company Aalborg CSP developed a new modular Nomalén lid (a cross-sectional view of the lid can be seen in Figure 1.10). The modular lid has been installed in the PTES in Marstal and Dronninglund and the newly constructed PTES in Høje Taastrup. This lid solution uses different types of insulation with varying insulating properties and resistance to high temperatures. A high-temperature resistant version of Nomalén is placed close to the storage water surface, on top of which a regular extruded polystyrene insulation (XPS) is placed. Additionally, for more efficient rainwater handling, the lid is divided into multiple modules. A slope is created towards the center of each module using varying levels of pebbles where a pump is located to remove the rainwater.

1.4 Research questions

Pit thermal energy storage systems have proven to be a cheap and efficient storage technology for district heating. As the technology is maturing, more district heating companies are expressing interest in the technology; hence, the number of PTES installations is expected to increase in the near future. However, the available knowledge on PTES derives primarily from short-term performance monitoring and a small number of scientific studies. Specifically, the effect of storage geometry, soil conditions, and storage operation remains largely uninvestigated, although they have a potentially great impact on performance. To this end, the following research questions were developed to cover this knowledge gap, which forms the basis of the present PhD study.

Performance:

1. How can the performance of PTES systems be assessed?
2. How does the geometry of a PTES affect its performance?
3. How does PTES operation affect the soil domain and vice versa?

Integration:

4. What is the impact of PTES on DH grids on a city scale?
5. What is the impact of PTES on a country scale?

1.5 Thesis outline

The remainder of this thesis is structured as follows:

Chapter 2 gives an overview of the methods used in this PhD study. Specifically, Section 2.1 presents a description of the investigated case studies along with the corresponding measurement equipment used at each system. Section 2.2, introduces the key performance indicators (KPIs) that were used to investigate stratification, efficiency, and economy of PTES. Section 2.3, provides a brief overview of the software used for simulating PTES systems. Last, Section 2.4, describes the drone thermal imaging method used to perform thermal inspections on PTES lids.

Chapter 3 presents the results obtained and answers the research questions introduced in Section 1.4. In Section 3.1, papers I, II, III, and IV were used for answering research question 1, paper V was used for question 2, and paper VI for question 3. In Section 3.2, paper VII was used for answering research question 4, and paper VIII was used for answering question 5.

Chapter 4 provides the conclusions for each research question, as well as recommendations for future work.

2 Methods

This chapter presents the case studies and methods used for conducting the present study. First, the case studies are presented in Section 2.1, followed by the key performance indicators (KPIs) used to assess and compare the performance of PTES systems in Section 2.2. Next, in Section 2.3, the software used in the simulations of this study (ANSYS, TRNSYS, and Balmorel) are introduced. Last, Section 2.4 gives details on thermal imaging, a technique used to detect leakages in PTES.

2.1 Investigated systems

Data from two PTES systems were used in this study for performance comparison and validation of simulation models. The systems in Marstal and Dronninglund were chosen as they were both part of previous research projects; hence, measurements were available from the plant operators.

2.1.1 Measurement data

It should be mentioned that obtaining system performance data from DH plants is a very time-consuming process. One of the reasons for this is that measurement data is usually spread across hundreds of individual files, which often contain erroneous data due to power outages, sensor malfunctions, etc. Thus, it is necessary first to write custom parsing scripts and quality control the data. However, the quality control process is user-dependent and poorly documented in most studies. For this reason, a quality control procedure and dataset were published for the PTES in Dronninglund (**Sifnaios** et al., 2023a), with the aim of creating a high-quality and transparent reference dataset. The quality control procedure was done in several Python scripts, which have been published on GitHub. It should be noted that the same quality control procedure was used for the dataset from the PTES in Marstal.

2.1.2 Marstal

The PTES in Marstal was constructed in 2012, having a volume of 75 000 m^3 and a storage capacity of approximately 6 000 MWh (PlanEnergi, 2013). The shape of the PTES was an inverse truncated obelisk (i.e., rectangular lid and bottom surfaces). The storage operated as a seasonal heat storage, charged by a solar collector field of 15 000 m^2 flat-plate collectors (FPC), and supplied heat to approximately 1600 consumers. The PTES was charged by the solar collector field during the spring and summer periods and was discharged during autumn and winter.

Three double-plated diffusers located at the top, middle, and bottom of the storage (see Figure 2.1) were used to charge and discharge the PTES. The diameter of the diffuser plates was 3 m, and the vertical spacing between the plates was 0.85 m. During operation, the average volume flow rate was 63 m^3/hr (PlanEnergi, 2013).

The PTES in Marstal had a 3-layered Nomalén lid (24 cm total thickness) and used high-density polyethylene (HDPE) liners. The lid had a slope toward its center, where a pump was located to remove rainwater from its surface. An aerial photo of the lid in 2013 is presented in Figure 2.1. In 2015, the lid insulation started to degrade due to contact with warm storage water, which led to increasing heat loss. Eventually, in 2018, the lid was replaced with the new modular Nomalén lid design from Aalborg CSP (see Section 1.3.0.4). Unfortunately, data from its operation were not available at the time of this study. Thus, measurement data from 2014 – 2017 were used.

Figure 2.1: Aerial photo from 2013 (left) and diffuser installation in the PTES in Marstal (right) (PlanEnergi, 2013).

The DH grid in Marstal had an average supply temperature of 73 °C and a return temperature of approximately 40 °C (PlanEnergi, 2013). If the discharged water from the PTES was higher than 73 °C, it was supplied directly to the DH grid. However, if its temperature was between 70 °C and 73 °C, it was mixed with warmer water from a biomass boiler in order to reach 73 °C. Alternatively, if the discharged water had a temperature lower than 70 °C, it was supplied to the heat source side of a heat pump that supplied heat to the DH grid. The operation of the heat pump cooled down the storage to approximately 15-20 °C. A schematic of the main components of the Marstal DH plant is presented in Figure 2.2.

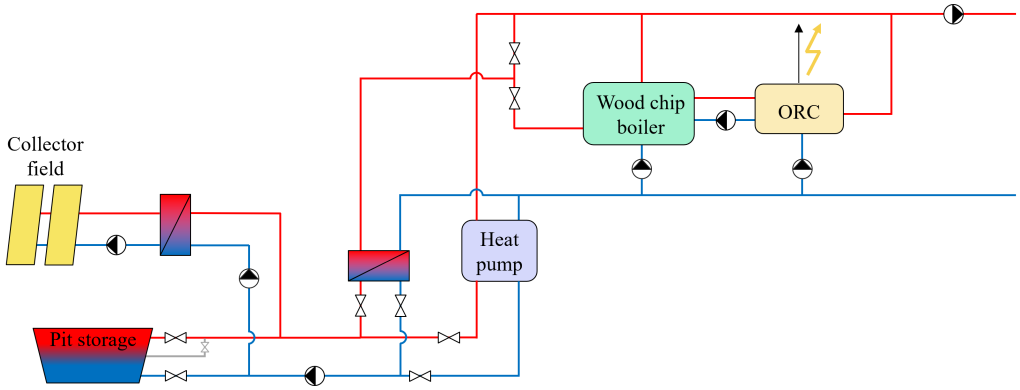

Figure 2.2: Simplified schematic of the PTES, solar collector field, biomass boiler, and ORC in the Marstal district heating system (Adapted from Schmidt, 2019).

2.1.3 Dronninglund

The PTES in Dronninglund was constructed in 2014 with a volume of 60 000 m^3 and an approximate storage capacity of 5 500 MWh (PlanEnergi, 2015b). The shape of the PTES

was an inverted truncated pyramid (i.e., square lid and bottom surfaces) and was based on an improved design of the PTES in Marstal. Similarly to Marstal, the Dronninglund storage also featured a 3-layered 24 cm Nomalén lid; however, an HDPE liner with a longer lifetime at high temperatures was used.

Despite the improvements, like the PTES in Marstal, the HDPE liner enclosing the lid insulation experienced multiple piercings at the end of 2020, leading to the replacement of the original lid with the new modular Nomalén lid from Aalborg CSP (see Section 1.3.0.4). However, data from the operation of the PTES with the new lid were not available during the period of the PhD study; thus, data from 2015 - 2019 were used.

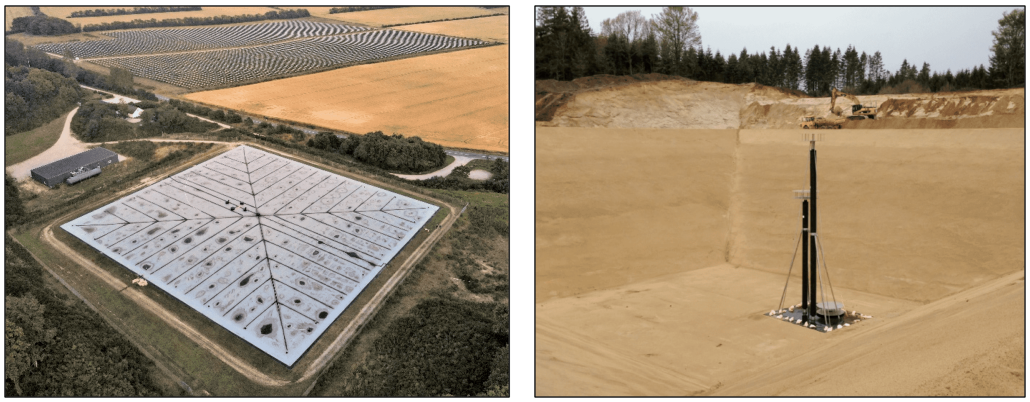

Figure 2.3: Aerial photo from 2015 (left) and diffuser installation (right) from the Dronninglund PTES (PlanEnergi, 2015b).

Similarly to Marstal, the PTES in Dronninglund was charged using three diffusers (at the top, middle, and bottom of the storage), as shown in Figure 2.3. However, the diffuser size was slightly smaller in Dronninglund, with a plate diameter of 2.5 m, a vertical spacing of 0.58 m, and an average flow rate of 80 m^3/hr during operation (PlanEnergi, 2015b).

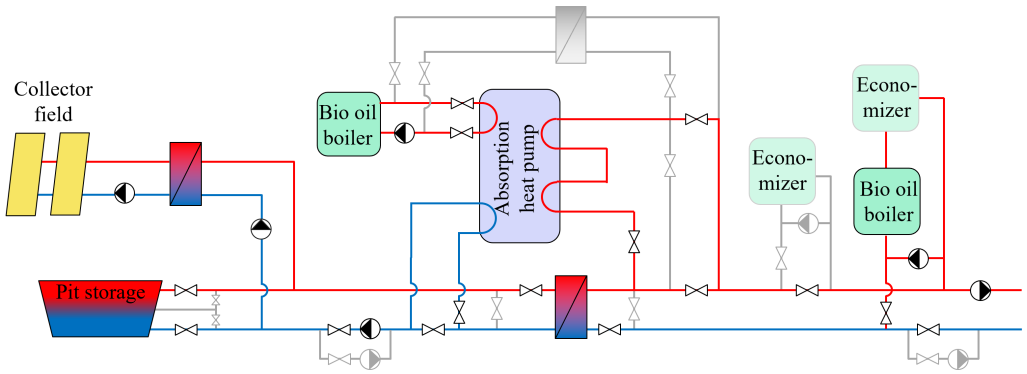

Figure 2.4: Simplified schematic of the collector field, PTES, and main components located at the Søndervangsvej DH plant, in Dronninglund (Adapted from PlanEnergi, 2015b).

The main difference between the PTES in Dronninglund and Marstal was their operation. While Marstal was only used as seasonal heat storage, the PTES in Dronninglund was used both as seasonal and short-term heat storage (mixed operation). Thus, the storage

was also used to even out the daily variation of the heat generation from the solar thermal collector field. Due to the mixed operation, the yearly charged and discharged energy of the PTES in Dronninglund was much higher than in Marstal.

The PTES in Dronninglund was charged by a 35 573 m^2 flat-plate solar collector field and supplied heat to 1350 consumers. The DH grid had an average supply temperature of 75 °C and an average return temperature of 42 °C (PlanEnergi, 2015b). If the discharged water temperature exceeded 75 °C, the PTES supplied heat directly to the DH grid. However, if it was lower than 75 °C, the system was used as a heat source for a heat pump. The heat pump usually operated from November to February and cooled down the PTES to approximately 10 °C. A schematic of the heating system in Dronninglund is presented in Figure 2.4.

2.1.4 Measurement equipment

This chapter presents the measurement equipment installed in the Marstal and Dronninglund PTES. It should be noted that more sensors than the ones mentioned in this chapter were installed; however, only the sensors used in this study are presented. For additional information on the topic, the reader is referred to **Sifnaios** et al. (2023a) and **Sifnaios** et al. (2022c).

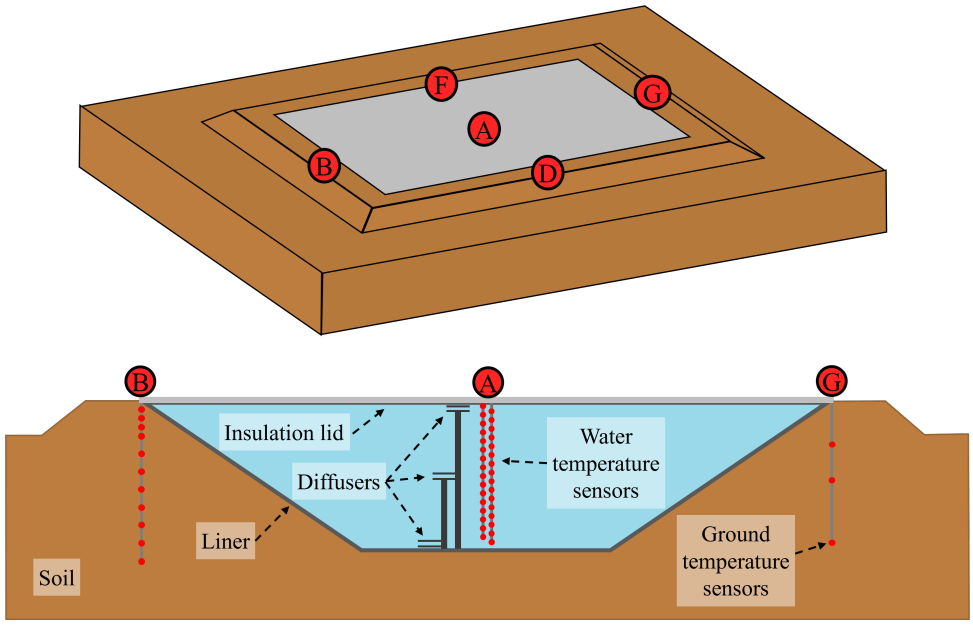

Figure 2.5: Measurement sensor locations in the Marstal PTES. The water temperature strings are attached at location A, and the soil temperature is measured at locations B, D, F, and G. Each small red dot corresponds to a temperature sensor (**Sifnaios** et al., 2023b).

2.1.4.1 Water temperature

The water temperature in each storage was measured using Class A PT100 temperature sensors, with an estimated uncertainty of ±0.15 K. These sensors were mounted on two strings hanging from the center of the lid. Each temperature string had 16 sensors placed at 1 m intervals, with the two strings offset by 0.5 m. Thus, the water temperature was

measured every 0.5 m. The same equipment was used to measure the water temperature in Marstal and Dronninglund. A schematic of the sensor locations can be seen in Figure 2.5 for Marstal and in Figure 2.6 for Dronninglund.

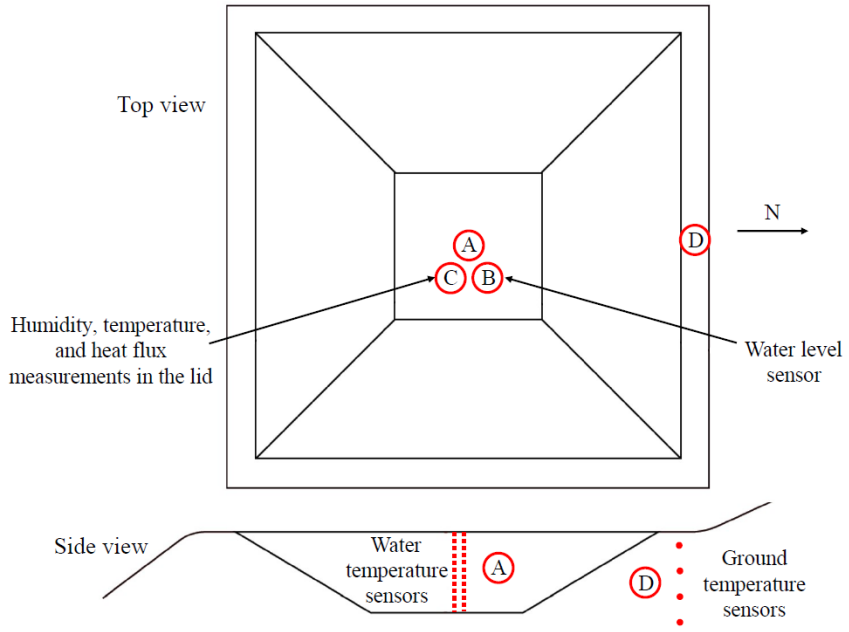

Figure 2.6: Measurement sensor locations in the Dronninglund PTES (**Sifnaios** et al., 2023a).

2.1.4.2 Inlet/outlet flow rates and temperatures

In Marstal, an ultrasonic flowmeter was installed in each diffuser pipe for measuring the volume flow rate to and from the storage. The estimated uncertainty of these sensors was 2%. In Dronninglund, the flow was measured using electromagnetic flowmeters with an uncertainty of 0.4%. However, in Dronninglund, the flow magnitude and direction were only measured for the middle diffuser. For the top and bottom diffusers, the reported flow rates and directions were calculated by the SCADA control system. Regrettably, the provided flow rates for Dronninglund had a significant mass-flow mismatch (i.e., a large imbalance between the entering and exiting flows). Therefore, a method for estimating the flow rates was developed, which is described in detail in **Sifnaios** et al. (2023a).

The temperatures in the inlet and outlet pipes were measured in both systems using immersed Class A PT100 sensors with an uncertainty of ±0.15 K.

2.1.4.3 Soil temperature

The soil temperature around the PTES was measured both in Marstal and Dronninglund. In Marstal, since it was the first large-scale PTES constructed, more sensors were installed for measuring the soil temperature. Thus, four temperature strings were installed near the edges of the storage embankment. Two of them had 11 temperature sensors, and two of them had three (see Figure 2.5).

In Dronninglund, four temperature sensors were installed in the ground (position D in Figure 2.6), approximately 1 m distance from the water edge and in the middle of the

embankment. The depths of the sensors were 10, 15, 20, and 25 m beneath the top of the embankment.

It is known that in both storages, the ground temperature sensors were PT100. However, their class is unknown; thus, their uncertainty was estimated to be ±0.5 K.

2.2 Key Performance Indicators (KPIs)

A key performance indicator (KPI) is a measurable result that can determine whether an objective is met. KPIs can be used to evaluate different aspects of a project but also compare it to other projects.

A number of KPIs exist in the literature for evaluating the economy and performance of individual TES but also TES as part of an energy system. The present study focuses on the thermal stratification and efficiency of PTES systems and on the economy of PTES as part of a DH system. The indicators used in each of these categories are presented in the following chapters.

2.2.1 Stratification

The working principle of a PTES is based on thermal stratification, i.e., a vertical temperature gradient of the water, which is maintained due to the dependence of buoyancy on temperature. Three main drivers decrease stratification: (1) mixing induced by the inlet flow, (2) heat diffusion caused by natural convection, and (3) thermal conduction (**Sifnaios** et al., 2022c). A storage with low heat losses can still perform poorly if stratification is not maintained; thus, it is of interest to be able to assess the level of stratification, e.g., to evaluate diffuser designs.

Several indicators have been used in the literature for assessing thermal stratification in TES systems. In this study, the two most common stratification indicators (i.e., the MIX number and the stratification coefficient) have been used to compare the level of stratification in the Marstal and Dronninglund PTES. Since both indicators were found to have drawbacks, a new stratification indicator was suggested, called exergy destruction, which was used to compare thermal stratification in the two storage systems (see **Sifnaios** et al. (2022b)).

As a first step when determining the stratification, each PTES was divided into a number of discrete horizontal layers corresponding to the position of the temperature sensors. In both Marstal and Dronninglund, water temperature sensors were installed every 0.5 m, and the PTES depth was 16 m. Thus, each storage was divided into 32 layers for which uniform temperature was assumed.

2.2.1.1 MIX number

The MIX number compares the investigated storage system's temperature profile with two idealized reference profiles, namely, a fully mixed and a fully stratified TES (Andersen et al., 2007). This way, a value between zero and one is obtained, with zero indicating a perfectly stratified TES and one indicating a fully mixed TES. It should be noted that when

calculating the idealized reference profiles, the corresponding energy content should be equal to the actual storage system. Equation 2.1, presents the expression for calculating the MIX number based on the moment of energy.

$$MIX = \frac{M_E^{stratified} - M_E^{actual}}{M_E^{stratified} - M_E^{fully\ mixed}} \tag{2.1}$$

The moment of energy for each storage layer is calculated by multiplying the energy content of each layer with the layer's distance from the bottom of the PTES. To find the moment of energy of a scenario (e.g., for the fully stratified), the moment of energy of each layer was summed, as shown in Equation 2.2.

$$M_E = \sum_{i=1}^{N} \rho_i \cdot V_i \cdot C_{p,i} \cdot (T_i - T_{ref}) \cdot z_i \tag{2.2}$$

where N is the total number of layers, ρ_i is the water density, V_i is the water volume, $C_{p,i}$ is the specific heat, and T_i is the water temperature of layer i. The distance from the centroid of layer i to the bottom of the PTES is denoted as z_i, and T_{ref} is the reference temperature, i.e., the temperature at which the storage system is considered empty.

2.2.1.2 Stratification coefficient

The stratification coefficient St was introduced by Wu and Bannerot (1987), where the degree of stratification is assessed based on the deviation of the storage temperature profile relative to the mean temperature. However, it should be noted that this indicator ranges from 0 to infinity, making it challenging to interpret. Generally, a higher stratification coefficient indicates a higher degree of thermal stratification. The mathematical expression for calculating the stratification coefficient is presented in Equation 2.3, where T_i is the temperature, and m_i is the water mass of layer i, T_{avg} is the weighted average storage temperature, and m_{total} is the total mass of the storage's water.

$$St = \sum_{i=1}^{N} \frac{m_i \cdot (T_i - T_{avg})^2}{m_{total}} \tag{2.3}$$

2.2.1.3 Exergy destruction

Exergy is a measure of the maximum useful work a system can produce until it reaches an equilibrium state with its environment (Dincer & Rosen, 2002). In other words, exergy is a measure of the quality of energy of a system. Exergy can be calculated using Equation 2.4, where ΔH is the change in enthalpy, ΔS is the change in entropy, and T_0 is the dead state temperature. The dead state of a system is when it is at temperature, pressure, elevation, velocity, and chemical equilibrium with its surroundings (Rosen & Dincer, 2004).

$$\Delta Ex = \Delta H - T_0 \cdot \Delta S \tag{2.4}$$

The exergy balance equation in a TES is given by Equation 2.5, indicating that the net exergy added to a TES (exergy charged minus discharged) is equal to the sum of the net change of exergy stored in the TES, exergy lost due to heat losses, and exergy destroyed due to reduction in stratification (i.e., mixing induced by the inlet flow, convection, and by downward thermal conduction).

This means that the last term of this equation (exergy destruction) can be used to assess the level of stratification in a TES as suggested by **Sifnaios** et al. (2022b). A high value would indicate poor thermal stratification, whereas a low value indicates good thermal stratification. One of the main benefits of exergy destruction is that it can be used to compare TES systems with different heat losses without having biased results since the exergy lost directly due to heat losses is accounted for.

$$\Delta Ex_{net} = \Delta Ex_{store} + \Delta Ex_{loss} + \Delta Ex_{destr} \tag{2.5}$$

Since the amount of exergy destroyed depends on the volume of the system, a normalized expression with the storage volume was used (see Equation 2.6) in order to be able to compare TES of different sizes.

$$\Delta Ex_{destr,norm} = \frac{\Delta Ex_{destr}}{\sum_{i=1}^{N} V_i} \tag{2.6}$$

2.2.2 Efficiency

In general terms, efficiency can be defined as the ratio between the useful output and the input to the system. Using this convention, two efficiency indicators were calculated in this study, namely energy and exergy efficiency, as presented in the following sections.

2.2.2.1 Energy efficiency

The energy balance expression in PTES is given by Equation 2.7, where E_{out} is the energy discharged from the PTES, E_{in} is the charged energy, and E_{loss} is the heat loss. ΔE_{int} is the change in the internal energy of the storage system, i.e., the difference between the internal energy at the end and start of the period under consideration.

$$E_{out} = E_{in} - E_{loss} - \Delta E_{int} \tag{2.7}$$

In general, two different expressions have been used so far for calculating the energy efficiency of PTES, which are presented in Equations 2.8 and 2.9. The main difference between these equations is in how the internal energy change of the PTES is accounted for.

$$\eta_{E1} = \frac{E_{out}}{E_{in} - \Delta E_{int}} \tag{2.8}$$

$$\eta_{E2} = \frac{E_{out} + \Delta E_{int}}{E_{in}} \tag{2.9}$$

Although these efficiency expressions have been extensively used in the literature and engineering studies, they can produce misleading results when comparing seasonal storage systems (e.g., Marstal) with storage systems used for both seasonal and short-term storage (e.g., Dronninglund). The main reason is that the total charged and discharged energy in a PTES used for seasonal and short-term operations is much higher compared to a PTES used only for seasonal operation. However, the heat loss of a seasonal storage is not proportionally higher. Thus, Equation 2.10 presents an expression for seasonal efficiency that attributes the heat losses only to the seasonally stored energy, regardless of the PTES operation. The seasonal energy stored can be calculated as the difference between the maximum and minimum energy content of the PTES during one year. Thus, the seasonal efficiency calculates the efficiency of the PTES as if it were solely used for seasonal heat storage.

$$\eta_{E,S} = \frac{E_{seasonal}}{E_{seasonal} + E_{loss}} \tag{2.10}$$

2.2.2.2 Exergy efficiency

Following the general convention for efficiency indicators, exergy efficiency can be calculated using Equation 2.11, where Ex_{in} is the exergy input to the system, and Ex_{out} is the exergy output of the system. The main difference between energy and exergy efficiency in TES systems is that exergy is influenced by the level of stratification, as mixing reduces exergy.

$$\eta_X = \frac{Ex_{out}}{Ex_{in}} \tag{2.11}$$

2.2.3 Economy

A number of indicators can be used for assessing the economy of an energy system. One of the most commonly used is the levelized cost of energy (LCOE). For energy systems that generate heat, this is often denoted as the levelized cost of heat (LCOH). In the present study, since the focus was on district heating, the LCOH was used for evaluating the systems' economy.

The LCOH quantifies the cost of providing one unit of heat over the system lifetime, considering the investment cost of the equipment, installation costs, operation and maintenance costs, etc. (International Energy Agency (IEA), 2022). A typical expression was used for calculating the LCOH, as described in (Yang et al., 2021). The used expression is pre-

sented in Equation 2.12, where I_0 is the investment cost, OM is the annual operation and maintenance cost, r is the discount rate, Q_H is the annual heat generation, t is the year, and T is the lifetime of the system in years.

$$LCOH = \frac{I_0 + \sum_{t=1}^{T} OM_t \cdot (1+r)^{-t}}{\sum_{t=1}^{T} Q_H \cdot (1+r)^{-t}} \tag{2.12}$$

It should be noted that a 4% discount rate was used in the calculations, as recommended by the Danish Energy Agency (Danish Energy Agency, 2018). Additionally, the operation and maintenance (OM) cost was taken as 1% of the total investment cost plus the fuel cost of the generation units (IEA Task 54, 2018).

Since the main focus of this investigation was the effect of adding a PTES system in an existing DH grid, the payback period (PPd) was also calculated as an economic KPI. This indicator can be used when comparing a reference system (e.g., a DH grid with no heat storage) with an investigated system (e.g., a DH grid with a PTES). The PPd is the time needed for the savings of the investigated system to compensate for the additional investment compared to the reference system. The expression for calculating the payback period is presented in Equation 2.13 as suggested by Zenhäusern (2020).

$$I_0 - I_{0,ref} = \sum_{t=1}^{PPd} (OM_{ref,t} - OM_t) \tag{2.13}$$

2.3 Software

To investigate the effect of various parameters on PTES performance and potential economic benefit, several simulations were carried out using different software. The software used in the present study are introduced below. The order of the introduced software is based on the level of detail used in the software's simulations. For example, ANSYS Fluent was used to simulate heat losses from the PTES in detail, whereas TRNSYS was used to simulate the integration of PTES in a local DH grid, and Balmorel was used to study the effect of including PTES in energy systems at a country level.

2.3.1 ANSYS Fluent

ANSYS Fluent is a software for computational fluid dynamics (CFD) simulations. It provides a wide range of pre-processing tools to the user in order to create the simulated geometry and the mesh for the computational domain. A number of meshing techniques are available, including structured and unstructured grids, enabling the user to create a mesh that is tailored to the desired application. Fluent utilizes the finite volume method (FVM) to discretize the computational domain into small control volumes and solves the governing equations of fluid flow and heat transfer phenomena between each of these volumes (ANSYS, 2022).

ANSYS Fluent was used to investigate the heat transfer in the soil domain surrounding

a PTES (no fluid was simulated). Specifically, the impact of the PTES geometry on its performance (research question 2) and the interaction between the PTES and its surroundings, such as groundwater (research question 3) was studied.

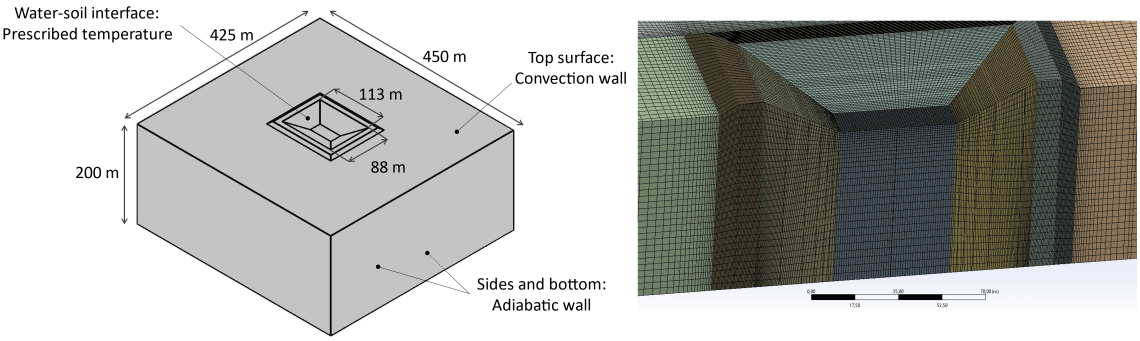

Figure 2.7: The simulated soil domain and boundary conditions (left) and a cross-cut of the created mesh (right) (**Sifnaios** et al., 2023b).

2.3.1.1 Simulation domain and boundary conditions

A simulation model in ANSYS Fluent was created to investigate the heat losses from the PTES toward the ground. Unlike the heat losses through the lid that can be reasonably assumed as one-dimensional and non-transient, accounting for the heat losses toward the ground is more complex due to the heat capacity of the soil and complex geometry. Thus, a 3D model must be used to accurately model the transient nature of the heat losses toward the ground. Consequently, a 3D model of the soil domain around the PTES was developed in ANSYS Fluent (see Figure 2.7). The boundary conditions of the soil domain were:

- Adiabatic walls for the sides and bottom of the soil domain. In reality, there is some small heat gain from the Earth's core, but it was assumed negligible.
- Convection wall for the top surface of the soil domain exposed to the ambient. The ambient air temperature was applied on the surface using a convection coefficient of 30 W/(m^{2}K), corresponding to a wind speed of 5 m/s (Laloui & Rotta Loria, 2020).
- A prescribed temperature wall for the water domain where the water temperature (varying with height) was applied as a boundary condition on the water-soil interface. The water temperature was described by 16 vertical uniform-temperature layers, each 1 m tall. By not modeling the PTES water movement, the computational time was dramatically reduced since only heat transfer was modeled (instead of a fluid dynamics simulation).

The soil domain was initialized with a uniform temperature of 8 °C. Heat gains due to solar radiation were assumed negligible. To obtain realistic ground temperatures at the start of the storage operation, a one-year preheating period was simulated, where the PTES was exposed to the ambient temperature (roughly corresponding to the construction period).

Due to the simple shape of the domain, the created mesh consisted only of hexahedral

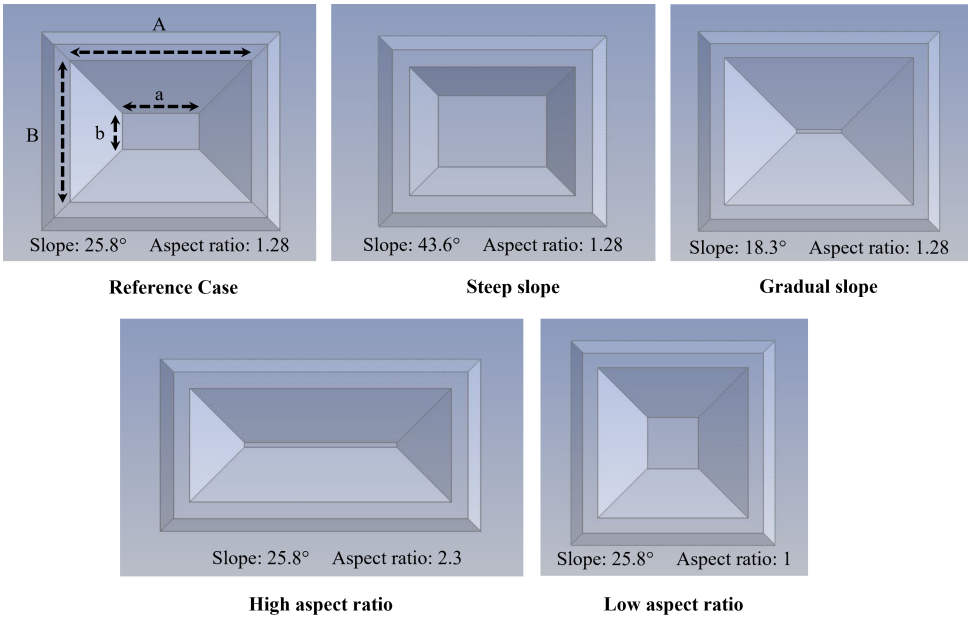

Figure 2.8: Investigated PTES geometries (**Sifnaios** et al., 2022a).

elements with a higher density (and smaller size) close to the water-soil boundary. In order to choose an appropriate mesh density and timestep duration, a mesh and timestep independence test was performed. Last, the created model was validated by comparison against measured ground temperature data from the Marstal PTES from 2013 to 2016.

Various PTES designs were investigated, having different slopes for the storage sides and aspect ratios, as seen in Figure 2.8. The aspect ratio is defined as the ratio of the long storage edge to the short edge. For example, a rectangular PTES has an aspect ratio greater than one, while a square PTES has an aspect ratio of one. All the investigated designs had the same height and volume in order to be directly comparable. More information on the specific designs can be found in (**Sifnaios** et al., 2022a).

2.3.1.2 PTES water and ambient temperature

To investigate the effect of seasonal and short-term PTES operations in the surrounding soil, theoretical temperature profiles were used in the boundary condition, as seen in Figure 2.9. The seasonal PTES operation performed one charge/discharge cycle per year, with a temperature range of 90–15 °C (similar to the PTES in Marstal). On the other hand, the short-term PTES operated one charge/discharge cycle every two weeks (thus, 26 cycles per year), with a temperature range of 90–45 °C (similar to the PTES in Høje Taastrup). It should be noted that the water temperature close to the lid was always assumed to be 90 °C, regardless of the operation.

For the simulations, the ambient temperature was taken from Denmark's Design Reference Year (DRY) (Nielsen, 2019). Since the typical lifetime of PTES is 25 years, the simulation duration was set to 25 years. Thus, the water and ambient temperature profiles presented in Figure 2.9 were repeated 25 consecutive times.

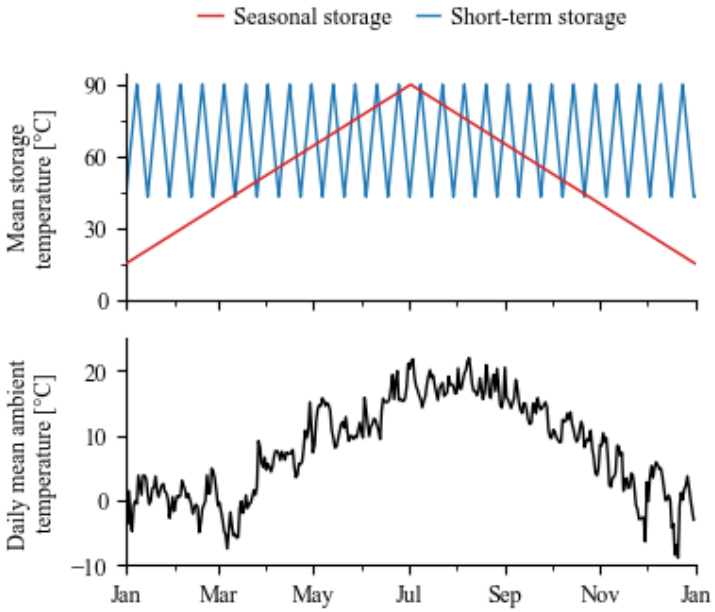

Figure 2.9: Mean storage and ambient temperature for the seasonal and short-term PTES operations. The same conditions were repeated for each year of the simulation. (**Sifnaios** et al., 2023b).

2.3.1.3 Groundwater properties

To investigate the interaction between the PTES and groundwater, a groundwater layer was added to the domain. The groundwater layer was modeled as a porous medium in Fluent, using Darcy's law to describe the flow, having an initial temperature of 8 °C. The properties of groundwater are presented in Table 2.1. For more information on the modeling of groundwater and the soil properties, the reader is referred to **Sifnaios** et al. (2023b).

Table 2.1: Groundwater properties (**Sifnaios** et al., 2023b).

Parameter	Value	Unit
Hydraulic conductivity	$3.6 \cdot 10^{-5}$	m/s
Effective porosity	0.25	-
Hydraulic gradient	1/300	-
Groundwater velocity	$4.8 \cdot 10^{-7}$	m/s

2.3.2 TRNSYS

TRNSYS, which stands for "Transient Systems Simulation Tool," is a graphically-based software designed for simulating and analyzing the performance of transient energy systems (Klein, 2017). It is primarily used for thermal and electrical energy systems in connection with building energy analysis and renewable energy research.

The software is based on a modular approach, where the user can connect components from a component library and create a complete energy system model. The components

are based on mathematical equations written in the Fortran programming language. TRNSYS models are particularly useful for performing feasibility studies for energy systems, evaluating control strategies, component dimensioning, and performance optimization.

TRNSYS was used to investigate the economic impact of a PTES integrated into a local DH grid that relied on electricity-based production units to cover its heat demand (research question 4). The specific case study is described below.

2.3.2.1 Investigated case study

The data used for the DH grid were operation data from the Danish city of Viborg for 2021. Viborg is a city of 41 000 people, with an annual heat demand of 342 GWh and a peak load of 107 MW. The supply temperature in the summer was approximately constant at 65 °C, while in the winter, it reached up to 80 °C, depending on the ambient temperature. The return temperature was approximately 45 °C in the summer and 40 °C in the winter.

Until 2022, Viborg's district heating operator relied on a traditional natural gas combined heat and power (CHP) plant and peak boiler units to cover the heat demand. However, a plan was launched in 2023 to eliminate the usage of natural gas by introducing electricity-based production units (i.e., heat pumps and electric boilers). The ultimate objective is to completely phase out the utilization of natural gas technologies by the year 2025. For more information on the DH in Viborg, the reader is referred to **Sifnaios** (2023). In general, there is a large increase in the number of electricity-based production units, particularly heat pumps, for DH production. As a reference, in 2017, there were 35 heat pump systems for DH in Denmark, while in 2022, there were 522 systems (PlanEnergi, n.d.). This increasing trend makes this study particularly relevant for future DH grids.

2.3.2.2 Modeled energy system

PTES have been traditionally used as seasonal heat storage, having a solar collector field as a heat source. However, since the Viborg DH grid will rely on electricity-based production units, it will become more dependent on the electricity market. Thus, it was decided to investigate the possible economic benefit of adding a short-term operating PTES to the DH grid with an aim to shift heat production to periods when the electricity price is low. This potential financial benefit has yet to be investigated in the literature.

To investigate the impact of a short-term operating PTES in the Viborg DH grid, a TRNSYS model was created. The main model components were a heat pump, an electric boiler, and a PTES (see Figure 2.10). This system was compared to a reference system, consisting of only a heat pump and an electric boiler. In order to ensure that the volatility of the heat demand and electricity prices was captured in the simulation, a 1-hour timestep was used.

For simulating the PTES, the TRNSYS components 1535/1301 were used. However, these components had not been validated in the past. Thus, it was decided to use the design of the PTES in Dronninglund for the simulated PTES and to validate its operation using data from the PTES in Dronninglund. Thus, the PTES was simulated as an inverse

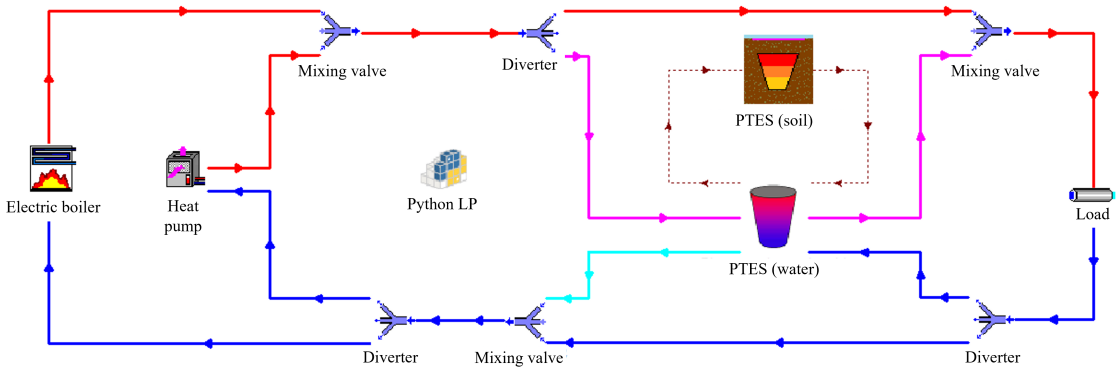

Figure 2.10: Model of the DH network and PTES in TRNSYS (**Sifnaios**, 2023).

truncated pyramid, with a height of 16 m and a volume of 60 000 m^3.

Regarding the heat pump, an air-to-water heat pump was selected. The reason for choosing an air-to-water heat pump was that it is universally applicable despite having a lower seasonal COP than other technologies (e.g., groundwater heat pumps). For example, an air-to-water heat pump does not require special permits for its installation and does not depend on the presence of specific heat sources (e.g., groundwater). For more information on the selected heat pump and its performance map, the reader is referred to **Sifnaios** (2023).

2.3.2.3 Control strategy

In order to determine the heat pump and electric boiler production for each timestep, as well as the PTES charge and discharge, a control strategy was developed. A linear programming optimization was developed based on the heat load and electricity price, with an optimization horizon of two weeks. The aim of the control strategy was to minimize the operation cost while always meeting the heat demand.

The linear programming equations solved are presented below. Equations 2.14 – 2.17 define the boundaries of the problem variables. Equation 2.18 specifies the system energy balance, and Equation 2.19 defines the storage constraints. Last, Equation 2.20 specifies the objective function to be minimized (i.e., the operation cost).

$$0 \leq Q_{HP}(t) \leq Q_{HP,max} \tag{2.14}$$

$$0 \leq Q_{Boiler}(t) \leq Q_{Boiler,max} \tag{2.15}$$

$$Q_{PTES,discharge,max} \leq Q_{PTES}(t) \leq Q_{PTES,charge,max} \tag{2.16}$$

$$0 \leq E_{PTES}(t) \leq E_{PTES,max} \tag{2.17}$$

$$Q_{HP}(t) + Q_{Boiler}(t) + Q_{PTES}(t) = Q_{load}(t) \tag{2.18}$$

$$Q_{PTES}(t) = E_{PTES}(t) - \eta_E \cdot E_{PTES}(t-1) \tag{2.19}$$

$$\text{Minimize } Obj = \sum_{t=1}^{T} El_{price}(t) \cdot \left(\frac{Q_{HP}(t)}{COP(t)} + Q_{Boiler}(t) \right) \tag{2.20}$$

where $Q_{HP}(t)$ is the heat generated by the heat pump, $Q_{Boiler}(t)$ is the heat generated by the boiler, $Q_{PTES}(t)$ is the heat charged (negative) or discharged (positive) from the PTES, $E_{PTES}(t)$ is the energy content of the PTES, $El_{price}(t)$ is the electricity price, $COP(t)$ is the heat pump's coefficient of performance, $Q_{load}(t)$ is the heat load, t is the timestep, and T is the forecast horizon in hours.

It should be noted that the PTES was not allowed to discharge if the temperature of the top layer was below the desired DH forward temperature. Thus, E_{PTES} is the usable energy content of the PTES, meaning the energy content above the DH forward temperature.

2.3.3 Balmorel

Balmorel (Wiese et al., 2018) is a high-level energy system model that calculates the least-cost solution for an energy system. In practice, it satisfies the energy demand while minimizing the investment and operation costs. Balmorel models the main energy sectors (i.e., power, heat, gas, and transport) and their interactions, allowing for complex energy system analyses. In this study, Balmorel was used to investigate the impact of PTES in future 100% renewable energy systems at a country level (research question 5).

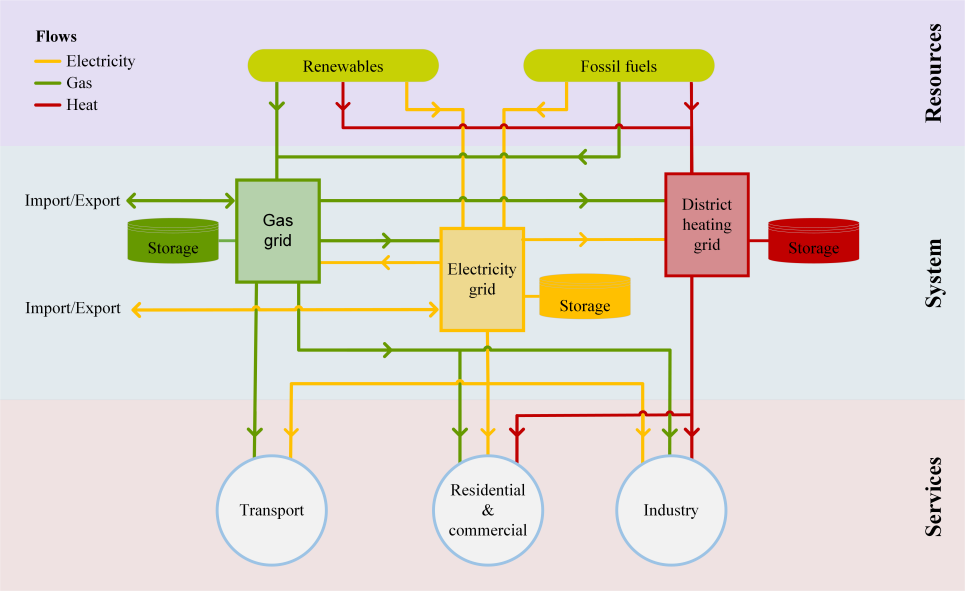

Figure 2.11: Schematic of energy sector modeling in Balmorel (Adapted from Münster et al., 2020).

In the investigated scenarios, the demand of the power sector is covered using electricity, while the demand of the transport sector is covered using liquid fuels or electricity. The demand of the heating sector can be covered using district heating, electricity, or fuels. In order to increase the flexibility of the energy system, the model can invest in storage (electricity, heat, and hydrogen) and transmission capacity or control the energy production and demand. A schematic of the energy sector modeling in Balmorel is presented in Figure 2.11.

2.3.3.1 Modeled energy system

The modeled energy system consisted of Denmark and its neighboring countries (Norway, Sweden, and Germany). However, since Denmark alone consists of 400 DH grids (Danish Energy Agency, 2017), an aggregation of the heat demand was performed to reduce the computation time. Thus, the DH areas in each region of Denmark (DK1 and DK2) were divided into three categories, i.e., DH-large, DH-medium, and DH-small. This meant that all large DH areas of one region were modeled as one DH grid, having a demand equal to the sum of the individual areas. The division of each country into regions is presented in Figure 2.12 A, and the division of each region of Denmark into areas is presented in Figure 2.12 B. Although the study focused on Denmark, the neighboring countries were included to account for electricity trading between the countries, which has a major impact on electricity prices.

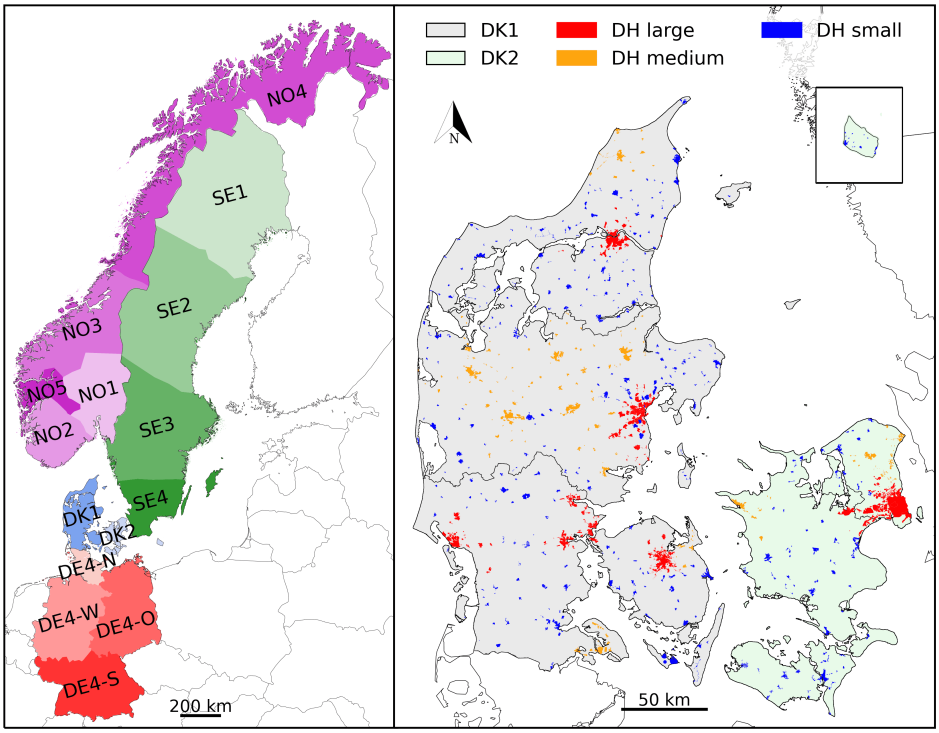

Figure 2.12: (A) Map of countries and regions (colored), and (B) aggregation of district heating areas in Denmark in Balmorel (**Sifnaios** et al., 2023c).

Similarly, since four different years were investigated (2020, 2030, 2040, 2050), time aggregation was performed, simulating only a number of representative weeks of each year. This way, each modeled week was repeated until the next modeled week arrived, thus accounting for an entire year. Detailed information on the spatial and temporal aggregation, as well as for the heat and electricity demand for each investigated year and country, can be found in **Sifnaios** et al. (2023c).

Balmorel utilizes two types of heat storage based on storage duration, namely short-term

and seasonal. Short-term has a storage duration of up to one week (usually using TTES), and seasonal has a storage duration longer than a week and up to one year (usually using PTES).

It should be noted that since Balmorel is performing country-level simulations, some simplifications are used in order to reduce the computation time. For example, unlike TRNSYS, Balmorel calculates only energy flows and does not account for the operation temperature of the investigated systems. Thus, regarding PTES, thermal stratification is not considered, and efficiency is calculated using a fixed coefficient (and does not depend on storage duration).

2.3.3.2 Techno-economic assumptions

The data used for simulating the PTES and TTES systems in Balmorel are presented in Table 2.2. Different PTES sizes were allowed to be installed in the various scales of DH grids in order to account for economy-of-scale effects. For example, only the large PTES could be installed in the DH-large areas, etc.

The investment cost of PTES and TTES were taken from data for existing systems. Apart from the capital cost, the PTES investment cost also included the land cost due to the large areas required for their construction. In general, the characteristics of the generation and storage technologies included in the simulations were based on data from the Danish Energy Agency's Technology Catalogs (Danish Energy Agency, 2023). It should be mentioned that PTES could be used for both seasonal and short-term operation; thus, the PTES efficiency (80%) was taken as an average between 70%, which is expected for PTES seasonal storage without a heat pump (Danish Energy Agency, 2018), and 90%, which is expected for PTES used for short-term storage. For more details on the settings of the simulations, the reader is referred to **Sifnaios** et al. (2023c).

Table 2.2: Data used for PTES and TTES simulation in Balmorel. The investment cost for PTES is assumed to decrease in the future as the technology matures, and there is a linear decrease from 2020 to 2050 (**Sifnaios** et al., 2023c).

Type	Size [m^3]	Investment year	Investment cost [10^3 €/MWh]	Efficiency [%]	(Dis)Charge capacity rate [MW]	Lifetime [years]
PTES (large)	250 000	2020	0.35	80	40	20
		2050	0.28			25
PTES (medium)	100 000	2020	0.49	80	40	20
		2050	0.40			25
PTES (small)	50 000	2020	0.64	80	40	20
		2050	0.52			25
TTES	3 000	-	2.90	98	40	40

2.3.3.3 Investigated scenarios

Balmorel was initially used to elucidate the effect of TES systems on a country scale; thus, a scenario without TES systems was compared to a scenario where TES systems could be used. Afterward, the investigation was focused on PTES and the benefit of their usage over the TTES alternative. The simulated scenarios are presented below:

- No TES: A No TES scenario was created in which Balmorel was not allowed to install thermal energy storage systems.
- TES: The TES scenario allowed investments in both TTES and PTES heat storage systems.
- PTES: In the PTES scenario, Balmorel was allowed to invest only in PTES systems as a heat storage technology (for both short-term and seasonal storage).
- TTES: In the TTES scenario, Balmorel was allowed to invest only in TTES systems as a heat storage technology (for both short-term and seasonal storage).

2.4 Thermal images

The performance of a PTES is directly related to the performance of the lid since it is the only insulated part of this technology. However, lid inspections are difficult and require manual work since the insulation is enclosed by the liner. Thus, it was decided to investigate and compare the different lid technologies using thermal cameras mounted on drones.

Figure 2.13: DJI Matrice 200 equipped with a Zenmuse XT2 camera flying over the solar collector field in Vojens (left) and close-up photo (right) (Drones Made Easy, n.d.).

Thermal cameras create images capturing the infrared (IR) radiation (750 to 1350 nm) emitted by objects. Therefore, thermal cameras do not directly detect temperature but instead rely on the principle that every object emits infrared radiation. In order to increase the accuracy of a thermal image, the emissivity of the object of interest should also be considered since it affects the wavelength of the emitted infrared radiation. The emissivity of an object can be affected by its surface material and finish (e.g., polished or painted) and by moisture on the surface. Water has a high emissivity; thus, there is a tendency to overestimate the temperature of wet surfaces.

The drone used for the inspection was a DJI Matrice 200 equipped with a DJI Zenmuse XT2 dual camera, able to capture thermal infra-red (IR) and regular (RGB) photos simultaneously. It is essential to have both photos of the investigated surface to easily identify different features. For example, in the case of pit storage inspection, a thermal image abnormality might be caused by debris, which can be detected in the RGB image and should not be further investigated. In order to have a high-quality thermal image for each PTES, a large number of images (250 - 700) were stitched together to form a large composite map called an orthomosaic. Photos of the used drone are seen in Figure 2.13. For more information on drone thermal imaging, the reader is referred to **Sifnaios** et al. (2021).

3 Results

Following the same convention as for the research questions, the results section was divided into two main parts: the performance of PTES (Section 3.1) and their integration into DH systems (Section 3.2).

3.1 PTES system performance

The first section of the results presents different approaches for assessing PTES performance. First, PTES performance is evaluated using KPIs, followed by inspections of PTES lid performance using thermal cameras (research question 1). Second, the effect of PTES geometry on PTES performance is analyzed (research question 2). Last, the impact of the surrounding soil domain on PTES performance is investigated (research question 3).

3.1.1 Comparison of PTES systems using KPIs

The performance of the PTES in Marstal and Dronninglund (described in Section 2.1) was evaluated in terms of thermal stratification and storage efficiency. The methods and equations used for this analysis are presented in Sections 2.2.1 and 2.2.2. A number of indicators were assessed in order to gain an understanding of the pros and cons of each indicator and determine best practices for assessing PTES performance.

3.1.1.1 Stratification indicators

The PTES water temperatures, MIX number, stratification coefficient, exergy destruction, diffuser energy supply, and normalized weekly flow rate for the Marstal PTES are shown in Figure 3.1.

Regarding the storage temperatures, the temperature of each layer is illustrated using a different color (green for the top and blue for the lowest layer). A thin, black curve is also used to indicate the temperature of the top, middle, and bottom layers. This figure shows that the annual maximum temperature of the Marstal PTES decreased over the investigated period. The main reason for this was the degradation of the lid insulation that led to the interruption of the PTES operation in 2018.

It should be noted that each sub-figure has a different temporal resolution in Figure 3.1. For example, the temperature, MIX number, and stratification coefficient are presented for each day, while the exergy destruction and diffuser energy supply were calculated for each month, and the volume flow rate for each week. The main reason was the low spatial resolution of the temperature in the storage that prevented an accurate calculation of exergy destruction and heat losses at a higher temporal resolution. Regarding the flow rate, the daily flows were too variable.

In Figure 3.1, the charge periods of the PTES are shown with a pink background. The periods when the PTES discharged directly to the DH grid are shown in grey, while the

periods when it was used as a heat source by a heat pump are illustrated using a dotted pattern. It may be observed that the periods that the PTES was used as a heat source by a heat pump were getting longer with time, directly resulting from the low storage temperatures.

Regarding stratification, in Marstal, the MIX number had an average value of 0.74 for the entire investigated period, indicating a low degree of stratification in the PTES. Additionally, the stratification coefficient had an average value of 64 K^2; however, this value is only useful for assessing stratification when used to compare two different storage systems or different storage operations. It may be observed that the MIX number negatively correlates with the stratification coefficient (i.e., when one increases, the other decreases). Both indicators agree that the maximum degree of stratification is achieved approximately at the middle of the charge/discharge periods, while there is a low degree of stratification (i.e., uniform temperature) at the end of the charge/discharge periods. In general, both indicators tend to calculate a higher degree of stratification when there is a large temperature difference between the top and bottom of the storage. However, this does not necessarily mean a high degree of stratification in the PTES.

Unlike the MIX number and stratification coefficient, exergy destruction indicates that the highest degree of mixing in a PTES occurred during the charging periods. This is mainly due to mixing induced by the inlet flow and secondary due to heat losses from the top of the storage during charging. Heat losses can affect the stratification in the storage system by cooling down the water layer under the lid, creating thermal inversion that induces mixing. Additionally, when there is no uniform temperature in the PTES, temperature equalization is caused by heat conduction and diffusion. These phenomena are captured by exergy destruction since its lowest values are documented when the PTES approaches a uniform temperature (i.e., when fully charged or discharged). It should be noted that some of the spikes in exergy destruction can be correlated with periods of high energy supply/extract from the diffusers, indicating mixing occurring during the diffuser operation. Last, there was generally no direct correlation between the volume flow rate passing through the PTES and the stratification indicators. The mean annual values of the stratification indicators for the PTES systems in Marstal and Dronninglund are presented in Table 3.1.

The main differences in the design and operation between the PTES in Marstal and Dronninglund were the following:

- Dronninglund was used for mixed storage operation (short and long-term storage), while Marstal was used only as a seasonal heat storage.
- Dronninglund featured an improved lid design, leading to lower heat losses than Marstal.
- The mean low temperature in the Dronninglund PTES was 10 °C, while in Marstal, it was around 20 °C; thus, the heat gains from the ground in the winter were much greater in Dronninglund.

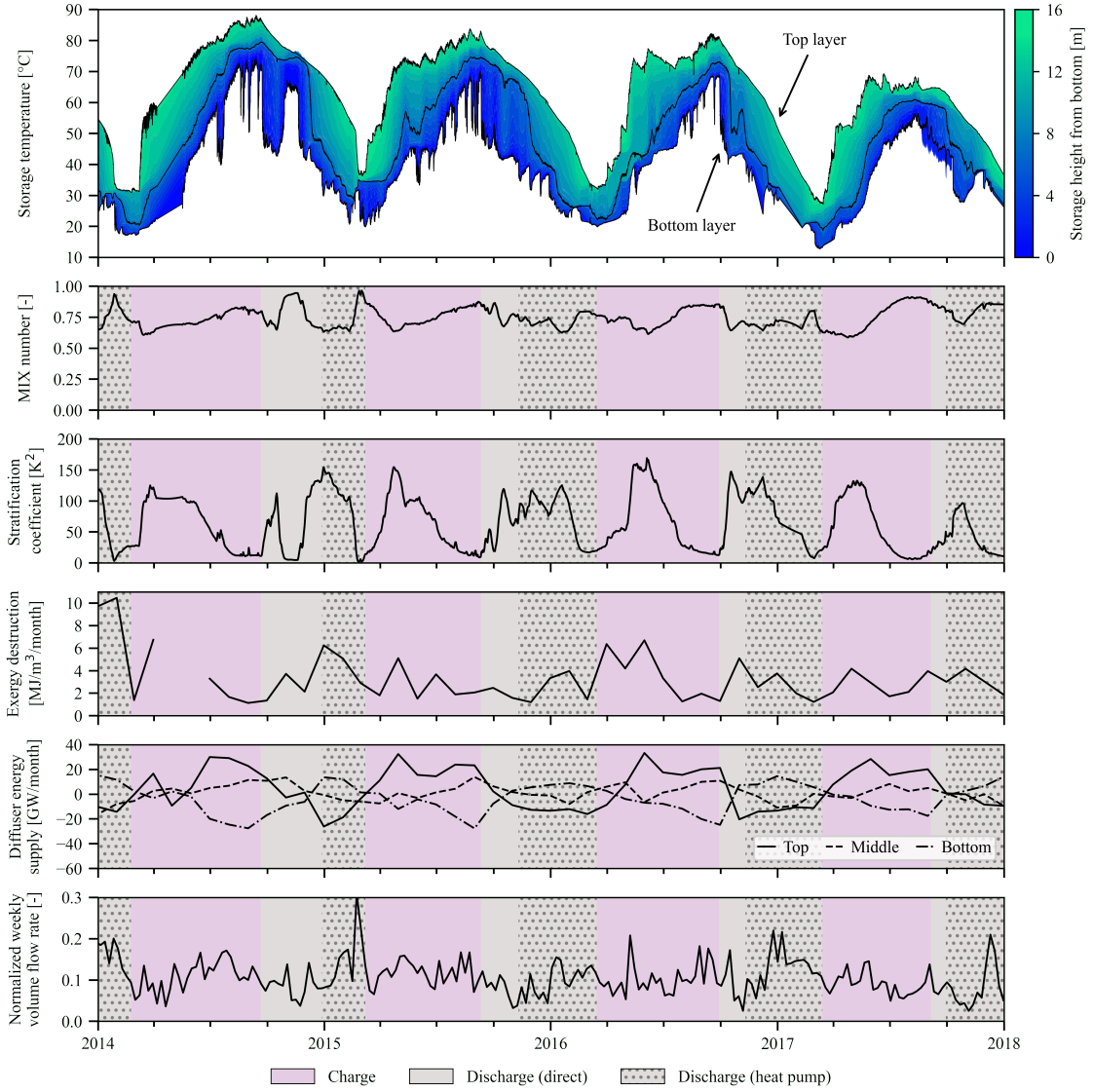

Figure 3.1: Storage temperature and stratification indicators for PTES in Marstal. The gap for exergy destruction in spring 2014 is due to missing flow rates from the dataset, probably due to data logging errors (**Sifnaios** et al., 2022c).

The effect of the lower heat losses is observed in Figure 3.2 where the Dronninglund storage temperature reached higher levels than Marstal. It should be noted that the short-term storage cycles created the spiky profile in the top layers of the Dronninglund PTES, unlike Marstal, which was caused by heat losses.

The mean MIX number value for the investigated period in the Dronninglund PTES was 46% lower than the one in Marstal, indicating a well-stratified storage. Similarly, the stratification coefficient demonstrated a higher degree of stratification for Dronninglund compared to Marstal since the maximum value was 3.2 times higher. However, it should be noted that due to the short-term cycles, there were many more spikes in the stratification

Table 3.1: Mean annual values for MIX number and stratification coefficient and the sum of the annual values for exergy destruction for the PTES in Marstal and Dronninglund (**Sifnaios** et al., 2022c).

	Marstal			**Dronninglund**		
	MIX number [-]	Stratification coefficient [K^2]	Exergy destruction [MJ/m^3]	MIX number [-]	Stratification coefficient [K^2]	Exergy destruction [MJ/m^3]
2014	0.75	60	38	-	-	-
2015	0.75	71	33	0.33	174	36
2016	0.73	75	42	0.34	187	39
2017	0.76	49	32	0.35	154	34
2018	-	-	-	0.32	115	31
2019	-	-	-	0.34	139	32
Overall	0.74	64	36	0.34	154	34

coefficient during the charge periods, indicating a higher degree of mixing during charge than in Marstal.

This can also be confirmed by the exergy destruction, where the maximum values occurred during the PTES charge periods. Although exergy destruction during the PTES charging is higher in Dronninglund than in Marstal, the discharging values are much lower. This led to Dronninglund having 6% lower mean annual exergy destruction than Marstal.

Overall, all stratification indicators agree that Dronninglund had a higher degree of stratification than Marstal. However, since the MIX number and stratification coefficient favor systems with low heat losses, exergy destruction is recommended as a non-biased indicator for assessing stratification.

3.1.1.2 Efficiency indicators

The calculated energy and exergy efficiencies for the PTES in Marstal and Dronninglund are presented in Table 3.2. It may be observed that very high efficiencies were achieved in Dronninglund, primarily due to the low heat losses and the utilization of low-temperature heat by the heat pump, which increased the amount of energy that could be discharged.

Regarding energy efficiency, using the efficiency expressions $\eta_{E,1}$ and $\eta_{E,2}$ gave different results for Marstal. The reason is that if the internal energy change is negative (meaning the energy content of the storage is lower at the end of the year than at the start), then $\eta_{E,1}$ indicates higher efficiency than $\eta_{E,2}$. The opposite occurs if the energy change is positive.

However, this difference is not spotted for Dronninglund since, due to the short-term storage cycles, the charged and discharged energy is much higher than the internal energy charge of the storage. Thus, $\eta_{E,1}$ and $\eta_{E,2}$ give the same results for Dronninglund.

In general, this investigation elucidated that the two energy expressions cannot be used interchangeably. However, it is firmly believed that the expression $\eta_{E,1}$ should be used

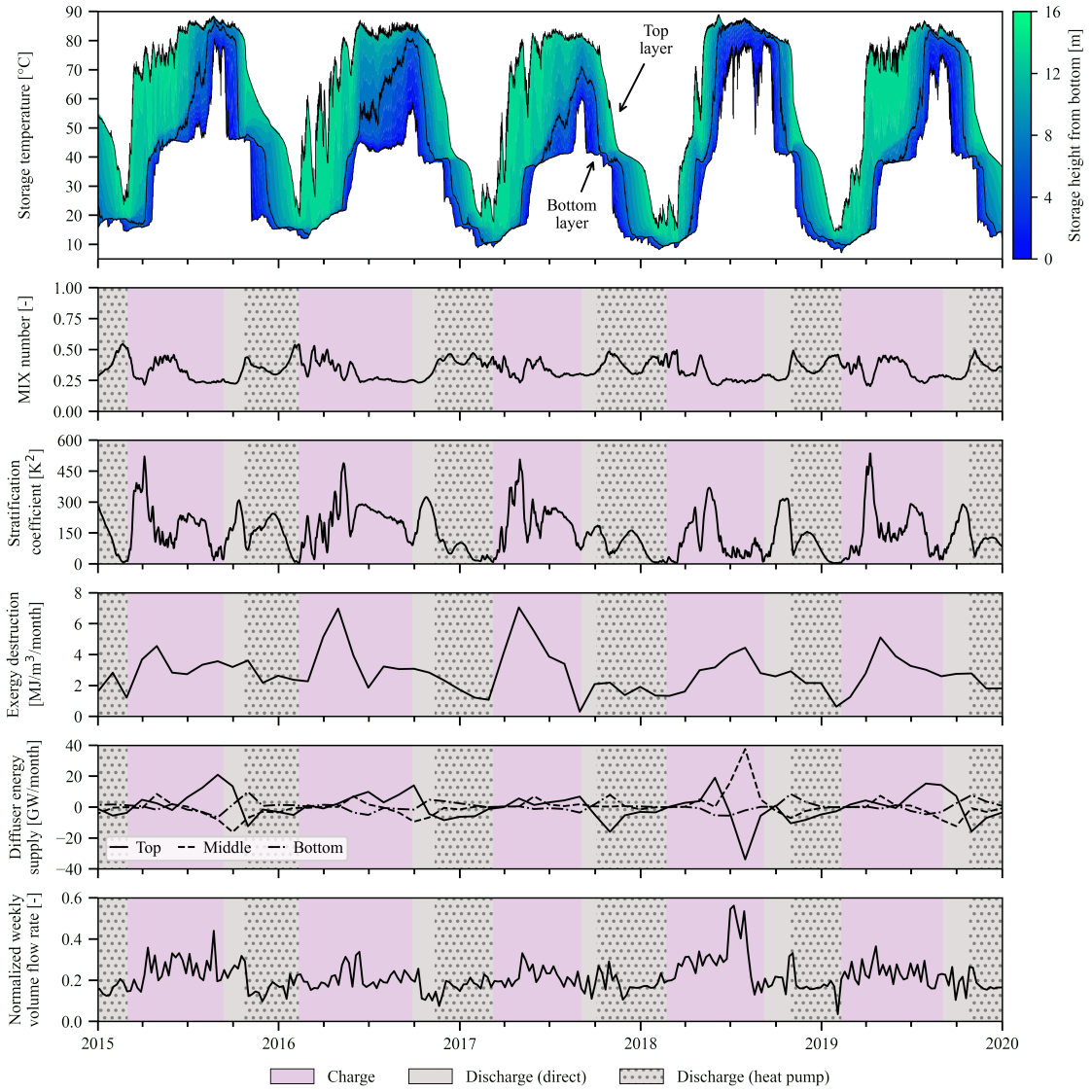

Figure 3.2: Storage temperature and stratification indicators for the Dronninglund PTES (**Sifnaios** et al., 2022c).

since it is considered more appropriate to subtract the internal energy change from the charged energy. This way, less energy has to be charged due to existing energy from the previous cycle.

The seasonal efficiency ($\eta_{E,S}$) calculates the efficiency of the storage system as if it had been used only for seasonal storage. Thus, for Marstal, which is used only for seasonal storage, the obtained energy and seasonal efficiency results are very close. On the contrary, the seasonal efficiency is much lower than the energy for Dronninglund since it is used as a short and seasonal PTES. Consequently, this indicator can be used to compare the equivalent efficiency of two PTES having different operations.

It should be noted that the energy efficiency expressions investigated in this study account only for heat losses. However, the exergy efficiency also accounts for the amount of

Table 3.2: PTES efficiencies (%) for Marstal and Dronninglund (**Sifnaios** et al., 2022c).

	Marstal				Dronninglund			
	$\eta_{E,1}$	$\eta_{E,2}$	$\eta_{E,S}$	η_X	$\eta_{E,1}$	$\eta_{E,2}$	$\eta_{E,S}$	η_X
2014	79	82	78	53	-	-	-	-
2015	68	66	59	58	88	88	74	73
2016	66	63	64	52	90	90	78	69
2017	41	34	47	27	96	96	90	73
2018	-	-	-	-	93	93	83	79
2019	-	-	-	-	93	93	84	73
Total	63	62	61	48	92	92	81	73

mixing in the storage. Thus, the calculated exergy efficiency was always lower than the energy efficiency expressions and is useful to consider in conjunction with the energy efficiencies.

Overall, all the efficiency indicators elucidated that the PTES in Dronninglund had higher efficiency than Marstal. This was due to the higher heat losses and the lower degree of thermal stratification in the Marstal PTES.

3.1.2 Comparison of PTES systems using drones

The use of KPIs is a way of evaluating and comparing the PTES performance based on operation data, although it can be difficult to know the exact cause of poor performance. Since the PTES performance is directly related to the lid performance, lid inspections can provide a way to determine if poor performance is caused by increased heat losses from the PTES lid. It should be noted that it is very difficult to compare thermal images of different PTES systems, but they can be used to identify leakages in the lids of individual systems.

As shown in Table 1.2, the main insulation types used in PTES are Nomalén and LECA. The following sections present thermal images of the lid constructions of different PTES systems; first, the PTES using Nomalén followed by the PTES using LECA. It should be noted that there are large differences in the surface temperatures of the PTES systems. This is mainly due to the different ambient and sky temperatures during filming; thus, temperatures between plots should not be compared.

3.1.2.1 PTES using Nomalén

Figure 3.3 presents an RGB and thermal image of the first generation Nomalén lid that was installed in Dronninglund. It can easily be observed that there is a large number of water puddles on the lid's surface that appear as having high temperatures in the thermal image (yellow color). However, as mentioned in Section 2.4, this is due to the high emissivity of water and not necessarily because they are warmer than their surroundings.

Although the water puddles can not be compared with the surrounding areas, they can be compared with each other. By such a comparison, it was identified that the puddle

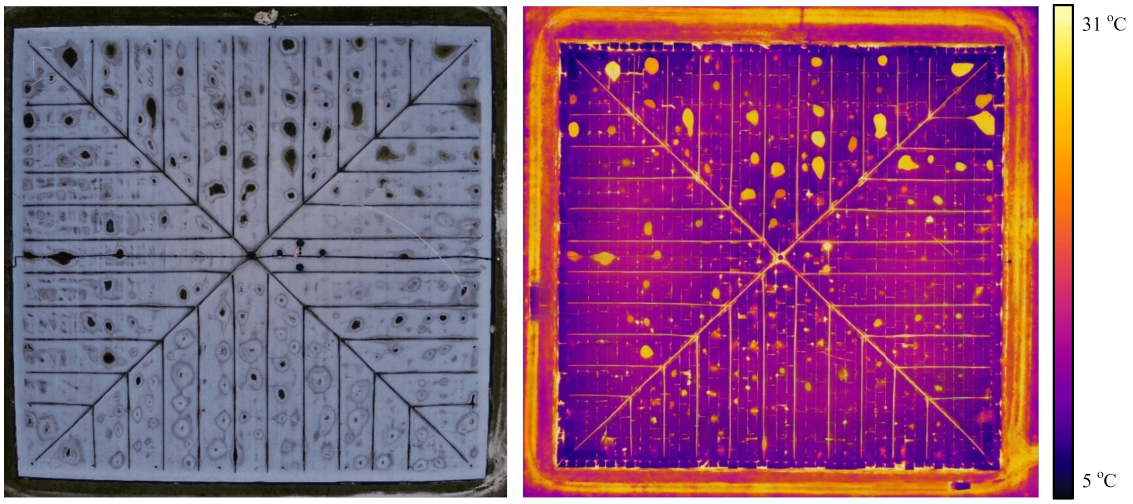

Figure 3.3: RGB (left) and thermal (right) image of the PTES in Dronninglund in 2020 (**Sifnaios** et al., 2021).

in the top left corner was warmer than the rest. Upon informing the plant manager, he confirmed that there was a leakage of warm storage water into the lid in that area. Such findings are very important since small repairs can improve the PTES performance and extend the insulation's lifetime.

Figure 3.4 presents the thermal and RGB images of the new generation of the Nomalén lid in Marstal (see Section 1.3.0.4). This modular lid consisted of 12 square sub-sections. Each of the sub-sections had a surface slope toward its center, where a rainwater drainage system was located. In general, no major issues were identified during the inspection of this lid.

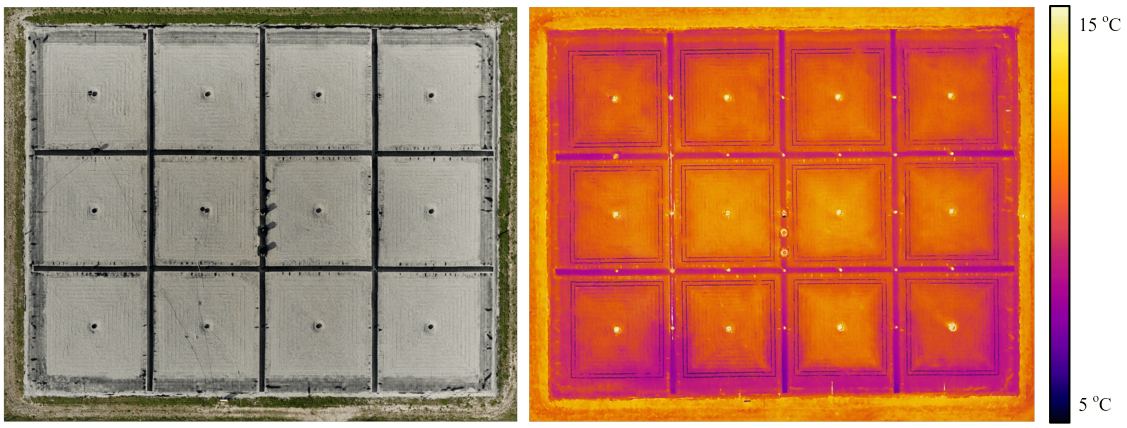

Figure 3.4: RGB (left) and thermal (right) image of the PTES in Marstal in 2021 (**Sifnaios** et al., 2021).

3.1.2.2 PTES using LECA

In Figure 3.5, the PTES in Gram is shown. It may be observed that the thermal signature looks vastly different compared to Figures 3.3 and 3.4, which is because of the use of LECA as an insulation material. The observed brain-like pattern is probably due to heat convection within the lid, which increases the heat losses of the PTES. Last, a very warm

water puddle was identified, indicating a leakage in the lid.

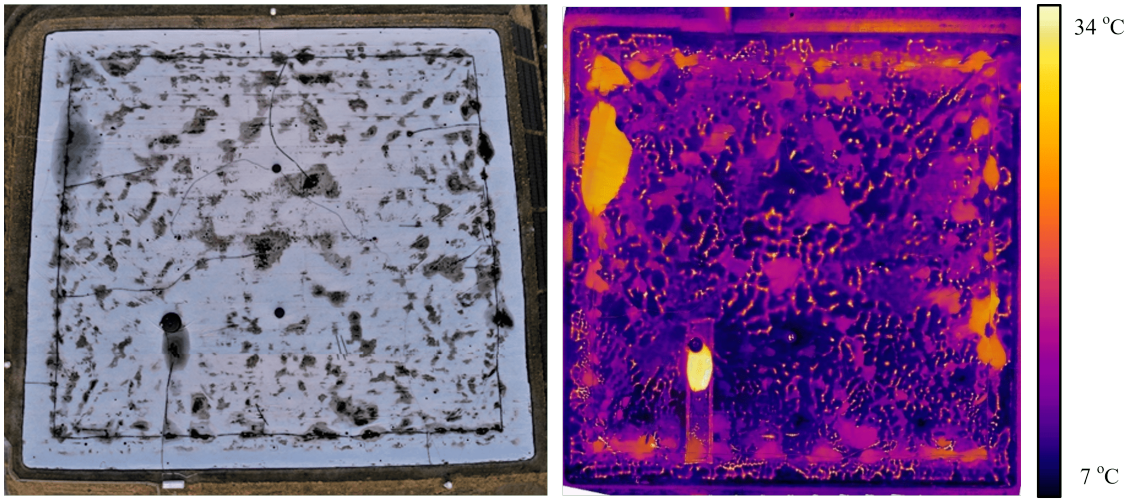

Figure 3.5: RGB (left) and thermal (right) image of the PTES in Gram in 2020 (**Sifnaios** et al., 2021).

The PTES in Vojens is presented in Figure 3.6, which looks fairly similar to the one in Gram. Again, due to LECA insulation, brain-like patterns can be identified in the thermal image. However, unlike Gram, this phenomenon is more intense in some areas, indicating either the existence of a thinner LECA layer or that the LECA is wet, resulting in higher heat losses. In any case, it is suggested that smaller clay pebbles should be used in LECA lids in the future, or a convection membrane should be installed to minimize this phenomenon.

Overall, these investigations proved that drone thermal imaging is an effective way of performing thermal inspections of PTES lids and identifying leakages.

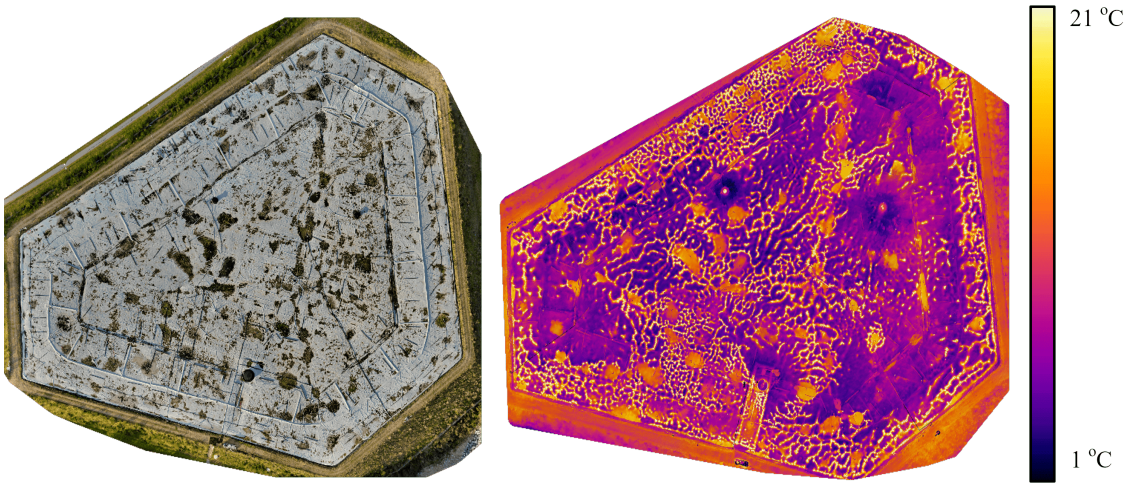

Figure 3.6: RGB (left) and thermal (right) image of the PTES in Vojens in 2020 (**Sifnaios** et al., 2021).

3.1.3 Effect of PTES geometry

A factor that can affect the performance of PTES but hasn't been investigated in the literature is their geometry. Figure 3.7 presents the heat losses for each investigated PTES geometry for three years of operation. It should be noted that the storage temperatures from the PTES in Marstal were used in this investigation. Consequently, the heat losses were affected by the storage operation for each year (e.g., in 2014, the mean storage temperature was higher than in 2013).

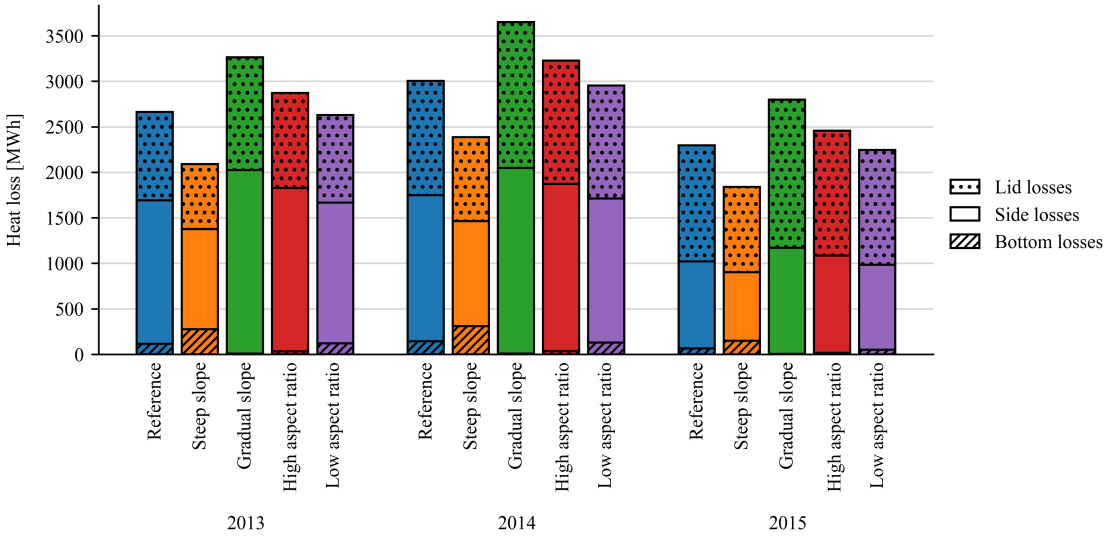

Figure 3.7: Annual heat loss for the investigated PTES configurations (**Sifnaios** et al., 2022a).

Figure 3.7 proves that the impact of the storage sides' slope on heat loss is much larger than that of the aspect ratio. For example, the *steep slope* scenario had overall 35% lower heat losses than the *gradual slope* scenario and 20% lower heat losses than the *reference* scenario. On the contrary, the *low aspect ratio* scenario (square-shaped lid and bottom) could decrease the overall heat loss only by 9% compared to the *high aspect ratio* scenario (rectangular-shaped lid and bottom). The reason for this difference is that the *steep slope* scenario has a much smaller surface area, leading to lower heat losses.

Table 3.3 reports the values of the last simulation year (2015) and the corresponding efficiency for each PTES geometry. Only the values for 2015 are shown since they are considered more representative of a long-term operating PTES. It should be noted that the storage energy efficiency was calculated using $\eta_{E,1}$ (see Section 2.2.2.1), as suggested by **Sifnaios** et al. (2022c). Since efficiency is directly affected by heat losses, a similar trend was obtained. The *steep slope* scenario featured the highest storage efficiency (78%), while only a 3% improvement in efficiency could be achieved by selecting a low aspect ratio for the PTES.

The results of this investigation identified the ideal PTES geometry to have a square-shaped lid and bottom (aspect ratio of one) with as steep as possible storage side slope.

Table 3.3: Heat loss and efficiency for 2015 for the investigated PTES configurations (**Sifnaios** et al., 2022a).

Case	Bottom heat loss [MWh]	Side heat loss [MWh]	Lid heat loss [MWh]	Efficiency [%]
Reference case	63	957	1274	72
Steep slope	150	751	936	78
Gradual slope	4	1167	1626	66
High aspect ratio	17	1068	1373	70
Low aspect ratio	50	933	1261	73

However, it should be noted that in many cases, the aspect ratio of a PTES is dictated by the shape of the available plot of land and its slope by the ground stability and soil properties. Thus, sub-optimal geometries have been selected in many existing PTES. Nevertheless, these results can aid in determining how much to compromise in terms of deviating from the optimal storage configuration.

3.1.4 Effect of surrounding soil domain

PTES is an underground TES system in direct contact with the soil since the sides and bottom surfaces are not insulated. Thus, the thermal properties of the surrounding soil domain and the possible presence of groundwater can affect its performance. However, it remains unknown if and how much the PTES operation is affected by the presence of groundwater and whether the impact differs depending on the operation of the PTES (short-term vs. seasonal).

In order to investigate the effect of the surrounding soil domain on the operation of PTES, a simulation model was developed in ANSYS Fluent (see Section 2.3.1). Initially, a mesh and timestep independence test was performed where a mesh of 900k cells and a timestep of 8 h were selected. Afterward, the model was validated against measured ground temperature data from the Marstal PTES for 2013 – 2015. The results showed a good agreement between the simulated and measured ground temperatures. For more information on the validation and the mesh and timestep independence studies, the reader is referred to **Sifnaios** et al. (2023b).

3.1.4.1 Heat loss and ground temperature stabilization

Figure 3.8 illustrates the heat losses toward the ground for a seasonal and short-term PTES operation for a period of 25 years. Due to the different operating temperatures between a seasonal and a short-term PTES (see Figure 2.9), the short-term PTES has approximately 15% higher heat losses than the seasonal PTES. However, it should be noted that, due to the greater number of storage cycles (i.e., shorter heat storage duration), the short-term PTES has lower heat losses relative to the stored energy and, consequently, higher storage efficiency.

Over the entire operation period of the PTES, heat losses consistently decrease, with the most significant reduction occurring in the first years of operation (assuming the same

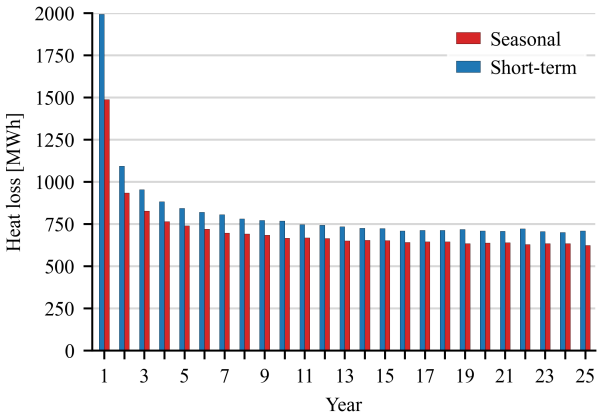

Figure 3.8: Yearly heat losses toward the ground for seasonal and short-term PTES operation (**Sifnaios** et al., 2023b).

yearly operation). This decrease is attributed to the temperature difference between the charged water in the PTES and the initially cooler soil. As the PTES operates, a high heat transfer rate occurs from the water to the soil, resulting in heat accumulation in the soil and a subsequent increase in soil temperature. As a result, the heat loss toward the soil is gradually reduced over time.

This can be seen in Figure 3.8, where there is a drastic decrease in heat losses in the first years of operation for both the seasonal and the short-term PTES. Overall, the heat losses for the last year of operation were 58% lower than the first for the seasonal PTES operation and 64% lower for the short-term. Nevertheless, the rate of decrease becomes smaller with time, and after a certain point, the annual heat loss decrease becomes smaller than 2%, so the heat losses could be considered stable after this point. Thus, a stable heat loss was achieved for the seasonal PTES after the 12^{th} year of operation, while for the short-term PTES, it was after the 8^{th} year of operation.

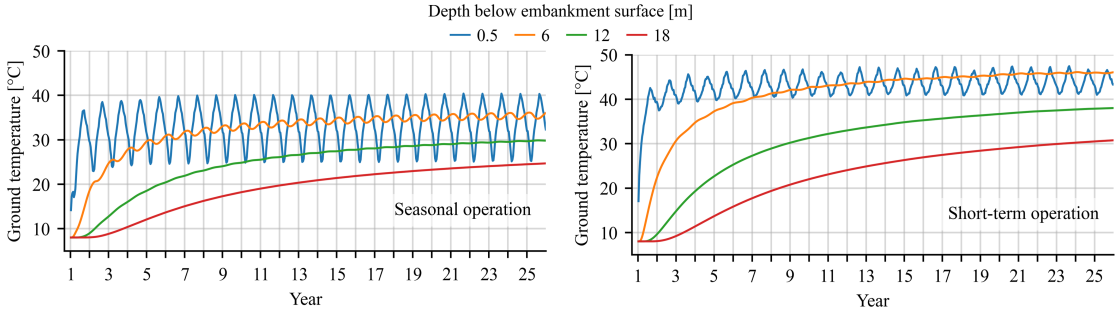

Figure 3.9: Ground temperature development at different depths for seasonal (left) and short-term (right) PTES operations. The horizontal location corresponds to location B in Figure 2.5 (**Sifnaios** et al., 2023b).

The stabilization of heat losses is directly related to the stabilization in ground temperatures around the PTES, which can be seen in Figure 3.9. It may be observed that the soil

temperature close to the surface shows yearly variations in both short-term and seasonal PTES operations induced by the ambient temperature. However, seasonal PTES have more intense variations due to lower discharge temperatures when used as a source for a heat pump. Similar to heat losses, the soil temperature close to the PTES does not stabilize even after 25 years, particularly at lower depths. This highlights the importance of considering the entire lifetime of a PTES when evaluating its impact on surrounding soil and groundwater temperatures.

3.1.4.2 PTES zone of influence

In many cases, the increase in the ground temperature caused by PTES operation can have a negative effect on the surroundings (e.g., if a drinking water well is located nearby). For this reason, a zone of influence was established that determined the dimensions of the soil domain affected by the PTES operation. To identify the zone of influence, the soil temperature was calculated on a horizontal and a vertical line, starting at the bottom of the PTES and extending to the end of the soil domain (see Figure 3.10). As expected, the soil domain reached higher temperatures for the short-term PTES. However, for both seasonal and short-term PTES operations, the temperature of the soil domain remained unaffected outside of a 100 m radius around the storage, regardless of the soil properties.

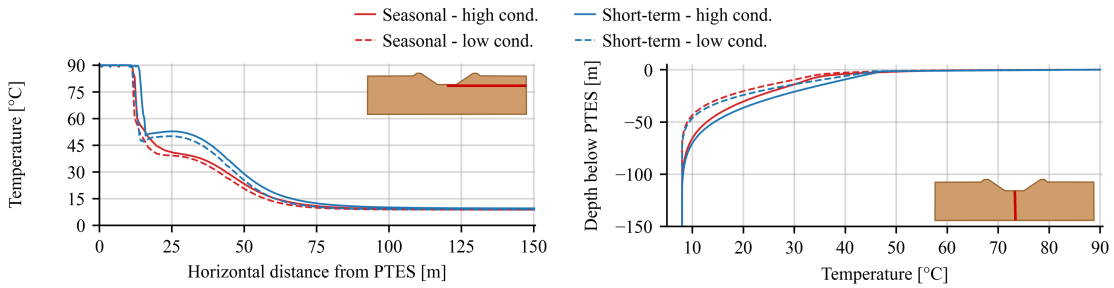

Figure 3.10: Ground temperature profile at the start of July (i.e., both storage types were fully charged) after 25 years of operation for a high and low conductivity (cond.) soil domain. The soil temperature was calculated on a horizontal line (left) and a vertical line (right). Both lines started at the bottom center of the PTES and extended to the end of the soil domain (**Sifnaios** et al., 2023b).

3.1.4.3 PTES and groundwater

As previously mentioned, it is possible for a PTES to be located close to (or even within) a groundwater layer. However, the presence of groundwater is expected to have a negative impact on the PTES performance. Thus, investigating the effect of groundwater on PTES operation can give insights into choosing an appropriate construction location based on geological conditions. Additionally, accurate prediction of a storage performance is of major importance for securing financing and delivering the promised results to the DH system.

The effect of groundwater on the soil temperature is illustrated in Figure 3.11 after 25 years of short-term PTES operation. The calculated soil temperature contours are presented for three scenarios: scenario (A) has no groundwater, (B) has a static groundwater layer, and (C) has a moving groundwater layer with a velocity of 15 m/year. It should be noted

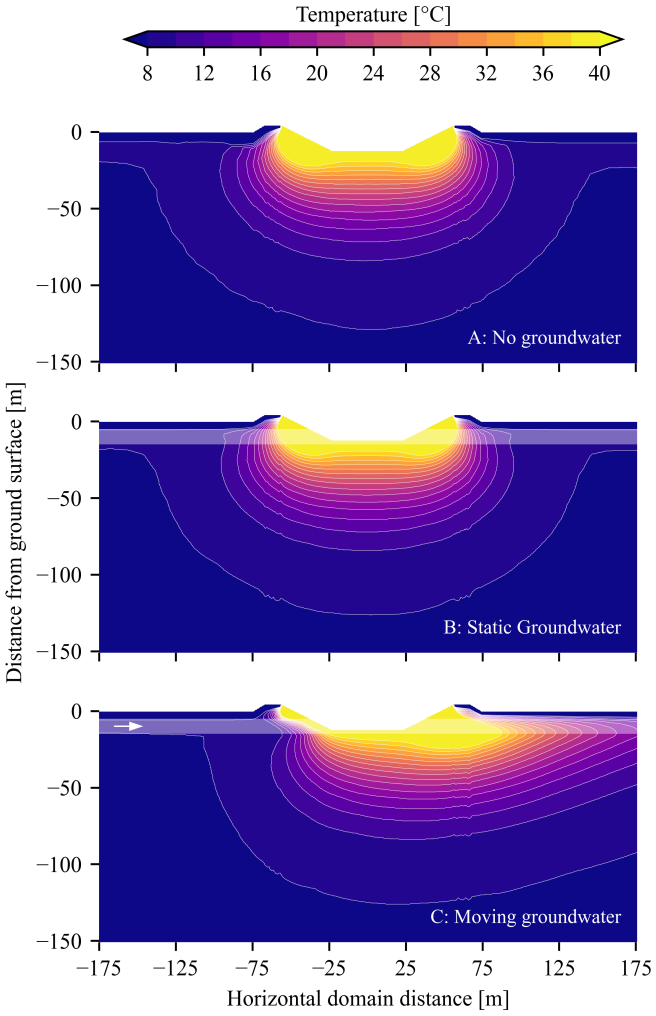

Figure 3.11: Soil temperature contours for short-term PTES operation where there is (A) no groundwater, (B) a static groundwater layer, and (C) a moving groundwater layer. The semi-transparent horizontal white bar in the bottom two subplots illustrates the groundwater layer (**Sifnaios** et al., 2023b).

that the depth of the groundwater layer was 5 m below the ground surface (average depth for Denmark (Koch et al., 2021)), resulting in the bottom half of the PTES being within the groundwater layer.

Minor differences can be spotted in the temperature contours of scenarios (A) and (B) since the main difference is an increased thermal conductivity of the soil domain where the groundwater is located. However, in sub-figure (C), the temperature contours are shifted in the direction of the moving groundwater. Apart from the contours, the presence of groundwater affected the heat losses. In the case of static groundwater (B), there were approximately 14% higher heat losses toward the ground and approximately 60% higher heat losses for moving groundwater (C) compared to the case without groundwater (A).

It should be noted that these results were obtained for a specific groundwater depth (5 m below the ground surface), so they are not directly applicable to other depths. Thus, it was decided to investigate the variation of heat losses with groundwater depth for a moving groundwater layer with a 15 m/year speed.

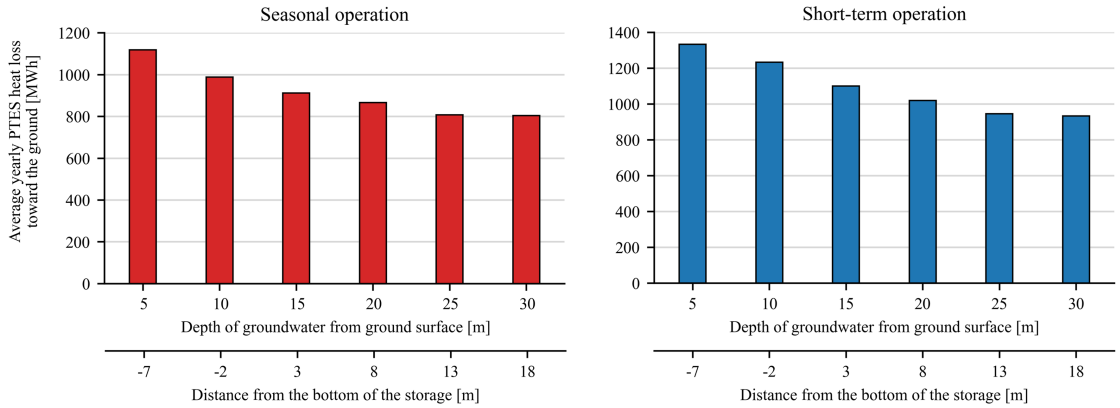

Figure 3.12: Average yearly heat losses toward the ground for seasonal (left) and short-term (right) PTES operations at different groundwater depths for a moving groundwater layer (**Sifnaios** et al., 2023b).

Figure 3.12 presents the results of this investigation for seasonal and short-term PTES operations. As expected, the heat losses decreased for larger groundwater depths, being up to approximately 30% lower compared to a groundwater layer 5 m below the surface. Furthermore, when the depth of the groundwater layer was 25 m below the surface (or 13 m below the bottom of the PTES), the heat losses were unaffected regardless of the PTES operation.

Although this is a very useful finding in terms of designing and planning a PTES system, many countries have regulations on the maximum groundwater temperature (20 – 25 °C) and the maximum permittable change in the groundwater temperature (±6 K) (see **Sifnaios** et al. (2023b) for more information). For this reason, the groundwater temperature was also investigated for these depths for the seasonal and short-term PTES operations, and the results are presented in Figure 3.13 A and B, respectively.

It may be observed that, in Figure 3.13 A, the highest temperature contours (>25 °C) only occur close to the top of the PTES since the heat pump operation cools the lower part down. On the contrary, for the short-term operation (Figure 3.13 B), the highest temperature contour is around the entire PTES. Thus, to comply with the 25 °C regulation, the groundwater layer should be below 20 m for the seasonal and below 30 m for short-term operations. In fact, a groundwater temperature below 20 °C was achieved at a groundwater depth of 25 m for the seasonal PTES operation, whereas it was not possible for short-term operation.

Nevertheless, in none of the investigated scenarios was it possible to limit the change of the groundwater temperature to ±6 K. Thus, in countries where this is required, ground-

water should not be present in the soil. Alternatively, the permissible level of groundwater heating could be increased within a specified radius of the PTES while requiring documentation that local groundwater wells remain unaffected.

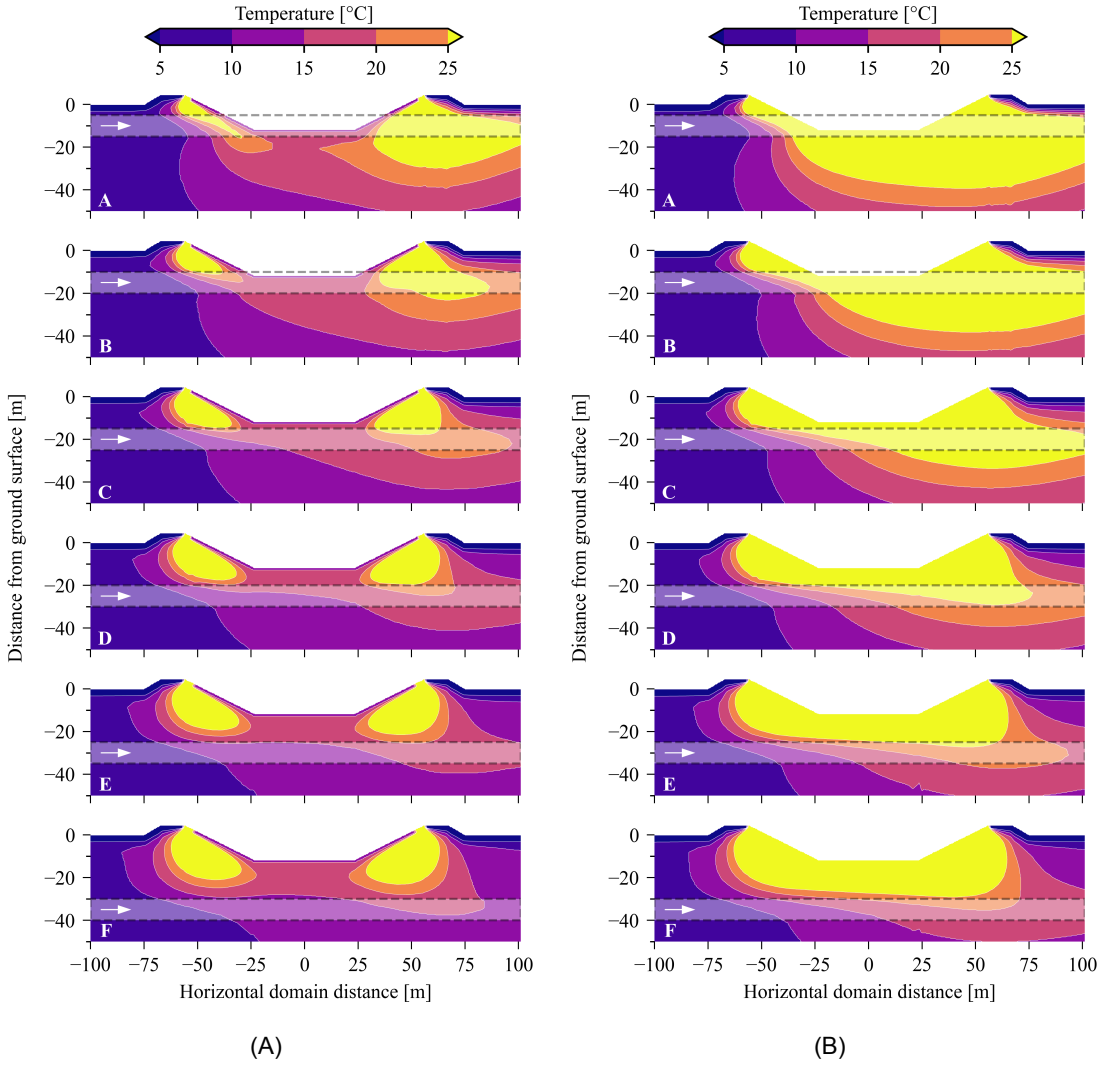

Figure 3.13: Ground temperature contour plots for (A) seasonal and (B) short-term PTES operations for different depths of moving groundwater. The semi-transparent horizontal white bar illustrates the groundwater layer (**Sifnaios** et al., 2023b).

3.2 PTES system integration

The second section of the results presents the impact of PTES integration on different scales. The first part investigates PTES as part of a local DH system (city scale), answering research question 4. The second part takes a macroscopic approach, assessing the impact of PTES as part of the Danish energy system (country scale), answering research question 5.

3.2.1 Impact of PTES on a city scale

PTES systems on a city scale were investigated using TRNSYS for the Danish city of Viborg (see Section 2.3.2), aiming to quantify the economic impact of PTES on the DH grid.

Initially, the TRNSYS 1535/1301 PTES components were validated using measurement data from the PTES in Dronninglund. The validation showed that for the investigated parameters, there was a bias of less than 5% between the measured and calculated data. Thus, the model accuracy was considered acceptable for the following study. For more details on the results of the validation study, the reader is referred to **Sifnaios** (2023).

3.2.1.1 Reference system

The first step of the study was to determine a reference system that could cover the entire heat load using a heat pump and an electric boiler (without heat storage). Figure 3.14 illustrates the possible combinations of minimum boiler and heat pump capacities for covering the heat load of the Viborg DH grid, along with the corresponding capital (CAPEX) and operational (OPEX) expenditures. The results demonstrated the different trends of the CAPEX and OPEX for heat pumps and electric boilers. Specifically, electric boilers have a low CAPEX but a high OPEX, while heat pumps are the opposite; thus, OPEX decreased for increasing heat pump capacities, but CAPEX increased.

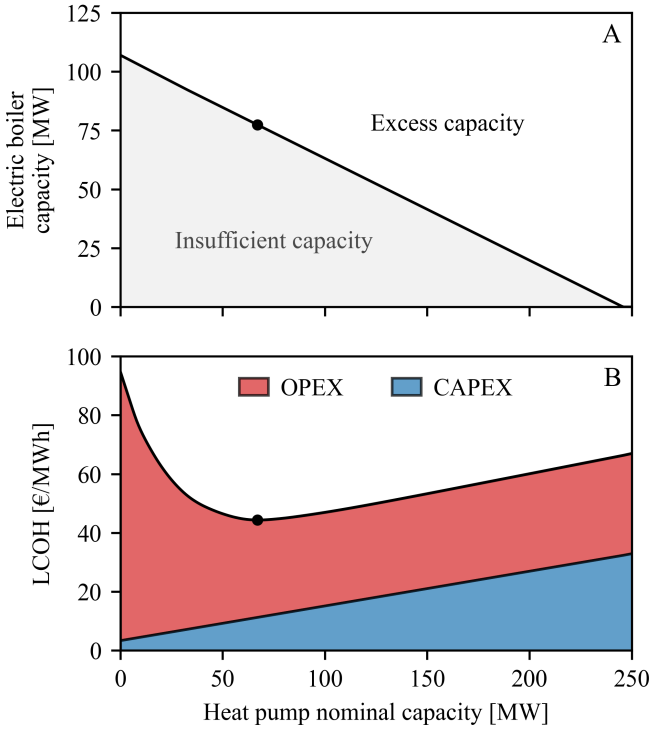

Figure 3.14: (A) Electric boiler vs. heat pump capacity and (B) LCOH vs. heat pump capacity for the reference system (**Sifnaios**, 2023).

An optimal combination of the two technologies can be selected to achieve the lowest levelized cost of heat (LCOH). It should be noted that air-to-water heat pumps have lower heat production and COP when the ambient temperature is low and the supply temperature is high, corresponding to the peak heat load periods. The periods of peak heat demand determine the minimum capacities. However, these periods of very high demand occur infrequently, and thus, it is not optimal to cover them entirely with heat pumps;

rather, it is economical to invest in cheaper boiler capacity despite the higher operating costs. Without storage, the lowest achievable LCOH was 44.4 €/MWh and was achieved for a 68 MW air-to-water heat pump capacity and 53 MW electric boiler capacity.

It should be noted that the calculated heat pump capacity is higher than what is currently planned to be installed in Viborg since the actual DH operator intends to use a larger variety of heat sources to cover the demand. However, Viborg's current electric boiler capacity is 50 MW, indicating that the calculated values are reasonable.

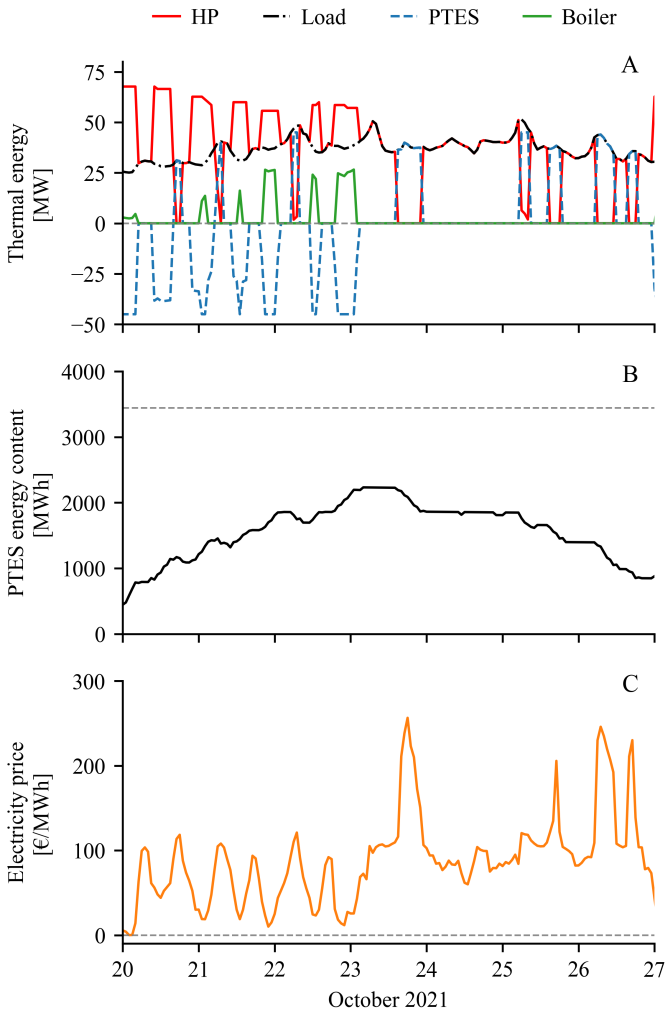

Figure 3.15: (A) Thermal energy produced by the heat pump, electric boiler, and PTES for a week in October and the corresponding heat load. (B) The energy content of the PTES during the same period as well as (C) the electricity price. The dotted line for the PTES energy content denotes the maximum PTES capacity (**Sifnaios**, 2023).

3.2.1.2 PTES integration in the DH grid

To evaluate the impact of integrating PTES, the economy of the reference system without storage was compared to a system with PTES. The system was simulated in TRNSYS (see Figure 2.10), with a PTES volume of 60 000 m^3, a 77 MW heat pump capacity, and a

90 MW electric boiler capacity. It should be noted that the heat pump and boiler capacity were increased compared to the reference system to ensure enough generation capacity to cover the heat load and charge the PTES. The charge/discharge capacity of the PTES in this scenario was 45 MW.

Figure 3.15 shows the operation of the DH grid for a week in October. The periods where the PTES supplied heat to the grid are denoted as positive PTES thermal energy, while the periods where the PTES was charged by the heat pump and the boiler were indicated as negative. In general, the boiler was used to cover the load in cases where the heat pump capacity was not sufficient or to charge the PTES during periods of low electricity prices.

The LCOH of this system was 39.9 €/MWh (10% lower than the reference system) with a payback period (PP) of 5.1 years. However, it should be noted that this system is not optimized in terms of heat pump and boiler capacity, charge/discharge rate, and PTES volume. Thus, there is potential for the LCOH and PP to be even lower. Nevertheless, it demonstrates the added value of a PTES in a DH grid with electricity-based generation.

3.2.1.3 Impact of PTES volume

The impact of PTES volume was assessed by investigating three different PTES volumes: 60 000 m^3, 120 000 m^3, and 200 000 m^3. The results are presented in Table 3.4. It should be noted that the CAPEX and OPEX are the capital and operation expenditures per MWh of produced energy for each unit, and were calculated for 25 years using the LCOH formula.

Table 3.4: CAPEX, OPEX, LCOH, and PP for the investigated PTES volumes (**Sifnaios**, 2023).

		Storage size [m^3]		
		60 000	**120 000**	**200 000**
CAPEX [€/MWh]	HP	6.9	6.9	6.9
	Boiler	22.0	21.6	21.4
	PTES	2.4	3.9	5.1
OPEX [€/MWh]	HP	25.7	25.7	25.7
	Boiler	32.2	34.0	34.0
	PTES	0.6	1.0	1.3
LCOH [€/MWh]	-	39.9	40.6	40.7
PP [years]	-	5.1	6.1	6.6

It can be observed that by increasing the PTES volume, the LCOH and PP increase as well, denoting that the investigated volumes were too large for the size of the investigated DH grid. The increase derived primarily from the increased CAPEX for the PTES. Nevertheless, all the investigated PTES volumes had a lower LCOH than the reference case and reasonable payback periods compared to their lifetime (i.e., 25 years), indicating the positive impact of PTES on DH grids (even if oversized).

3.2.1.4 Impact of PTES charge temperature

As mentioned before, air-to-water heat pumps have their lowest COP and heat supply for high supply temperatures. However, it is common practice to charge the PTES at 90 °C, as a higher charge temperature increases the available heat storage capacity. Consequently, when air-to-water heat pumps are used to charge the PTES, they can perform poorly (i.e., reduced COP, resulting in consuming more electricity), especially in the winter. For this reason, the impact of PTES charge temperature was assessed on the economy of the DH system. The investigation results can be seen in Table 3.5.

Table 3.5: Effect of the PTES charge temperature on LCOH and PP for a 60 000 m^3 PTES (**Sifnaios**, 2023).

	PTES charge temperature [°C]		
	80	**85**	**90**
LCOH [€/MWh]	38.5	39.8	39.9
PP [years]	4.2	5.0	5.1

The results indicate that when charging the PTES using 80 °C, despite the 20% lower storage capacity, the LCOH was decreased by approximately 4% and the PP by 18%. Thus, when heat pumps are the main heat generator unit in a DH grid, a lower PTES charge temperature should be considered. Apart from the economic benefit, a lower PTES charge temperature would benefit the lifetime of the PTES liner since one of the biggest challenges is to find polymer liners that can withstand temperatures close to 90 °C for a long period of time.

It was not investigated charging the PTES with a temperature lower than 80 °C since this was the highest supply temperature for the Viborg DH grid in the winter. To be able to charge the PTES with lower temperatures, the supply temperature of the DH grid should also be decreased. Alternatively, different charging temperatures could be used throughout the year.

Last, it should be mentioned that the impact of PTES on a city scale is an ongoing investigation. Thus, the optimal dimensioning of the heat pump and boiler capacities will be investigated, as well as the impact of the DH charge/discharge rates.

3.2.2 Impact of PTES on a country scale

The techno-economical impact of PTES on a country scale was investigated using Balmorel. As mentioned in Section 2.3.3, the first step of the investigation was to compare a No TES scenario (where TES systems could not be installed in the energy system) with a TES scenario (where storage technologies could be used normally). The study focused on Denmark and its neighboring countries (Norway, Sweden, and Germany); however, the results presented in the following sections only concern Denmark.

3.2.2.1 Comparison between the TES and No TES scenarios

The installed generation capacities for the two scenarios are presented in Figure 3.16 A. Overall, it may be observed that TES systems enabled the installation of higher renew-

able capacities. Specifically, over the entire simulated period, when TES systems were utilized, 35% more PV and 10% more offshore wind capacity was installed compared to a system without TES. The heat and electricity demand in the system without TES were covered using a larger capacity of dispatchable technologies (e.g., boilers, CHP, and heat pumps). Thus, larger amounts of biomass and fossil fuels were used to cover the heat and electricity demand for energy systems without TES. Consequently, only energy systems utilizing TES could reach zero CO_2 emissions by 2050.

It should be noted that a number of factors influenced the amount of installed generation capacities. For example, a higher total capacity was installed when TES systems were utilized since a larger share of low-capacity factor technologies was used (e.g., PV and wind). On the contrary, in 2020, where both scenarios relied mainly on dispatchable technologies, the use of storage led to a smaller total generation capacity than the No TES scenario.

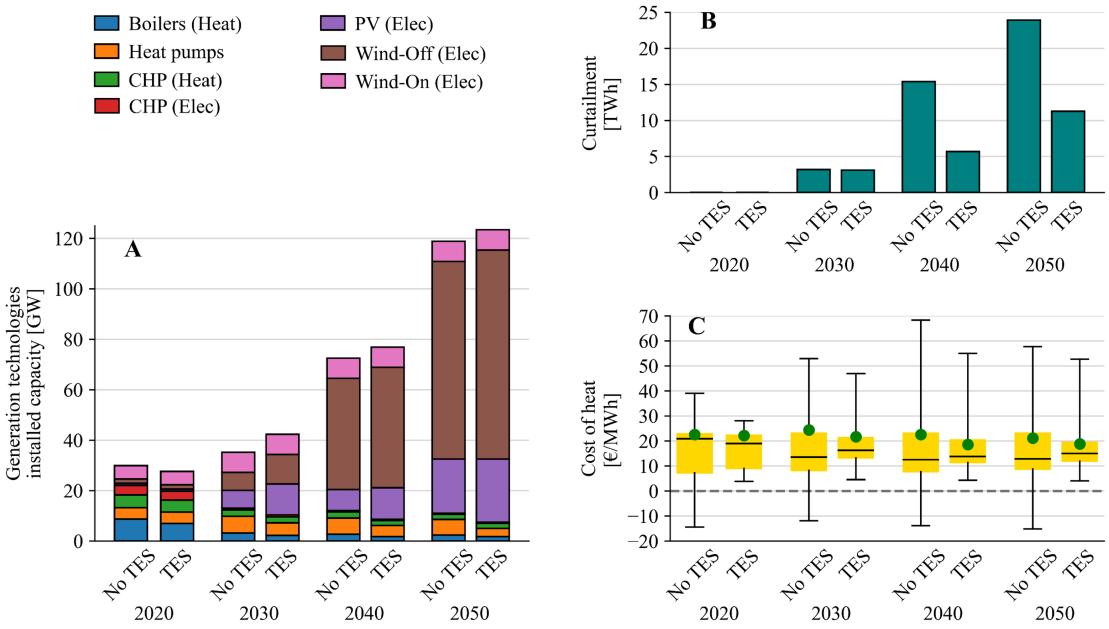

Figure 3.16: Comparison between the No TES and TES scenarios for Denmark regarding the (A) installed capacities, (B) curtailment, and (C) cost of heat. The weighted mean yearly heat prices are indicated with a green circle (**Sifnaios** et al., 2023c).

In periods with high energy production and low demand, renewables can be shut down (curtailed). In general, energy generation is curtailed if it is more profitable than expanding the infrastructure (e.g., electricity transmission grid, Power-to-Heat technologies, or storage). Figure 3.16 B illustrates that, on average, the No TES scenario had 2.2 times higher curtailment than the TES scenario, primarily deriving from the lack of heat storage (and thus flexibility). Essentially, including TES allowed for less curtailment as the energy produced during peak generation periods could be stored for later use.

Additionally, the use of TES in periods of high demand instead of expensive peak units (e.g., natural gas boilers) reduced the peak heat price by 24%. Overall, the presence of

TES systems enabled the lowering of the average price of heat by 11% compared to the No TES scenario.

In order to visualize the role of TES in the heating sector, a Sankey diagram for the Denmark 2050 TES scenario is presented in Figure 3.17. It can be seen that 41% of the heat is produced by heat pumps, while 27% is produced by excess heat and 25% by waste-burning CHP plants. Moreover, the TES systems supplied 20% of the total demand (19% and 1% for long-term and short-term, respectively). The installed TES capacity in this scenario was 3 858 GWh (66 GWh of TTES and 3 792 GWh of PTES). To put this into perspective, it corresponds to approximately 390 TTES systems, each having a volume of 3 000 m^3, and 240 PTES systems, each having a volume of 250 000 m^3. It should be noted that, in Denmark, there are already more than 390 TTES systems today since every DH grid has at least one TTES system used for short-term heat storage. However, there are only six operational PTES, indicating a substantial potential to increase the utilization of PTES in future energy systems.

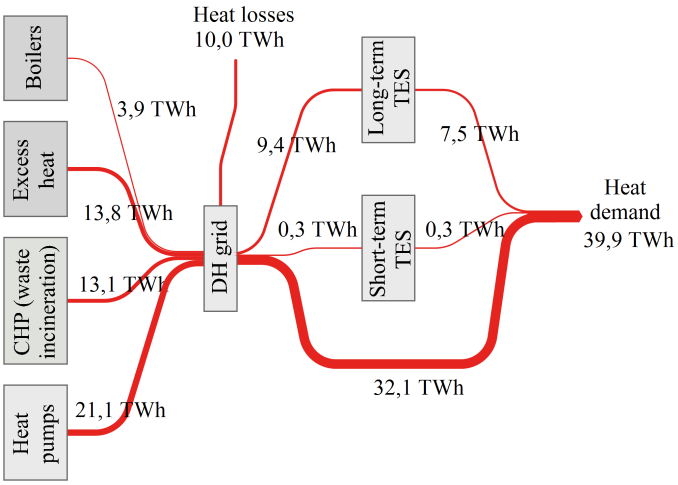

Figure 3.17: Sankey diagram showing the energy flows for Denmark's heat sector in the 2050 TES scenario. Excess heat is produced primarily from hydrogen production (**Sifnaios** et al., 2023c).

3.2.2.2 Comparison between the PTES and TTES scenarios

This section aimed to elucidate the differences between using PTES or TTES as the only heat storage technology on a country scale.

One of the main advantages of PTES over TTES is their low investment cost (PTES systems have a specific cost of approximately 24 €/m^3 while TTES have 121 €/m^3). Due to this, the installed capacity for PTES was five times higher than TTES (see Figure 3.18 A). Thus, the available heat storage capacity for the PTES scenario was much larger, enabling the installation of 6% higher PV and 6% higher wind capacity.

The high storage capacity also affected the cost of heat as illustrated in Figure 3.18 B. Since the PTES scenario could transfer large amounts of heat from summer to winter

but also provided arbitrage (i.e., charging with cheap energy when there is an energy surplus), lower heat prices were achieved. Although the peak prices were similar for the two scenarios, the TTES scenario had a higher mean price for heat (22.1 vs. 20.6 €/MWh).

It should be noted that the installed TES capacity depends not only on the heat demand and the characteristics of the storage technologies but also on the cost of alternative options (e.g., transmission capacity). For example, the model might find it more profitable to invest in electricity transmission over a TES technology to utilize excess electricity production. Thus, very different results can be obtained for each TES technology. Nevertheless, PTES systems seem more favorable than TTES regarding costs and performance, especially considering that they are not yet a mature technology and there is still a margin for improvement.

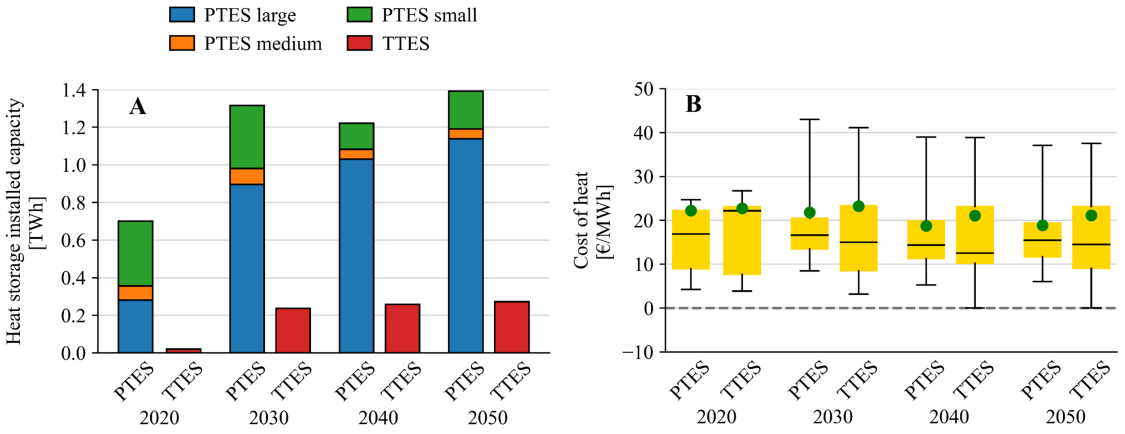

Figure 3.18: Comparison between the PTES and TTES scenarios for Denmark regarding the (A) installed heat storage capacity and the (B) hourly cost of heat. The weighted mean yearly heat prices are indicated with a green circle (**Sifnaios** et al., 2023c).

4 Conclusions

This study aimed to investigate five research questions related to the performance, operation, and integration of water pit thermal energy storage (PTES) systems in the district heating sector. The conclusions to the individual research questions are presented below:

Research question 1: *How can the performance of PTES systems be assessed?*

This study identified multiple ways of assessing the performance of PTES systems. First, the performance can be assessed using energy and exergy efficiency indicators. Specifically, two different expressions of energy efficiency were investigated, leading to the recommendation of the one that could account for the internal energy change in the most appropriate way. Moreover, the significance of considering exergy efficiency was elucidated as it was the only efficiency indicator that accounted for heat losses and mixing in the storage. Since there are different PTES operations (seasonal, short-term, or mixed) that have a direct impact on efficiency, it was considered essential to determine a way to compare their performance fairly. Thus, the seasonal efficiency was suggested, which calculated the equivalent efficiency of a PTES as if it was used as a seasonal storage. Apart from storage efficiency, performance was also assessed in terms of stratification. In fact, this study suggested using exergy destruction as an indicator that can evaluate stratification without being biased by differences in heat losses. Last, an alternative way of assessing PTES performance was demonstrated, where drone thermal images were successfully used for inspecting the PTES lids and identifying leakages.

Research question 2: *How does the geometry of a PTES affect its performance?*

Two key PTES geometry parameters were investigated, namely the slope of the storage sides and the aspect ratio, and their effect on heat losses and storage efficiency. It was found that, due to a smaller surface area, changing the slope of the side walls from 26° (typical PTES side-wall slope) to 44° could reduce the total heat losses by 20%. In general, the slope of the side walls had a bigger impact both on the heat losses and on efficiency compared to the aspect ratio. For example, the variation in efficiency due to different side slopes was 12%, while the efficiency only varied by 3% due to different aspect ratios. Overall, the results of this investigation identified the ideal PTES geometry to have a square-shaped lid and bottom (aspect ratio of one) with as steep storage side slopes as possible.

Research question 3: *How does PTES operation affect the soil domain and vice versa?*

Due to the absence of insulation between the PTES water domain and the surrounding soil, it was found that the soil thermal properties (especially if groundwater is present) have a large impact on the heat losses of a PTES. Specifically, static groundwater increased the

PTES heat losses toward the ground by 14% while moving groundwater increased heat losses by 60%, compared to a case without groundwater. Furthermore, it was shown that groundwater should generally be at least 13 m below the bottom of the PTES for the heat losses to remain unaffected.

However, PTES operation also affected the groundwater temperature, which is subject to regulations in some countries. For countries with a maximum limit of 25 °C, the groundwater layer should be below 20 m from the ground surface for seasonal PTES operation and below 30 m for short-term operation. If a limit of 20 °C is desirable, the groundwater layer should be below 25 m from the ground surface for the seasonal operation, whereas this limit cannot be achieved for short-term operation. Overall, the soil temperature continues to increase during the entire lifetime of the PTES, impacting the soil within a radius of 100 m around the PTES. With increasing soil temperature, the heat losses are constantly decreasing. Nevertheless, the heat losses could be considered stable (relative change per year less than 2%) after eight years of operation for the short-term and 12 years of operation for the seasonal PTES operation.

Research question 4: *What is the impact of PTES on DH grids on a city scale?*

The economic impact of PTES on DH grids was investigated using the Danish city of Viborg as a case study. Following the trend of installing electricity-based generation technologies (particularly heat pumps) in DH grids, there is a plan for Viborg to phase out conventional natural gas units and switch to electricity-based alternatives. Thus, a reference system was determined that could cover the entire heat load using heat pumps and electric boilers without any heat storage. Boilers were mainly used when the heat pump capacity was insufficient to meet the load or when the electricity price was negative. Without storage, the lowest achievable LCOH was 44.4 €/MWh, which was achieved for a 68 MW air-to-water heat pump capacity and 53 MW electric boiler capacity. This system was compared to a DH system that utilized a 60 000 m^3 PTES, 77 MW air-to-water heat pump capacity, and 90 MW electric boiler capacity. It was found that the LCOH of the system with a PTES was 10% lower than without a PTES. Moreover, the additional investment cost for the PTES installation was paid off over a period of 5.1 years.

In order to increase the available heat storage capacity, it is common practice for PTES to be charged at a high temperature, e.g., 90 °C. However, air-to-water heat pumps have their lowest COP and heat capacity when the supply temperature is high. Thus, the impact of lowering the PTES charge temperatures was investigated. It was found that although the available PTES capacity was 20% lower, charging the PTES at 80 °C led to an overall 4% reduction in LCOH and 18% reduction in the payback period. Thus, when heat pumps are the main heat generator unit in a DH grid, a lower PTES charge temperature should be considered. Overall, this investigation revealed the economic benefit of using PTES in DH grids, elucidating their potential as short-term heat storages contrary to traditional seasonal systems.

Research question 5: *What is the impact of PTES on a country scale?*

The impact of TES, and particularly PTES, was investigated for future scenarios for Denmark. It was found that including TES systems enabled higher utilization of renewable technologies (i.e., 35% higher PV capacity and 10% higher wind capacity) compared to scenarios without heat storage. In parallel, TES systems enabled the utilization of excess electricity (through power-to-heat technologies), leading to 53% lower curtailment and ultimately to 11% lower average heat price (with a 24% lower peak price). Additionally, the utilization of TES systems enabled carbon neutrality for the energy system by 2050.

When comparing PTES and TTES, there was a much greater deployment of PTES on a country scale (approximately five times) due to their lower cost. This reduced the energy system costs and enabled higher utilization of renewables compared to TTES. Additionally, a 1.5 €/MWh lower average heat price was achieved for PTES compared to TTES. In general, it was found that when large volumes of TES were available (e.g., PTES), the use of PV and wind was increased, while for smaller TES volumes (e.g., TTES), greater dispatchable capacities (e.g., heat pumps, boilers, and CHP) were used to cover the demand.

4.1 Future work

This study investigated different aspects of water pit thermal energy storage (PTES) systems. During the study, a number of possible future investigations regarding PTES were identified, which are presented below:

- Most existing lid designs have encountered issues with water entering the lid construction (either rainwater from above or storage water from below), which reduced the insulation performance and the lifetime of the lid. Thus, more research and development is required to develop lid solutions with low heat losses and a long lifetime. However, since the lid performance and lifetime are directly connected to the liner, investigations should also be focused on developing more durable liner materials. Moreover, the performance of the state-of-the-art Nomalén lid by Aalborg CSP, which has been installed in Marstal, Dronninglund, and Høje Taastrup, should be monitored in order to identify potential issues and improvements.
- Since PTES have recently started being used as short-term storage, the impact of storage operation (seasonal or short-term) on efficiency and stratification should be investigated in the future, preferably by investigating operational data.
- Stratification was not identified as an issue in the existing PTES systems. However, since the short-term PTES systems are expected to operate with higher flow rates compared to the seasonal, guidelines should be developed on selecting the optimal diffuser construction and operation.
- The number of PTES systems is expected to increase drastically in the near future; thus, it is expected that in many situations, they will be close to or inside a ground-

water layer. In the presence of moving groundwater, the PTES heat losses toward the ground were increased by 60%. Thus, research is required to identify possible solutions to reduce heat losses when groundwater is present (e.g., channeling). Additionally, the impact of the groundwater speed on the PTES heat losses should also be investigated.

- Last, all the investigations conducted in this study assumed that the maximum temperature stored in PTES is 90 °C, which is typical for Denmark in 2023. However, it is expected in the future to have lower temperatures in the district heating network. Thus, the effect of lower storage temperatures on the performance and operation of PTES should be investigated.

References

Aalborg CSP. (2019). 15,000 M3 PTES for district heating, Tibet. Retrieved July 9, 2023, from https://web.archive.org/web/20210418202632/https://www.aalborgcsp.com/projects/15000-m3-ptes-for-district-heating-tibet/

Aalborg CSP. (2022). Lid solution for PTES. Retrieved July 8, 2023, from https://www.aalborgcsp.com/projects/ptes-projects/11000-m2-lid-solution-for-ptes-denmark

Andersen, E., Furbo, S., & Fan, J. (2007). Multilayer fabric stratification pipes for solar tanks. *Solar Energy*, *81*(10), 1219–1226. https://doi.org/10.1016/j.solener.2007.01.008

ANSYS. (2022). *ANSYS Fluent, Academic Research Mechanical, Release 2022 R2*. Retrieved July 12, 2023, from https://www.ansys.com/products/fluids/ansys-fluent

Cabeza, L. (2012). Thermal Energy Storage. In *Comprehensive renewable energy* (pp. 211–253). Elsevier. https://doi.org/10.1016/B978-0-08-087872-0.00307-3

Clifford, K. H., & Ambrosini, A. (2020). Thermal energy storage technologies. In *Sandia energy storage handbook*. https://www.sandia.gov/ess-ssl/wp-content/uploads/2020/12/ESHB_Ch12_Thermal_Ho.pdf

Dahash, A., Ochs, F., Janetti, M. B., & Streicher, W. (2019). Advances in seasonal thermal energy storage for solar district heating applications: A critical review on large-scale hot-water tank and pit thermal energy storage systems. *Applied Energy*, *239*(October 2018), 296–315. https://doi.org/10.1016/j.apenergy.2019.01.189

Danish Energy Agency. (2017). Regulation and planning of district heating in Denmark. https://ens.dk/sites/ens.dk/files/Globalcooperation/regulation_and_planning_of_district_heating_in_denmark.pdf

Danish Energy Agency. (2018). Technology data for Energy storage. https://ens.dk/sites/ens.dk/files/Analyser/technology_data_catalogue_for_energy_storage.pdf

Danish Energy Agency. (2023). Technology data. Retrieved March 21, 2023, from https://ens.dk/en/our-services/projections-and-models/technology-data

Dincer, I., & Rosen, M. A. (2002). *Thermal Energy Storage: Systems and Applications*. Wiley.

Drones Made Easy. (n.d.). Matrice 200 + Zenmuse XT2. Retrieved July 11, 2023, from https://dronesmadeeasy.com/zenmuse-xt2/

Fleuchaus, P., Godschalk, B., Stober, I., & Blum, P. (2018). Worldwide application of aquifer thermal energy storage – A review. *Renewable and Sustainable Energy Reviews*, *94*, 861–876. https://doi.org/10.1016/j.rser.2018.06.057

Gao, L., Zhao, J., An, Q., Liu, X., & Du, Y. (2019). Thermal performance of medium-to-high-temperature aquifer thermal energy storage systems. *Applied Thermal Engineering*, *146*(October 2018), 898–909. https://doi.org/10.1016/j.applthermaleng.2018.09.104

Guelpa, E., & Verda, V. (2019). Thermal energy storage in district heating and cooling systems: A review. *Applied Energy*, *252*(June), 113474. https://doi.org/10.1016/j.apenergy.2019.113474

Hansen, K., Hansen, P., & Ussing, V. (1983). Seasonal heat storage in underground warm water stores-Construction and testing. *LFV report no. 134*.

Heller, A. (1994). Floating lid constructions for pit water storage - A survey. Retrieved August 4, 2023, from https://www.osti.gov/etdeweb/servlets/purl/524183

Holm, L. (2009). Solar plants together with district heating. http://dgener.caib.es/www/user/portalenergia/ponencies/solar_plants.pdf

IEA Task 54. (2018). LCOH for solar thermal applications. Retrieved October 1, 2021, from http://task54.iea-shc.org/Data/Sites/1/publications/A01-Info-Sheet--LCOH-for-Solar-Thermal-Applications.pdf

International Energy Agency (IEA). (2021). Task 55: Integrating Large SHC Systems into District Heating and Cooling Networks. Retrieved July 3, 2023, from https://task55.iea-shc.org/Data/Sites/1/publications/2021-07-Task55-Solar-District-Heating.pdf

International Energy Agency (IEA). (2022). Levelised cost of heating in selected cold climate countries. Retrieved July 19, 2023, from https://www.iea.org/data-and-statistics/charts/levelised-cost-of-heating-in-selected-cold-climate-countries

Jensen, A. R., & **Sifnaios**, **I.** (2022). Modeling, validation, and analysis of a concentrating solar collector field integrated with a district heating network. *Solar*, *2(2)*, 234–250. https://doi.org/10.3390/solar2020013

Jensen, A. R., **Sifnaios**, **I.**, & Anderson, K. (2022a). twoaxistracking – a python package for simulating self-shading of two-axis tracking solar collectors. *MethodsX*, *9*, 101876. https://doi.org/10.1016/j.mex.2022.101876

Jensen, A. R., **Sifnaios**, **I.**, Caringal, G. P., Furbo, S., & Dragsted, J. (2022b). Thermal performance assessment of the world's first solar thermal Fresnel lens collector field. *Solar Energy*, *237*, 447–455. https://doi.org/10.1016/j.solener.2022.01.067

Jensen, A. R., **Sifnaios**, **I.**, Furbo, S., & Dragsted, J. (2022c). Self-shading of two-axis tracking solar collectors: Impact of field layout, latitude, and aperture shape. *Solar Energy*, *236*, 215–224. https://doi.org/10.1016/j.solener.2022.02.023

Jensen, A. R., **Sifnaios**, **I.**, Perers, B., Rothmann, J. H., Mørch, S. D., Jensen, P. V., Dragsted, J., & Furbo, S. (2022d). Demonstration of a concentrated solar power and biomass plant for combined heat and power. *Energy Conversion and Management*, *271*, 116207. https://doi.org/10.1016/j.enconman.2022.116207

Jensen, M. V., & Nielsen, J. E. (2020). Seasonal pit heat storages - Guidelines for materials & construction. Retrieved July 3, 2023, from https://task55.iea-shc.org/Data/Sites/1/publications/IEA-SHC-T55-C-D.2-FACT-SHEET-Guidelines-seasonal-storages.pdf

Kallesøe, A., & Vangkilde-Pedersen, T. (2019). *Underground Thermal Energy Storage (UTES) – state-of-the-art, example cases and lessons learned.* (tech. rep.). https:

//www.heatstore.eu/documents/HEATSTORE_UTES%20State%20of%20the%20Art_WP1_D1.1_Final_2019.04.26.pdf

Klein, S. (2017). TRNSYS 18: A Transient System Simulation Program. http://sel.me.wisc.edu/trnsys

Koch, J., Gotfredsen, J., Schneider, R., Troldborg, L., Stisen, S., & Henriksen, H. J. (2021). High resolution water table modeling of the shallow groundwater using a knowledge-guided gradient boosting decision tree model. *Frontiers in Water*, *3*. https://doi.org/10.3389/frwa.2021.701726

Korsgaard, V. (1979). Sæsonlagring af varme i store vandbassiner. Retrieved April 8, 2023, from https://backend.orbit.dtu.dk/ws/portalfiles/portal/234778521/lfv_091.pdf

Kumi, E. N. (2023). Energy storage technologies. In *Pumped hydro energy storage for hybrid systems* (pp. 1–21). Elsevier. https://doi.org/10.1016/B978-0-12-818853-8.00002-9

Laloui, L., & Rotta Loria, A. F. (2020). Heat and mass transfers in the context of energy geostructures. In *Analysis and design of energy geostructures* (pp. 69–135). Academic Press. https://doi.org/10.1016/b978-0-12-816223-1.00003-5

Lund, H., Werner, S., Wiltshire, R., Svendsen, S., Thorsen, J. E., Hvelplund, F., & Mathiesen, B. V. (2014). 4th Generation District Heating (4GDH). Integrating smart thermal grids into future sustainable energy systems. *Energy*, *68*, 1–11. https://doi.org/10.1016/j.energy.2014.02.089

Meliß, M., & Späte, F. (2000). The solar heating system with seasonal storage at the solarcampus jülich. *Solar Energy*, *69*(6), 525–533. https://doi.org/10.1016/s0038-092x(00)00116-x

Münster, M., Møller Sneum, D., Bramstoft, R., Bühler, F., Elmegaard, B., Giannelos, S., Zhang, X., Strbac, G., Berger, M., Radu, D., Elsaesser, D., Oudalov, A., & Iliceto, A. (2020). Sector Coupling: Concepts, State-of-the-art and Perspectives. Retrieved December 15, 2022, from https://smart-networks-energy-transition.ec.europa.eu/sites/default/files/documents/working%20groups/ETIP-SNEP-Sector-Coupling-Concepts-state-of-the-art-and-perspectives-WG1.pdf

Narula, K., Filho, F. D. O., Chambers, J., & Patel, M. K. (2020). Simulation and comparative assessment of heating systems with tank thermal energy storage – A Swiss case study. *Journal of Energy Storage*, *32*(September), 101810. https://doi.org/10.1016/j.est.2020.101810

Nielsen, K. P. (2019). *2001-2010 Danish Design Reference Year* (tech. rep.). https://www.dmi.dk/fileadmin/Rapporter/2018/DMI_report_18-20.pdf

NMC Termonova. (2011). Nomalen 28N. Retrieved July 10, 2023, from https://web.archive.org/web/20220426161150/https://azupcs365certviewer.azurewebsites.net/api/GetSDB?env=se&articleNr=550984

Pauschinger, T., Schmidt, T., Alex Soerensen, P., Aart Snijders, D., Djebbar, R., Boulter, R., & Jeff Thornton, C. (2018). Integrated Cost-effective Large-scale Ther-

mal Energy Storage for Smart District Heating and Cooling - Design Aspects for Large-Scale Aquifer and Pit Thermal Energy Storage for District Heating and Cooling. *International Energy Agency Technology Collaboration Programme on District Heating and Cooling including Combined Heat and Power*, (September).

Perez-Mora, N., Bava, F., Andersen, M., Bales, C., Lennermo, G., Nielsen, C., Furbo, S., & Martínez-Moll, V. (2018). Solar district heating and cooling: A review. *International Journal of Energy Research*, *42*(4), 1419–1441. https://doi.org/10.1002/er.3888

PlanEnergi. (2013). *Design of the pit heat storage of the demonstration plant at Marstal Fjernvarme* (tech. rep.). https://docplayer.net/40878119-Sunstore-4-deliverable-d-2-2-version-3-design-of-the-pit-heat-storage-of-the-demonstration-plant-at-marstal-fjernvarme.html

PlanEnergi. (2015a). Long term storage and solar district heating. Retrieved July 8, 2023, from https://web.archive.org/web/20220306155726/https://planenergi.dk/wp-content/uploads/2017/06/sol_til_fjernvarme_brochure_endelig.pdf

PlanEnergi. (2015b). *Sunstore 3 - Phase 2: Implementation* (tech. rep.). https://planenergi.dk/wp-content/uploads/2018/05/26-Sunstore-3-Final-report.pdf

PlanEnergi. (2016). Long term storage and solar district heating. Retrieved April 11, 2022, from https://ens.dk/sites/ens.dk/files/Forskning_og_udvikling/sol_til_fjernvarme_brochure_endelig.pdf

PlanEnergi. (2020). Roles in HEATSTORE & Monitoring results for 2019-2020 for Marstal, Dronninglund and Gram. Retrieved July 9, 2023, from https://www.heatstore.eu/documents/20201028_DK-temadag_PlanEnergi_Monitoring%20results%20for%202019%E2%80%902020%20for%20Marstal,%20Dronninglund%20and%20Gram.pdf

PlanEnergi. (n.d.). Varme pumpe data. Retrieved August 29, 2023, from https://varmepumpedata.dk/

Rad, F. M., & Fung, A. S. (2016). Solar community heating and cooling system with borehole thermal energy storage – Review of systems. *Renewable and Sustainable Energy Reviews*, *60*, 1550–1561. https://doi.org/10.1016/j.rser.2016.03.025

Rambøll. (2015). South-Jutland stores the sun's heat in the world's largest pit heat storage. Retrieved July 8, 2023, from https://web.archive.org/web/20210827074933/https://ramboll.com/projects/re/south-jutland-stores-the-suns-heat-in-the-worlds-largest-pit-heat-storage?utm_source=alias&utm_campaign=sun-storage

Rambøll. (2016). Damvarmelagre. Retrieved July 8, 2023, from https://web.archive.org/web/20220504080511/https://dk.ramboll.com/-/media/3fc11649e25942c195fa90e63ea41e11.pdf

Rambøll. (2020). Experience from Toftlund. Retrieved July 9, 2023, from https://www.heatstore.eu/documents/20201028_DK-temadag_Ramb%C3%B8ll%20PTES%20project.pdf

REN21. (2022). *Renewables 2022 global status report*.

Reuss, M. (2020). The use of borehole thermal energy storage systems. In L. F. Cabeza (Ed.), *Advances in thermal energy storage systems: Methods and applications* (2nd, pp. 139–171). https://doi.org/10.1016/C2019-0-00061-1

Ritchie, H., Roser, M., & Rosado, P. (2022). Energy. *Our World in Data*. https://ourworldindata.org/energy

Rosen, M. A., & Dincer, I. (2004). Effect of varying dead-state properties on energy and exergy analyses of thermal systems. *International Journal of Thermal Sciences*, *43*(2), 121–133. https://doi.org/10.1016/j.ijthermalsci.2003.05.004

Schmidt, T. (2019). Marstal district heating monitoring data evaluation for the years 2015-2017. Retrieved July 9, 2023, from https://www.solar-district-heating.eu/wp-content/uploads/2019/10/Marstal-evaluation-report-2015-2017_2019.05.28.pdf

Schmidt, T., Pauschinger, T., Sørensen, P. A., Snijders, A., Djebbar, R., Boulter, R., & Thornton, J. (2018). Design Aspects for Large-scale Pit and Aquifer Thermal Energy Storage for District Heating and Cooling. *Energy Procedia*, *149*, 585–594. https://doi.org/10.1016/j.egypro.2018.08.223

Sibbitt, B., McClenahan, D., Djebbar, R., Thornton, J., Wong, B., Carriere, J., & Kokko, J. (2012). The Performance of a High Solar Fraction Seasonal Storage District Heating System – Five Years of Operation. *Energy Procedia*, *30*, 856–865. https://doi.org/10.1016/j.egypro.2012.11.097

Sifnaios, **I.** (2023). Integration of a pit thermal energy storage in a district heating network [Draft].

Sifnaios, **I.**, Dragsted, J., & Jensen, A. R. (2021). Thermal inspection of water pit heat storages using drones. *Proceedings - ISES Solar World Congress 2021*, 925–931. https://doi.org/10.18086/swc.2021.35.02

Sifnaios, **I.**, Gauthier, G., Trier, D., Fan, J., & Jensen, A. R. (2023a). Dronninglund water pit thermal energy storage dataset. *Solar Energy*, *251*, 68–76. https://doi.org/10.1016/j.solener.2022.12.046

Sifnaios, **I.**, Jensen, A. R., Furbo, S., & Fan, J. (2022a). Effect of Design Characteristics on Pit Thermal Energy Storage Performance. *Proceedings - EuroSun 2022*.

Sifnaios, **I.**, Jensen, A. R., Furbo, S., & Fan, J. (2022b). Evaluation of stratification in thermal energy storages. *Renewable Energy Systems in Smart Grid*, 57–69. https://doi.org/10.1007/978-981-19-4360-7_6

Sifnaios, **I.**, Jensen, A. R., Furbo, S., & Fan, J. (2022c). Performance comparison of two water pit thermal energy storage (PTES) systems using energy, exergy, and stratification indicators. *Journal of Energy Storage*, *52*, 104947. https://doi.org/10.1016/j.est.2022.104947

Sifnaios, **I.**, Jensen, A. R., Furbo, S., & Fan, J. (2023b). Heat losses in water pit thermal energy storage systems in the presence of groundwater. *Applied Thermal Engineering*, *235*, 121382. https://doi.org/10.1016/j.applthermaleng.2023.121382

Sifnaios, **I.**, Sneum, D. M., Jensen, A. R., Fan, J., & Bramstoft, R. (2023c). The impact of large-scale thermal energy storage in the energy system. *Applied Energy*, *349*, 121663. https://doi.org/10.1016/j.apenergy.2023.121663

Soerensen, P. A., & From, N. (2011). High solar fraction with pit heat storages. *30th ISES Biennial Solar World Congress 2011, SWC 2011*, *4*, 3020–3030. https://doi.org/10.18086/swc.2011.21.07

Suárez, C., Pino, J., Rosa, F., & Guerra, J. (2019). Analytical approach to ground heat losses for high temperature thermal storage systems. *International Journal of Energy Research*, *43*(1), 439–454. https://doi.org/10.1002/er.4278

Sveinbjörnsson, D., From, N., Sørensen, P. A., Schmidt, T., Klöck, M., & Pauschinger, T. (2020). *Pit Thermal Energy Storage for Smart District Heating and Cooling* (tech. rep.).

Sveinbjörnsson, D., Laurberg Jensen, L., Trier, D., Ben Hassine, I., & Jobard, X. (2017). *Large Storage Systems for DHC Networks* (tech. rep.).

Texas Education Agency. (2023). World Energy Use. Retrieved July 4, 2023, from https://www.texasgateway.org/resource/79-world-energy-use

Tschopp, D., Tian, Z., Berberich, M., Fan, J., Perers, B., & Furbo, S. (2020). Large-scale solar thermal systems in leading countries: A review and comparative study of denmark, china, germany and austria. *Applied Energy*, *270*. https://doi.org/10.1016/j.apenergy.2020.114997

United States Environmental Protection Agency. (2023). What is CHP? Retrieved July 31, 2023, from https://www.epa.gov/chp/what-chp

W.E District. (2023). Interactive map: Share of District Heating and Cooling across Europe. Retrieved March 22, 2023, from https://www.wedistrict.eu/interactive-map-share-of-district-heating-and-cooling-across-europe/

Wiese, F., Bramstoft, R., Koduvere, H., Pizarro Alonso, A., Balyk, O., Kirkerud, J. G., Tveten, Å. G., Bolkesjø, T. F., Münster, M., & Ravn, H. (2018). Balmorel open source energy system model. *Energy Strategy Reviews*, *20*, 26–34. https://doi.org/10.1016/j.esr.2018.01.003

Winterscheid, C., & Schmidt, T. (2017). *Dronninglund District Heating Monitoring Data Evaluation for the Years 2015-2017* (tech. rep.).

Wu, L., & Bannerot, R. (1987). An experimental study of the effect of water extraction on thermal stratification in storage. *Proceedings of the 1987 ASME-JSME-JSES Solar Energy Conference, Honolulu*, 445–451.

Yang, T., Liu, W., Kramer, G. J., & Sun, Q. (2021). Seasonal thermal energy storage: A techno-economic literature review. *Renewable and Sustainable Energy Reviews*, *139*(January). https://doi.org/10.1016/j.rser.2021.110732

Zenhäusern, D. (2020). *Key Performance Indicators for PVT Systems* (tech. rep.). IEA Solar Heating and Cooling Programme. https://doi.org/10.18777/ieashc-task60-2020-0007

Part II

Papers

I. Performance comparison of two water pit thermal energy storage (PTES) systems using energy, exergy, and stratification indicators

Ioannis Sifnaios, Adam R. Jensen, Simon Furbo, and Jianhua Fan

Journal of Energy Storage, 52, 104947 (2022)

Journal of Energy Storage 52 (2022) 104947

Contents lists available at ScienceDirect

Journal of Energy Storage

journal homepage: www.elsevier.com/locate/est

Research Papers

Performance comparison of two water pit thermal energy storage (PTES) systems using energy, exergy, and stratification indicators

Ioannis Sifnaios [a,b,*], Adam R. Jensen [a], Simon Furbo [a], Jianhua Fan [a]

[a] Department of Civil and Mechanical Engineering, Technical University of Denmark, Brovej, Building 118, 2800 Kgs. Lyngby, Denmark
[b] Sino-Danish College (SDC), University of Chinese Academy of Sciences, Beijing, China

ARTICLE INFO

Keywords:
District heating
Water pit heat storage
Efficiency indicators
Thermal stratification
Large-scale heat storage

ABSTRACT

Water pit thermal energy storage systems have been demonstrated in Denmark and have proven effective in increasing the solar thermal fractions of district heating systems and in covering the mismatch between heat demand and production. This study analyzed five years of measurement data for two PTES systems in Denmark, namely Marstal and Dronninglund. Their efficiency was assessed using energy, exergy, and a seasonal efficiency indicator. The degree of stratification was investigated using the MIX number, the stratification coefficient, and a newly-introduced indicator, exergy destruction. Exergy destruction was shown to be a promising indicator for assessing stratification since it can be used to compare PTES systems with different heat losses, providing a quantitative evaluation of the amount of mixing. In addition, the seasonal efficiency was found to be suitable for estimating the long-term efficiency of combined seasonal and short-term storage systems. The storage in Dronninglund had 92% energy and 73% exergy efficiency, while Marstal had 63% energy and 48% exergy efficiency. All stratification and efficiency indicators showed that the storage in Dronninglund performed better overall than the one in Marstal.

1. Introduction

Approximately 64% of residential heat consumers in Denmark use district heating to cover their heat demand [1]. A benefit of district heating systems is that, in principle, they can use a variety of heat sources, both renewable and non-renewable. However, due to the intermittent nature of renewables, e.g., wind and solar, there is often a mismatch between heat demand and production. In order to accommodate a high share of renewables in district heating grids, a solution is needed to deal with this mismatch [2]. Research has demonstrated that an effective solution is the use of thermal energy storage (TES) in district heating systems. According to Sveinbjörnsson et al. [3], the mismatch between heat demand and production typically limits the solar thermal fraction of district heating systems to 20%. However, by using seasonal TES, solar thermal fractions higher than 40% can be achieved.

Obtaining a high storage efficiency is crucial in order to obtain a high system performance. For this reason, storage efficiency has been thoroughly studied in the literature, primarily in terms of energy and exergy. Historically, energy efficiency analysis has been favored as it is based on relatively simple concepts and is easy to implement. However, Rosen et al. [4] demonstrated that exergy analysis provides a more realistic and accurate assessment of TES performance than energy analysis.

Rezaie et al. [5] investigated the performance of a TES in a district heating system in Germany and calculated an energy and exergy efficiency of 60% and 19%, respectively. Lake and Rezaie [6] presented similar results for a cold TES where the overall energy efficiency of the storage was 75%, while the exergy efficiency was only 20%. Exergy efficiency is lower than energy efficiency as it accounts not only for losses but also reversibility [7]. For example, exergy can identify temperature degradation in a storage system caused by ambient temperature but also due to mixing [8]. Also, exergy can account for temperature differences in storage systems with the same energy content, resulting in a performance indicator that is more accurate than one based only on energy.

The main factors impacting TES performance are heat losses and thermal stratification. Thermal stratification occurs when fluid is stored at different temperature levels in the same tank, creating a vertical temperature gradient. Rosen et al. [9] concluded that achieving a high degree of stratification is essential for high TES performance since it increases the amount of stored exergy. Additionally, Sifnaios et al. [10] showed that a stratified tank could increase a heat pump system's coefficient of performance (COP) by up to 32% compared to a fully mixed tank. The reason is that a stratified TES can have a higher exergy content

* Corresponding author at: Department of Civil and Mechanical Engineering, Technical University of Denmark, Brovej, Building 118, 2800 Kgs. Lyngby, Denmark.
E-mail address: iosif@dtu.dk (I. Sifnaios).

https://doi.org/10.1016/j.est.2022.104947
Received 9 March 2022; Received in revised form 4 May 2022; Accepted 21 May 2022
Available online 27 May 2022

Nomenclature

Latin letters

C_p	Specific heat [J/(kg·K)]
d	Diameter [m]
E	Energy [J]
Ex	Exergy [J]
h	Height [m]
H	Enthalpy [J]
m	Mass [kg]
M_E	Moment of energy [J·m]
S	Entropy [J/K]
T	Temperature [K]
v	Water speed [mm/s]
V	Volume [m^3]
$\dot{V}$	Volume flow rate [m^3/h]
z	Distance [m]

Greek letters

η_E	Energy efficiency [%]
$\eta_{E,\,S}$	Seasonal energy efficiency [%]
η_X	Exergy efficiency [%]
ρ	Density [kg/m^3]

than a fully mixed tank for the same heat input [11].

While stratification naturally occurs due to the temperature dependence of the buoyancy force (i.e., the density of water generally decreases with an increase of temperature), several phenomena decrease stratification. Stratification is decreased by mixing induced by the inlet flow, by heat diffusion caused by natural convection, and by downward thermal conduction [12]. As a consequence, thermal stratification is affected by the inlet/outlet design, storage geometry, and operation strategy of the TES. To decide if a TES performs adequately, it is necessary to evaluate the degree of stratification, usually by calculating stratification indicators.

Many stratification indicators have been investigated in the literature without determining which performs best. Castell et al. [13] compared many dimensionless numbers for assessing thermal stratification and concluded that the Richardson number is the most suitable for predicting the expected stratification. However, the Richardson number does not quantify the actual storage stratification and can only be used for comparing two or more similar storage systems. In addition, in a review performed by Han et al. [14], it was found that various studies report inconsistent interpretations of the relation between the Richardson number and mixing.

Haller et al. [15] reported a comprehensive investigation of most available stratification indicators. The study concluded that all of the assessed indicators had limitations in their application, e.g., some indicators could not be used for scenarios including charging and discharging, whereas others failed to separate the effects of heat losses from mixing. To overcome these limitations, Sifnaios et al. [16] suggested using the internal exergy destruction for elucidating the specific times at which mixing occurs. Compared to other indicators, a benefit of this method is that it does not rely on a reference storage simulation, which can be difficult to implement in real life. It can also be applied to storage systems regardless of their application (e.g., short term, long term, or a combination).

In the present paper, two large-scale water pit thermal energy storage (PTES) systems were assessed and compared in terms of their efficiency and degree of stratification. A water PTES is a large water reservoir used to store thermal energy for a period ranging from days to months, depending on the application. It is constructed by excavating a pit in the ground, which is subsequently lined with a watertight polymer liner [17]. The storage is then filled with water and covered with an insulated floating lid [18]. Water PTES technology was developed in Denmark and demonstrated with solar collector fields as the heat source [19]. The main advantage of a water PTES is its low cost compared to other storage technologies. For example, the investment cost of a water PTES ranges from 20 to 40 €/m^3 while the investment cost of conventional storage tanks is from 150 to 320 €/m^3 [20].

To the authors' knowledge, there has never been a study assessing the performance and stratification of a PTES using actual measurement data. In addition, although simple energy efficiencies have been calculated for individual storage systems, e.g., by Dahash et al. [21], a comparison of the performance of two PTES systems in terms of energy, exergy, and stratification indicators has never been performed.

For this reason, the efficiency and thermal stratification of two water PTES systems were determined experimentally in this study. The two systems were located in Denmark, in Marstal and Dronninglund. Long-term measurements at each of the two PTES systems were carried out. The data obtained were analyzed using a number of energy and exergy efficiency expressions. Their suitability for evaluating PTES performance was assessed. Lastly, an exergy destruction indicator was for the first time applied to actual storage systems to determine its suitability for assessing stratification.

2. Methods

The construction and operation of the water PTES systems in Marstal and Dronninglund are briefly described below, followed by an account of the measurements that were made and the definitions of the stratification and efficiency indicators.

2.1. The storage systems investigated

2.1.1. Marstal

The water PTES system in Marstal was constructed in 2012, with a capacity of approximately 6000 MWh. The heat storage system was integrated with the local district heating system, which supplies heat to approximately 1600 consumers. The pit was excavated in the shape of an inverse truncated pyramid with a volume of 75,000 m^3. This PTES system is used for seasonal storage of heat generated by a solar collector field consisting of 15,000 m^2 of flat-plate collectors.

The core of the lid construction consists of three layers of close cell structure polyethylene (PE) foam insulation (Nomalén 28N manufactured by the company NMC Termonova [23,24]) with a total thickness of 24 cm. The layers of Nomalén were enclosed between two high-density polyethylene (HDPE) liners. Weight pipes were used to ensure a slope towards the center of the lid, where a pump well was located to remove rainwater from the surface of the lid. Fig. 1 shows an aerial photo of the PTES and the solar thermal collector field in Marstal. The heat storage system was primarily charged during the spring and summer periods and discharged during autumn and winter.

The district heating supply temperature in Marstal was approx. 73 °C [25], while the average return temperature was 40 °C (lower in winter and higher in summer). When the temperature at the top of the storage was higher than the supply temperature, heat was supplied directly to the district heating grid. However, when the temperature at the top of the storage was between 70 °C and 73 °C, water from the storage system was mixed with higher temperature water from a biomass boiler in order to reach the desired supply temperature. Whenever the storage temperature dropped below 70 °C, the PTES acted as the heat source for a heat pump that supplied heat to the district heating network. The heat pump cooled down the storage to approximately 15–20 °C.

The storage system was charged and discharged using three double-plated diffusers located at the top, middle, and bottom of the storage (see Fig. 2). In the same figure, it may be seen that the pipes leading to the diffusers were uninsulated and passed through the storage side wall. The diameter of the diffuser plates was 3 m, and the vertical spacing between

Fig. 1. Aerial photo of the PTES in Marstal in 2013 [22].

Fig. 2. Diffuser installation in Marstal [22].

the diffuser plates was 0.85 m. The diffusers were constructed of steel, and the average exit velocity for the water was 2.2 mm/s, corresponding to a Reynolds number of 5731 (for water at 90 °C). Eq. (1) was used to calculate the average diffuser velocity for an average volume flow rate of 63 m^3/h.

$$v_{diffuser} = \frac{\dot{V}}{d_{diffuser} \bullet h_{diffuser} \bullet \pi} \quad (1)$$

where $\dot{V}$ is the volumetric flow rate, $d_{diffuser}$ is the diameter of the diffuser plate, and $h_{diffuser}$ is the vertical spacing between the diffuser plates.

The lid insulation in the PTES in Marstal started to degrade in the course of 2015 due to contact with water at high temperatures. In 2017, multiple piercings in the HDPE liner led to water entering the lid (rainwater from above and storage water from below), causing a large increase in the rate of heat loss. In 2018 the heat storage operation was interrupted during the replacement of the lid. The data used in this study are thus from 2014 to 2017.

2.1.2. Dronninglund

The water PTES system in Dronninglund was constructed in 2014, based on the same design as the storage in Marstal, but including some improvements (Fig. 3). It had a volume of 60,000 m^3 and an approximate storage capacity of 5500 MWh. The storage system was charged from a 35,573 m^2 flat-plate solar collector field and supplied heat to 1350 consumers. As in the storage system in Marstal, the lid was made of three layers of Nomalén enclosed in two HDPE liners. However, the HDPE liner used in Dronninglund had a longer lifetime at high temperatures.

The main difference between the two storage systems was in their operation. The storage in Dronninglund was used both as seasonal and short-term heat storage. This means that not only was heat stored from summer to winter, but the storage was also used to even out the diurnal variation, i.e., heat charged during the day might be discharged in the evening and at night. This operation strategy increased the yearly charged and discharged energy compared to the PTES system in Marstal.

The supply temperature of the district heating network in Dronninglund was 75 °C [26], while the average return temperature was 42 °C. When the temperature at the top of the storage was higher than the supply temperature, heat was supplied directly to the district heating grid, but when the storage temperature was lower than 75 °C, the system was used as a heat source for a heat pump. The heat pump was only operated in winter and cooled down the storage to approximately 10 °C.

The Dronninglund PTES system was also charged using three diffusers, placed at the top, middle, and bottom of the pit, as shown in Fig. 4. However, the diffuser construction in Dronninglund differed

Fig. 3. Aerial photo of the PTES in Dronninglund in 2019.

Fig. 4. Diffuser installation in Dronninglund [27].

somewhat from the one in Marstal. For example, Fig. 4 shows that the pipes leading to the diffusers were insulated and entered the storage from below, thus minimizing any temperature exchange with the stored water. The diffusers were made of stainless steel and were slightly smaller than those in Marstal, with a plate diameter of 2.5 m and vertical spacing of 0.58 m. Consequently, the average flow rate was higher, with an average diffuser exit velocity of 5 mm/s at 80 m^3/h volume flow rate. The corresponding Reynolds number for this exit velocity was 8887 (for water at 90 °C).

However, as at Marstal, the HDPE liner enclosing the lid insulation experienced multiple piercings during 2020 and 2021, and eventually, the entire lid had to be replaced. The data from Dronninglund are thus from 2015 to 2019. Both storage systems had a different lid construction at the time of writing compared to those described, which are the ones that were in place when the measurements were made.

2.1.3. Measurement equipment

The temperature in each storage was measured using two vertical temperature sensor strings hanging from the middle of the lid. Each temperature string had 16 temperature sensors placed at 1 m intervals. The two strings were located next to each other and offset by 0.5 m; thus, the vertical temperature profile was measured every 0.5 m. The temperature sensors were Class A PT100, with an accuracy of ±0.15 °C. The equipment used to measure the storage temperature was the same for Dronninglund and Marstal. The location of the water temperature sensors relative to the diffusers in the PTES is presented in Fig. 5.

The volume flow rate to and from the storage in Dronninglund was measured using electromagnetic flowmeters with an accuracy of 0.4%. In Marstal, the flow was measured using ultrasonic flowmeters with an estimated uncertainty of 2%. The temperatures in the inlet and outlet pipes were measured in both systems using immersed Class A PT100 sensors, with an accuracy of ±0.15 °C.

2.2. Stratification indicators

The present study derived three indicators to assess thermal stratification: the MIX number, the stratification coefficient, and exergy destruction. In order to calculate these indicators, the storage systems were divided into discrete layers corresponding to the position of the installed temperature sensors. The temperature sensors in both storage systems were installed every 0.5 m from the bottom to the top of the water pit, and since both storage systems had a depth of 16 m, each storage was divided into 32 layers.

2.2.1. MIX number

The MIX number is a dimensionless indicator assessing storage stratification by comparing the storage system temperature profile with a fully mixed and a fully stratified reference storage system [28]. The MIX number ranges between zero and one, corresponding to a perfectly stratified and a fully mixed storage, respectively. As presented in Eq. (2), the MIX number is calculated based on the moment of energy.

$$MIX = \frac{M_E^{stratified} - M_E^{actual}}{M_E^{stratified} - M_E^{fully\ mixed}} \quad (2)$$

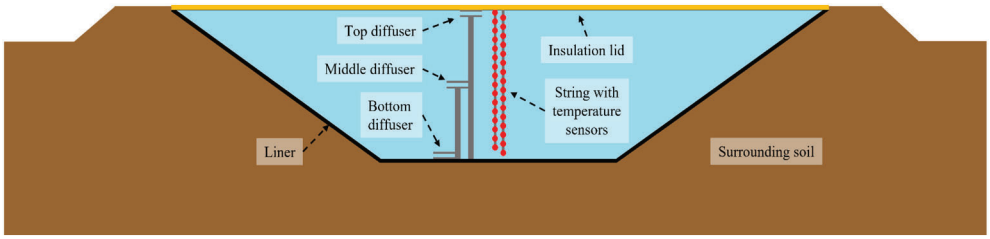

Fig. 5. Sketch of the location of the water temperature sensors (red dots) relative to the diffusers for the PTES in Dronninglund and Marstal. (For interpretation of the references to color in this figure legend, the reader is referred to the web version of this article.)

The moment of energy for each scenario is calculated as the sum of the moment of energy of each layer. Each layer's moment of energy is calculated by multiplying the layer's energy content with the height from the bottom of the storage:

$$M_E = \sum_{i=1}^{N} \rho_i \bullet V_i \bullet C_{p,i} \bullet \left(T_i - T_{ref}\right) \bullet z_i \tag{3}$$

where N is the number of storage layers, ρ_i represents the water density of layer i, V_i is the water volume of the layer, $C_{p,\,i}$ is the specific heat, and T_i is the water temperature of the ith layer. The distance from the centroid of the layer to the bottom of the storage system is denoted as z_i, and T_{ref} is the reference temperature, i.e., the temperature at which the storage system is considered empty.

The moment of energy for the fully stratified and fully mixed storage systems is calculated such that they have the same energy content as the actual storage system.

2.2.2. Stratification coefficient

The stratification coefficient expresses the degree of thermal stratification based on the deviation of the storage temperature profile relative to the mean temperature. The expression developed by Wu and Bannerot [29] is presented below:

$$St = \sum_{n=1}^{N} \frac{m_i \bullet \left(T_i - T_{avg}\right)^2}{m_{total}} \tag{4}$$

where T_i is the temperature and m_i is the mass of the ith layer, T_{avg} is the average storage temperature, and m_{total} is the total mass of the storage system.

2.2.3. Exergy destruction

The internal exergy destruction is calculated based on the exergy balance of the TES, using Eq. (5):

$$\Delta Ex_{destr} = \Delta Ex_{flow} - \Delta Ex_{store} - \Delta Ex_{loss} \tag{5}$$

Exergy destruction is the sum of the exergy destroyed due to mixing, heat conduction, and diffusion. This means that a storage system with high exergy destruction will experience a low level of stratification. It should be noted that the exergy destruction calculated in Eq. (5) includes the exergy lost directly due to heat losses. This is one of the main benefits of using exergy destruction compared to other methods, as it is possible to compare storage systems with different heat losses without having biased results. The exergies were calculated as:

$$\Delta Ex = \Delta H - T_0 \bullet \Delta S \tag{6}$$

where ΔH is the change in enthalpy, ΔS is the change in entropy and T_0 is the dead state temperature. The dead state of a system is a state in which it is at temperature, pressure, elevation, velocity, and chemical equilibrium with its surroundings [30].

In order to be able to compare storage systems of different sizes fairly, the exergy destruction should be normalized with the storage volume. The normalized exergy destruction is therefore calculated as:

$$\Delta Ex_{destr,norm} = \frac{\Delta Ex_{destr}}{\sum_{n=1}^{N} V_i} \tag{7}$$

2.3. Efficiency indicators

Many different efficiency indicators have been proposed, although they can generally be expressed as the ratio between the useful output and input to the system:

$$\eta = \frac{useful\ output}{input} \tag{8}$$

In this study, two efficiency indicators were calculated, namely energy and exergy efficiency, as defined in the following sub-sections.

2.3.1. Energy efficiency

The energy balance of a thermal storage system can be expressed as:

$$E_{out} = E_{in} - E_{loss} - \Delta E_{int} \tag{9}$$

where E_{out} is the energy discharged from the storage system, E_{in} is the charged energy, and E_{loss} is the energy lost due to heat losses. ΔE_{int} is the change in the internal energy of the storage system, i.e., the difference between the internal energy at the start and end of the period under consideration.

Two expressions have been used to calculate energy efficiency and are presented in Eqs. (10) and (11). It should be noted that these expressions are slightly different from Eq. (8) since they also account for the internal energy change of the storage system.

$$\eta_{E,1} = \frac{E_{out}}{E_{in} - \Delta E_{int}} = \frac{E_{out}}{E_{out} + E_{loss}} \tag{10}$$

$$\eta_{E,2} = \frac{E_{out} + \Delta E_{int}}{E_{in}} = \frac{E_{in} - E_{loss}}{E_{in}} \tag{11}$$

The main difference between the two expressions is the treatment of the internal energy change, i.e., either subtracting it from the charged energy or adding it to the discharged energy. Both expressions have been used in engineering reports and are included in this study to investigate whether they can be used interchangeably.

Nevertheless, energy efficiencies calculated in this way can be misleading when comparing seasonal storage systems (such as Marstal) with storage systems used for both seasonal and short-term storage (such as Dronninglund). The main reason is that the total energy charged and discharged in a seasonal and short-term storage system is much higher than a storage system that is only used for seasonal storage. However, the heat losses of a seasonal and short-term storage are not proportionally higher since they depend on the storage duration. For this reason, Jensen [31] proposed a seasonal efficiency, which attributes the heat losses only to the seasonally stored energy:

$$\eta_{E,S} = \frac{E_{seasonal}}{E_{seasonal} + E_{loss}} \tag{12}$$

where $E_{seasonal}$ is the stored seasonal energy. The stored seasonal energy

can be calculated as the difference between the minimum and maximum energy content in the course of one year. Seasonal efficiency quantifies the efficiency of the storage system as if it was solely used for seasonal heat storage.

2.3.2. Exergy efficiency

Exergy is a measure of the quality of energy and indicates the work potential of a system relative to its environment [32]. Following the general format of efficiency indicators, Rosen et al. [4] calculated the exergy efficiency as:

$$\eta_X = \frac{Ex_{out}}{Ex_{in}} \tag{13}$$

where Ex_{in} is the exergy entering the system and Ex_{out} is the exergy exiting the system. Unlike energy efficiency, exergy efficiency also accounts for the level of stratification, as mixing reduces the exergy content.

3. Results

The first section of the results derives the stratification indicators for the PTES systems in Marstal and Dronninglund. The second section calculates the energy and exergy efficiencies of the storages.

3.1. Stratification indicators

3.1.1. Marstal PTES system

The storage temperatures, stratification indicators, diffuser energy supply, and normalized weekly flow rate for the PTES system in Marstal are shown in Fig. 6. The storage temperature, diffuser energy supply, and normalized volume flow rate are included in the plot to demonstrate the storage operation and assist in understanding the stratification indicators.

For the PTES temperature, the temperature of each storage layer is illustrated using a different color, namely green for the top of the storage and blue for the lowest level. Additionally, a thin black curve indicates the temperature for the top, middle, and lowest layers. It may be seen that the annual maximum temperature of the PTES system in Marstal decreased over the investigated period. As previously mentioned, this was because of the high heat losses due to the degradation of the lid insulation after 2014 (see also Table 2).

In Fig. 6, the MIX number and the stratification coefficient are presented for each day, while the exergy destruction and diffuser energy supply are tabulated for each month and the volume flow rate for each

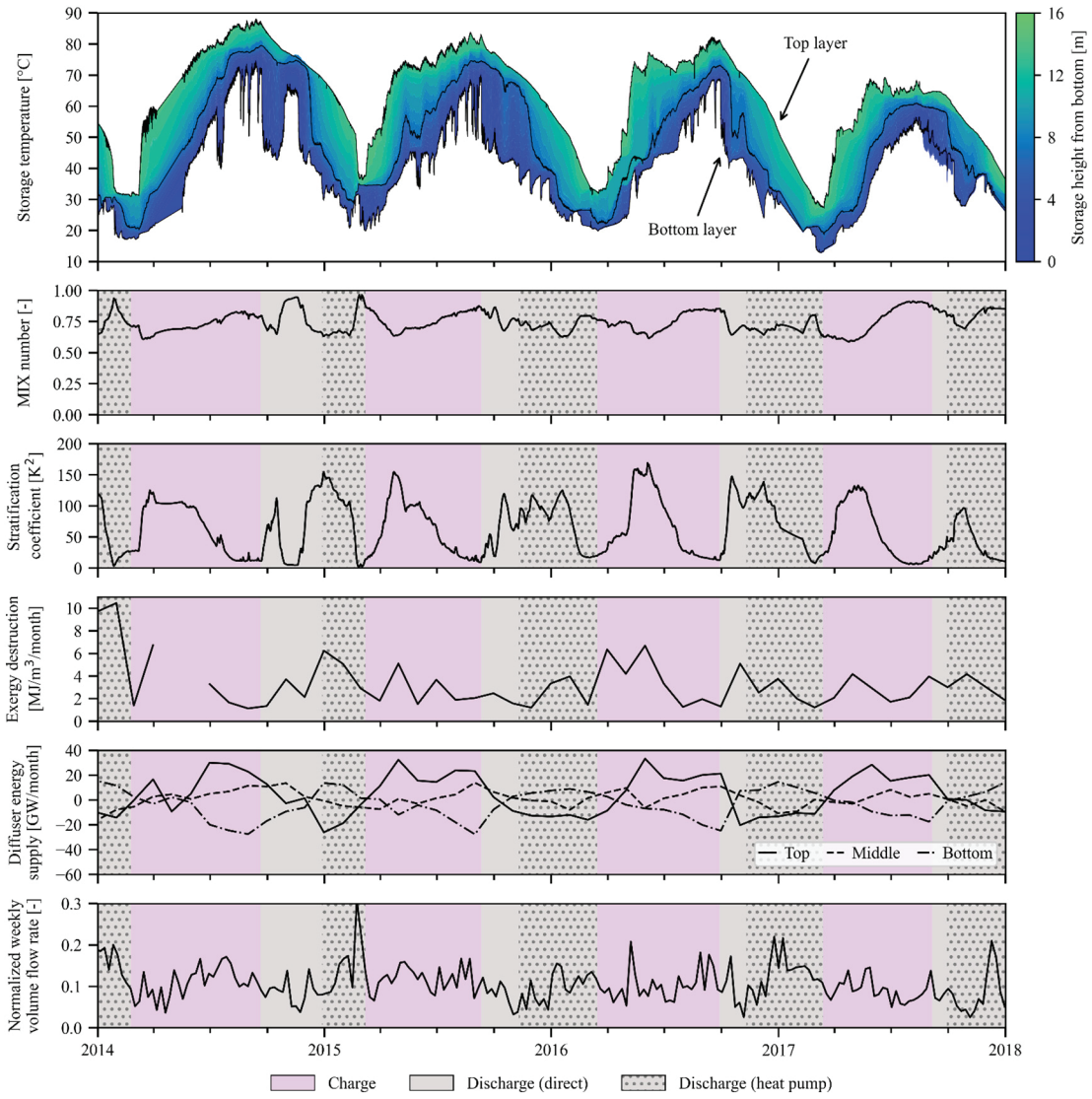

Fig. 6. Storage temperature and stratification indicators for PTES in Marstal. The gap for exergy destruction in spring 2014 is due to missing flow rates from the dataset, probably due to data logging errors.

week. Ideally, all of the indicators should be calculated for each day. However, the exergy destruction and heat losses can only be calculated with reasonable accuracy on a monthly basis due to the low spatial resolution of the temperature in the storage. The volume flow rate was plotted weekly since the daily flow was very variable. The charging periods are illustrated in Fig. 6 using a pink background, while the discharging periods are shown in grey. The heat pump discharge periods are illustrated using a dotted pattern so as to be distinguishable from the periods of direct discharge of the PTES. As mentioned before, the duration of the direct discharge period varies from year to year, depending on the storage temperature. It may be seen that for years with low storage temperatures, e.g., in 2017, the storage system was almost exclusively used as a source for the HP.

The maximum value of the MIX number in Marstal was 0.97, and the minimum was 0.56. The average MIX number value for the entire period under investigation was 0.74, indicating a high degree of mixing. It may be seen that the MIX number generally approaches one towards the end of each charging and discharging period when there is an almost uniform temperature in the PTES system.

Comparing the MIX number with the stratification coefficient, it can be stated that they have a negative correlation, i.e., when one increases, the other decreases. For example, at the end of each charging and discharging period, the stratification coefficient approaches its lower value, i.e., zero, indicating a uniform temperature in the PTES. However, the variation of the values of the stratification coefficient is more pronounced, providing more information about the mixing within the storage. The stratification coefficient reached its maximum value when there was the largest temperature difference between the top and bottom of the storage. In Marstal, this value was 169 K^2 and occurred in the summer of 2016. Like the MIX number, the value of the stratification coefficient has no physical meaning, but it can be used to compare two different storage systems or different storage operations. The maximum value of the stratification coefficient was achieved approximately at the middle of each charge/discharge period. The small spikes during charge and discharge indicate mixing since a more uniform temperature decreases the value of the coefficient. Apart from in 2014, the stratification coefficient indicates better stratification during charge than discharge periods. However, these values are caused by higher temperatures at the top of the PTES system and not necessarily by better stratification.

Also, in Fig. 6, it is evident that, in general, there is high exergy destruction during the charging periods. The reason for this is that most of the heat losses take place from the top of the storage during charging, leading to the spiky temperature profile shown in Fig. 6. Heat losses can affect the stratification in the storage system by cooling down the top layer of water just under the lid, creating thermal inversion that induces mixing. Besides mixing caused by heat losses, heat conduction and diffusion in the storage system also generate mixing. These phenomena occur when there is a non-uniform temperature profile in the storage system. The exergy destruction indicator captures the effect of heat conduction and diffusion since it reaches its lowest values when the storage system approaches a uniform temperature (i.e., when fully charged or discharged). Last, some of the spikes in exergy destruction can be correlated with periods of high energy supply/extract from the diffusers, indicating mixing occurring during the diffuser operation. The mean annual exergy destruction in Marstal for the analyzed period was 36 MJ/m^3/year. This number indicates the amount of mixing in the storage and will be used for comparison with the Dronninglund storage.

Periods with high exergy destruction occurred when there were spikes in the stratification coefficient. As previously mentioned, a rapid decrease in the stratification coefficient indicates mixing, which is well captured by exergy destruction. However, it should be noted that the exergy destruction values were calculated monthly, so it is not easy to match them with the other stratification indicators.

From Fig. 6, it is apparent that there is no direct correlation between the normalized volume flow rate passing through the storage and the stratification indicators. This indicates that the diffusers were functioning appropriately and were reducing the water velocity even when high flows were entering the PTES.

The mean annual value for the MIX number and stratification coefficient are presented in Table 1, along with the sum of exergy destruction per year for the two PTES systems under investigation.

3.1.2. Dronninglund PTES

Table 2 shows the energy balance for the PTES system in Dronninglund. It shows that more energy was being charged and discharged annually in Dronninglund than in Marstal due to their different modes of operation. In addition, the heat losses in the Dronninglund system were much lower than in Marstal, primarily because of lower heat losses from the lid, but also because of the mode of operation. For example, in Dronninglund, the mean low temperature of the PTES system was around 10 °C, while in Marstal it was around 20 °C, so the heat gains from the ground in wintertime were much greater in Dronninglund.

The effect of the lower heat losses can be seen in Fig. 7, where the temperature in the storage system is shown. Compared to Marstal, the storage temperature in Dronninglund remained at higher levels. It should be noted that the temperature spikes occurring in the top layers of the storage were mainly caused by the short-term storage cycles and not by heat losses, as they were in Marstal.

In Dronninglund, the MIX number for the period analyzed ranged from 0.20 to 0.67 with an average of 0.34, which is 46% lower than in Marstal. This value indicates a well-stratified storage as a value of zero represents a perfectly stratified storage. As in Marstal, there seems to be a negative correlation between the MIX number and the stratification coefficient.

However, the maximum value reached in Dronninglund for the stratification coefficient was 538 K^2, which is 3.2 times higher than in Marstal, indicating a higher degree of thermal stratification. Nonetheless, due to the short-term storage cycles, there were many more spikes in the stratification coefficient during the charge periods, indicating a higher degree of mixing during charge than in Marstal.

This phenomenon is better illustrated in terms of exergy destruction, where the maximum values occur for the charge periods where the short-term storage cycles occur. Although these values are higher than those in Marstal in some cases, very little mixing took place in Dronninglund during discharge. Unlike the PTES in Marstal, in Dronninglund, there was no correlation between exergy destruction spikes and the diffuser operation, except from the summer of 2018. Overall, the mean annual exergy destruction for Dronninglund was 34 MJ/m^3/year, which is approximately 6% lower than for Marstal.

In both PTES systems, most charged/discharged energy was supplied using the top and bottom diffusers. However, in Dronninglund, the middle diffuser was used more than in Marstal, especially during discharge operations. The authors are not aware of whether the operation strategy differed between the two systems or if this was a result of the difference between their temperature profiles. In either case, increased usage of the middle diffuser would be expected to affect the storage stratification positively.

Higher flow rates were measured at Dronninglund than at Marstal on average, but the higher flow rates do not seem to have affected the stratification indicators.

Overall, all stratification indicators indicate that Marstal had a lower degree of stratification than Dronninglund. However, the MIX number and stratification coefficient are both affected by heat losses, favoring systems with low heat loss. Since exergy destruction is the amount of exergy lost only due to mixing, it is considered by the authors to be the best indicator for comparing storage systems with different heat losses. Additionally, its value has a physical meaning, quantifying the exergy lost through mixing. Consequently, it is the only indicator investigated that can present a quantitative evaluation of the amount of mixing that takes place in a storage system.

Calculating these indicators requires a knowledge of the vertical distribution of the storage system temperature. However, for calculating

Table 1
Mean annual values for MIX number and stratification coefficient and sum of the annual values for exergy destruction for the PTES in Marstal and Dronninglund.

	Marstal			Dronninglund		
	MIX number [–]	Stratification coefficient [K^2]	Exergy destruction [MJ/m^3]	MIX number [-]	Stratification coefficient [K^2]	Exergy destruction [MJ/m^3]
2014	0.75	60	38	–	–	–
2015	0.75	71	33	0.33	174	36
2016	0.73	75	42	0.34	187	39
2017	0.76	49	32	0.35	154	34
2018	–	–	–	0.32	115	31
2019	–	–	–	0.34	139	32
Overall	0.74	64	36	0.34	154	34

Table 2
Annual energy values for the storages in Marstal and Dronninglund. All quantities are in MWh.

	Marstal					Dronninglund				
	E_{in}	E_{out}	ΔE_{int}	E_{loss}	$E_{seasonal}$	E_{in}	E_{out}	ΔE_{int}	E_{loss}	$E_{seasonal}$
2014	7654	5124	1134	1396	4875	–	–	–		–
2015	7568	5571	−609	2606	3802	13,164	12,127	−559	1596	4551
2016	7452	5392	−695	2755	4823	12,107	10,842	13	1252	4317
2017	6975	3179	−822	4618	4021	11,442	11,555	−585	472	4225
2018	–	–	–	–	–	14,793	13,893	−159	1059	5101
2019	–	–	–	–	–	12,733	11,573	234	926	4803

the MIX number, a perfectly stratified and a fully mixed scenario have to be simulated as a reference for the actual storage system under investigation, increasing the complexity of the calculation. In addition, the MIX number can be affected by the choice of reference temperature for calculating the moment of energy. For this reason, it is essential to choose as reference temperature the one that indicates that the storage system is considered as empty. Choosing a lower reference temperature will cause the storage system to appear to be more mixed, while choosing a higher reference temperature will cause it to appear to be more stratified. Lastly, for calculating the MIX number, the moment of energy must be calculated for each of the layers in the PTES system. This is a more demanding task than for a tank due to the truncated pyramid geometry of the PTES systems under consideration.

3.2. Efficiency indicators

Table 2 sets out the annual energy values for the PTES systems in Marstal and Dronninglund. It may be seen that the energy input of each storage system, E_{in}, was similar each year. However, the discharged energy, E_{out}, varied, as it was affected by the heat losses for the specific year and the internal energy change of the storage, ΔE_{int}. The internal energy change depends on the storage system's energy content at the start and the end of each year, and, as shown in Table 2, it can be positive or negative.

A visualization of the monthly charged and discharged energy and the energy content of the storage system is given in Figs. 8 and 9 for Marstal and Dronninglund, respectively. These figures illustrate the different operations of the two storages, e.g., the Dronninglund water pit is also discharged during the charging periods. In addition, the charged energy per month in Dronninglund is approximately twice that in Marstal since the size of the solar collector field is twice as large. Last, it may be seen that Dronninglund is discharged to a lower energy content than Marstal.

The calculated energy and exergy efficiencies for the storage systems in Marstal and Dronninglund are shown in Table 3. It may be seen that the efficiencies achieved in Dronninglund are very high. The main reasons for this are the lower heat losses and the utilization of low-temperature heat by the heat pump, which increases the amount of energy that can be discharged.

When considering energy efficiency, the results for Marstal differ whether $\eta_{E,\,1}$ or $\eta_{E,\,2}$ are used. The reason is that if the internal energy change is negative (meaning the energy content of the storage is lower at the end of the year than at the start), then $\eta_{E,\,1}$ indicates higher efficiency than $\eta_{E,\,2}$. The opposite occurs if the energy change is positive. For example, in Marstal, in 2014, the internal energy change was positive, leading to a higher $\eta_{E,\,2}$, while in 2015, where ΔE_{int} was negative, $\eta_{E,\,1}$ was higher.

When comparing the results of using $\eta_{E,\,1}$ or $\eta_{E,\,2}$ for Dronninglund and Marstal, the two expressions give the same results for Dronninglund but are slightly different for Marstal. The reason is that in Dronninglund, due to the short-term storage cycles, the charged and discharged energy is much higher than the internal energy charge of the storage, so $\eta_{E,\,1}$ and $\eta_{E,\,2}$ give essentially the same results. However, for Marstal, since the charged and discharged energy are of the same order of magnitude as the internal energy charge, selecting one energy expression over the other leads to different PTES system efficiencies. The authors believe that the two expressions cannot be used interchangeably and that it is preferable to use $\eta_{E,\,1}$. The reason is that subtracting the internal energy change from the charged energy is more appropriate since less energy has to be charged due to existing energy from the previous cycle. This results in the heat losses from each year being attributed to the heat discharged during the year. In contrast, $\eta_{E,\,2}$ attributes the heat losses to the energy charged during the year.

From the efficiencies in Table 3, it may be seen that the energy efficiencies $\eta_{E,\,1}$ and $\eta_{E,\,2}$ give higher efficiency values compared to the seasonal efficiency, primarily for Dronninglund. As explained in Section 2.3.1, the seasonal energy efficiency, $\eta_{E,\,S}$, estimates the efficiency of the storage system as if it had been used only for seasonal storage. This is why the energy efficiency and seasonal efficiency for Marstal are very close. In contrast, the seasonal efficiency is lower than the energy efficiency for Dronninglund, which is used for both seasonal and short-term storage. While the short-term storage operation increases the heat losses, the total amount is approximately the same regardless of the length of the storage cycle. The reason is that most heat losses occur from the lid, and the temperature at the top of the storage system is the same whether it is used for seasonal storage only or combined seasonal and short-term storage. Therefore, the seasonal efficiency is a good indicator for finding the equivalent efficiency of a PTES if it was only used for seasonal storage.

It was found that exergy efficiency is always lower than the energy efficiencies for all the investigated years. This is because it accounts for both heat losses and the amount of mixing in the storage, while the

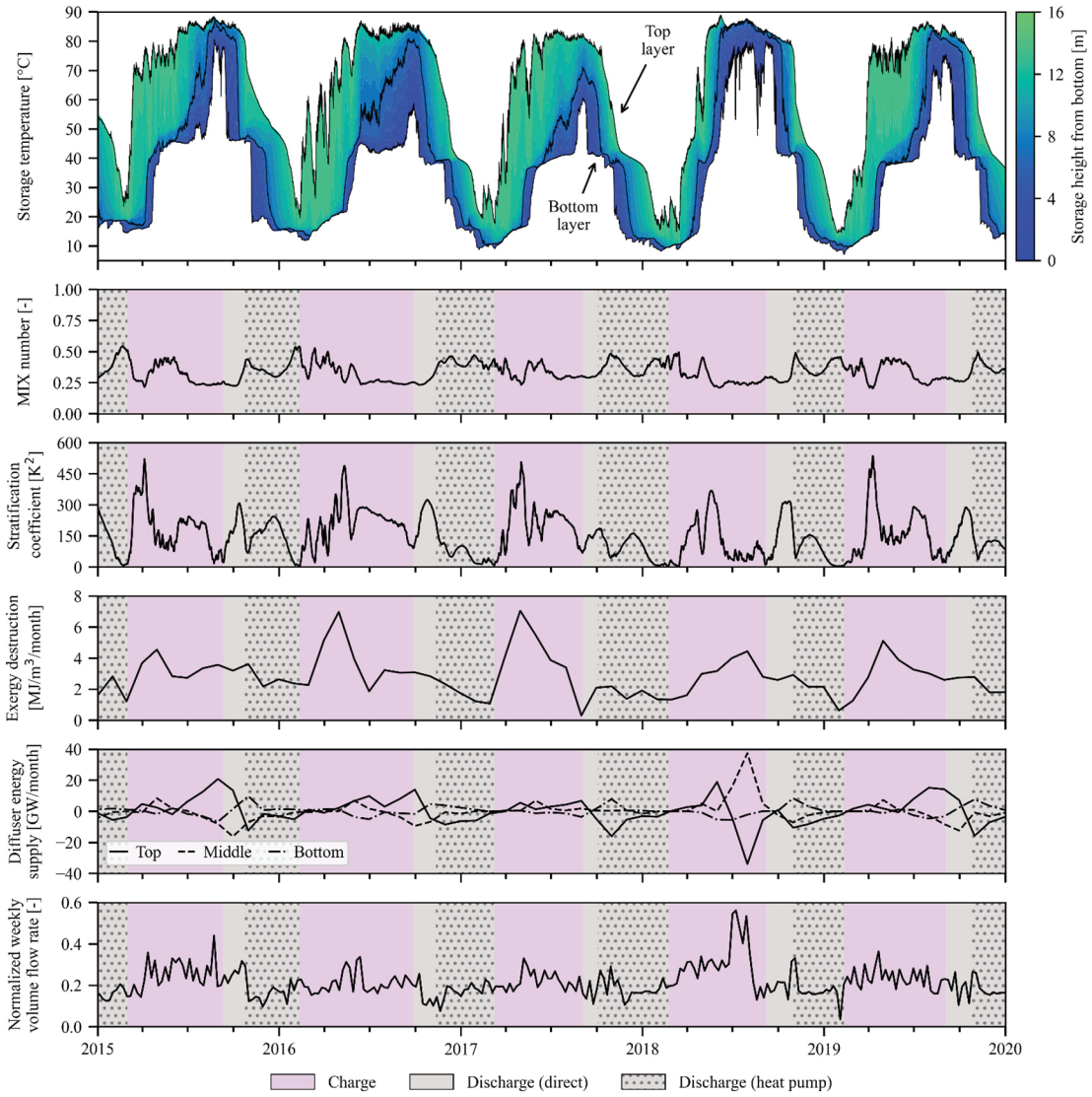

Fig. 7. Storage temperature and stratification indicators for PTES in Dronninglund.

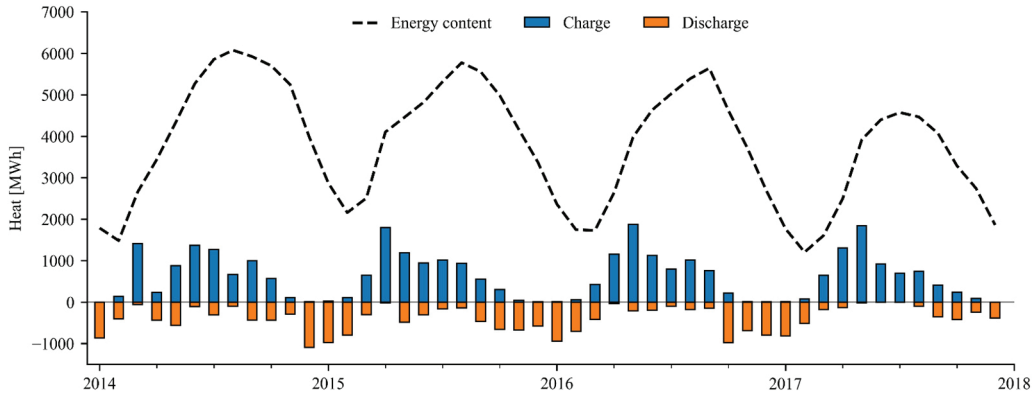

Fig. 8. Monthly charged/discharged energy and energy content for the PTES in Marstal.

typical energy efficiencies account only for heat losses. As a result, it can complement the energy efficiency expressions and provide a more detailed indicator for the comparison of different storage systems. However, it is apparent that it does not follow the same trend as the energy efficiencies, as it indicates different years as having the highest exergy efficiency. For both PTES systems, the highest exergy efficiency values corresponded to years with the highest charged/discharged energy.

All the efficiency indicators considered show that the PTES system in Dronninglund had a higher efficiency than Marstal. The main reasons

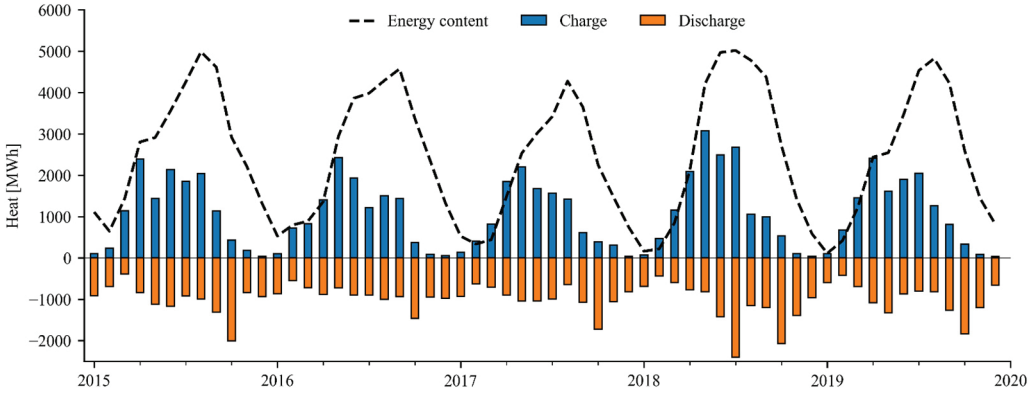

Fig. 9. Monthly charged/discharged energy and energy content for the PTES in Dronninglund.

Table 3
PTES efficiencies for Marstal and Dronninglund.

	Marstal				Dronninglund			
	$\eta_{E,1}$ (%)	$\eta_{E,2}$ (%)	$\eta_{E,S}$ (%)	η_X (%)	$\eta_{E,1}$ (%)	$\eta_{E,2}$ (%)	$\eta_{E,S}$ (%)	η_X (%)
2014	79	82	78	53	–	–	–	–
2015	68	66	59	58	88	88	74	73
2016	66	63	64	52	90	90	78	69
2017	41	34	47	27	96	96	90	73
2018	–	–	–	–	93	93	83	79
2019	–	–	–	–	93	93	84	73
Total	63	62	61	48	92	92	81	73

seem to be the high heat losses and the lower degree of stratification in the Marstal PTES. The high heat losses in Marstal are most likely due to water entering the lid (either rainwater from above or storage water from below), which reduces the performance of the insulation. Thus, it is crucial that the lid insulation is maintained dry since the thermal barrier of the lid is key to limiting the heat loss of a PTES. Regarding stratification, research should be conducted on selecting the optimal diffuser construction and operation.

4. Conclusions

This study investigated the efficiency and stratification of two existing large-scale water pit thermal energy storage (PTES) systems. Both systems were located in Denmark, namely in Marstal and Dronninglund. Long-term measurements at the two systems were analyzed.

The MIX number, stratification coefficient, and exergy destruction indicators were used for assessing the stratification of the PTES. Although all these indicators show that Marstal had a lower degree of stratification than Dronninglund, exergy destruction was considered the most promising indicator for assessing the amount of mixing in a storage. One of the benefits of exergy destruction is that it can be used to compare storage systems with different heat losses without necessarily favoring the one with the lowest heat losses, but instead providing a quantitative evaluation of the amount of mixing.

The storage efficiency was assessed using energy, exergy, and a seasonal efficiency indicator. It was found that the two energy expressions compared cannot be used interchangeably since they give different results for seasonal storage systems, in which the internal energy change is of the same order of magnitude as the charged and discharged energy.

The seasonal efficiency was found to be a suitable indicator for comparing storage systems with different operations. Calculating the equivalent efficiency of a PTES system as if it was used as seasonal storage enables a fair comparison between a seasonal and a combined seasonal and short-term storage.

Exergy efficiency is recommended as an indicator complementing energy efficiency since it is able to account for the effects of heat losses and mixing in the storage. In addition, the exergy efficiency can more fairly compare storage systems with different operations.

In comparing the performance of the two PTES systems, all of the stratification and efficiency indicators considered in this study showed that the Dronninglund system performed better than the Marstal system. The reason is that the PTES system in Dronninglund had lower heat losses and better stratification.

Future work should investigate the impact of storage operations on efficiency and stratification by assessing the performance of PTES systems with different storage configurations. At the time of writing, there is one pit storage system that is under construction and another that is being planned in Denmark, both of which are designed to be used as short-term storage systems. They will both be connected directly to the district heating grid, and neither will use a heat pump. This means that measurements from short-term PTES systems operation will be available in the near future.

CRediT authorship contribution statement

Ioannis Sifnaios: Conceptualization, Methodology, Visualization, Investigation, Data analysis, Writing - Original draft. **Adam R. Jensen:** Methodology, Visualization, Data analysis, Writing - Review & editing. **Simon Furbo:** Writing - Review & editing, Supervision, Funding acquisition. **Jianhua Fan:** Writing - Review & editing, Supervision, Funding acquisition.

Declaration of competing interest

The authors declare that they have no known competing financial interests or personal relationships that could have appeared to influence the work reported in this paper.

Acknowledgments

The authors would like to thank Lasse Kjærgaard Larsen and PlanEnergi for providing the data for the PTES in Marstal and Dronninglund, respectively, thus enabling the conduction of this study. This study was funded by the Danish Energy Agency through EUDP grant no. 64018-0134 and by the Sino-Danish Center for Education and Research (SDC) Ph.D. program.

References

[1] Danish District Heating Association, Facts about district heating in Denmark [WWW document], URL, https://www.danskfjernvarme.dk/sitetools/english/about-us, 2021 (accessed 12.17.20).
[2] S.H. Li, Y.X. Zhang, Y. Li, X.S. Zhang, Experimental study of inlet structure on the discharging performance of a solar water storage tank, Energy Build. 70 (2014) 490–496, https://doi.org/10.1016/j.enbuild.2013.11.086.

[3] D. Sveinbjörnsson, L. Laurberg Jensen, D. Trier, I. Ben Hassine, X. Jobard, Large Storage Systems for DHC Networks, 2017.
[4] M.A. Rosen, N. Pedinelli, I. Dincer, Energy and exergy analyses of cold thermal storage systems, Int. J. Energy Res. 23 (1999) 1029–1038, https://doi.org/10.1002/(SICI)1099-114X(19991010)23:12<1029::AID-ER538>3.0.CO;2-C.
[5] B. Rezaie, B.V. Reddy, M.A. Rosen, Exergy analysis of thermal energy storage in a district energy application, Renew. Energy 74 (2015) 848–854, https://doi.org/10.1016/j.renene.2014.09.014.
[6] A. Lake, B. Rezaie, Energy and exergy efficiencies assessment for a stratified cold thermal energy storage, Appl. Energy 220 (2018) 605–615, https://doi.org/10.1016/j.apenergy.2018.03.145.
[7] I. Dincer, 1.6 Exergy, in: Comprehensive Energy Systems, Elsevier, 2018, pp. 212–264, https://doi.org/10.1016/B978-0-12-809597-3.00106-1.
[8] M.A. Rosen, The exergy of stratified thermal energy storages, Sol. Energy 71 (2001) 173–185, https://doi.org/10.1016/S0038-092X(01)00036-6.
[9] M.A. Rosen, R. Tang, I. Dincer, Effect of stratification on energy and exergy capacities in thermal storage systems, Int. J. Energy Res. 28 (2004) 177–193, https://doi.org/10.1002/er.960.
[10] I. Sifnaios, J. Fan, L. Olsen, C. Madsen, S. Furbo, Optimization of the coefficient of performance of a heat pump with an integrated storage tank – a computational fluid dynamics study, Appl. Therm. Eng. 160 (2019), https://doi.org/10.1016/j.applthermaleng.2019.114014.
[11] Y.P. Chandra, T. Matuska, Stratification analysis of domestic hot water storage tanks: a comprehensive review, Energy Build. 187 (2019) 110–131, https://doi.org/10.1016/j.enbuild.2019.01.052.
[12] J. Fan, S. Furbo, Thermal stratification in a hot water tank established by heat loss from the tank, Sol. Energy 86 (2012) 3460–3469, https://doi.org/10.1016/j.solener.2012.07.026.
[13] A. Castell, M. Medrano, C. Solé, L.F. Cabeza, Dimensionless numbers used to characterize stratification in water tanks for discharging at low flow rates, Renew. Energy 35 (2010) 2192–2199, https://doi.org/10.1016/j.renene.2010.03.020.
[14] Y.M. Han, R.Z. Wang, Y.J. Dai, Thermal stratification within the water tank, Renew. Sust. Energ. Rev. 13 (2009) 1014–1026, https://doi.org/10.1016/j.rser.2008.03.001.
[15] M.Y. Haller, C.A. Cruickshank, W. Streicher, S.J. Harrison, E. Andersen, S. Furbo, Methods to determine stratification efficiency of thermal energy storage processes - review and theoretical comparison, Sol. Energy 83 (2009) 1847–1860, https://doi.org/10.1016/j.solener.2009.06.019.
[16] I. Sifnaios, A.R. Jensen, S. Furbo, J. Fan, Evaluation of stratification in thermal energy storages, in: Accepted for 8th International Conference on Renewable Energy Technologies (ICRET). Kuala Lumpur, Malaysia, 2022.
[17] M.V. Jensen, Seasonal Pit Heat Storages - Guidelines for Materials & Construction IEA-SHC Tech Sheet 45.B.3.2, 2014.
[18] T. Schmidt, T. Pauschinger, P.A. Sørensen, A. Snijders, R. Djebbar, R. Boulter, J. Thornton, Design aspects for large-scale pit and aquifer thermal energy storage for district heating and cooling, Energy Procedia 149 (2018) 585–594, https://doi.org/10.1016/j.egypro.2018.08.223.
[19] P.A. Soerensen, N. From, High solar fraction with pit heat storages, in: 30th ISES Biennial Solar World Congress 2011, SWC 2011, 2011, pp. 3020–3030, https://doi.org/10.18086/swc.2011.21.07.
[20] A.J. Kallesøe, T. Vangkilde-Pedersen, Underground Thermal Energy Storage (UTES) – State-of-the-art, Example Cases and Lessons Learned., HEATSTORE Project Report, GEOTHERMICA – ERA NET Cofund Geothermal, 2019.
[21] A. Dahash, F. Ochs, A. Tosatto, W. Streicher, Toward efficient numerical modeling and analysis of large-scale thermal energy storage for renewable district heating, Appl. Energy 279 (2020), 115840, https://doi.org/10.1016/j.apenergy.2020.115840.
[22] PlanEnergi, Design of the Pit Heat Storage of the Demonstration Plant at Marstal Fjernvarme, 2013.
[23] NMC Termonova, Thermal properties of Nomalen 28N [WWW document], /https://dms.etra.fi:9900/72192/conversions/original?version=0, https://web.archive.org/web/20220428093554, 2015 (accessed 4.28.22).
[24] NMC Termonova, Nomalen 28N [WWW Document], URL, https://web.archive.org/web/20220426161150/https://azupcs365certviewer.azurewebsites.net/api/GetSDB?env=se&articleNr=550984, 2011 (accessed 4.20.22).
[25] Dansk Fjernvarme, Inspirations-katalog om solvarme [WWW document], URL, https://www.danskfjernvarme.dk/-/media/danskfjernvarme/kurser_og_arrangementer/modematerialer/temamoder/2017/temadag-om-etablering-og-drift-af-solvarme/inspirationskatalog-om-solvarme.pdf, 2017 (accessed 1.6.22).
[26] Dronninglund Fjernvarme, Niras PlanEnergi, Dronninglund solar thermal plant [WWW document], URL, https://planenergi.dk/wp-content/uploads/2017/06/Brochure_Dronninglund_2015_booklet_ENG_web_.pdf, 2014 (accessed 1.6.22).
[27] PlanEnergi, Sunstore 3 - Phase 2: Implementation, 2015.
[28] E. Andersen, S. Furbo, J. Fan, Multilayer fabric stratification pipes for solar tanks, Sol. Energy 81 (2007) 1219–1226, https://doi.org/10.1016/j.solener.2007.01.008.
[29] L. Wu, R.B. Bannerot, An experimental study of the effect of water extraction on thermal stratification in storage, in: Proceedings of the 1987 ASME-JSME-JSES Solar Energy Conference, Honolulu, 1987, pp. 445–451.
[30] M.A. Rosen, I. Dincer, Effect of varying dead-state properties on energy and exergy analyses of thermal systems, Int. J. Therm. Sci. 43 (2004) 121–133, https://doi.org/10.1016/j.ijthermalsci.2003.05.004.
[31] A.R. Jensen, Investigation of a Pit Thermal Energy Storage - CFD Simulations and Experimental Analysis, Technical University of Denmark (DTU), 2018.
[32] I. Dincer, M.A. Rosen, Thermal Energy Storage: Systems and Applications, Wiley, 2002.

II. Evaluation of stratification in thermal energy storages

Ioannis Sifnaios, Adam R. Jensen, Simon Furbo, and Jianhua Fan

Renewable Energy Systems in Smart Grid, 57-69 (2022)

II

Evaluation of stratification in thermal energy storages

Ioannis Sifnaios[1,2,*[0000-0003-0933-2952]], Adam R. Jensen[1[0000-0002-5554-9856]], Simon Furbo[1[0000-0003-2578-4780]] and Jianhua Fan[1[0000-0003-0936-6677]]

[1] DTU Civil and Mechanical Engineering, Technical University of Denmark, Kgs. Lyngby, Denmark
[2] Sino-Danish College (SDC), University of Chinese Academy of Sciences, Beijing, China
*iosif@byg.dtu.dk

Abstract. Thermal stratification in water-based storages can be destroyed by mixing, heat diffusion, and thermal conduction. For this reason, the evaluation of stratification in water-based thermal energy storages is important for assessing their performance. The most promising indicators were identified and assessed based on their suitability for use in practical applications. The selected stratification indicators were calculated for four simulated storage scenarios comprising a fully stratified, a fully mixed, and two realistic storages. It was found that most indicators had severe limitations in their application. For this reason, a new indicator called internal exergy destruction was proposed, which can be used in combination with the overall exergy efficiency for assessing the performance and stratification of thermal energy storages. The main benefit of internal exergy destruction is that it can be used to compare storages with different heat loss coefficients. In addition, it separates the effects of mixing from the heat losses and is easily applied to real-life storages.

Keywords: Thermal stratification, Heat storage, Exergy analysis.

1 Introduction

Thermal energy storages (TES) are often used for bridging the time gap between heat generation and heat demand, especially when using non-dispatchable renewable energy sources [1]. Thermal energy is stored in a TES using heating or cooling in order to be used later. The thermal performance of a heating system utilizing a TES is strongly influenced by stratification. Stratification occurs when a temperature gradient in the TES separates fluid at different temperatures. One study found that by creating stratification in a TES with the use of a diffuser, increased the heating system's coefficient of performance (COP) by 32% compared to having a fully mixed tank [2].

However, achieving a good thermal stratification inside a TES is challenging due to mixing induced by the inlet flow, heat diffusion caused by natural convection in the TES, and downward thermal conduction [3]. The TES geometry, diffuser design, and operation strategy strongly influence the level of stratification. For this reason, it is critical to be able to quantify the degree of stratification inside a TES.

Usually, stratification indicators are used to assess stratification in a TES. Expressions have been developed that can be applied to any water-based heat storage that is directly charged/discharged, i.e., does not use a heat exchanger, e.g., in district heating tanks, domestic hot water tanks, pit thermal energy storages, etc.

Haller et al. summarized most of the available stratification indicators [4]. The same study employed some of these indicators to characterize a theoretical TES case comprised of one charge, standby, and discharge period. The study pointed out that all of the available methods have some drawbacks, e.g., some of them cannot be used for both charge and discharge, whereas others fail to separate the effects of heat losses from mixing. Overall, the study concluded that the available stratification indicators had limitations in their applications. However, the investigated simulation case was very simplified, including only mixing around the inlet and outlet of the storage and did not include heat losses to the ambient and thermal conduction between the water layers.

This study identifies the most promising stratification indicators for assessing the stratification in thermal energy storages for practical applications. The indicators are evaluated on how well they can be used to determine stratification inside a thermal energy storage. Finally, it suggests a new indicator for assessing stratification in TES.

2 Methods

First, the stratification indicators used in this study are presented, namely the MIX number, stratification coefficient, exergy efficiency, and overall exergy efficiency, followed by a description of the investigated scenarios.

2.1 MIX number

The MIX number is a dimensionless indicator that quantifies the degree of mixing inside a TES by comparing it to a fully mixed and a fully stratified reference storage [5]. Its range is between zero and one, corresponding to a perfectly stratified and a fully mixed tank, respectively. The MIX number is defined as the ratio of the difference in the moment of energy between a perfectly stratified storage and actual storage to the difference in the moment of energy between a perfectly stratified storage and a fully mixed one:

$$MIX = \frac{M_E^{stratified} - M_E^{actual}}{M_E^{stratified} - M_E^{fully-mixed}} \quad (1)$$

The moment of energy is calculated for the two theoretical reference cases (stratified and fully mixed) such that they have the same energy content as the actual storage. To calculate the MIX number, the storage is divided into discrete layers (typically corresponding to the number of temperature sensors). The moment of energy for each layer is then calculated by weighing each layer's energy content with the height from the bottom of the storage to the centroid of the layer. The total moment of energy of the storage is then calculated as the sum of all layers, as seen in Equation (2).

$$M_E = \sum_{n=1}^{N} \rho_i \cdot V_i \cdot C_{p,i} \cdot \left(T_i - T_{ref}\right) \cdot z_i \tag{2}$$

Where N is the total number of layers in the storage, ρ_i is the water density, V_i is the water volume of the layer, $C_{p,i}$ is the specific heat, T_i is the water temperature, and z_i is the distance from the center of the layer to the bottom of the storage. T_{ref} is the reference temperature, meaning the temperature at which the storage is considered empty.

2.2 Stratification coefficient

The stratification coefficient expresses the degree of stratification based on the mass-weighted square of the difference of the actual storage temperature to the mean storage temperature [6]:

$$St = \sum_{n=1}^{N} \frac{m_i \cdot \left(T_i - T_{avg}\right)^2}{m_{total}} \tag{3}$$

Where T_i is the temperature of each layer, m_i is the mass of each layer, T_{avg} is the average storage temperature, and m_{total} is the total mass of the storage.

2.3 Exergy efficiencies

There are several expressions suggested regarding exergy efficiency. In this study, the two expressions presented by Haller et al. [7] and Rosen et al. [8] are used.

Haller et al. define the exergy efficiency as the internal exergy loss of an experimental TES relatively to the internal exergy destruction of a fully mixed TES:

$$\eta_{st,\xi} = 1 - \frac{\Delta\xi_{destr,exp}}{\Delta\xi_{destr,mix}} \tag{4}$$

Where the internal exergy destruction is found through the exergy balance of the TES, using Equation (5):

$$\Delta\xi_{int,destr} = \Delta\xi_{flow} - \Delta\xi_{store} - \Delta\xi_{heat\ loss} \tag{5}$$

The fully mixed storage is simulated with the same flow rate, inlet temperature, and heat loss coefficient as the experimental storage. For further details, the reader is referred to the paper by Haller et al. [7].

Conversely, Rosen et al. used a general expression for the overall exergy efficiency of a TES, comparing the exergy recovered from the TES to the exergy input of the TES, as defined in Equation (6).

$$\eta_{overall} = \frac{\xi_{output}}{\xi_{input}} \tag{6}$$

It has to be noted that the two expressions are very different in their application, i.e., the former gives information about the precise time when mixing occurs during one storage cycle. In contrast, the latter gives an overall efficiency for one TES cycle.

2.4 Simulated scenarios

In order to demonstrate the performance of the investigated stratification indicators, four idealized storage scenarios were simulated. Mixing was implemented using the methodology recommended by Haller et al. [7].

The investigated scenarios were a fully stratified storage, a fully mixed storage, and two realistic storages. Each case was investigated for two full charge/discharge cycles. The scenarios have been simulated, including and excluding heat losses. The heat loss coefficient used in the simulations was selected such that the "realistic scenario 1" has an energy efficiency of 90%. It has to be noted that the effect of the storage walls was neglected.

Table 1. Simulation parameters.

Parameter	Value	Unit
Storage volume	1	m^3
Water density	980	kg/m^3
Water specific heat capacity	4200	J/(kg K)
Charging temperature	90	°C
Discharging temperature	45	°C
Threshold temperature	10	°C
Number of nodes	60	-
Time step duration	1	min
Flow rate charge/discharge	980	kg/hr
Heat loss coefficient	6	$W/(m^2 K)$
Effective vertical thermal conductivity	2.5	W/(m K)
Storage height	1	m

Each storage was charged using a constant temperature of 90 °C and discharged with a constant inlet temperature of 45 °C. The time step of the simulation was 1 minute, such that the charged/discharged flow was equal to the volume of one node. This ensured that numerical diffusion was avoided. An overview of the simulation parameters is presented in Table 1. Note that constant values for ρ_i and $C_{p,i}$ were used in order to simplify the simulations and focus on mixing effects. In addition, the value of the effective thermal conductivity was set to 2.5 W/(m K) as suggested by Haller et al. [7].

Fully stratified scenario. There is no mixing between the tank nodes and no vertical heat conduction inside the tank in this scenario. Essentially the flow during charge and discharge is simulated as plug flow.

Fully mixed scenario. In the fully mixed scenario, the temperature of the water entering the tank at each time step is instantaneously mixed with the temperature of the rest of the storage.

Realistic scenarios. The realistic case mimics the actual conditions inside a storage, hence the naming. In this scenario, as water enters the storage, the nodes' temperatures close to the inlet are mixed, simulating the inlet jet-mixing phenomenon. Two variations of the realistic scenario were simulated, corresponding to a better performing and a worse performing diffuser. For the case of the better diffuser, denoted from now on as realistic scenario 1, the total tank volume used for imitating the inlet jet mixing was approximately 10% of the tank's total volume. Similarly, for the case of the worse diffuser, denoted from now on as realistic scenario 2, 20% of the entire tank volume was used. The rest of the simulation conditions were the same for the two realistic scenarios. After mixing, vertical heat conduction was applied between the tank nodes based on the temperature distribution in the storage. Last, heat losses to the ambient were calculated based on the temperature difference between the storage nodes and the ambient temperature (for the cases where heat losses were enabled). An illustration of the investigated storage during charging and discharging is presented in Fig. 1.

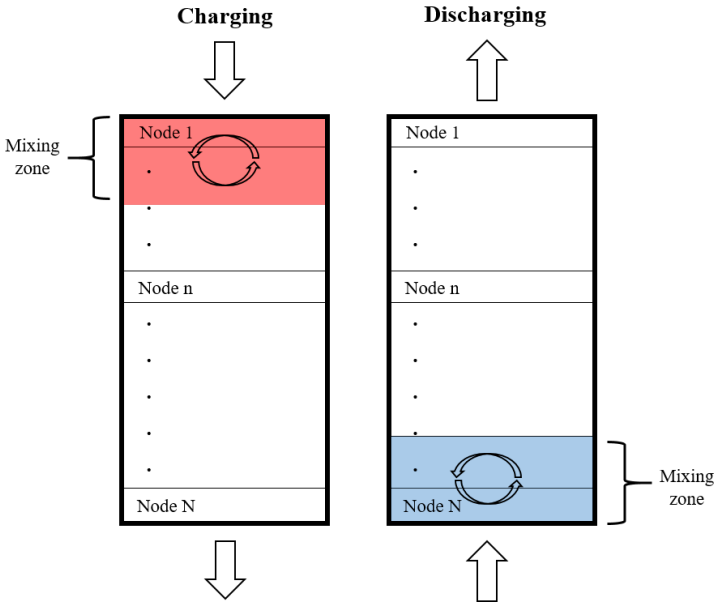

Fig. 1. Illustration of the tank charging and discharging.

2.5 Charging and discharging conditions

The storage in each simulation starts with charging and is initialized as empty, i.e., having a uniform temperature of 45 °C. The storage immediately switches from charging (operation=1) to discharging (operation=0), or vice versa, when the storage

is identified as empty or full. The criteria for the storage being full or empty were implemented using a threshold temperature for the top and bottom node, as indicated in Equation (7).

$$operation = \begin{cases} 1, if \;\; T_{bottom} \geq T_{charge} - T_{threshold} \\ 0, if \;\; T_{top} \leq T_{discharge} + T_{threshold} \end{cases} \quad (7)$$

The temperature profile inside the tank during the two storage cycles is presented in Fig. 2. The top figure shows the temperature profile for the realistic scenario 1 without heat losses, while the bottom figure is the same case but includes heat losses. It can be observed that the presence of heat losses lowers the temperature in the tank, predominantly at the top of the storage, and also slightly increases the required time to charge the storage.

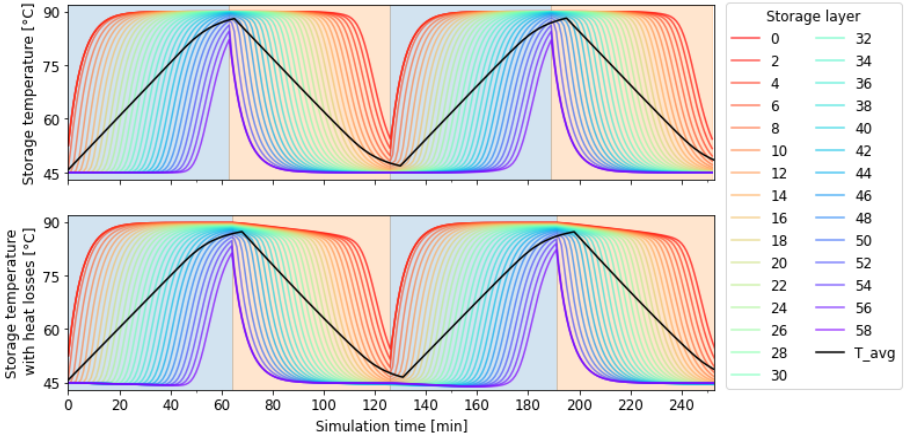

Fig. 2. Temperature profile in the storage for the realistic scenario 1. The top figure does not include heat losses.

3 Results

The results of the calculated stratification indicators are presented in Fig. 3 - Fig. 6. Each indicator is applied to all the possible storage scenarios, i.e., fully mixed (with and without heat losses), realistic 1 and 2 (with and without heat losses), and fully stratified. The fully stratified scenario is only simulated without heat losses since if heat losses did occur, it would no longer be a fully stratified case.

3.1 MIX number

As expected, the MIX number for the fully mixed storage is constantly equal to one, regardless of heat losses. Similarly, the MIX number is always equal to zero for the fully stratified storage. For the realistic storages, the MIX number varies throughout the storage cycles. This is partly because the MIX number is strongly affected by the

energy content of the storage. Large spikes can be noticed at high (fully charged) and low (fully discharged) energy contents in the MIX number because a fully charged and discharged storage is considered not stratified.

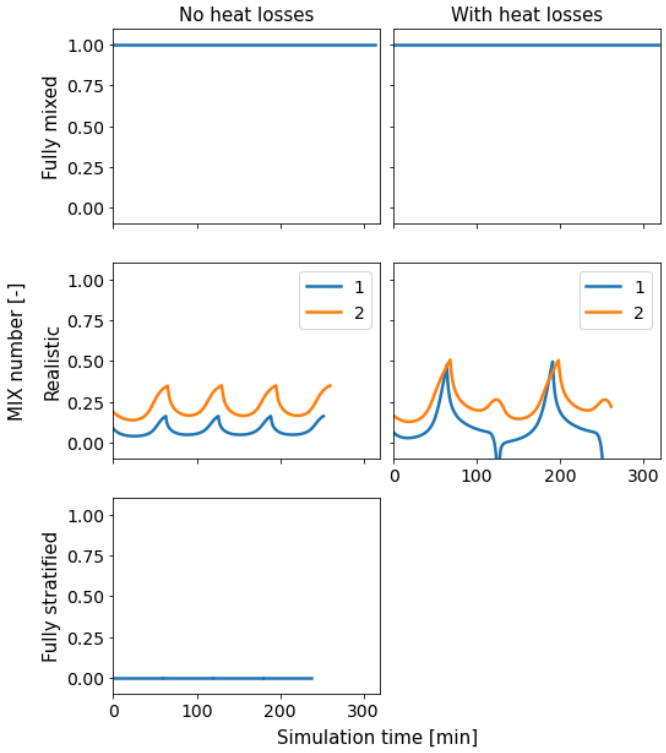

Fig. 3. MIX number for the investigated storages.

By comparing the two realistic storages, it is clear that a worse performing diffuser (case 2) creates more mixing in the TES; thus, it has a higher MIX number. By adding heat losses to the simulation, the MIX number shows the storage to be more stratified during discharging than charging. In fact, the MIX number becomes negative for a few time steps for Case 1, as the heat losses bring the average storage temperature below the reference temperature. While the MIX number does provide some use in comparing similar storages, it is difficult to draw a conclusion regarding stratification. In addition, it is highly influenced by the heat losses and the choice of the reference temperature.

3.2 Stratification coefficient

For the fully mixed storage, the stratification coefficient was zero since there was a uniform temperature in the storage at all times. The stratification coefficient was proportional to the energy content for the fully stratified storage and ranged from 0 to approximately 500 K^2. The values were between the two ideal cases for the realistic cases, with a maximum of approximately 400 K^2 and 300 K^2 for cases 1 and 2, respectively. The results of this indicator are much easier to interpret than the MIX

number and were more useful in comparing the two storages. Similar to the MIX number, the stratification coefficient shows a low level of stratification when the storage is almost full or empty. However, this indicator has the benefit of not depending on a reference temperature and, therefore, never becomes negative.

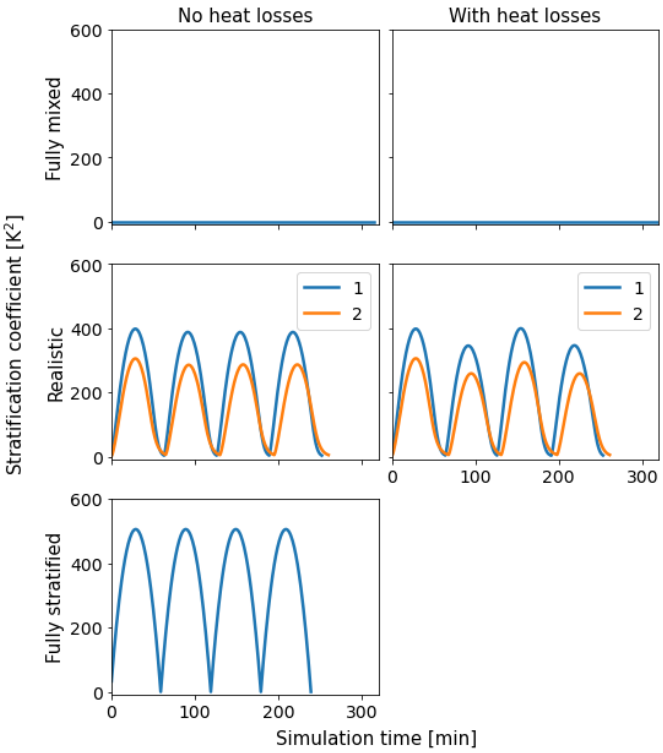

Fig. 4. Stratification coefficient for the investigated storages.

Nonetheless, the absolute value of the stratification coefficient has no physical meaning and, like the MIX number, is affected by heat losses. When applying heat losses to the realistic cases, the stratification coefficient shows a smaller degree of stratification during discharging compared to charging. This is because, when charging, the temperature at the top of the storage is constantly 90 °C, while during discharge, the top temperature decreases due to heat losses, as can be seen in Fig. 2. This leads to a lower stratification coefficient during discharge. Overall, this indicator can be used to compare the stratification degree in two storages, but one needs to be cautious when the two storages have different heat loss coefficients.

3.3 Exergy efficiencies

In Fig. 5, the exergy efficiency of the investigated storages is presented. As expected, the fully mixed storage had an exergy efficiency of 0%, while the fully stratified had an efficiency of 100%. Again, the realistic storages had an efficiency between the

other two, and applying heat losses reduced the exergy efficiency. The method of Haller et al. [7] gives significantly different results compared to the MIX number and the stratification coefficient.

However, it is difficult to apply Haller's exergy efficiency method to real-life scenarios. This method can only be applied for specific, well-defined time periods in the storage operation. For example, it requires a clear distinction between the charge and discharge periods, which in some cases is not possible, e.g., for storages that are used both for short and long-term storage. In addition, it can only be used if the charging and discharging mass flow and inlet temperature are constant during the storage operation.

In general, the methods that compare a real-life storage with reference fully mixed or fully stratified cases, i.e., the MIX number and exergy efficiency, are difficult to use in practice.

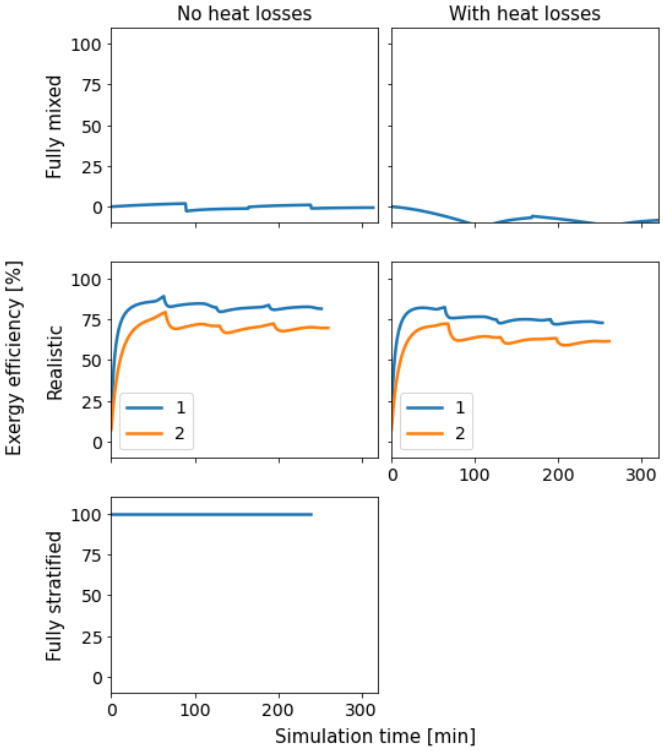

Fig. 5. Exergy efficiency for the investigated storages.

The overall exergy efficiency, presented in Table 2, is considered the most reliable indicator of stratification performance. This table gives information about the percentage of exergy lost due to mixing and heat losses. For example, the realistic storage 1 has a 10% lower efficiency due to mixing compared to the fully stratified storage, but 18% lower exergy efficiency, including mixing and heat losses.

Table 2. Overall exergy efficiency for investigated storages.

Overall exergy efficiency	Value [%]
Fully mixed storage	54
Fully mixed with heat losses	51
Realistic storage 1	90
Realistic storage 1 with heat losses	82
Realistic storage 2	85
Realistic storage 2 with heat losses	77
Fully stratified storage	100

In order to get information about the precise time when mixing occurred in the storage, it is suggested to use the internal exergy destruction as given in Equation (5). Exergy destruction gives the amount of exergy lost in the storage due to mixing caused by inlet jet mixing and vertical thermal conduction. Since the exergy loss due to heat losses is subtracted from the expression, the internal exergy destruction can be used for comparing the amount of mixing in two or more storages, even if they do not have the same heat loss coefficient.

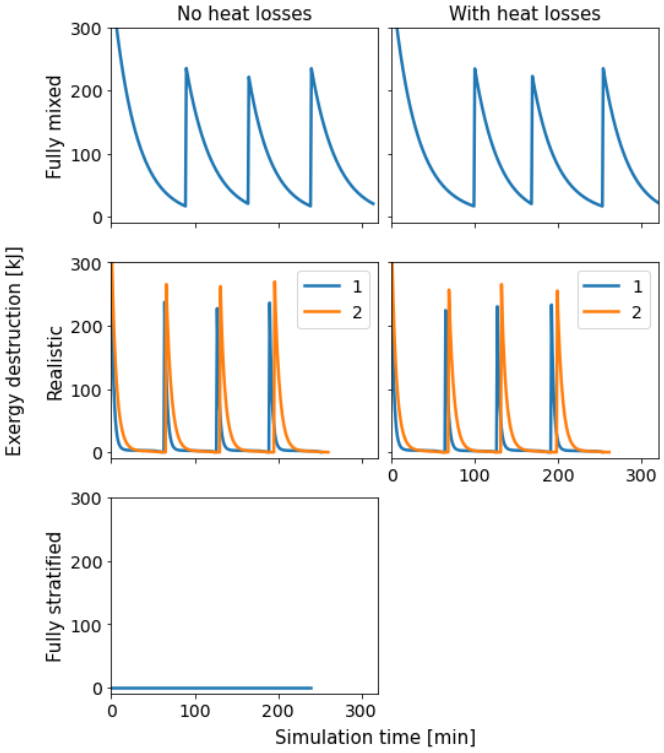

Fig. 6. Internal exergy destruction for the investigated storages.

Fig. 6 presents the internal exergy destruction for the investigated storages. It can be observed that, apart from the fully stratified storage, the exergy destruction mainly occurs at the start of the charge and discharge period, as this is when the thermocline develops. In the case of the realistic storage 1, which is well stratified, the exergy destruction only occurs at the beginning of charge and discharge and is close to zero during most of the storage operation. However, for a less stratified tank (e.g., for the realistic storage 2), the internal exergy destruction occurs over a longer period, as it takes longer to build up the thermocline. In addition, the internal exergy destruction remains essentially the same regardless of heat losses, allowing the comparison of the level of stratification independent from the heat losses.

4 Conclusions

This paper investigated stratification for four different storage scenarios: a fully mixed, a fully stratified, and two realistic scenarios. Four stratification indicators were assessed from the literature: the MIX number, stratification coefficient, exergy efficiency, and overall exergy efficiency.

Apart from the overall exergy efficiency, all the other investigated indicators had significant drawbacks leading to either results that were difficult to interpret or results applicable to specific, well-defined periods in the storage operation. It is suggested to use the overall exergy efficiency and supplement it with the internal exergy destruction for assessing stratification in a storage. The overall exergy efficiency gives a thermodynamically based quantification of the stratification performance of a TES. The internal exergy destruction can then be used to illustrate the specific times at which mixing occurs in the storage. The main benefit of these two methods is that they do not rely on a fully mixed or fully stratified reference storage simulation, which can be difficult or impossible to implement in real-life cases.

Applying the recommended methods to real-life storages is a topic of future work. It is believed that they have a great potential for comparing the stratification among storages since they can be applied to all storages regardless of their use, e.g., short term, long term, or combination of the two.

References

1. Li, S.H., Zhang, Y.X., Li, Y., Zhang, X.S.: Experimental study of inlet structure on the discharging performance of a solar water storage tank. Energy Build. 70, 490–496 (2014). https://doi.org/10.1016/j.enbuild.2013.11.086
2. Sifnaios, I., Fan, J., Olsen, L., Madsen, C., Furbo, S.: Optimization of the coefficient of performance of a heat pump with an integrated storage tank – A computational fluid dynamics study. Appl. Therm. Eng. 160, (2019). https://doi.org/10.1016/j.applthermaleng.2019.114014
3. Fan, J., Furbo, S.: Thermal stratification in a hot water tank established by heat loss from the tank. Sol. Energy. 86, 3460–3469 (2012). https://doi.org/10.1016/j.solener.2012.07.026
4. Haller, M.Y., Cruickshank, C.A., Streicher, W., Harrison, S.J., Andersen, E., Furbo, S.: Methods to determine stratification efficiency of thermal energy storage processes - Re-

view and theoretical comparison. Sol. Energy. 83, 1847–1860 (2009). https://doi.org/10.1016/j.solener.2009.06.019
5. Andersen, E., Furbo, S., Fan, J.: Multilayer fabric stratification pipes for solar tanks. Sol. Energy. 81, 1219–1226 (2007). https://doi.org/10.1016/j.solener.2007.01.008
6. Wu, L., Bannerot, R.B.: An experimental study of the effect of water extraction on thermal stratification in storage. In: Proceedings of the 1987 ASME-JSME-JSES Solar Energy Conference, Honolulu. pp. 445–451 (1987)
7. Haller, M.Y., Yazdanshenas, E., Andersen, E., Bales, C., Streicher, W., Furbo, S.: A method to determine stratification efficiency of thermal energy storage processes independently from storage heat losses. Sol. Energy. 84, 997–1007 (2010). https://doi.org/10.1016/j.solener.2010.03.009
8. Rosen, M.A., Pedinelli, N., Dincer, I.: Energy and exergy analyses of cold thermal storage systems. Int. J. Energy Res. 23, 1029–1038 (1999). https://doi.org/10.1002/(SICI)1099-114X(19991010)23:12<1029::AID-ER538>3.0.CO;2-C

Acknowledgements

This study was funded by the Danish Energy Agency through EUDP grant no. 64018-0134 and by the Sino-Danish Center for Education and Research (SDC) Ph.D. program.

III. Dronninglund water pit thermal energy storage dataset

Ioannis Sifnaios, Geoffroy Gauthier, Daniel Trier, Jianhua Fan, and Adam R. Jensen

Solar Energy, 251, 68-76 (2023)

Solar Energy 251 (2023) 68–76

Contents lists available at ScienceDirect

Solar Energy

journal homepage: www.elsevier.com/locate/solener

III

Dronninglund water pit thermal energy storage dataset

Ioannis Sifnaios [a,b,*], Geoffroy Gauthier [c], Daniel Trier [c], Jianhua Fan [a,*], Adam R. Jensen [a]

[a] Department of Civil and Mechanical Engineering, Technical University of Denmark, Koppels Allé, Building 404, 2800 Kgs. Lyngby, Denmark
[b] Sino-Danish College (SDC), University of Chinese Academy of Sciences, Beijing, China
[c] PlanEnergi, Nørregade 13, 1165 København K, Denmark

ARTICLE INFO

Keywords
Heat storage
Seasonal storage
Data analysis
Python
PTES

ABSTRACT

Water pit heat storage has been proven a cheap and efficient storage solution for solar district heating systems. The 60,000 m^3 pit storage in Dronninglund represents in many ways the state-of-the-art large-scale heat storage, demonstrating a storage efficiency higher than 90% during its operation. The storage is used for seasonal and short-term heat storage of solar heat generated by a 37,573 m^2 solar collector field and supplies heat directly to the district heating grid or is used during winter as an alternative heat source to a heat pump. This study aims to provide an overview of the available information on the Dronninglund water pit heat storage, including a detailed description of the design, ground conditions, and operating strategy. The used dataset (2014–2020) has been the foundation for most investigations and simulations of pit thermal energy storages. However, due to a lack of public documentation, various studies have used different post-processing methods and assumptions, leading to inconsistent results. Therefore, the dataset has been manually quality-controlled, and erroneous data have been removed with the aim of establishing a high-quality reference dataset. Moreover, an overview of the available parameters and metadata is provided, along with example plots. To promote the usage of the quality-controlled dataset, all the developed quality-control routines and Python scripts are made available on GitHub.

1. Introduction

In Denmark, where 64% of residential consumers use district heating, incorporating large-scale solar heating plants has become increasingly popular after 2010. Due to the seasonal mismatch between solar heat generation and heat demand, typical district heating systems are limited to achieving a solar thermal fraction of up to 20% (Perez-Mora et al., 2018). To cover this mismatch, seasonal heat storage systems have been used to store the produced thermal energy in summer and use it in winter. By incorporating a seasonal heat storage, the solar thermal fraction of a district heating system can increase up to 50% (Sveinbjörnsson et al., 2017). Four main types of thermal energy storages have been utilized so far for seasonal thermal energy storage (TES), namely, tanks (TTES), boreholes (BTES), aquifers (ATES), and pit thermal energy storages (PTES) (Pauschinger et al., 2018).

The main driver for the PTES technology was to develop a low-cost heat storage for solar district heating systems. PTES systems have been demonstrated combined with large-scale collector fields providing a promising storage solution (Soerensen and From, 2011). Due to the simple storage design, it has been possible to achieve costs below 27 €/m^3 (Schmidt et al., 2018).

In principle, a PTES is a large water reservoir lined with a watertight polymer liner (to prevent water from leaking to the ground) and covered with a floating insulating lid (to reduce heat losses). At the moment of writing, there are six operational pit storages in the world, located in Denmark and Tibet, China. The Danish PTES systems are located in Marstal (75,000 m^3) (Jensen, 2014), Vojens (200,000 m^3) (Rambøll, 2015), Toftlund (70,000 m^3) (Rambøll, 2016), Gram (122,000 m^3) (PlanEnergi, 2015a), and Dronninglund (60,000 m^3) (Schmidt and Sørensen, 2018). In Tibet, there is a PTES in Langkazi (15,000 m^3) (Aalborg CSP, 2019). Apart from these storages, there is a 70,000 m^3 PTES under construction in Høje Taastrup, Denmark, and detailed plans have been made for two storages in Odense, Denmark.

The performance of the existing PTES varies, with Gram having an efficiency of 60% (PlanEnergi, 2020), Marstal 66% (Schmidt, 2019), Toftlund 70% (Rambøll, 2020), and Dronninglund greater than 90% (Winterscheid and Schmidt, 2017). The difference in efficiencies is mainly due to different technologies used for the PTES components (especially the lid) but also due to improved PTES construction. It has to be noted that it was not possible to find information on the performance

* Corresponding authors.
E-mail addresses: iosif@dtu.dk (I. Sifnaios), jifa@dtu.dk (J. Fan).

https://doi.org/10.1016/j.solener.2022.12.046
Received 15 November 2022; Received in revised form 14 December 2022; Accepted 27 December 2022
Available online 17 January 2023

Fig. 1. Aerial view of the PTES and solar collector field in Dronninglund.

of the PTES systems in Vojens and Tibet.

The water pit heat storage in Dronninglund (see Fig. 1) represents, in many ways, the state-of-the-art heat storage technology. For this reason, the majority of investigations and simulations of PTES have used this storage as a reference case, e.g., Dahash et al. (2020,2019), Gauthier (2020), Ochs et al. (2020), Sorknæs (2018), Xie et al. (2021), Pan et al. (2022), Sifnaios et al. (2022).

Nonetheless, some reports for the storage in Dronninglund are only available in Danish. This has led some previously published articles (e.g., Dahash et al. (2021) and Dahash et al. (2020)) to report different ground properties and groundwater levels compared to the official measurement reports. In addition, the published studies are generally limited to only using one or two years of data, even though the storage has been in operation for more than seven years.

However, since the spring of 2021, the operation data of the Dronninglund PTES has been obtained from the Danish company PlanEnergi. According to the data license agreement with the plant, data has not been made available online.

The main objective of this article is to summarize the available knowledge on the Dronninglund PTES and give a detailed explanation of its design and operation. The paper also aims to make interested parties aware of the value of a comprehensive dataset and establish a standardized post-processing procedure, to avoid erroneous measurements being used. Additionally, the paper provides users with an overview of available parameters, which have not been published before, and references to existing documentation of the system, along with the available metadata. Finally, it provides code examples of how to use the data. The developed code is publicly available on the GitHub repository https://github.com/PitStorages/DronninglundData, along with the data for the first year of the plant's operation for testing the code.

The present paper provides a description of the Dronninglund PTES, briefly introducing the storage design and construction. Afterward, information about the location and type of measurement sensors is presented, followed by a description of the data quality control procedure and handling of missing data. Last, several example plots using the quality-controlled dataset are presented.

2. Storage description

Dronninglund is a Danish town in Northern Jutland with approximately 1,350 district heating (DH) consumers and an annual heat demand of approximately 40 GWh (12 MW peak load) (Dronninglund Fjernvarme, 2020). The research project SUNSTORE 3 started in 2008, intending to demonstrate seasonal heat storage coupled with a solar thermal collector field and a heat pump. A 60,000 m^3 pit thermal energy storage (PTES), 37,573 m^2 of flat-plate solar collectors, and an absorption heat pump were constructed as part of the project. The solar collectors installed were Arcon 35/10 HEATstore collectors with insulating foil (Epp, 2014). The cost related to the storage was approximately 2.3 million € (38.3 €/m^3), while the total project cost was approximately 14.1 million € (PlanEnergi, 2015b). The project costs are presented in Table 1.

Table 1
Project costs (PlanEnergi, 2015b).

Component	Cost [€]
Solar collectors	5,856,000
Solar field, excavation, and mounting of pipes	321,000
District heating pipes	985,000
Transmission pipe, excavation, and mounting	344,000
Technique building	3,201,000
Storage heat exchangers, pumps, valves, pipes, diffusers	350,000
Storage excavation and landscaping	673,000
Storage lid and liner	1,263,000
Other costs	1,137,000

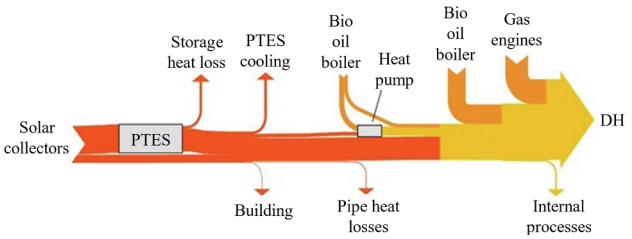

Fig. 2. Schematic of the expected energy flows for the original plant (modified from Winterscheid and Schmidt, 2017).

2.1. Dronninglund heating system

The priority for the solar thermal collectors was to supply heat directly to the district heating grid. If the solar heat production was higher than the demand, the surplus heat was used to charge the PTES. In periods with low or no solar heat production, the storage could supply heat directly to the district heating grid, but only if the outlet temperature was above 75 °C. Net charging of the storage typically occurred from February to August, whereas net discharging occurred from September to January. Depending on the specific year, February, August, and September could either have net charging or discharging (see Fig. 14 for monthly charged/discharged energy).

If the temperature of the PTES was not sufficiently high, the storage was used as the low-temperature heat source for a 5.2 MW absorption heat pump (2.1 MW cooling capacity) with a COP of 1.67. The heat pump was driven by high-temperature heat from a 5 MW bio-oil boiler. The heat pump generally started operating around the start of November and continued until January or February. The inlet temperature of the heat pump's source side was 75 °C or lower (depending on the temperature at the top of the PTES), and it cooled the storage down to approximately 10 °C. The connection of the heat pump to the storage is illustrated in Fig. 3.

The absorption heat pump, the 5 MW bio oil boiler, and an additional 10 MW bio-oil boiler were located at the Søndervang district heating plant in the town, approx. 2.5 km away from the PTES. At a second location in the town, Tidselbak Alle, there was also an 8 MW natural gas boiler and four 1.6 MW natural gas engines. A Sankey diagram of the expected energy flows for the original plant is illustrated in Fig. 2, and a schematic of the plant is shown in Fig. 3.

It should be mentioned that the PTES system in Dronninglund has been significantly modified during 2022. For example, the original lid solution was replaced with a newer, improved design since the original

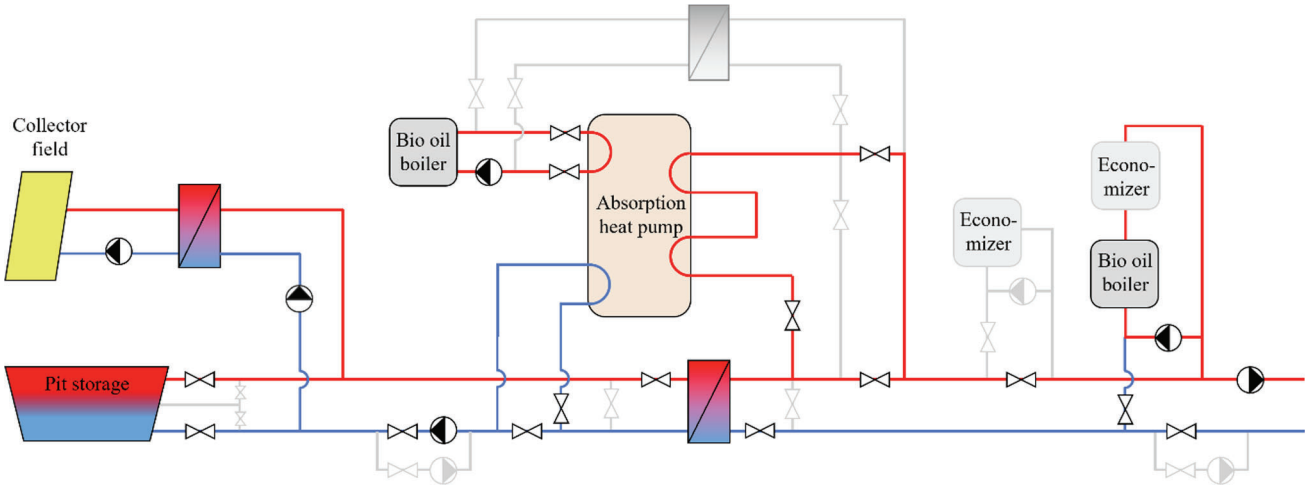

Fig. 3. Simplified schematic of the collector field, the PTES, and the components located in the Søndervang plant (modified from (PlanEnergi, 2015b)).

Fig. 4. Excavation and pipe layout in Dronninglund PTES (PlanEnergi).

Fig. 5. Installation of the bottom liner of the Dronninglund PTES (PlanEnergi).

lid was damaged beyond feasible repair. The damage was caused due to water entering the lid construction through a tear in the bottom lid liner. In addition, the absorption heat pump and bio-oil boiler were replaced by a compression heat pump. However, since the dataset is from 2014 to 2020, the information presented below refers to the original plant configuration.

2.2. Storage design and dimensions

The PTES has the shape of a truncated pyramid with a depth of 16 m and a volume of 60,000 m^3. The bottom of the pit is a square of 26 × 26 m, and the lid surface is approximately 91 × 91 m, corresponding to a surface area of 8,300 m^2. The storage sides have a slope of 1:2 in order to ensure soil stability.

Three pipes are entering the storage from below, as seen in Fig. 4. At the end of each pipe, there is a diffuser for reducing the mixing caused by the inlet jet flow, assisting in establishing a high degree of stratification in the PTES. Each diffuser consists of two parallel discs with a diameter of 2.5 m and vertical spacing of 0.58 m. The three diffusers are placed at different heights from the bottom of the storage: the top diffuser at 15.3 m, the middle diffuser at 10.9 m, and the bottom diffuser at 0.4 m. These heights are measured at the center of the diffuser opening.

2.3. Storage construction

The PTES construction started in March 2013 and was officially completed in April 2014. Different construction stages are illustrated in Figs. 4 and 5. The solar collectors' heat production (and thus the charging of the storage) began in February 2014.

The excavated soil from the pit was used to form embankments around the pit so that soil would not have to be transported off the site, thus minimizing construction costs. The soil excavation was completed after two months.

After the soil excavation and pipe installation, the PTES was lined with a polymer liner to prevent the stored water from leaking into the ground (see Fig. 5). The watertight liner was a 2.5 mm welded high-density polyethylene (HDPE) with a guaranteed lifetime of 20 years when exposed to temperatures lower than 90 °C. The liner installation took one month and was completed by mid-June 2013; afterward, it took two months to fill the storage with water.

The storage was filled with treated water from the district heating grid to avoid corrosion of the metallic components, e.g., the pipes and diffusers. As part of the water treatment, all salts were removed (including chlorides) in addition to ensuring a low hardness (<0.1 °dH), low conductivity (130 μS/cm), low iron (<0.005 mg/l), low oxygen content (<20 μg/L), and a pH value of 9.8 ± 0.2 (Klingaard and Andersen, 2018). The water quality is analyzed at least annually, and a sodium hydroxide solution is added at regular intervals to maintain the pH level.

After the storage was filled with water, the lid construction started. The original lid design was based on flexible insulation mats enclosed within a top and bottom liner. This allowed the lid to move as the water level changed due to the change of water density with temperature.

The lid insulation consisted of three 80 mm thick layers of Nomalén

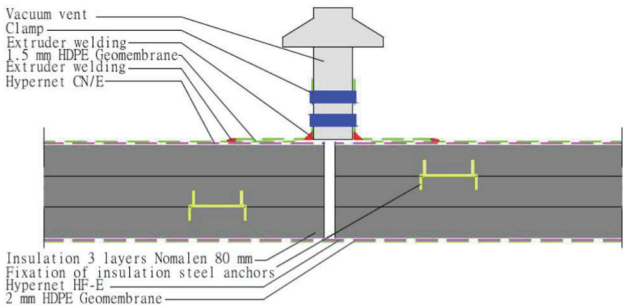

Fig. 6. Sketch of the Dronninglund lid cross-section (PlanEnergi, 2015b).

Table 2
Groundwater properties (GEO, 2012).

Parameter	Value	Unit
Hydraulic conductivity	$3.6 \cdot 10^{-5}$	m/s
Effective porosity	0.25	–
Hydraulic gradient	1/300	–
Groundwater velocity	$4.8 \cdot 10^{-7}$	m/s

Table 3
Thermal properties of soil around storage (GEO, 2010).

	Bulk density [kg/m^3]	Thermal conductivity [W/(m K)]	Specific heat capacity [J/(kg K)]
Above groundwater	1830	0.3–0.5	800
Below groundwater	2040	1	1632

28 N insulation mats manufactured by NMC (NMC Termonova, 2011). Nomalén is made of a closed-cell structure polyethylene (PE) foam with an operating temperature of up to 95 °C. The manufacturer stated that the thermal conductivity of the insulation was 0.04 W/(m K) at 10 °C (NMC Termonova, 2015). Analysis of the operation data showed that the long-term average value of the insulation's thermal conductivity was 0.047 W/(m K) since it was exposed to temperatures up to 90 °C. Nonetheless, it has to be mentioned that the heat flux through the lid was measured at a specific spot in the lid, thus it is not necessarily representative of the heat flux through the entire lid and might underestimate the actual heat flux at times.

Concrete-filled weight pipes were placed inside and on top of the lid. The pipe diameter was increased closer to the center of the lid, creating a slope towards the center. Due to the sloped surface, rainwater was collected at the center of the lid, where it was pumped off the lid's surface. Removal of rainwater is one of the biggest challenges with the PTES lid designs, and inadequate handling of rainwater increases maintenance, heat losses, and shortens the lifetime of the lid.

Additionally, vacuum vents were installed close to the lid's edge to ventilate the interior of the lid construction. Some of the vents were modified in order to allow cold, dry air to be drawn into the lid, where it would absorb heat and moisture. The warm, humid air was vented out by the remaining vents creating natural ventilation. A cross-sectional view of the original lid's construction is shown in Fig. 6.

2.4. Soil and groundwater properties

During the pre-feasibility study, the Danish company GEO was hired to carry out geological investigations, which included measurements of the groundwater level, soil characterization, and estimation of the soil thermal properties. The groundwater level was found to be 1–1.5 m below the bottom of the storage and flowing north to south with an estimated velocity of 15 m/year (GEO, 2012). The same report mentions

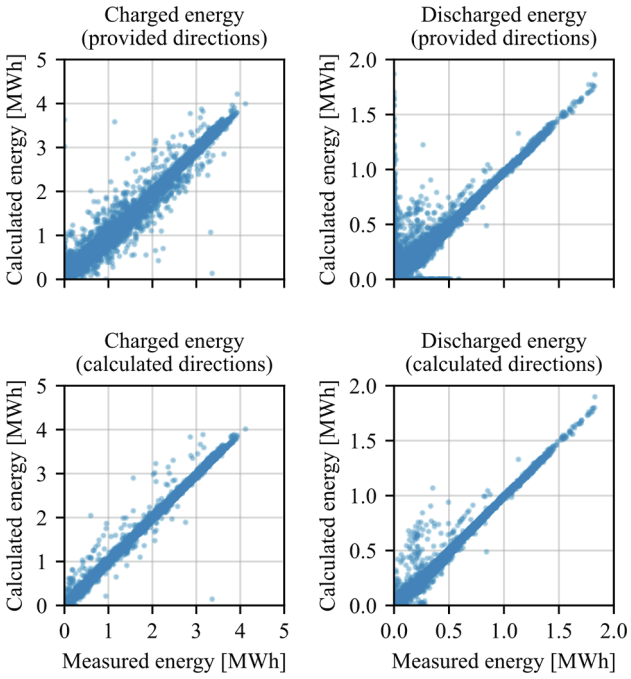

Fig. 7. Calculated charged and discharged energy using the provided and the calculated flow rates, and comparison to the measured energy quantities.

that the groundwater table is not entirely flat (there is a slope of around 1%) and stresses the fact that the depth of groundwater depends on the period of the year, as rainfall, snowmelt, and dry periods can affect it. Nonetheless, in temperate-cold climates (like Denmark), the seasonal level of change for groundwater is below 10% (Nygren et al., 2020). The groundwater properties are presented in Table 2.

Soil investigations revealed that the surrounding soil type is mainly fine sand with a few clay layers (PlanEnergi, 2011). The thermal properties of the soil surrounding the storage were reported by GEO (2010) and are presented in Table 3. According to the report, the soil thermal conductivity was estimated based on theoretical values. The specific heat capacity was not reported and thus has been estimated from the soil type, based on the research from Hamdhan and Clarke (2010).

2.5. Storage flow rates

The PTES is charged by the solar collector field via a heat exchanger. During the PTES charge, water can enter the storage via the top or middle diffuser, depending on its temperature and storage operation. Similarly, water can either be drawn from the middle or top diffuser during discharge.

It has to be mentioned that the magnitude and direction of the storage flows were only measured for the middle diffuser. For the top and bottom diffusers, the flow rates and directions reported in the dataset were calculated by the SCADA control system. However, using the provided data for flows results in a significant mass-flow mismatch of the storage (large imbalance between entering and exiting flows). Therefore, the authors have developed a method for deriving the flow magnitudes and directions based on the energy and mass-flow balance of the storage.

There are three diffusers with each two possible flow directions (in or out), and as a result, there are six unique combinations of flow directions. One of the six combinations could be: flow into the storage through the top and middle diffusers (positive direction) and flow out of the storage through the bottom diffuser (negative direction). For each possible combination of flow directions, the flow and energy balances of the storage were calculated for each time step. The mismatch in the flow and energy balances was then normalized using their standard

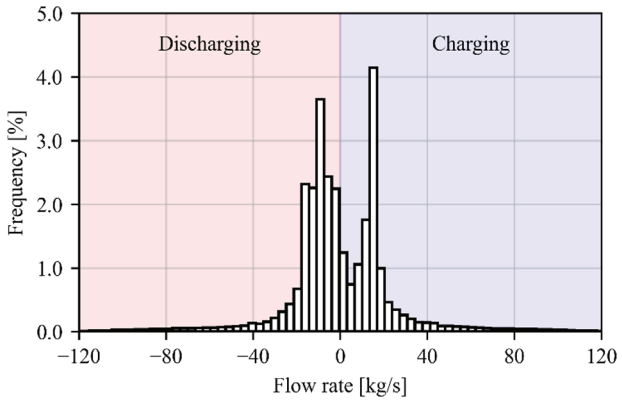

Fig. 8. Histogram with the flow rates used during charging and discharging.

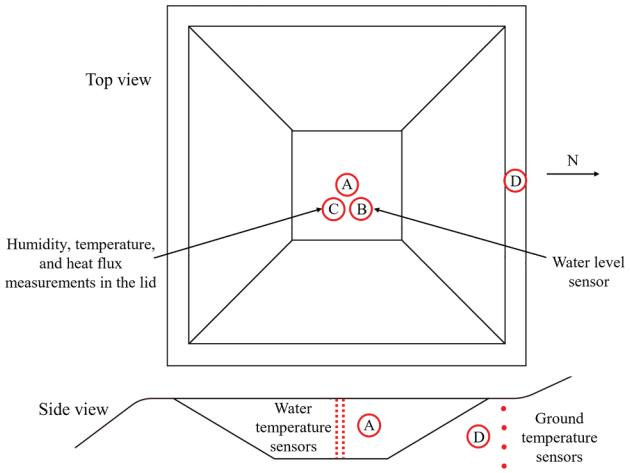

Fig. 9. Measurement locations in and around the Dronninglund pit storage.

deviations for the entire period and added to give a joint "score" for how well each set of directions obeys the flow and energy balance. The set of flow directions that gave the minimum score was then selected for each step.

The calculated flows are in better agreement with the measured charged and discharged energy rates compared to the provided flow directions in the dataset. The exact method for calculating the flow directions is provided in a Python (Python Core Team, 2008) script in the dedicated GitHub repository: https://github.com/PitStorages/DronninglundData.

The energy flows derived from the provided and calculated flow directions are compared in Fig. 7. It can be observed that using the provided flow rate data results in a significant mismatch between the calculated and measured energy. Additionally, mass-flow balance is not achieved when using the provided flow rates. However, mass-flow balance is necessary when using the data as input in simulation models. Thus, the authors recommend using the calculated flow rate magnitudes and directions described in this section.

The frequency distribution of the derived flow rates during charging and discharging is presented in Fig. 8. The mean charge flow rate was 20.2 kg/s, while the mean discharge flow rate was 15.1 kg/s.

It has to be stated that the presented method, though effective, should only be used for the Dronninglund case due to the lack of flow measurements in all diffusers. In the future, it is recommended that the flow magnitude and direction be measured in all diffuser pipes.

3. Measurement sensors

The locations of the sensors in the Dronninglund water pit heat storage are presented in Fig. 9. It has to be noted that although the storage is symmetric, the surrounding ground is very uneven, as can be seen in the side view drawing of Fig. 9; thus, symmetry should not necessarily be assumed for the ground when performing simulations.

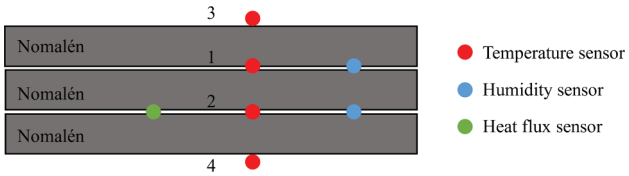

Fig. 10. Placement of temperature sensors in the lid.

3.1. Water temperature measurements

The water temperature is measured with two vertical temperature sensor strings located approximately in the middle of the storage (position A). Each temperature string had 16 temperature sensors placed at 1 m intervals. The two strings are located next to each other and have an offset in their measurement positions of 0.5 m.

3.2. Lid measurements

Initially, a water level sensor was mounted above the top diffuser at position B; however, it operated only from 2015 to 2017 due to the harsh environment. Four temperature and two humidity sensors are installed at position C between the insulation layers, along with a heat flux sensor, as illustrated in Fig. 10. It has to be noted that it is unknown between which two insulation layers the heat flow sensor is placed; however, the specific position should not affect the measurement.

3.3. Ground temperature measurements

Four temperature sensors were installed at position D to measure the ground temperature close to the storage. The exact location of these sensors has not been documented and is thus uncertain. However, according to the plant operator, they are approximately placed in the middle of the storage's northern edge at a 1 m distance from the water edge. The four temperature sensors are located at a depth of 10, 15, 20, and 25 m beneath the top of the embankment.

3.4. Ambient air temperature

The ambient temperature close to the storage is measured in two different locations in the solar collector field in the original dataset. However, the locally measured temperatures are very high (reaching 50 °C during summer). The reason is that the ambient temperature sensors are not properly shielded from direct solar irradiance and that the measurements are probably affected by the emitted heat from the solar collectors.

However, the ambient temperature is also measured by a nearby weather station (06031 Tylstrup) operated by the Danish Meteorological Institute (DMI). The DMI station is approximately 18 km west of the storage, but it is considered representative for long-term studies of the storage heat losses. An added benefit of using DMI's station for the ambient temperature is that the measurements are high quality from ventilated enclosures and are freely available for download from DMI.

3.5. Description of measurement tags

Measurements are made every 10 s and saved every 10 min. The saved values are averaged during the 10-minute periods, except for energy values, which are integrated over the period (MWh). A list of the sensors related to the pit storage is given in Table 4, including the tag name, description, sensor type, unit, and uncertainty for each sensor.

III

Table 4
List and description of sensors in Dronninglund storage.

Tag name	Description	Sensor Type	Unit	Uncertainty
SO.DA. TT.401.1	Temperature of pit storage bottom layer (0.5 m)	PT100	°C	0.15 K
SO.DA. TT.402.1	Temperature of pit storage at 1 m	PT100	°C	0.15 K
SO.DA. TT.401.2	Temperature of pit storage at 1.5 m	PT100	°C	0.15 K
⋮	⋮	⋮	⋮	⋮
SO.DA. TT.402.15	Temperature of pit storage at 15 m	PT100	°C	0.15 K
SO.DA. TT.401.16	Temperature of pit storage at 15.5 m	PT100	°C	0.15 K
SO.DA. TT.402.16	Temperature of pit storage top layer (16 m)	PT100	°C	0.15 K
SO.DA. HT.422.1.F	Lid humidity at position C point 1	–	%	–
SO.DA. HT.422.1.T	Lid temperature at position C point 1	PT100	°C	0.15 K
SO.DA. HT.422.2.F	Lid humidity at position C point 2	–	%	–
SO.DA. HT.422.2.T	Lid temperature at position C point 2	PT100	°C	0.15 K
SO.DA. TT.422.3	Temperature above lid at position C point 3	PT100	°C	0.15 K
SO.DA. TT.422.4	Temperature below lid at position C point 4	PT100	°C	0.15 K
SO.DA. ET.422.5	Heat flux through lid at position C	Hukseflux HFP01	W/ m^2	6–20%
SO.DA. TT.426.1	Ground temperature at 25 m depth	PT100	°C	0.15 K
SO.DA. TT.426.2	Ground temperature at 20 m depth	PT100	°C	0.15 K
SO.DA. TT.426.3	Ground temperature at 15 m depth	PT100	°C	0.15 K
SO.DA. TT.426.4	Ground temperature at 10 m depth	PT100	°C	0.15 K
SO.DA. LT.421	Storage water level measurement	–	m	–
SO.LA. TT.414	Top diffuser temperature	PT100	°C	0.15 K
SO.LA. TT.415	Middle diffuser temperature	PT100	°C	0.15 K
SO.LA. TT.416	Bottom diffuser temperature	PT100	°C	0.15 K
SO.LA.FT.466	Flow rate from the top diffuser	Derived	m^3/ hr	–
SO.LA.FT.467	Flow rate from the middle diffuser	Electromagnetic	m^3/ hr	0.4 %
SO.LA.FT.468	Flow rate from the bottom diffuser	Derived	m^3/ hr	–
SO.LA. FT.466. RETN	Flow direction from the top diffuser[1]	–	–	–
SO.LA. FT.467. RETN	Flow direction from middle diffuser[1]	–	–	–
SO.LA. FT.468. RETN	Flow direction from bottom diffuser[1]	–	–	–
SO.LA. ENERGI. TIL.LAGER. T	The cumulative sum of the charged energy	PT100 + ultrasonic	MWh	0.15–0.5 %
SO.LA. ENERGI. FRA. LAGER.T	The cumulative sum of the discharged energy	PT100 + ultrasonic	MWh	0.15–0.5 %
SO.LA.FT.464	Flow rate to grid/ heat pump	Electromagnetic	m^3/ hr	0.4 %
SO.LA. TT.411	Supply temperature to grid/heat pump	PT100	°C	0.15 K
SO.LA. TT.410	Return temperature from grid/heat pump	PT100	°C	0.15 K
SO.F.TT.405	Temperature at the north side of the collector field[2]	PT100	°C	0.15 K
SO.F.TT.413	Temperature at the south side of the collector field[2]	PT100	°C	0.15 K
SO.F1.PRO. ENERGI.T	Produced solar energy from field 1	PT100 + ultrasonic	MWh	0.15–0.5 %
SO.F1.AFBL. ENERGI.T	Energy used for storage night cooling field 1	PT100 + ultrasonic	MWh	0.15–0.5 %
SO.F1. FROST. ENERGI.T	Energy used for defrosting field 1 in the winter	PT100 + ultrasonic	MWh	0.15–0.5 %
SO.F2.PRO. ENERGI.T	Produced solar energy from field 2	PT100 + ultrasonic	MWh	0.15–0.5 %
SO.F2.AFBL. ENERGI.T	Energy used for storage night cooling field 2	PT100 + ultrasonic	MWh	0.15–0.5 %
SO.F2. FROST. ENERGI.T	Energy used for defrosting field 2 in the winter	PT100 + ultrasonic	MWh	0.15–0.5 %

[1]The flow directions contained in the original dataset have been found to be erroneously and not maintain flow balance. These flow directions should not be used, and instead be derived from the remaining variables.
[2]The ambient air measurements in the dataset have been found erroneous, probably affected by insufficient shading or by heat emitted from the solar collectors. Since these might be unreliable, data from the Danish Meteorological Institute (DMI) could be used as an alternative.

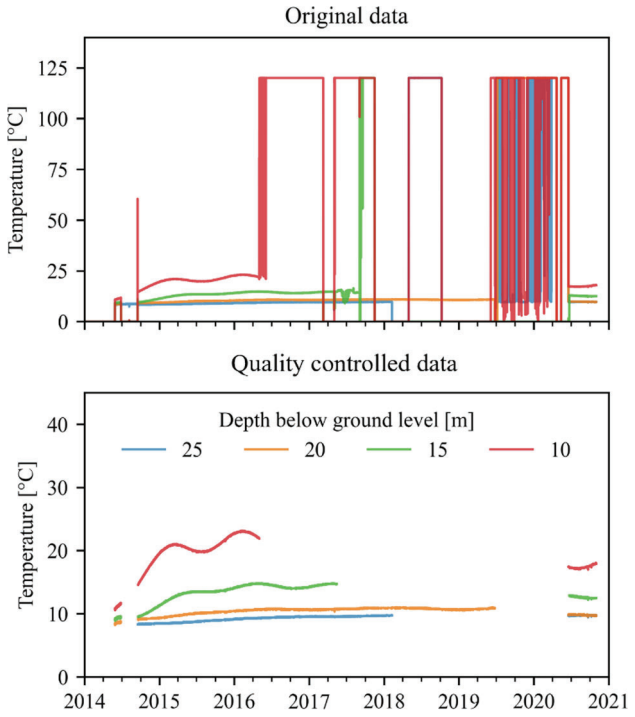

Fig. 11. Soil temperature measurements before and after quality control.

The tag name of each sensor follows a specific structure. The first field is common for all sensors (SO) and represents the solar energy system. The second field describes the subsystem, e.g., DA stands for "damvarmelager" (pit storage) and refers to sensors in or around the storage, LA stands for "lager" (storage) and refers to the sensors located

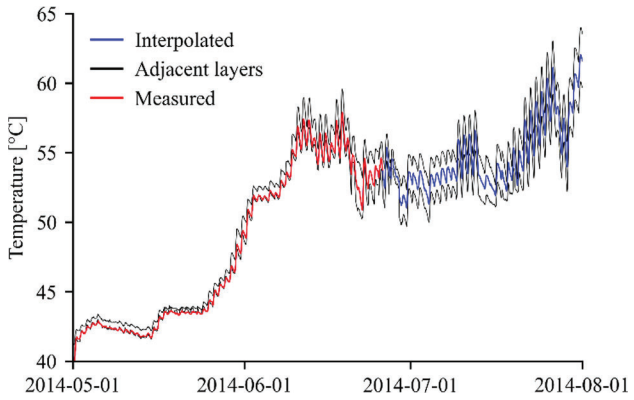

Fig. 12. Measured and interpolated water temperature for the sensor at 1.5 m from the bottom of the storage.

in the pumphouse adjacent to the storage, and F stands for "felt" (field – short form for solar field). The third field is the measured quantity, e.g., TT is temperature, FT is flow, HT is humidity and temperature, ET is heat flux, ENERGI is energy, and LT is water level.

4. Quality control and handling of missing data

The raw measurement data contains many periods with "bad data" due to power outages, sensor failures, etc. These periods have been filtered out using automatic filters and manual inspection. For example, temperatures outside the range 0–100 °C were flagged as erroneous. Afterward, unfeasible temperature spikes were manually removed. The ground temperature data before and after the quality-control procedure is illustrated in Fig. 11.

It has to be noted that all the ground temperature sensors were eventually replaced in the fall of 2021. However, a different position had to be used, approximately 3 m north of the storage's inner edge, as the hole in which the old sensors were installed was closed. Since the new temperature sensors were installed further away from the storage, the measured temperatures are inevitably lower than the previous measurements.

A similar quality control for removing erroneous data was applied to the water temperature measurements. However, in the case of the water temperature sensors, since there were measurements every 0.5 m, the following method was applied in order to reduce the gaps in the data.

Due to the slow time constant of the storage, periods of missing data shorter than 24 h were linearly interpolated. Additionally, missing temperatures were interpolated across the layers. For example, if the temperature at 2.0 m was missing for one month, it was replaced by the average of the sensors at 1.5 m and 2.5 m. This method proved very effective in reducing the number of gaps, as it was infrequent that adjacent temperature sensor data were missing. By interpolating among the layers, most of the long-term gaps were filled. Lastly, we interpolated the missing data for each sensor, filling the remaining gaps and ensuring a complete dataset. Depending on the scope of the analysis, this final step could also be omitted; however, some types of analyses require a complete time series.

As an example, the temperature profile for the sensor at 1.5 m from the storage bottom (SO.DA.TT.401.2) is shown in Fig. 12. The red curve shows the measured temperature, the blue curve is the interpolated temperature based on the sensors above and below, and the black curves are the temperatures of the adjacent layers.

5. Example plots

In this section, example plots are presented to demonstrate the dataset's potential uses. The demonstrated plots aim to provide inspiration to users and only showcase just a small fraction of the available data and possible plots.

Fig. 13 presents the temperature profile in the storage on the first day of each month for 2018. Such figures can be used to inspect the storage temperature profile and the presence of a thermocline layer during different times of the year.

The top subplot of Fig. 14 presents the temperature of the storage layers from 2014 to 2020. The upper layers are illustrated using green color, while the bottom layers are shown in blue. In addition, three thin, black curves are drawn, indicating the temperature of the top, middle, and bottom layers. Such a figure can be used to showcase the seasonally changing temperature profile and identify the years with the highest temperatures in the storage. For example, it is evident that in 2018, the storage had a higher average temperature than in other years, as the temperature of the middle layer was almost equal to the top layer during the charge period. The main reason for this was the increased solar radiation in 2018 compared to an average year.

The middle subplot of Fig. 14 presents the monthly charged and discharged energy as well as the monthly energy content of the storage. When combined with the top subplot, it gives a complete image of the storage operation, e.g., it can be verified that there was more energy charged into the storage in 2018. The middle subplot also demonstrates that the storage was used for both long- and short-term heat storage as a

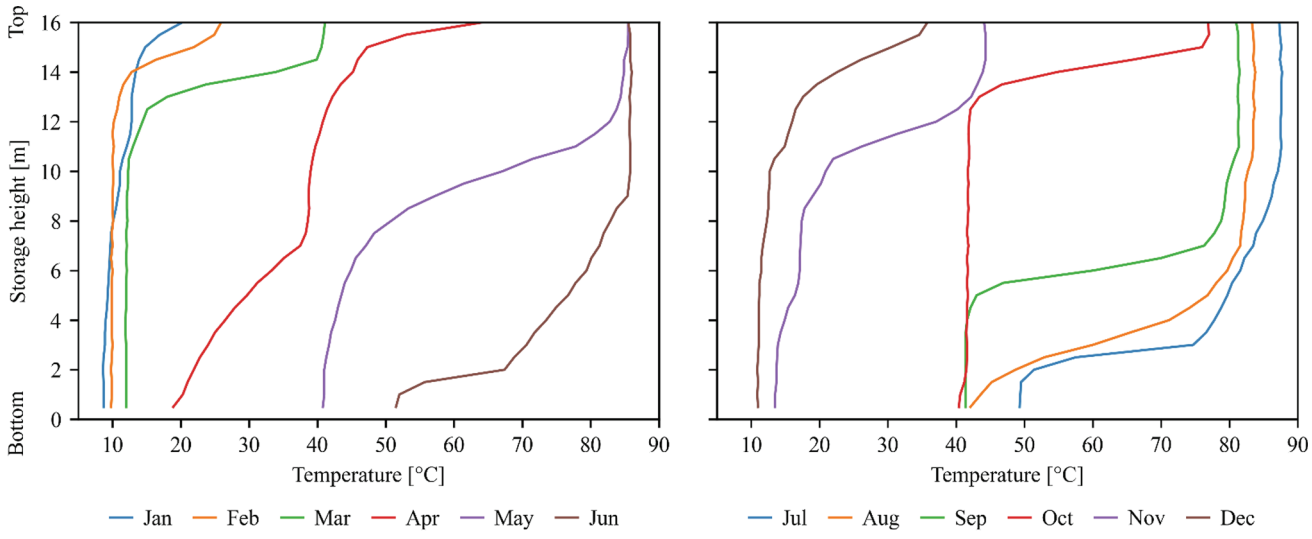

Fig. 13. Temperature profile inside the Dronninglund storage on the 1st day of each month in 2018.

III

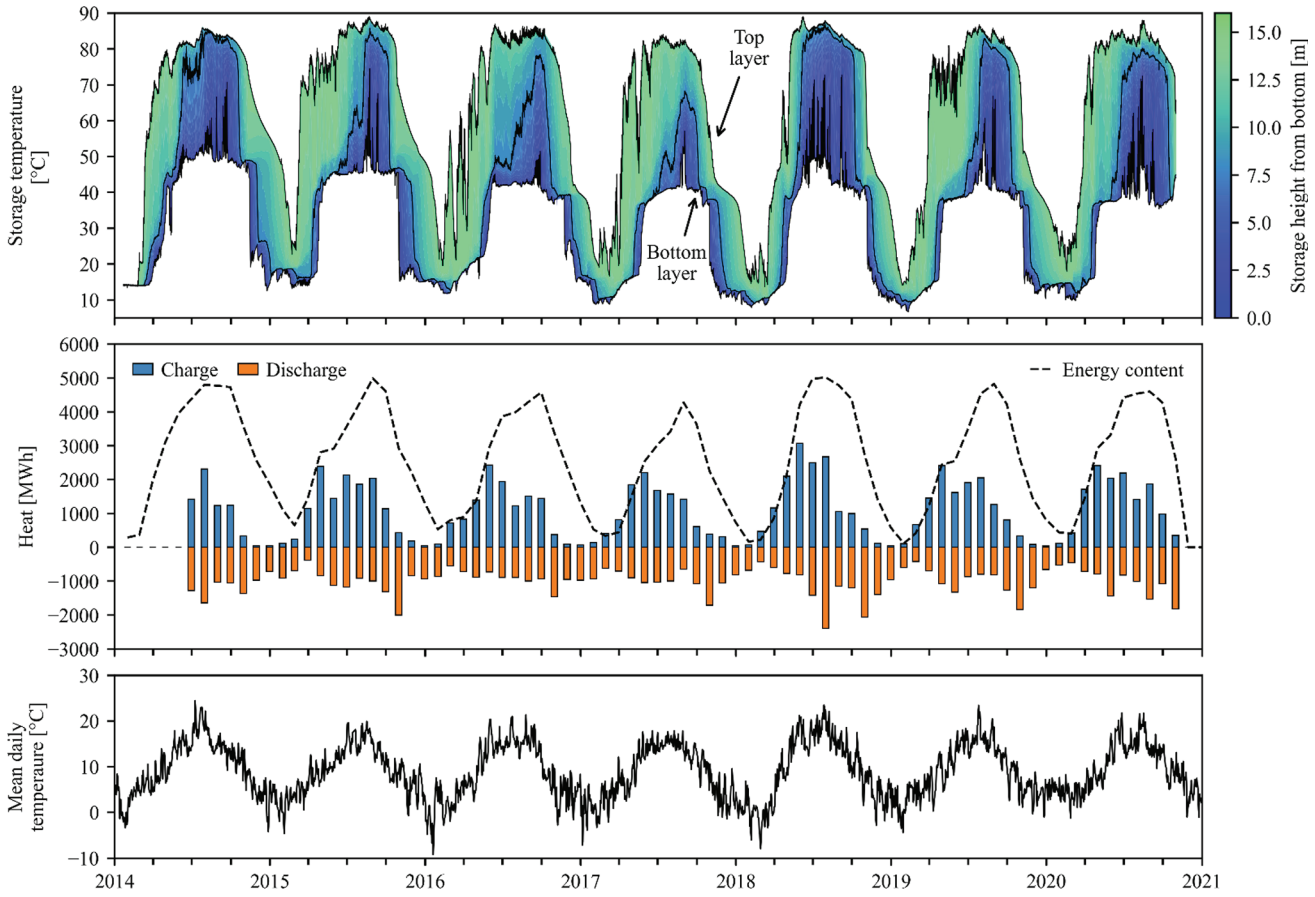

Fig. 14. Dronninglund ambient temperature, storage temperatures, charged and discharged heat, and energy content of the PTES from 2014 to 2020.

significant amount of heat was also discharged in the summer months.

Last, the bottom subplot illustrates the mean daily temperature around the PTEs in Dronninglund, which can be used to identify the yearly high and low ambient temperatures.

5.1. *Moving forward*

This article provides a detailed description of the available information on the Dronninglund water pit heat storage. A reference dataset from the storage operation for the period 2014 – 2020 has been introduced. The goal is for this article to be used as a reference point for future research in the field of seasonal storage of solar thermal heat and specifically for studies regarding the Dronninglund pit storage.

Declaration of Competing Interest

The authors declare that they have no known competing financial interests or personal relationships that could have appeared to influence the work reported in this paper.

Acknowledgments

The authors would like to express their gratitude to Johan Frey for his valuable contributions to the paper. This study was funded by the Danish Energy Agency through EUDP grants' IEA ECES Annex 39 LTES' (no. 64018-0134), 'Participation in the IEA task on efficient solar district heating systems' (no. 134-21027) and 'Participation in the IEA ES TCP Task 41 on Economics of Energy Storage' (no. 134223-495989) and by the Ph.D. program of the Sino-Danish Center for Education and Research (SDC).

References

Aalborg CSP, 2019. 15,000 M3 PTES for district heating, Tibet [WWW Document]. <https://web.archive.org/web/20210418202632/https://www.aalborgcsp.com/projects/15000-m3-ptes-for-district-heating-tibet/> (Accessed 5.4.22).

Dahash, A., Ochs, F., Giuliani, G., Tosatto, A., 2021. Understanding the interaction between groundwater and large-scale underground hot-water tanks and pits. Sustain. Cities Soc. 71, 102928 https://doi.org/10.1016/j.scs.2021.102928.

Dahash, A., Ochs, F., Janetti, M.B., Streicher, W., 2019. Advances in seasonal thermal energy storage for solar district heating applications: a critical review on large-scale hot-water tank and pit thermal energy storage systems. Appl. Energy 239, 296–315. https://doi.org/10.1016/j.apenergy.2019.01.189.

Dahash, A., Ochs, F., Tosatto, A., Streicher, W., 2020. Toward efficient numerical modeling and analysis of large-scale thermal energy storage for renewable district heating. Appl. Energy 279, 115840. https://doi.org/10.1016/j.apenergy.2020.115840.

Dronninglund Fjernvarme, 2020. Dronninglund district heating [WWW Document]. <https://www.dronninglundfjernvarme.dk/>.

Epp, B., 2014. Denmark: Dronninglund Inaugurates 26 MWth Solar District Heating Plant [WWW Document]. Sol. Therm. World. <https://www.solarthermalworld.org/news/denmark-dronninglund-inaugurates-26-mwth-solar-district-heating-plant>.

Gauthier, G., 2020. Benchmarking, and improving models of subsurface heat storage dynamics. Comparison of Danish PTES and BTES installation measurements with their corresponding TRNSYS models. GEOTHERMICA – ERA NET Cofund Geothermal [WWW Document]. <https://www.heatstore.eu/documents/20201028_DK-temadag_PlanEnergi_Monitoring%20results%20for%202019%E2%80%902020%20for%20Marstal,%20Dronninglund%20and%20Gram.pdf>.

GEO, 2012. Dronninglund. Lunderbjerg 8A Damvarmelager - Vurdering af varmelagerets påvirkning af grundvand.

GEO, 2010. Dronninglund. Lunderbjerg 8A Damvarmelager - Geoteknisk undersøgelse.

Hamdhan, I.N., Clarke, B.G., 2010. Determination of Thermal Conductivity of Coarse and Fine Sand Soils, in: Proceedings World Geothermal Congress. Bali, Indonesia.

Jensen, M.V., 2014. Seasonal pit heat storages - Guidelines for materials & construction IEA-SHC Tech Sheet 45.B.3.2.

Klingaard, S., Andersen, A., 2018. Analyse af vandkvalitet og iltindhold i damvarmelageret i Dronninglund.

NMC Termonova, 2015. Thermal properties of Nomalen 28N [WWW Document]. <https://web.archive.org/web/20220428093554/https://dms.etra.fi:9900/72192/conversions/original?version=0> (Accessed 4.28.22).

NMC Termonova, 2011. Nomalen 28N [WWW Document]. <https://web.archive.org/web/20220426161150https://azupcs365certviewer.azurewebsites.net/api/GetSDB?env=se&articleNr=550984> (Accessed 4.20.22).
Nygren, M., Giese, M., Kløve, B., Haaf, E., Rossi, P.M., Barthel, R., 2020. Changes in seasonality of groundwater level fluctuations in a temperate-cold climate transition zone. J. Hydrol. X 8, 100062. https://doi.org/10.1016/j.hydroa.2020.100062.
Ochs, F., Dahash, A., Tosatto, A., Bianchi Janetti, M., 2020. Techno-economic planning and construction of cost-effective large-scale hot water thermal energy storage for Renewable District heating systems. Renew. Energy 150, 1165–1177. https://doi.org/10.1016/j.renene.2019.11.017.
Pan, X., Xiang, Y., Gao, M., Fan, J., Furbo, S., Wang, D., Xu, C., 2022. Long-term thermal performance analysis of a large-scale water pit thermal energy storage. J. Energy Storage 52, 105001. https://doi.org/10.1016/j.est.2022.105001.
Pauschinger, T., Schmidt, T., Alex Soerensen, P., Aart Snijders, D., Djebbar, R., Boulter, R., Jeff Thornton, C., 2018. Integrated Cost-effective Large-scale Thermal Energy Storage for Smart District Heating and Cooling - Design Aspects for Large-Scale Aquifer and Pit Thermal Energy Storage for District Heating and Cooling. Int. Energy Agency Technol. Collab. Program. Dist. Heat. Cool. Incl. Comb. Heat Power, 2018.
Perez-Mora, N., Bava, F., Andersen, M., Bales, C., Lennermo, G., Nielsen, C., Furbo, S., Martínez-Moll, V., 2018. Solar district heating and cooling: a review. Int. J. Energy Res. 42, 1419–1441. https://doi.org/10.1002/er.3888.
PlanEnergi, 2020. Roles in HEATSTORE & Monitoring results for 2019-2020 for Marstal, Dronninglund and Gram [WWW Document]. <https://www.heatstore.eu/documents/20201028_DK-temadag_PlanEnergi_Monitoring%20results%20for%202019%E2%80%902020%20for%20Marstal,%20Dronninglund%20and%20Gram.pdf> (Accessed 12.9.20).
PlanEnergi, 2015a. Long term storage and solar district heating [WWW Document]. <https://web.archive.org/web/20220306155726/https://planenergi.dk/wp-content/uploads/2017/06/sol_til_fjernvarme_brochure_endelig.pdf> (Accessed 5.4.22).
PlanEnergi, 2015b. Sunstore 3 - Phase 2: Implementation.
PlanEnergi, 2011. Sunstore 3, Fase 1 - Projektering og udbud [WWW Document]. <https://energiforskning.dk/sites/energiforskning.dk/files/slutrapporter/slutrapport_incl._bilag_1_12042011_1824.pdf>.
Python Core Team, 2008. Python: A dynamic, open source programming language. Python Software Foundation. <https://www.python.org/>.
Rambøll, 2020. Experience from Toftlund [WWW Document]. <https://www.heatstore.eu/documents/20201028_DK-temadag_Ramb%C3%B8ll%20PTES%20project.pdf> (Accessed 12.9.22).
Rambøll, 2016. Damvarmelagre [WWW Document]. <https://web.archive.org/web/20220504080511/https://dk.ramboll.com/-/media/3fc11649e25942c195fa90e63ea41e11.pdf> (Accessed 5.4.22).
Rambøll, 2015. South-Jutland stores the sun's heat in the world's largest pit heat storage [WWW Document]. <https://web.archive.org/web/20210827074933/https://ramboll.com/projects/re/south-jutland-stores-the-suns-heat-in-the-worlds-largest-pit-heat-storage?utm_source=alias&utm_campaign=sun-storage> (Accessed 5.4.22).
Schmidt, T., 2019. Marstal district heating monitoring data evaluation for the years 2015-2017 [WWW Document]. <https://www.solar-district-heating.eu/wp-content/uploads/2019/10/Marstal-evaluation-report-2015-2017_2019.05.28.pdf> (Accessed 12.9.22).
Schmidt, T., Pauschinger, T., Sørensen, P.A., Snijders, A., Djebbar, R., Boulter, R., Thornton, J., 2018. Design aspects for large-scale pit and aquifer thermal energy storage for district heating and cooling. Energy Proc. 149, 585–594. https://doi.org/10.1016/j.egypro.2018.08.223.
Schmidt, T., Sørensen, P.A., 2018. Monitoring Results from Large Scale Heat storages for District Heating in Denmark.
Sifnaios, I., Jensen, A.R., Furbo, S., Fan, J., 2022. Performance comparison of two water pit thermal energy storage (PTES) systems using energy, exergy, and stratification indicators. J. Energy Storage 52, 104947. https://doi.org/10.1016/j.est.2022.104947.
Soerensen, P.A., From, N., 2011. High solar fraction with pit heat storages, in: 30th ISES Biennial Solar World Congress 2011, SWC 2011. pp. 3020–3030. <https://doi.org/10.18086/swc.2011.21.07>.
Sorknæs, P., 2018. Simulation method for a pit seasonal thermal energy storage system with a heat pump in a district heating system. Energy 152, 533–538. https://doi.org/10.1016/j.energy.2018.03.152.
Sveinbjörnsson, D., Laurberg Jensen, L., Trier, D., Ben Hassine, I., Jobard, X., 2017. Large Storage Systems for DHC Networks.
Winterscheid, C., Schmidt, T., 2017. Dronninglund District Heating Monitoring Data Evaluation for the Years 2015-2017.
Xie, Z., Xiang, Y., Wang, D., Kusyy, O., Kong, W., Furbo, S., Fan, J., 2021. Numerical investigations of long-term thermal performance of a large water pit heat storage. Sol. Energy 224, 808–822. https://doi.org/10.1016/j.solener.2021.06.027.

IV. Thermal inspection of water pit heat storages using drones

Ioannis Sifnaios, Janne Dragsted, and Adam R. Jensen

Proceedings of the ISES Solar World Congress 2021, 925-931

IV

Thermal inspection of water pit heat storages using drones

Ioannis Sifnaios[1,2], Janne Dragsted[1], and Adam R. Jensen[1]

[1]DTU Civil Engineering, Technical University of Denmark, Kgs. Lyngby [Denmark]

[2]Sino-Danish College (SDC), University of Chinese Academy of Sciences, Beijing [China]

Abstract

Water pit heat storages can be used to cover the mismatch between solar thermal generation and heat demand and achieve high solar thermal fractions in district heating systems. The most expensive part of such storages is the floating insulating lid, which is crucial to ensuring high efficiency by minimizing heat losses. So far, two different insulation materials have been used in the lids, namely Nomalén and LECA, both of which are sensitive to moisture. Therefore, it is important that leakages, which existing storages have been prone to develop, are fixed quickly. Manual inspection is costly and inefficient due to the lids' large surface area (>10.000 m2). This study investigates whether thermal drone imaging can identify leakages in pit storage lids by inspecting all existing pit storages in Denmark. The investigations identified leakages in two different pit storages and proved that drone thermal imaging is a very effective tool for leakage detection.

Keywords: drones, thermal imaging, pit thermal energy storage, heat storage, leak detection

1. Introduction

In Denmark, district heating supplies heat to more than 60% of residential consumers (Danish Energy Agency, 2017). The district heating networks utilize heat from various sources, including gas, waste incineration, coal, oil, combined heat power (CHP) plants, and surplus heat from industry. Renewables are also used, including solar thermal, geothermal energy, biomass, and heat pumps powered by renewable electricity (Lund et al., 2014). Although there is an effort to increase the share of renewables, there are many situations where the heat demand and supply do not coincide. This mismatch can happen either due to short-term weather-induced fluctuations or seasonal variations. For example, most solar irradiation in North and Central Europe is received between May and September, whereas two-thirds of the heat demand occurs between October and April.

As a solution to this problem, seasonal heat storages can store heat produced by solar thermal collector fields during summer and deliver it in winter (Mangold and Deschaintre, 2015). The mismatch between consumption and production typically limits district heating systems from achieving solar thermal fractions greater than 20%. However, using seasonal energy storages, solar thermal fractions can be increased up to 50% (Sveinbjörnsson et al., 2017).

One of the cheapest and most promising types of large-scale heat storage technologies is pit thermal energy storages (PTES), which have been demonstrated in combination with large solar collector fields in Denmark (Soerensen and From, 2011). In principle, a PTES is a large water reservoir that is used to store thermal energy. The storage duration depends on the application, ranging from days to months. First, a pit is excavated in the ground and is lined with a watertight polymer (Jensen, 2014). The excavated soil from the pit is used to form embankments around the pit, such that soil does not have to be transported off the site to minimize construction costs. Then, the storage is filled with treated water, which has the advantages of being inexpensive, non-toxic, allows stratification, and has a high thermal capacity (Schmidt et al., 2018). After the pit has been filled with water, it is covered with an insulated floating lid. One of the main advantages of the PTES technology is the low cost compared to other storage technologies and that high charge and discharge rates can be achieved.

The floating lid is the most expensive part of the storage; hence, many investigations have been performed for various designs and materials (Jensen, 2014). Nonetheless, liner ruptures or penetration has occurred in

doi:10.18086/swc.2021.35.02 Available at http://proceedings.ises.org

numerous situations, causing water to leak into the lid, significantly reducing insulation performance. This leads to increased heat losses and reduces storage efficiency.

From experience, it has been proven that liner ruptures in the lids are difficult to locate due to their large surface area (>10.000 m2). In the past, leakages have been located by manual inspection, which is costly and inefficient. This paper presents experiences from drone thermal imaging of PTES, seeking to provide an effective and cost-efficient alternative to traditional methods.

2. Methods

In this section, the specifications of the PTES in Denmark are first presented, along with the corresponding insulation materials. Next, drone thermal imaging is introduced as a method for inspecting the lids of PTES for leakages due to the large lid areas. A major benefit of drone thermal leakage inspection is speed since the entire PTES lid area can be mapped in approximately 20 minutes. The specific setup used for the drone mapping is discussed in Section 2.3.

2.1. Lid insulation materials

Until 2020, only two different insulation materials have been used for PTES, namely Nomalén and LECA. Nomalén insulation is sold as mats made of cross-linked polyethylene foam (PEX) with a closed-cell structure, while LECA (Light Expanded Clay Aggregate) are small, expanded clay pebbles. However, there have been issues related to the usage of both technologies. Nomalén has in some cases collapsed to a fourth of its original thickness due to exposure to moisture and high temperatures (~90 °C) for long periods. LECA, on the other side, has a natural tendency to absorb water, and mechanical ventilation is necessary in order to dry out the material. Both of these issues decrease the insulating properties of the insulation material and increase the heat loss of the PTES. In Tab. 1, information about the existing PTES in Denmark is presented, along with the used insulation types.

Tab. 1: Information about PTES in Denmark

Storage	Size (m^3)	Estimated lid area (m^2)	Insulation type	Reference
Dronninglund	60,000	8,300	Nomalén	(PlanEnergi, 2015, 2013)
Marstal	75,000	10,900	Nomalén	(PlanEnergi, 2013)
Toftlund	70,000	11,500	LECA	(Rambøll, 2016)
Gram	125,000	14,500	LECA	(PlanEnergi, 2016)
Vojens	200,000	22,500	LECA	(Rambøll, 2015)

2.2. Thermal imaging

Thermal cameras, also known as infrared or thermographic cameras, create images based on infrared (IR) radiation emitted by objects. They detect wavelengths in the infrared spectrum, typically from 750 to 1350 nm, whereas regular cameras detect visible light in the range of 400 to 700 nm. Therefore, thermal cameras do not directly detect temperature but instead rely on the principle that every object emits infrared radiation. Thermal cameras can detect radiation in the IR part of the spectrum that the human eye cannot see (OPGAL, 2018).

However, the conversion of infrared radiation to temperature can be complex. For example, in most cases, the emissivity of an object must be estimated since it affects the wavelength of the emitted infrared radiation. Emissivity is a surface radiative property, quantified as the ratio of emitted energy from a surface to that of an ideal blackbody surface. The emissivity range is from 0 to 1, corresponding to a perfect mirror and an ideal blackbody, respectively. A surface's emissivity depends primarily on the material and the surface finish, e.g., polished, painted, etc. Water affects emissivity, as wet or even moist surfaces have a different emissivity than dry. The water emissivity is 0.96, which results in damp areas of an object being erroneously detected as having a higher temperature. Surface water can also affect an object's temperature due to the evaporation of the water, reducing the temperature of the object. For obtaining an accurate surface temperature, images should be taken of dry surfaces, and the correct emissivity should be used, which can be adjusted in the settings of most thermal cameras.

2.3. Drone thermal imaging

The drone used for the inspection of PTES is a DJI Matrice 200 equipped with a DJI Zenmuse XT2 640x512 resolution thermal camera. The Zenmuse XT2 is a dual camera that captures a regular image concurrently with the thermal image. The thermal camera has a 13 mm lens that detects radiation in the spectral band 7.5-13.5 µm. Capturing both RGB and thermal images is helpful as it makes it easy to compare the features of the thermal image with that of a regular photo. For example, in the case of pit storage inspection, a thermal image abnormality might be caused by debris, which can be detected in the RGB image, and should not be further investigated.

The thermal investigation of the PTES was carried out during nighttime to avoid reflections from the sun. For this reason, RGB images of the storage were taken before the thermal inspection while it was still daylight. Pictures of the drone used can be seen in Fig. 1. The drone images were taken using the app DJI Pilot. Between 250-700 images were taken and stitched together for each inspection to form a large overall image called an orthomosaic. It was found that the images had to be taken at the height of 60 m for best orthomosaic results and a high level of detail. In order to ensure sharp images, the flight speed has to be set at a low value, depending on the battery capacity of the drone. For the orthomosaics presented in this study, a speed of approximately 2.3 m/s was used.

The stitching of the images was done using either DroneDeploy (commercially available) or OpenDroneMap (open-source). Unfortunately, neither software can generate a colormap for the orthomosaics for indicating the temperature at each spot. However, this is not of major concern, as the images are primarily used to detect differences in the relative temperature between different lid areas.

Fig. 1: DJI Matrice 200 equipped with a Zenmuse XT2 camera flying over the solar collector field in Vojens (left) and close-up photo (right) (Drones Made Easy, n.d.).

3. Results

This section presents the results of the investigations of the PTES using Nomalén, followed by the storages that use LECA as insulation. The presented thermal images are accompanied by a color bar indicating the temperature range on the storage's surface. The large differences between the temperatures of the plots are mainly due to the different ambient and sky temperature at the time of filming; thus, temperatures between plots should not be compared.

3.1. PTES using Nomalén

Nomalén is used as insulation material for the lid in the PTESs in Dronninglund and Marstal. Fig. 2 shows a thermal image and daylight photo of the Dronninglund PTES lid. One of the most noticeable observations in the thermal image is the many warm (yellow color) oval shapes on the lid. When comparing the locations and shapes of these to the RGB image on the left, it can be seen that they are water puddles. They are detected as warmer than the adjacent areas because the emissivity of water is higher than that of the lid surface. The water puddles can therefore not be compared with the surrounding areas; however, the puddles' temperatures can be compared with each other. By comparing the detected temperature of the different water puddles, it was identified that the puddle in the top left corner was warmer than the rest. The puddle temperature in the top left corner was 30.6 °C, while the average temperature of the rest of the puddles was 20 °C. The plant manager was informed about this finding, and the warmer pond was manually inspected. The inspection showed that

the liner under the lid was torn in this area, and warm water from the storage was entering the lid. Afterward, the leak was fixed, resulting in a positive impact on the storage performance and lifetime of the insulation. By inspecting the thermal image in Fig. 2, a rectangular grid of thermal bridges can be noticed, corresponding to the gaps between the insulation mats underneath the top liner. The average temperature of the thermal bridges was 18 °C.

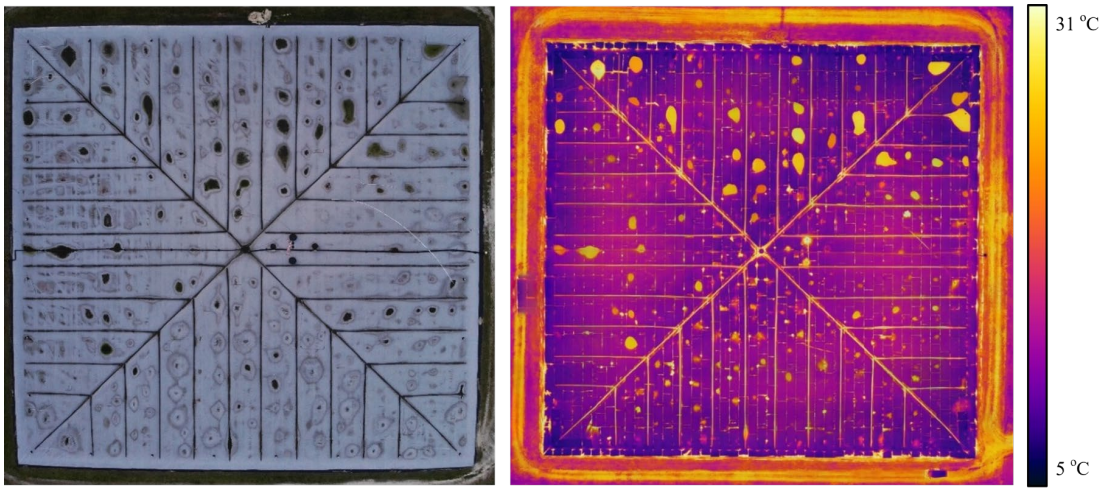

Fig. 2: RGB (left) and thermal (right) image of the PTES in Dronninglund.

In Fig. 3, the thermal and RGB images of the Marstal PTES are presented. As of April 2020, a new lid was installed consisting of twelve square sub-sections. Each sub-section is covered with gravel to ensure a slope towards the center, where a rainwater drainage system is located. Consequently, it is the only inspected PTES with no water ponds on its surface, and thus an easier assessment of the thermal image can be made. The bright yellow dots indicate the pump wells at the center of each sub-section. Additionally, several air vents and the three maintenance holes can be identified in the thermal image. The average temperature of the pump wells, vents, and maintenance holes was 20 °C. No issues were identified during the inspection that took place in October 2020. It can be observed that there was a small problem with the thermal image stitching at the top of the thermal image, though this did not significantly alter the thermal inspection.

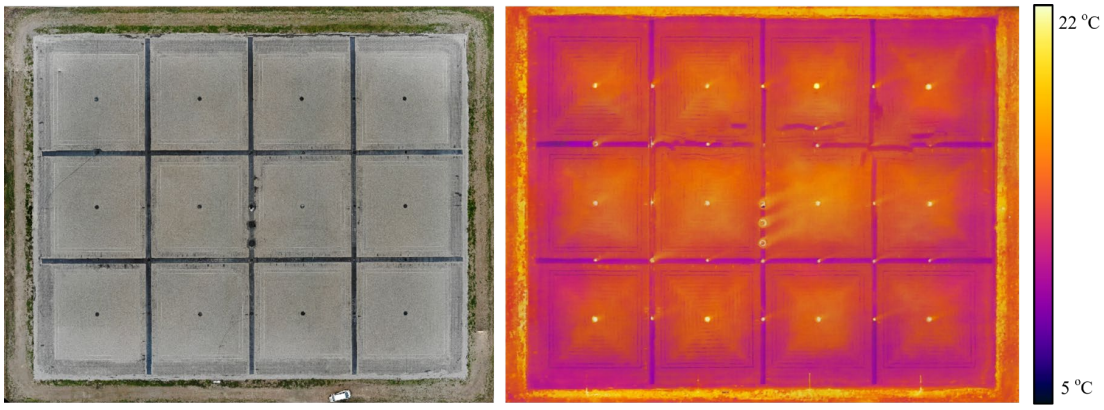

Fig. 3: RGB (left) and thermal (right) image of the PTES in Marstal (October 2020).

A second inspection of the Marstal PTES was done in October 2021, a year after the first one, to verify the performance of the new lid technology. The results can be seen in Fig. 4. Overall, no significant differences were spotted between the two inspections, indicating that the performance of the lid has not degraded significantly during this period. However, a warmer area was detected at the connections of the left-most modules (marked with a white oval in Fig. 4). This is due to the separation of insulation covering the joint between the modules, which is thought to be caused by lid expansion. In general, the temperature of the hot spots where the insulation was separating was between 10 – 12 °C, whereas the temperature of the rest connections was around 8 °C. The separation of the insulation creates a thermal bridge and increases the heat

loss of the lid.

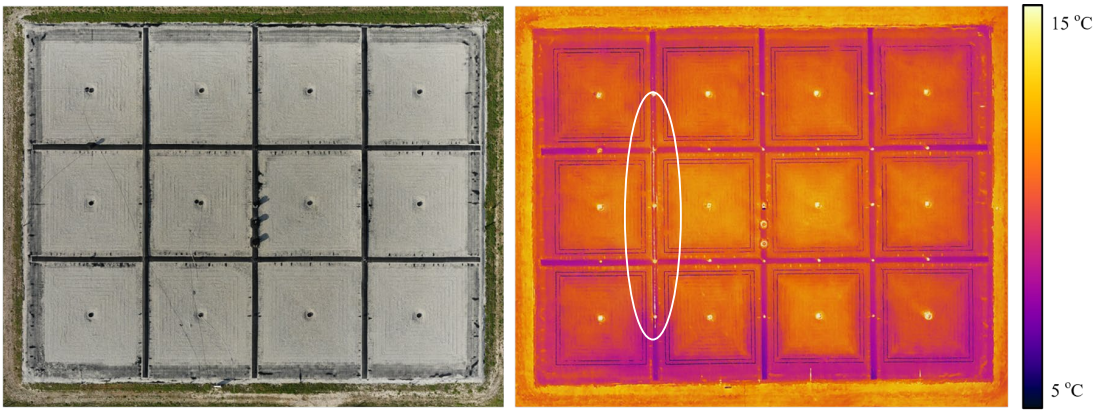

Fig. 4: RGB (left) and thermal (right) image of the PTES in Marstal (October 2021).

3.2. PTES using LECA

LECA is used as insulation material in the lid for the PTESs in Gram, Toftlund, and Vojens. Fig. 5 illustrates the orthomosaic for the PTES in Gram. This image looks vastly different from the PTESs in Dronninglund and Marstal. The reason for this is the different insulation materials used within the PTES lids. The brain-like pattern visible in Fig. 5 is thought to be due to heat convection within the lid. This phenomenon should be minimized as much as possible, as it enhances the thermal losses from the storage. The image clearly illustrates the presence of thermal bridges, which are most likely due to convection. The average temperature of the thermal bridges was 22 °C. It is suggested that smaller clay pebbles should be used in the future, or a convection membrane should be installed. Lastly, in Fig. 5, it was possible to identify a significantly warmer puddle (33 °C) on the lid near the top diffuser, indicating a potential leak.

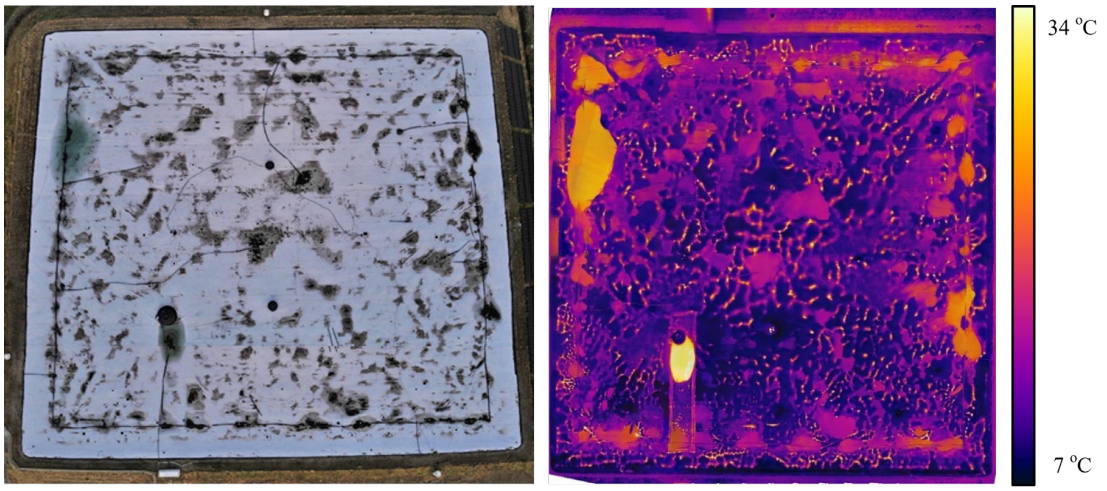

Fig. 5: RGB (left) and thermal (right) image of the PTES in Gram.

In Fig. 6 and Fig. 7, the RGB and thermal images of the PTESs in Toftlund and Vojens are shown, respectively. Similar to Gram, these PTESs use LECA as lid insulation, and thus brain-like patterns due to convection can be observed in the thermal image. However, contrary to Gram, in both PTES, there seem to be areas of the lid where this phenomenon is more intense, indicating that either a thinner layer of LECA exists in these areas or that LECA is wet, resulting in higher heat losses.

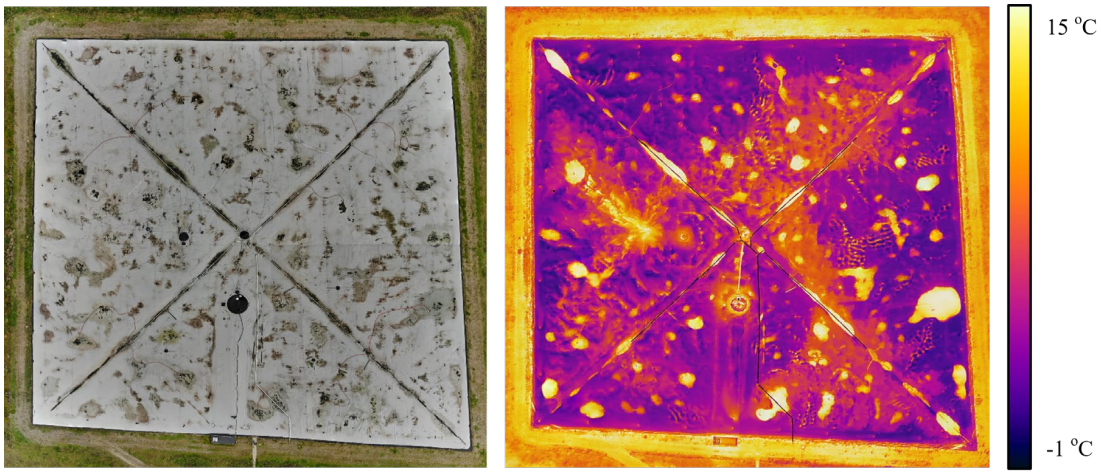

Fig. 6: RGB (left) and thermal (right) image of the PTES in Toftlund.

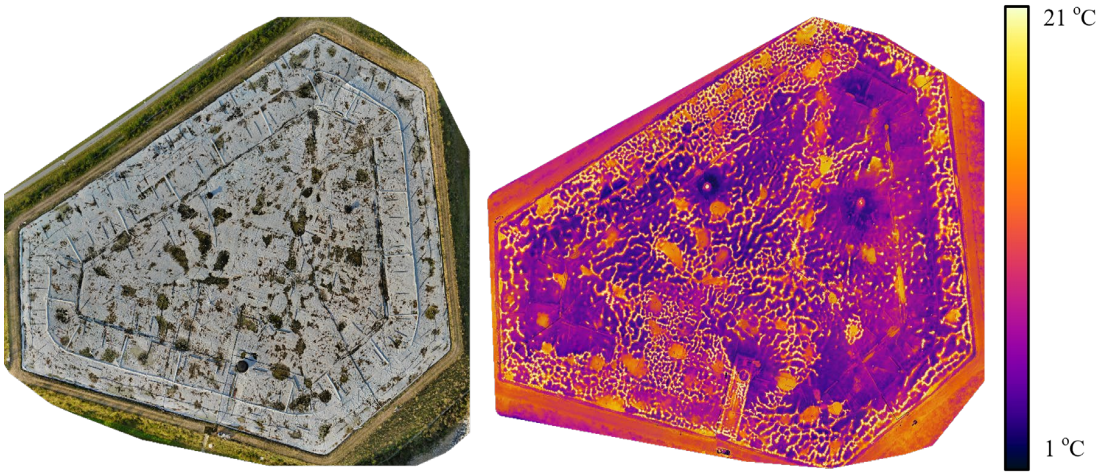

Fig. 7: RGB (left) and thermal (right) image of the PTES in Vojens.

4. Conclusions

This article presents results from thermal inspection of pit thermal energy storages using drone thermal imaging. Two different technologies for lid insulation were investigated, namely Nomalén used in Dronninglund and Marstal, and LECA used in Gram, Toftlund, and Vojens. The results showed that although water ponds on the lid make thermal inspection more difficult, their relative temperature to each other can be used as an indication for leakages. In addition, the thermal images for Nomalén indicate more uniform heat losses than LECA, where brain-like patterns are created due to convection. Lastly, in some pit storages with LECA, areas with very intense brain-like patterns were identified, indicating possibly a thinner layer of LECA or moisture in the insulation. Overall, the performed investigations proved that drone thermal imaging is an effective tool for leakage detection in pit storages.

5. Acknowledgments

The research was financed by the Bjarne Saxhofs Fond.

6. References

Danish Energy Agency, 2017. Regulation and planning of district heating in Denmark.

Drones Made Easy, n.d. Matrice 200 + Zenmuse XT2 [WWW Document]. URL https://dronesmadeeasy.com/zenmuse-xt2/ (accessed 10.6.21).

Jensen, M.V., 2014. Seasonal pit heat storages - Guidelines for materials & construction IEA-SHC Tech Sheet 45.B.3.2.

Lund, H., Werner, S., Wiltshire, R., Svendsen, S., Thorsen, J.E., Hvelplund, F., Mathiesen, B.V., 2014. 4th Generation District Heating (4GDH). Integrating smart thermal grids into future sustainable energy systems. Energy 68, 1–11. https://doi.org/10.1016/j.energy.2014.02.089

Mangold, D., Deschaintre, L., 2015. Seasonal thermal energy storage: Report on state of the art and necessary further R+D.

OPGAL, 2018. Introduction to IR (Part 1): The physics behind thermal imaging [WWW Document]. URL https://www.opgal.com/blog/thermal-cameras/the-physics-behind-thermal-imaging (accessed 3.4.21).

PlanEnergi, 2016. Long term storage and solar district heating.

PlanEnergi, 2015. Sunstore 3 - Phase 2: Implementation.

PlanEnergi, 2013. Udredning vedrørende varmelagringsteknologier og store varmepumper til brug i fjernvarmesystemet.

Rambøll, 2016. Damvarmelagre.

Rambøll, 2015. South-Jutland stores the sun's heat in the world's largest pit heat storage [WWW Document]. URL https://ramboll.com/projects/re/south-jutland-stores-the-suns-heat-in-the-worlds-largest-pit-heat-storage?utm_source=alias&utm_campaign=sun-storage (accessed 2.17.22).

Schmidt, T., Pauschinger, T., Sørensen, P.A., Snijders, A., Djebbar, R., Boulter, R., Thornton, J., 2018. Design Aspects for Large-scale Pit and Aquifer Thermal Energy Storage for District Heating and Cooling. Energy Procedia 149, 585–594. https://doi.org/10.1016/j.egypro.2018.08.223

Soerensen, P.A., From, N., 2011. High solar fraction with pit heat storages, in: 30th ISES Biennial Solar World Congress 2011, SWC 2011. pp. 3020–3030. https://doi.org/10.18086/swc.2011.21.07

Sveinbjörnsson, D., Laurberg Jensen, L., Trier, D., Ben Hassine, I., Jobard, X., 2017. Large Storage Systems for DHC Networks.

IV

V. Effect of Design Characteristics on Pit Thermal Energy Storage Performance

Ioannis Sifnaios, Adam R. Jensen, Simon Furbo, and Jianhua Fan

Proceedings of EuroSun 2022

Effect of Design Characteristics on Pit Thermal Energy Storage Performance

Ioannis Sifnaios[1,2], Adam R. Jensen[1], Simon Furbo[1] and Jianhua Fan[1]

[1] DTU Civil and Mechanical Engineering, Technical University of Denmark, Kgs. Lyngby (Denmark)

[2] Sino-Danish College (SDC), University of Chinese Academy of Sciences, Beijing (China)

Abstract

Pit thermal energy storage (PTES) systems have been developed as a low-cost, water-based storage technology for district heating networks. While annual efficiencies greater than 90% have been realized, many existing storages have suffered from high heat losses and poor stratification. Thus, research is still necessary for identifying and optimizing the parameters that affect the operation and performance of PTES. This study investigated the effect of design characteristics and ambient temperature on PTES heat loss and efficiency. More specifically, the influence of aspect ratio and slope of the storage sides were investigated for three locations (Denmark, Finland, and Greece) using the software ANSYS Fluent. It was found that the slope of the PTES sides had a larger impact on the storage efficiency than the aspect ratio. The investigated PTES with steeper side-wall slopes had a 12% higher efficiency than one with a gradual slope, while the PTES with a rectangular shape had a 3% lower efficiency than a square one. Regarding different locations, a PTES in Greece would have 5% higher efficiency than one in Finland due to higher ambient temperatures that reduce heat losses.

Keywords: Heat storage, design optimization, heat loss, heat transfer, PTES

1. Introduction

Many different heat sources can be utilized in the district heating (DH) networks, such as waste incineration, biomass, wind, solar, geothermal energy, natural gas, oil, coal, and surplus heat from industry (Danish District Heating Association, 2021). In Denmark, where DH covers 64% of the country's residential heat demand, there is an effort to increase the share of renewables in the DH sector in order to be carbon neutral by 2050 (Ministry of Foreign Affairs of Denmark, 2020). To achieve this, energy storage has to be utilized due to the intermittent nature of renewable energy sources like solar and wind. For example, typical DH networks can achieve a solar fraction of 20%, whereas DH networks with seasonal energy storage systems can achieve solar fractions higher than 40% (Sveinbjörnsson et al., 2017).

One of the most promising storage technologies in the district heating sector is pit thermal energy storage (PTES), which is a low-cost technology that utilizes water as the storage medium. Several PTES systems have been demonstrated in Denmark and connected to large-scale solar collector fields (Soerensen and From, 2011). The current state-of-the-art PTES has an efficiency greater than 90% (Winterscheid and Schmidt, 2017), demonstrating that PTES can be a cost-effective heat storage technology with a large potential.

At the time of writing, there are five storages in operation in Denmark, namely in Dronninglund (60,000 m^3) (Schmidt and Sørensen, 2018), Marstal (75,000 m^3) (Jensen, 2014) , Vojens (200,000 m^3) (Rambøll, 2015), Toftlund (70,000 m^3) (Rambøll, 2016), and Gram (122,000 m^3) (PlanEnergi, 2015). Additionally, there is one PTES under construction in Høje Taastrup (70,000 m^3) (Aalborg CSP, 2020) and one in the planning stage in Odense (1,000,000 m^3). Outside of Denmark there is only one operational PTES, which is in Lagkazi, Tibet (15,000 m^3) (Aalborg CSP, 2019).

All the existing PTES systems were constructed after 2012, and the technology has mainly been developed by making minor changes to existing designs based on previous practical experience. For this reason, research is necessary on topics of major importance to their operation and performance, e.g., their design.

This paper investigated the effect of two key design characteristics of PTES; the slope of the storage sides and the

aspect ratio (AR). Steeper side walls reduce the surface area of a storage, thus reducing heat losses. Similarly, an aspect ratio equal to one is desired from a heat loss perspective as it reduces the surface area of the storage. The effect of these parameters on heat loss and energy efficiency was investigated using a numerical simulation model in the software ANSYS Fluent. Last, the effect of ambient temperature on heat loss and efficiency was investigated using the same method.

2. Methods

The heat loss from a PTES can be divided into heat loss from the water through the insulated lid and the uninsulated side walls. The heat loss through the lid can be estimated as one-dimensional with high accuracy if the insulation properties are known. However, the heat loss to the soil is complex as it has to be modeled in 3D, and the soil's thermal capacity must be considered.

In order to investigate the effect of the design characteristics on the PTES performance, a model of the soil domain around the PTES was developed in ANSYS Fluent. Fluent is a computational fluid dynamics (CFD) software that uses the Green-Gauss Finite Volume Method (FVM) to discretize the conservation form of the partial differential equations.

The heat loss from the water to the soil was simulated by applying the water temperature (varying with height) to the soil boundary. This simplification is valid under the assumption that the convection coefficient between the water-soil interface is negligible relative to the conduction in the soil. By not including the PTES water in the model, only heat conduction in the soil had to be simulated instead of a fluid dynamics study; thus, the computation time was dramatically reduced.

2.1 Simulated PTES designs

The annual heat loss to the ground was calculated for five different storage configurations. The geometry of the reference case was modeled after the PTES in Marstal, and the water-soil interface was simulated using 16 vertical layers, each having a height of 1 m and a constant temperature for each time step.

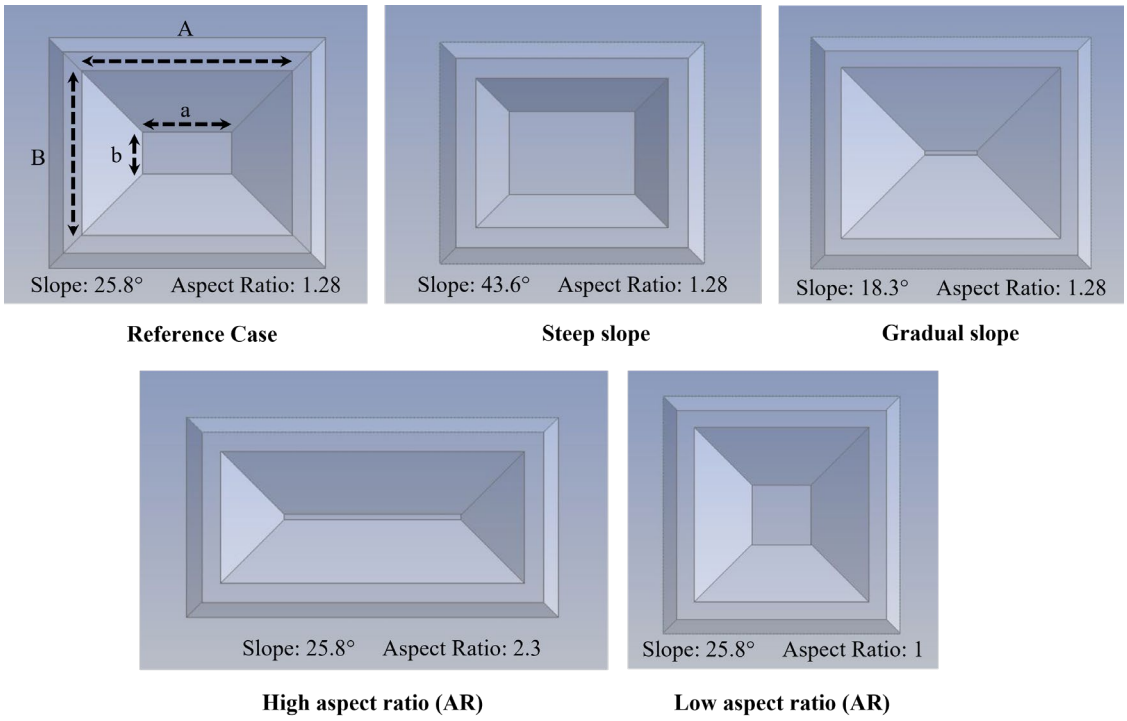

Fig. 1: Investigated PTES configurations.

The slope of the storage sides and the storage aspect ratio (AR) were investigated. The aspect ratio is the ratio of the long edge of the storage relative to the short edge, i.e., a square storage has an aspect ratio of 1, and a rectangular storage has an aspect ratio greater than 1. The five storage configurations are illustrated in Fig. 1, and their key characteristics are listed in Tab. 1. All the investigated storage configurations had the same storage volume, height, number of vertical layers, and volume per layer across PTES. Consequently, the area of the lid, side walls, and bottom walls varied greatly for the different designs. Also, it should be noted that the layers in each storage had different

heights for them to have the same water volume.

Tab. 1: Dimensions of the investigated scenarios.

Parameter	Reference case	Different slope tilt		Different aspect ratio		Units
		Steep slope	Gradual slope	High AR	Low AR	
Side slope	25.8	43.6	18.3	25.8	25.8	°
Lid aspect ratio	1.28	1.28	1.28	2.3	1	-
Bottom side length (a)	47.6	63.4	30.3	92	34.1	m
Bottom side width (b)	22.6	42	2	3.2	34.1	m
Top side length (A)	113.1	97	127.9	157.2	99.3	m
Top side width (B)	88.1	75.6	99.6	68.4	99.3	m
Sides and bottom area	11,022	9,110	13,396	11,971	10,886	m^2
Lid area	9,972	7,331	12,732	10,745	9,868	m^2
Storage height			16			m
Storage volume			76,929			m^3

From Tab. 1, it can be observed that the different slope tilts have a larger effect on the surface area of the storage. For example, the Steep slope case has 22% less surface area overall than the reference case, whereas the Gradual slope case has a 24% larger surface area compared to the reference case. On the other hand, the High AR case has an overall 8% larger area than the reference case, and the Low AR case has only a 1% smaller surface area than the reference case. These differences in the surface area are expected to impact the heat losses and efficiency of the PTES significantly.

2.2 Thermal properties of the ground and lid

It must be noted that the selected ground thermal properties are not necessarily exact for the PTES in Marstal. Instead, the selected values are indicative of the general soil conditions in eastern and central Denmark, which have moraine landforms with loamy soils rich in silt, clay, and sand (Adhikari et al., 2014). Typical values for moraine soil were taken from (Ditlefsen et al., 2012):

- Density: 2200 kg m^{-3}
- Specific heat: 1700 J kg^{-1} K^{-1}
- Thermal conductivity: 2 W m^{-1} K^{-1}

These values were used for the entire soil domain, which was initialized having a uniform temperature of 8 °C. The bottom of the soil domain (50 m below the bottom of the PTES) was simulated to have a fixed boundary temperature of 8 °C. The side walls of the soil domain were modeled using adiabatic boundary conditions. The top of the soil domain (which was in contact with the ambient air) was simulated to have a forced convection coefficient of 30 W m^{-2} K^{-1}, indicative of an average airflow velocity of 5 m/s according to Laloui and Rotta Loria (2020).

Regarding the lid, the thermal properties used in the calculations were chosen based on values of the original Nomalén (NMC Termonova, 2011) lid, which was initially installed in Marstal and Dronninglund. For calculating the heat loss through the lid, the following equation was used:

$$E_{lid\ loss} = A_{lid} \cdot k_{lid} \cdot h_{lid} \cdot (T_{top\ layer} - T_{amb}) \qquad \text{(eq. 1)}$$

where A_{lid} is the surface area of the lid, k_{lid} is the effective thermal conductivity of the lid structure (0.06 W m^{-1} K^{-1}), h_{lid} is the thickness of the lid (0.24 m), $T_{top\ layer}$ is the temperature of the storage's top layer, and T_{amb} is the ambient air temperature.

2.3 PTES and ambient temperature

The water temperatures from the Marstal PTES were used to simulate a seasonal heat storage operation from January 2013 to December 2015. The reference case (located in Denmark) was used for comparison, and with the same water-temperature profile, the storage was simulated for two additional locations, namely Finland and Greece. Regarding the ambient temperatures, Typical Meteorological Year (TMY) temperatures were used for Copenhagen (Denmark), Helsinki (Finland), and Athens (Greece). The data used in the simulations are presented in Fig. 2.

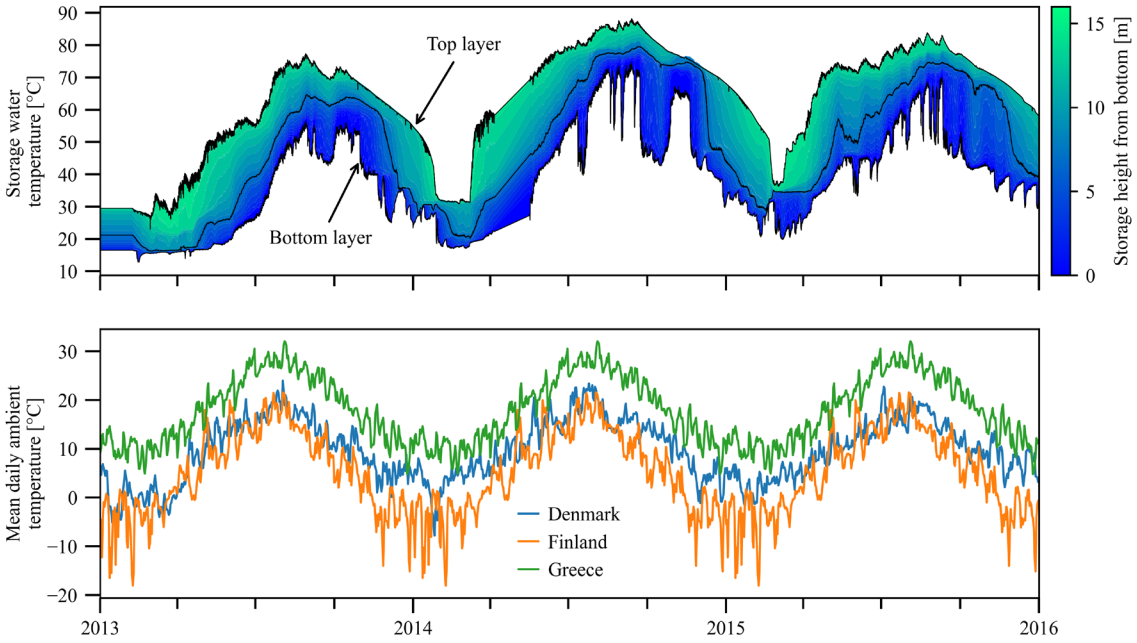

Fig. 2: PTES and ambient temperatures used in the simulations.

2.4 Efficiency calculation

The energy balance of a thermal storage system can be expressed as follows:

$$E_{out} = E_{in} - E_{loss} - \Delta E \qquad \text{(eq. 2)}$$

where E_{out} is the energy discharged from the storage, E_{in} is the charged energy, and E_{loss} is the energy lost due to heat losses. ΔE is the internal energy change of the storage, i.e., the difference between the internal energy at the start and end of the period of consideration.

Since all simulated PTES have the same volume and temperature per storage layer, they all have the same internal energy change. Assuming that they all have the same charged energy (E_{in}) and that the heat loss is calculated by the heat transfer CFD simulation, the discharged energy (E_{out}) can be calculated using Equation 2. Then the PTES energy efficiency can be calculated using Equation 3, as explained in (Sifnaios et al., 2022).

$$\eta_E = \frac{E_{out}}{E_{in} - \Delta E} = \frac{E_{out}}{E_{out} + E_{loss}} \qquad \text{(eq. 3)}$$

3. Results

So far, in all the constructed PTES, only the lid area has been insulated, whereas the sides and bottom have had no insulation. This decision was made for two main reasons:

1. It was difficult and expensive to find an insulation material that could withstand the weight of the water without collapsing.
2. It was not considered important due to most heat loss occurring through the lid's surface.

This last statement can be observed in Fig. 3, where the annual heat loss for the investigated PTES is presented. After three years of operation, for all cases, approximately 55% of the heat loss comes from the lid, while 42% from the sides and 3% from the bottom. However, it must be noted that the heat loss from the sides and bottom of the PTES decreases with time as the ground temperature stabilizes and that three years of operation are insufficient for a seasonal storage to stabilize the ground temperature.

In Fig. 3, it can be observed that the storage sides' slope considerably impacts the annual heat loss toward the ground. The main reason is that a steeper slope leads to a smaller surface area, thus leading to lower heat losses. The Steep slope case had 21% lower total heat loss overall and 16% lower heat loss toward the ground compared to the reference case. On the other hand, in the Gradual slope case, where the slope of the sides was less steep than in the reference case, the total heat loss was 22% higher, and the heat loss toward the ground was 17% higher. The Gradual slope case had lower bottom heat losses than the Steep slope case, but overall, the Steep slope had 35% lower heat losses.

Comparing the cases with the same slope (i.e., High AR and Low AR cases), it was found that a square PTES shape (aspect ratio=1) can decrease the lid heat loss by 9% and the loss toward the ground by also 9%.

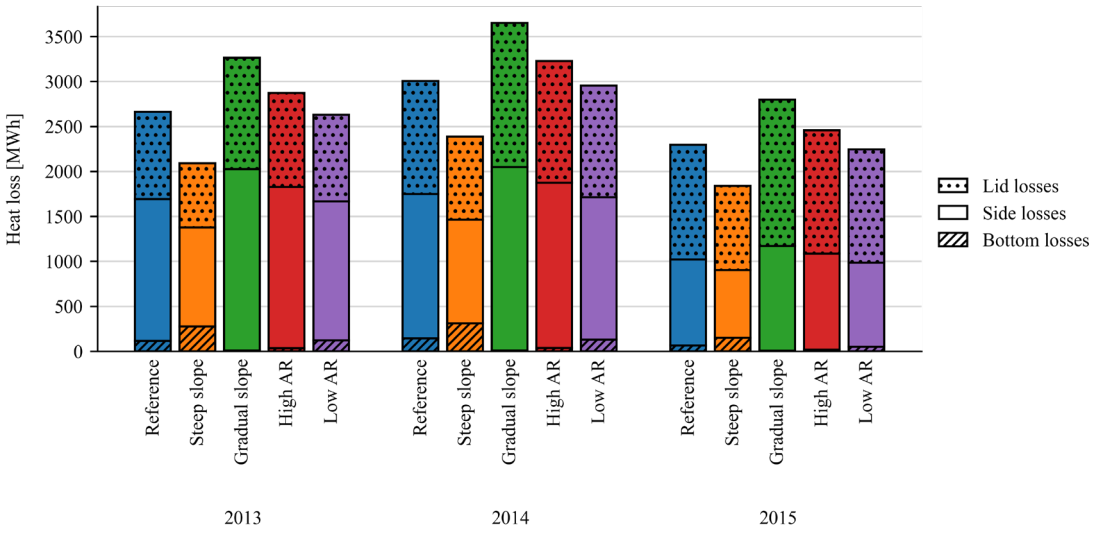

Fig. 3: Annual heat loss for the investigated PTES configurations.

The heat loss values for the last year of the simulation (2015) are reported in Tab. 2. The reason for showing only the values for 2015 is that, since there was preheating of the ground during the previous two years, the values for 2015 are considered more representative of the long-term operation of the PTES. The PTES energy efficiency was also calculated for 2015 for the different PTES configurations. It may be observed that the Steep slope had 6% higher efficiency than the reference case, while there was a 12% difference between the Steep and Gradual slope cases. Last, the square-shaped PTES of the Low AR case had 3% higher efficiency than the rectangular one of the High AR case. Although it is evident that the PTES design has a big impact on its performance, it has to be noted that, in many cases, its aspect ratio is dictated by the shape of the available plot of land. In addition, the side-wall slope is dictated by ground stability and, thus, the soil properties.

Tab. 2: Heat loss and efficiency for 2015 for the investigated PTES configurations.

Case	Bottom heat loss [MWh]	Side heat loss [MWh]	Lid heat loss [MWh]	Efficiency [%]
Reference case	63	957	1274	72
Steep slope	150	751	936	78
Gradual slope	4	1167	1626	66
High AR	17	1068	1373	70
Low AR	50	933	1261	73

The annual PTES heat loss for the different simulated countries is presented in Fig. **4**. As expected, the storage in Finland had the highest heat loss as Finland had the lowest ambient temperature of the investigated countries. On the contrary, the lowest heat loss occurred in Greece, which had the highest ambient temperature. The PTES in Finland had, on average, 5% higher total heat losses compared to Denmark, while the one in Greece had 8% lower.

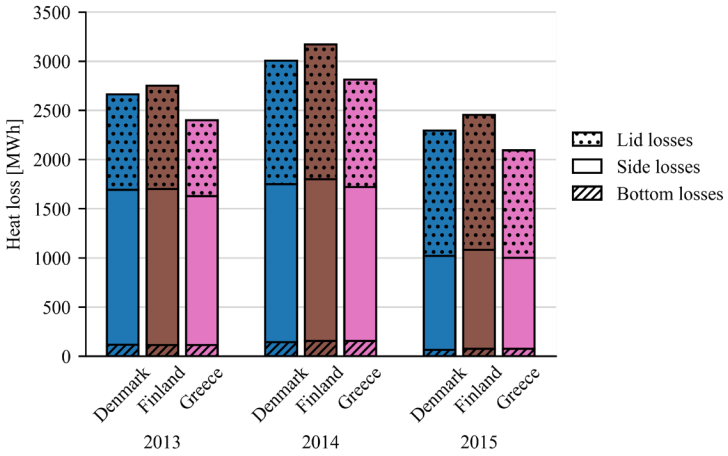

Fig. 4: Annual heat losses for Denmark, Finland, and Greece.

Table 3 presents the heat losses and efficiency for 2015 for the reference case for the three locations. The results show that the bottom heat loss is primarily affected by the storage temperature since all locations had the same bottom heat loss each year. The side heat losses were also comparable for the three locations, having a variation of approximately 9%. In contrast, the variation was much larger for the lid heat losses, namely 22%. Thus, the different ambient temperatures primarily affect the heat loss from the lid and, to a lesser extent, the heat loss from the sides. Last, a 5% variation in efficiency was calculated for the same storage water temperatures.

Tab. 3: Heat losses and efficiency for 2015 for Denmark, Finland, and Greece.

Country	Bottom heat loss [MWh]	Side heat loss [MWh]	Lid heat loss [MWh]	Efficiency [%]
Denmark	63	957	1274	72
Finland	63	1007	1373	70
Greece	63	923	1095	75

4. Conclusions

This study investigated the effect of two key design characteristics of pit thermal energy storage systems (the slope of the storage sides and the aspect ratio) and the effect of ambient temperature on storage heat loss and efficiency. A numerical simulation model was created in ANSYS Fluent that considered the soil domain around the PTES for investigating the heat loss from the water to the soil. Temperature data from the Marstal PTES were used to simulate the water domain from 2013 to 2015, and the design of the Marstal storage was used as the reference case. It was found that, due to a smaller surface area, a PTES with a steeper side slope had 21% lower total heat loss and 16% lower heat loss toward the ground compared to the reference one. Additionally, the square PTES design (aspect ratio=1) was shown to have a 9% lower total heat loss than the rectangular one. Furthermore, the slope of the PTES sides had a larger impact on the storage's efficiency than the aspect ratio; the variation in efficiency due to different side slopes was 12%, while the efficiency only varied by 3% due to different aspect ratios. Regarding different locations, a PTES in Greece was found to have 5% higher efficiency than one in Finland due to the higher ambient temperature that decreases the lid and side heat losses. Last, the heat losses through the bottom of a PTES were primarily affected by the storage temperature and not the ambient temperature since all simulated locations had the same bottom heat loss for each year.

5. Acknowledgments

This study was funded by the Danish Energy Agency through EUDP grant no. 64018-0134 and by the Sino-Danish Center for Education and Research (SDC) Ph.D. program.

6. References

Aalborg CSP, 2020. Aalborg CSP receives order for lid solution for Integrated Pit Thermal Energy Storage (PTES) System [WWW Document]. URL https://web.archive.org/web/20210417200554/https://www.aalborgcsp.cn/index.php?id=321&tx_news_pi1%5Bnews%5D=775&tx_news_pi1%5Bcontroller%5D=News&tx_news_pi1%5Baction%5D=detail&cHash=6

d7aff98a878e1d08d5ecd7f38e4fdbb (accessed 5.4.22).

Aalborg CSP, 2019. 15,000 M3 PTES for district heating, Tibet [WWW Document]. URL https://web.archive.org/web/20210418202632/https://www.aalborgcsp.com/projects/15000-m3-ptes-for-district-heating-tibet/ (accessed 5.4.22).

Adhikari, K., Minasny, B., Greve, M.B., Greve, M.H., 2014. Constructing a soil class map of Denmark based on the FAO legend using digital techniques. Geoderma 214–215, 101–113. https://doi.org/10.1016/j.geoderma.2013.09.023

Danish District Heating Association, 2021. Facts about district heating in Denmark [WWW Document]. URL https://web.archive.org/web/20220331213035/https://www.danskfjernvarme.dk/sitetools/english/about-us (accessed 5.4.22).

Ditlefsen, C., Vangkilde-Pedersen, T., Højberg, A.L., 2012. Geologi og jordvarmeboringer. Oversigt over geologiske forhold af betydning ved etablering af jordvarmeboringer i Danmark [WWW Document]. Natl. Geol. Undersøgelser Danmark og Grønl. URL https://geoenergi.org/xpdf/jordvarme-og-geologi-d3_2.pdf (accessed 9.5.22).

Jensen, M.V., 2014. Seasonal pit heat storages - Guidelines for materials & construction IEA-SHC Tech Sheet 45.B.3.2.

Laloui, L., Rotta Loria, A.F., 2020. Heat and mass transfers in the context of energy geostructures, Analysis and Design of Energy Geostructures. https://doi.org/10.1016/b978-0-12-816223-1.00003-5

Ministry of Foreign Affairs of Denmark, 2020. Global Climate Action Strategy [WWW Document]. URL https://web.archive.org/web/20220331213212/https://um.dk/en/foreign-policy/new-climate-action-strategy (accessed 5.4.22).

NMC Termonova, 2011. Nomalen 28N [WWW Document]. URL https://web.archive.org/web/20220426161150/https://azupcs365certviewer.azurewebsites.net/api/GetSDB?env=se&articleNr=550984 (accessed 4.20.22).

PlanEnergi, 2015. Long term storage and solar district heating [WWW Document]. URL https://web.archive.org/web/20220306155726/https://planenergi.dk/wp-content/uploads/2017/06/sol_til_fjernvarme_brochure_endelig.pdf (accessed 5.4.22).

Rambøll, 2016. Damvarmelagre [WWW Document]. URL https://web.archive.org/web/20220504080511/https://dk.ramboll.com/-/media/3fc11649e25942c195fa90e63ea41e11.pdf (accessed 5.4.22).

Rambøll, 2015. South-Jutland stores the sun's heat in the world's largest pit heat storage [WWW Document]. URL https://web.archive.org/web/20210827074933/https://ramboll.com/projects/re/south-jutland-stores-the-suns-heat-in-the-worlds-largest-pit-heat-storage?utm_source=alias&utm_campaign=sun-storage (accessed 5.4.22).

Schmidt, T., Sørensen, P.A., 2018. Monitoring Results from Large Scale Heat storages for District Heating in Denmark.

Sifnaios, I., Jensen, A.R., Furbo, S., Fan, J., 2022. Performance comparison of two water pit thermal energy storage (PTES) systems using energy, exergy, and stratification indicators. J. Energy Storage 52, 104947. https://doi.org/10.1016/j.est.2022.104947

Soerensen, P.A., From, N., 2011. High solar fraction with pit heat storages, in: 30th ISES Biennial Solar World Congress 2011, SWC 2011. pp. 3020–3030. https://doi.org/10.18086/swc.2011.21.07

Sveinbjörnsson, D., Laurberg Jensen, L., Trier, D., Ben Hassine, I., Jobard, X., 2017. Large Storage Systems for DHC Networks.

Winterscheid, C., Schmidt, T., 2017. Dronninglund District Heating Monitoring Data Evaluation for the Years 2015-2017.

V

VI. Heat losses in water pit thermal energy storage systems in the presence of groundwater

Ioannis Sifnaios, Adam R. Jensen, Simon Furbo, and Jianhua Fan

Applied Thermal Engineering, 235, 121382 (2023)

VI

Applied Thermal Engineering 235 (2023) 121382

Contents lists available at ScienceDirect

Applied Thermal Engineering

journal homepage: www.elsevier.com/locate/apthermeng

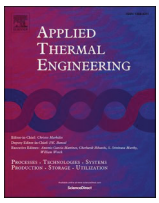

Research Paper

Heat losses in water pit thermal energy storage systems in the presence of groundwater

Ioannis Sifnaios [a,b,*], Adam R. Jensen [a], Simon Furbo [a], Jianhua Fan [a]

[a] Department of Civil and Mechanical Engineering, Technical University of Denmark, Koppels Allé 404, 2800, Kgs. Lyngby, Denmark
[b] Sino-Danish College (SDC), University of Chinese Academy of Sciences, Beijing, China

ARTICLE INFO

Keywords:
PTES
Heat storage
Computational Fluid Dynamics
CFD
Ground water

ABSTRACT

Water pit thermal energy storage (PTES) systems have proven a cheap and efficient storage solution for solar district heating systems. This is partly due to their low cost, deriving from low material usage as the ground is used as the weight-bearing structure. Further savings are obtained by the absence of insulation toward the ground, although this makes the ground-storage thermal interaction more pronounced than other storage technologies. However, it remains unclear how the different operation strategies affect the ground temperature and heat losses, especially in cases where groundwater is present. A simulation model was created using ANSYS and validated using operation data from the PTES in Marstal to investigate this. Using the validated model, it was found that the presence of groundwater could increase heat losses up to 60%, while the heat losses were unaffected when the groundwater table was more than 13 m below the storage bottom. The groundwater temperature could be maintained below 20 °C for a seasonal PTES if the groundwater table was at a depth of 25 m. However, maintaining this temperature for a short-term PTES operation was not feasible. Generally, the soil temperature was unaffected outside of a 100 m radius around the storage regardless of the operation type or the soil's thermal properties.

VI

1. Introduction

Thermal energy storage (TES) systems have been used in connection with large-scale solar heating plants for district heating (DH), enabling DH systems to achieve solar fractions of up to 50% [1]. For seasonal storage, four main types of TES have been utilized, namely, pit thermal energy storage (PTES), borehole (BTES), aquifer (ATES), and tank (TTES) [2]. While TTES and PTES typically use water as a storage medium, BTES systems use the soil itself [3], and ATES use natural underground aquifers as the storage medium [4]. Classification of TES can also be based on installation; ATES, BTES, and PTES are all underground, while TTES are usually placed above ground. Nonetheless, in some cases, large-volume TTES can be placed partially underground (e.g., as in [5]).

Except for TTES, which are insulated against the ground, the other seasonal storage technologies are in direct contact with the soil. For example, the sides and bottom of PTES systems are uninsulated and only lined with a watertight polymer liner to prevent water from leaking into the ground [6]. Consequently, the soil's thermal properties directly affect the heat losses and performance of PTES.

Heat transfer in the soil is mainly driven by thermal conduction [7], although it should be noted that soil is a multi-phase material and can consist of solid, gas, and liquid particles. While the presence of gas (i.e., air) obstructs heat conduction, its replacement with liquid (i.e., water) increases the thermal conductivity of the soil [8]. Additionally, higher moisture content can increase the soil's specific and volumetric heat capacity [9]. In general, the effective thermal properties of soil depend on the soil type, mineralogy, particle size, packing geometry, porosity, degree of saturation, and the state of the water (i.e., liquid or solid) [10,11].

High soil thermal conductivity (e.g., water-saturated soils) has been shown to increase heat losses, negatively impact efficiency, and reduce the achievable temperature of seasonal heat storage systems [12]. Thus, from a heat loss perspective, it is evident that placing underground TES systems in locations with low soil thermal conductivity is beneficial.

Similarly, the presence of groundwater, especially flowing groundwater, has been found to affect the efficiency of TES systems negatively. For example, the efficiency of ATES can drop as low as 10% for cases with groundwater flow rates higher than 50 m/year [13]. Depending on the velocity of the groundwater flow, the efficiency of BTES systems can

* Corresponding author.
E-mail address: iosif@dtu.dk (I. Sifnaios).

https://doi.org/10.1016/j.applthermaleng.2023.121382
Received 1 June 2023; Received in revised form 14 July 2023; Accepted 14 August 2023
Available online 16 August 2023

be reduced by up to 30% [14]. Similarly, PTES systems can have approximately 15% higher heat loss due to groundwater [15]. Last, the efficiency of TTES systems can be reduced by 8% due to the presence of groundwater [16]. In general, it is acknowledged that the most favorable geological conditions for TES systems are when there is no groundwater [17,18] or with a low flow rate (e.g., groundwater flow rates less than 1 m/year are acceptable for BTES [19]). Nonetheless, there are cases where TES systems are located within the groundwater table due to the absence of local sites with favorable soil conditions or poor planning.

The TES-groundwater interaction leads to reduced TES performance but also to an increase in the groundwater temperature. Since approximately half of the world's population relies on groundwater for potable water supply [20], it is paramount to ensure that the water quality is not negatively affected by the change in groundwater temperature. Studies have shown that temperature can considerably alter the groundwater's chemical composition, and an increase of 5–10 K is generally acceptable [21]. As a rule of thumb, as temperature increases, there is an increase in the concentration of some bacteria and chemical elements (e.g., manganese), which can be harmful to humans [22].

For this reason, some European countries have placed limits on the maximum groundwater temperature, e.g., in Austria (20 °C), Denmark (25 °C), and the Netherlands (25 °C) [23]. Additionally, a relative change in the groundwater temperature of ±6 K is given in the geothermal installation guidelines in Austria (legally binding) and Germany (recommended) [23] and ± 3K in Switzerland (legally binding) [24].

To adhere to these regulations, Dahash et al. [16] investigated the impact of a groundwater barrier and the addition of insulation between the groundwater surface for PTES or the increase in the insulation thickness for TTES. They found that, for maintaining the groundwater temperature below 20 °C, a vertical water barrier (blocking groundwater movement around the storage) should be placed 25 m from the TES, combined with insulation around the TES. However, the study only investigated seasonal storage operation. In seasonal operation, PTES systems may act as the source for heat pumps; thus, the temperature operation range is usually 15 – 90 °C, while it is 45 – 90 °C for short-term operation. Due to the lack of research, it is unclear how the differences in long-term and short-term operations affect groundwater temperature. In addition, the study by Dahash et al. only considered a ten-year period, while the expected lifetime is 25 for a PTES and 40 years for a TTES. Thus, different results could be expected when simulating the full lifetime of the storage systems.

Besides the thermal conductivity of the soil domain and the presence of groundwater, the soil temperature can also affect the TES operation. The temperature of the upper soil layer fluctuates during the year mainly due to heat exchange with the ambient air, whereas an almost constant temperature is typically achieved at depths below 10 m [25]. However, heat losses from heat storage will gradually increase the temperature of the surrounding soil. Dahash et al. found that the ground temperature in the vicinity of a PTES or TTES can reach up to 50 °C during charging periods [26]. Moreover, simulations of a seasonal BTES system using the finite element simulation software COMSOL [27] indicated a 10 K temperature increase in the soil around the boreholes within one year and predicted a 16 K increase after five years [28]. In general, the ground heat losses of a TES can be divided into a periodic variation with an annual cycle and an initial part with a transient thermal build-up around the storage [29]. The transient temperature built-up around the storage is significant during the initial two to ten years of operation (depending on the storage size), while the periodic yearly variation is the most important long-term. Hence, it is important to investigate the heat loss of a TES system for several years as it is not constant, even if constant operation and ambient conditions can be assumed. However, it is not evident from the literature how long it takes for TES heat losses to stabilize due to the warm-up of the surrounding ground and if the length of this period depends on the operation (i.e., seasonal vs. short-term) and soil properties.

Traditionally, PTES had been used only for seasonal heat storage in conjunction with large-scale solar heating plants. However, in 2023, a new PTES was put into operation in Høje Taastrup (Denmark), which is operated as a short-term storage (two-week cycle) and is directly connected to the DH grid [30]. Thus, PTES can be used for both seasonal and short-term operations, unlike other storage technologies (e.g., ATES and BTES).

However, the change in operation strategy significantly alters the seasonality of the heat losses to the ground, although this has yet to be studied in detail. For this reason, the aim of this study is to elucidate the effect of different PTES operations on the surrounding ground and groundwater. Additionally, the effect of seasonal and short-term operations on groundwater will be investigated.

The present study focused on PTES, a promising heat storage technology combining low construction costs with high storage efficiency. The efficiency of the existing seasonal PTES varies from 60% to greater than 90% [31]. However, there are no specific guidelines regarding the optimal ground conditions for a PTES, and it is currently unclear how large of an impact ground conditions have on PTES performance. For example, at the Dronninglund PTES, there is a groundwater Table 1–1.5 m below the storage bottom with a flow rate of 15 m/year [32]. For maintaining a lower construction cost than TTES, PTES systems are not insulated toward the ground. Thus, they are expected to be influenced by the ground conditions much more than insulated technologies (e.g., TTES). Nevertheless, it remains unknown if and how much the groundwater affects the PTES performance and if the storage operation increases the groundwater temperature.

For this reason, the present study aims to investigate the following research questions:

- How long does it take for the ground temperature around a PTES to stabilize under short- and long-term operation?
- How large is the temperature zone of influence for a PTES?
- At what depth does the groundwater need to be for it not to affect PTES performance?
- How far from the PTES should groundwater be to satisfy the groundwater temperature regulations?

To answer these questions, a simulation model of the soil surrounding a PTES was developed and used to study the heat losses from the water-ground interface and the temperature development in the soil domain. The model was validated by comparison against measurement data from the PTES in Marstal. The validated model was used to simulate heat losses to the ground assuming different soil conductivities and groundwater conditions for short-term and seasonal PTES operations.

The PTES in Marstal is described in Section 2.1, followed by the description of the developed simulation model in Section 2.2. Section 2.3 presents the PTES water temperature profiles, and Section 2.4 the groundwater settings used in the simulations. The validation of the simulation model is presented in Sections 3.1 and 3.2, followed by the investigations for heat loss stabilization in Section 3.3. The PTES interaction with the surrounding soil is presented in Section 3.4, followed by the interaction with groundwater in Section 3.5. Last, the conclusions are presented in Section 4.

2. Methods

2.1. The PTES in Marstal

The PTES system in Marstal was constructed in 2012 with an approximate storage capacity of 6,000 MWh. The storage had the shape of an inverse truncated pyramid, with a volume of 75,000 m^3. The storage depth was 16 m, and the floating lid measured 113 by 88 m. The PTES was charged with heat from a 15,000 m^2 flat-plate solar collector field and used primarily for seasonal storage. Hence, the PTES was mainly charged during spring and summer and discharged during

autumn and winter.

The DH supply temperature in Marstal was approx. 73 °C, while the average return temperature was 40 °C [33]. When the temperature in the top layers of the PTES was sufficiently high, the storage could supply heat directly to the grid. However, when the storage temperature was below the supply temperature, the storage acted as a heat source for a 1.5 MW_{th} heat pump that supplied heat to the DH network. During autumn and winter, the heat pump operation lowered the PTES temperature to 15–20 °C. A more detailed description of the design and operation of the Marstal PTES can be found in [31]. An aerial photo of the solar collector field and PTES in Marstal can be seen in Fig. 1.

It should be mentioned that the Marstal PTES was used for validating the developed model due to the extensive ground temperature measurements.

2.1.1. Measurement locations and uncertainty

The water temperature inside the storage was measured using two temperature sensor strings mounted in the center of the lid. Each string had 16 temperature sensors placed at 1 m intervals. The two temperature strings were located next to each other but offset vertically by 0.5 m; thus, the vertical temperature profile was measured every 0.5 m. The temperature sensors were Class A PT100, with an accuracy of ±0.15 K.

Additionally, to monitor the change in ground temperature, four temperature sensor strings were installed near the edges of the storage embankment. The ground temperature sensors were PT100, but since their class is unknown, their accuracy was estimated to be ±0.5 K. The locations of all the temperature sensors are illustrated in Fig. 2.

2.1.2. Soil domain

The soil properties and groundwater conditions were assessed before the storage construction. Specifically, soil samples were taken from ten boreholes at a depth of either 14 or 24 m, with a uniform spatial distribution. Both intact soil samples were taken, and field vane tests were performed. The report of the soil investigations stated that the soil conditions were “messy,” with alternating deposits of sand and clay and varying groundwater levels [35]. The stratigraphy of the terrain can be found in.

In many cases, groundwater was found at two different levels in the same borehole. However, the groundwater levels were different at each borehole. This indicated that there were probably isolated groundwater pockets in the area. Consequently, the exact dimensions and depth of the groundwater are unknown. Additionally, groundwater levels tend to change throughout the year due to rainfall, snowmelt, and dry periods [36].

According to the literature, the mean annual soil surface temperature in Denmark is 8 °C, and while there is a small increase with increasing depth, the temperature is within 8–12 °C down to a depth of 250 m [37]. No measurements were made of the soil’s thermal properties; thus, the properties used in the simulations were taken from the literature, as summarized in Table 1. It has to be noted that, due to the high uncertainty regarding the extent of groundwater, uniform thermal properties were assumed for the entire soil domain.

Fig. 1. Aerial photo of the Marstal PTES in 2013 [34].

2.2. Simulation model of the PTES in Marstal

Heat losses from a PTES consist of heat losses through the insulated lid and through the uninsulated side and bottom walls. Accounting for the heat losses through the insulation lid is relatively straightforward as the phenomena can reasonably be assumed as one-dimensional. The heat losses through the lid are generally uniform, with some thermal bridges at the connection points of the insulation blocks. The main parameters affecting the lid heat losses are the ambient temperature, the top water layer temperature, and the effective heat loss coefficient of the lid. On the other hand, accounting for the heat losses to the ground is much more complex due to the non-negligible heat capacity of the soil. Consequently, the transient nature of the heat losses to the ground has to be considered and requires modeling in 3D. Several other parameters also affect the ground heat losses, e.g., the temperature gradient within the PTES, the soil’s thermal properties, and the presence of groundwater.

For this reason, a 3D model of the soil domain around the PTES was developed using the finite volume method (FVM) software ANSYS Fluent. Fluent uses a numerical approach to solve the governing equations of fluid flow, offering a range of capabilities for simulating laminar and turbulent flows, heat transfer, etc. [39]. The simulation is conducted on a user-defined domain that is discretized using a computational mesh. Since this investigation focused on the heat losses toward the ground, the water and lid of the PTES were not explicitly modeled. By not modeling the movement of the water inside the PTES, only heat conduction in the soil had to be simulated instead of a fluid dynamics study, drastically reducing the computation time.

The heat losses from the water to the soil were simulated by applying the water temperature (varying with height) as a boundary condition on the soil’s surface. This simplification was based on the following assumptions:

- The water temperature in the PTES can reasonably be described by 16 uniform-temperature layers, each 1 m tall.
- The convection coefficient between the water-soil interface is negligible relative to the thermal conduction in the soil.
- The water temperature profile is predominantly affected by charging/discharging and not by heat losses to the ground.

In the simulations, the soil domain was initialized with a uniform temperature of 8 °C. Heat exchange between the soil surface and the ambient air was simulated by applying a convection coefficient of 30 W/(m^2 K) to the exposed ground surface (corresponding to an average airflow velocity of 5 m/s) [40]. It has to be noted that the simulation of the soil domain did not account for solar radiation. In the first simulated year, corresponding to the construction period, the PTES soil was only exposed to the ambient temperature (pre-heating period) in order to achieve a realistic ground temperature profile to develop.

The extent of the surrounding soil domain had to be large enough to avoid the boundary conditions influencing the PTES operation. For this reason, the soil domain was extended 150 m away from the PTES edges, and the model had a depth of 200 m (see Fig. 3). Adiabatic boundary conditions were used for the side and bottom of the soil domain. In reality, there is some small heat gain from the Earth’s core, but it was assumed negligible.

The created mesh consisted of hexahedral elements. The cells closer to the water-soil boundary have a higher density and a smaller size. This was done to ensure a high mesh density close to the heat source where large temperature gradients are expected. A mesh and timestep independence investigation was performed to confirm that the mesh was of sufficient quality and that an appropriate timestep had been selected

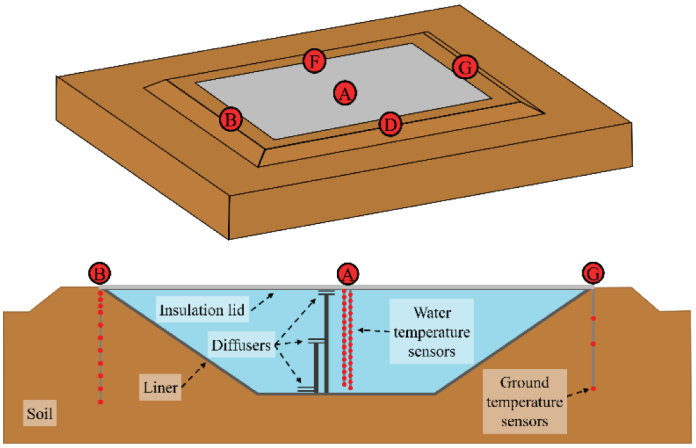

Fig. 2. Measurement sensor locations in the Marstal PTES. The water temperature strings are attached at location A, and the soil temperature is measured at locations B, D, F, and G. Each small red dot corresponds to a temperature sensor. (For interpretation of the references to color in this figure legend, the reader is referred to the web version of this article.)

Table 1
Thermal properties of sand and clay for different water contents (up to 25% for sand and 50% for clay) [38].

Soil type	Thermal conductivity [W/(m K)]	Specific heat capacity [J/(kg K)]	Bulk density [kg/m^3]
Sand (dry-moist)	0.3 – 1.9	590 – 1158	1800 – 2200
Sand (saturated)	2.0 – 3.0	956 – 1474	1900 – 2300
Clay (dry-moist)	0.4 – 1.0	789 – 842	1800 – 2000
Clay (saturated)	1.1 – 3.1	952 – 1333	2000 – 2200

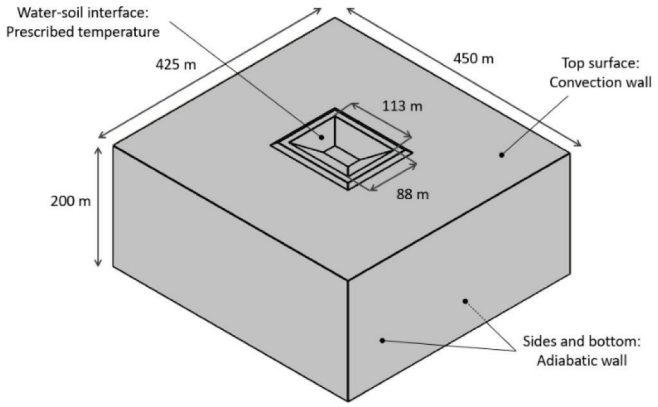

Fig. 3. The simulated soil domain and boundary conditions.

(see Section 3.1). Different mesh densities and timestep durations were selected and compared based on the calculated heat losses to the ground.

The model was validated by comparison against measured ground temperature data from the Marstal PTES from 2013 to 2016 (see Section 3.2).

2.3. Water temperature profiles

Theoretical temperature profiles were made corresponding to seasonal and short-term PTES operations. The seasonal PTES operation performed one charge–discharge cycle per year, with a temperature range of 90 – 15 °C (based on the actual operation of the PTES in Marstal [31]). The short-term operation was modeled as performing one charge–discharge cycle every two weeks (26 cycles per year), and the temperature range of the short-term operation was between 90 and 45 °C. The operation of the short-term PTES resembled the PTES in Høje Taastrup, Denmark [30,41]. It should be noted that for both storage operations, the top water layer was assumed to be constantly at 90 °C. The ambient temperature profile was taken from Denmark's Design Reference Year (DRY) [42]. Fig. 4 illustrates the mean storage temperature for the seasonal and short-term operations and the daily mean ambient temperature used in the simulations. The simulation duration was 25 years, so these profiles were repeated 25 consecutive times.

2.4. Groundwater simulation

For the initial investigations, the soil domain thermal properties were considered uniform and without the presence of groundwater. However, to investigate the interaction between the PTES and the groundwater, a groundwater layer was added to the domain for the simulations presented in Section 3.5. Realistic groundwater characteristics were taken from the PTES in Dronninglund [32] (presented in Table 2), as there was no pronounced groundwater layer at Marstal. This assumption was considered acceptable since similar geological

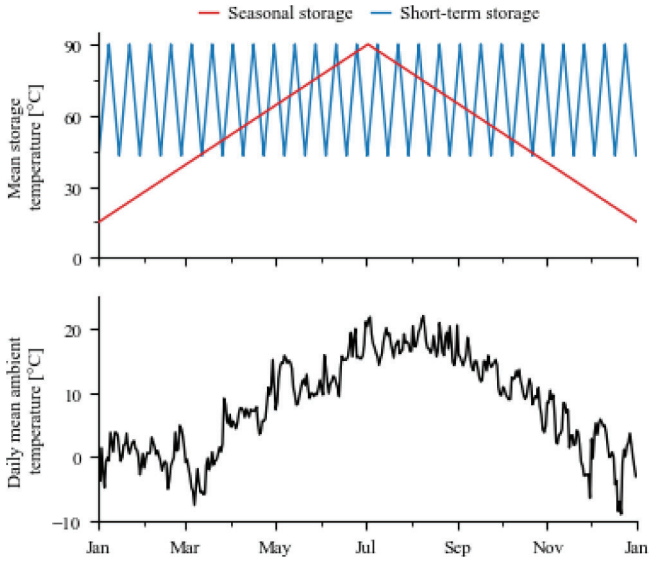

Fig. 4. Mean storage and ambient temperature for the simulated storage operations. The same conditions were repeated for each year of the simulation.

Table 2
Groundwater properties [44].

Parameter	Value	Unit
Hydraulic conductivity	$3.6 \cdot 10^{-5}$	m/s
Effective porosity	0.25	–
Hydraulic gradient	1/300	–
Groundwater velocity	$4.8 \cdot 10^{-7}$	m/s

conditions exist in Marstal and Dronninglund (i.e., the soil consists primarily of clay and sand). The groundwater was simulated as a 10 m layer, which is a representative value for confined aquifers [43] (and was also used in [16]) and was assumed to have the same temperature as the initial soil domain (i.e., 8 °C). However, it should be noted that groundwater characteristics can be very different depending on the investigated location.

The groundwater layer was simulated in ANSYS as a porous medium, and the flow was described using Darcy's law, as shown in Eqs. (1) and (2). Darcy's equations assume that the flow is laminar, viscous, and ignores convective acceleration and diffusion.

$$q = -\frac{\kappa}{\mu}\Delta p \tag{1}$$

$$u = \frac{q}{\varphi} \tag{2}$$

where q is the flux discharge per unit area, Δp is the pressure gradient vector, κ is the permeability, μ is the dynamic fluid viscosity, u is the fluid velocity, and φ is the porosity [45].

3. Results

3.1. Mesh and timestep independence of the CFD model

First, the mesh independence study was performed, where the heat losses for one year of operation were calculated for models with different numbers of cells. The calculated heat losses and the corresponding simulation time for each model are presented in Fig. 5. It can be observed that as the number of cells increased, the calculated heat loss for the scenarios with cells above 900 k reached an almost constant value, thus independent of the density of the mesh. The calculated heat loss for the scenario with 900 k cells differed only by 1% compared to the 3600 k case, while the simulation time was reduced by 73%. For this reason, it was decided that a mesh having 900 k cells was a good compromise between accuracy and simulation time. The mesh independence study was done using an 8 h timestep.

Next, the timestep independence was investigated using the mesh with 900 k cells. Similarly to the mesh independence, the calculated heat loss and simulation time for a simulation of one year of operation is presented in Fig. 5. The calculated heat loss for the case with the 8 h timestep differed by 0.7% compared to the 2 h case, while the simulation time was reduced by 68%. For this reason, a timestep of 8 h was chosen.

3.2. Model validation

The simulation model was validated against measured ground temperature data from the Marstal PTES for 2013 – 2015. As described in Section 2.2, the year 2012 was used as a pre-heating period.

In Fig. 6, measured ground temperatures can be observed at various depths. Depending on the level, each depth has two or four temperature sensors (see Fig. 2 and Section 2.1.1). The variation in the measured temperatures at the same depth demonstrates the mixed soil conditions around the PTES. In some cases, the temperature measured from two different sensors at the same height differed by up to 10 K, indicating the possible presence of groundwater pockets.

Comparing the simulated and measured temperatures in Fig. 6, it may be observed that the simulated ground temperatures follow the same trend as the measured ones at all depths, with an RMSE ranging from 0.22 to 1.54 K. Due to the highly uncertain ground conditions around the Marstal PTES (and also considering the sensor uncertainty), the difference between the simulated and measured temperatures was considered satisfactory. The following ground thermal properties were used in the simulation: thermal conductivity of 1.6 W/(m K), specific heat capacity of 800 J/(kg K), and bulk density of 2000 kg/m^3. These values are in line with the literature (see Table 1).

3.3. Heat loss and ground temperature stabilization

Fig. 7 presents the yearly heat losses toward the ground for a seasonal and short-term PTES operation for a period of 25 years. It can be observed that the heat losses decrease during the entire operation period of the PTES, with the first years having the most dramatic decrease. The reason for the reduction of heat loss with time is that when the PTES starts operating, the soil temperature around it is much lower than the charged water temperature. Thus, high heat transfer occurs from the PTES water to the soil. As the PTES continues to operate, heat accumulates in the soil, and the soil temperature increases; thus, the heat loss toward the soil decreases. More specifically, for the seasonal operation, the heat losses for the second year were 37% lower than the first.

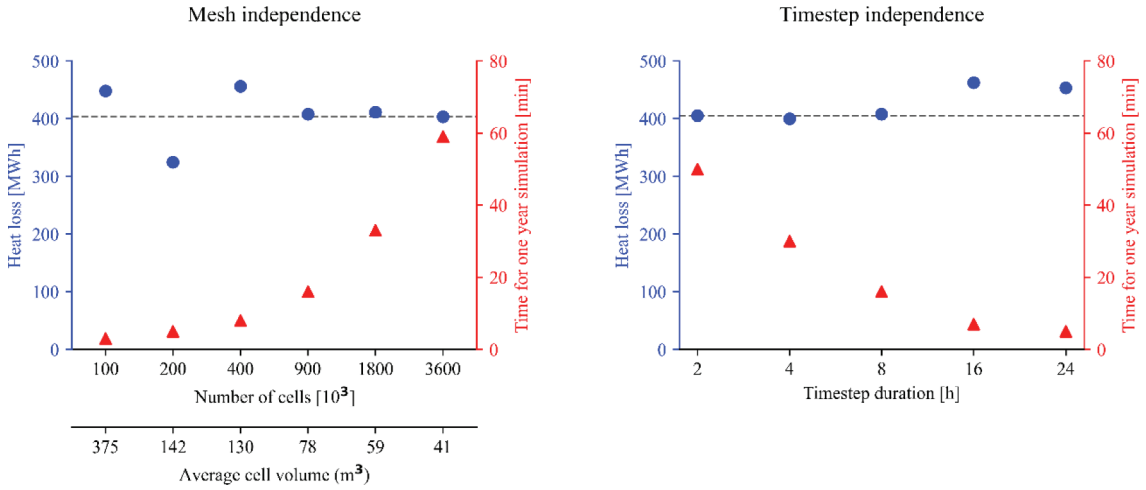

Fig. 5. Mesh (left) and timestep (right) independence results. The yearly heat loss is shown on the left y-axis (blue circles), and the time for one year of simulation is shown on the right y-axis (red triangles). (For interpretation of the references to color in this figure legend, the reader is referred to the web version of this article.)

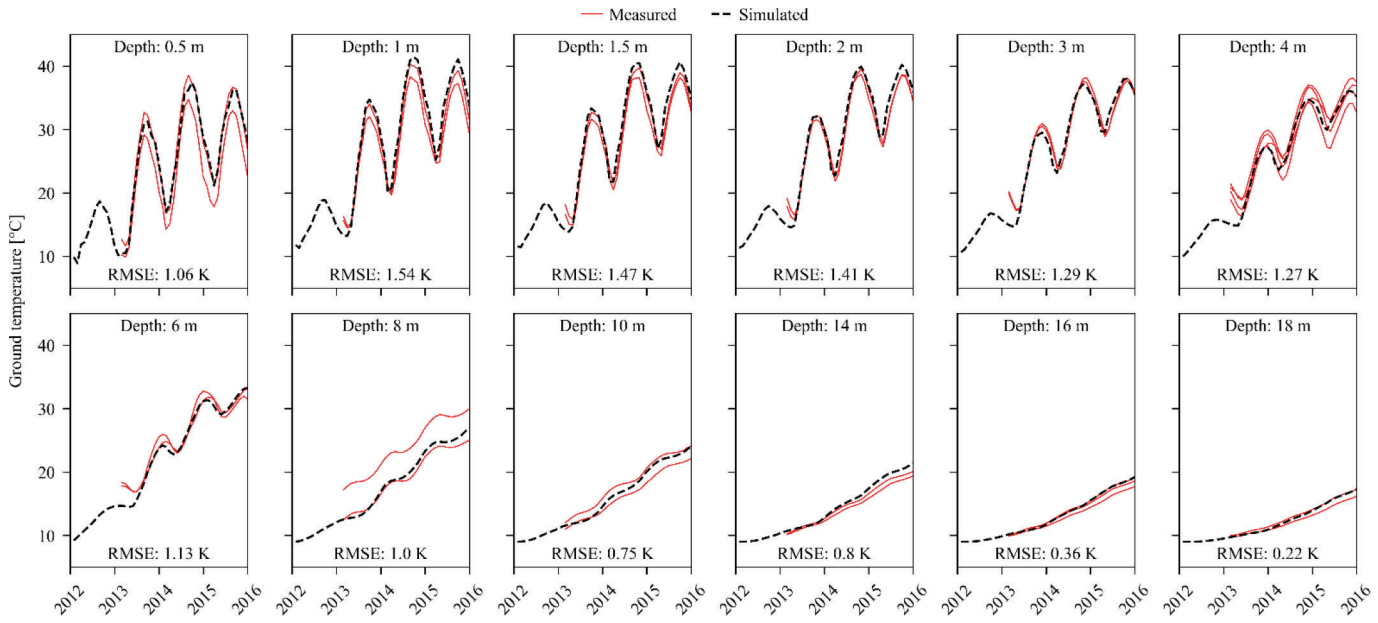

Fig. 6. Measured and simulated ground temperatures for the Marstal PTES from 2012 to 2015. Note that depending on the depth, there are two or four measured temperature curves.

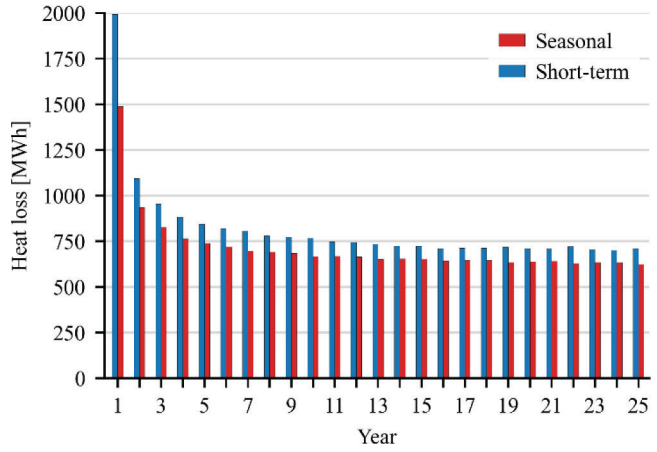

Fig. 7. Yearly heat losses toward the ground for seasonal and short-term PTES operation.

However, the third year was only 12% lower than the second. The heat losses in the last year of operation were 58% lower than the first. Although there was a decrease during the entire operation period (25 years), after the 12th year, the change in the heat losses from one year to the next was less than 2%, so the heat losses could be considered stable after this point.

A similar trend can be observed for the short-term PTES operation. For example, the second year of operation had 45% lower heat losses than the first, while the last year had 64% lower heat losses than the first. Overall, the heat losses stabilized quicker than the seasonal operation, i.e., in the 8th year of operation. It should also be noted that the short-term PTES had approximately 15% higher heat losses than the seasonal one due to the higher average water temperature. However, the relative heat losses of the short-term storage are lower than the seasonal, and thus the short-term efficiency is higher, although the annual heat losses are higher. This is due to the greater number of storage cycles of the short-term PTES, i.e., 10 – 20 times as much energy is stored annually.

The ground temperatures around the PTES for the 25 years of operation are presented in Fig. 8. It can be observed that, for both PTES operations, there is a yearly variation in the soil temperature close to the surface induced by the ambient temperature variation during the year. However, this variation is much more intense in the case of seasonal PTES operation. The reason is that a seasonal storage is discharged to much lower temperatures than a short-term (due to the heat pump operation). Thus, the soil temperature around the seasonal PTES is much lower in the winter (when it is empty) than the short-term PTES.

Fig. 8 also demonstrates that the soil temperature close to the PTES is not stabilized even after 25 years of operation (especially in lower depths). The increase in the soil temperature, even after 25 years of operation for the short-term PTES, is due to the higher minimum

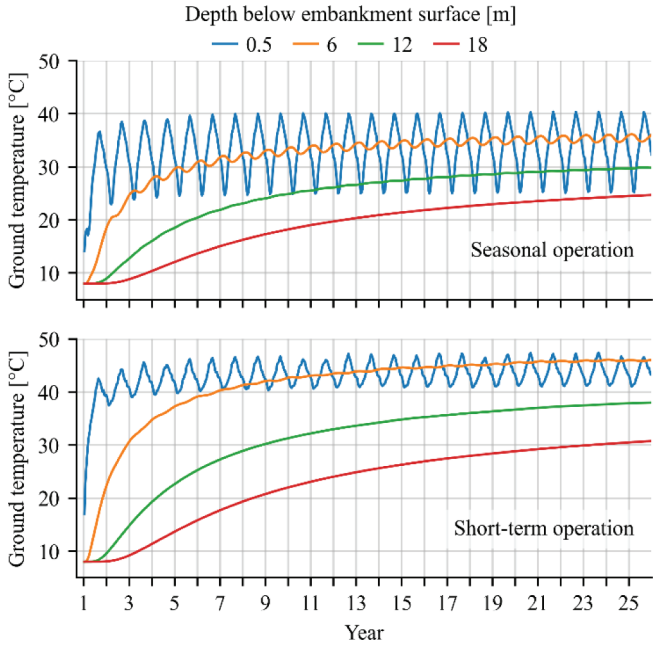

Fig. 8. Ground temperature development at different depths for seasonal and short-term PTES operations. The horizontal location corresponds to location B in Fig. 2.

temperatures of the short-term PTES compared to the seasonal. It is thus important to consider the entire lifetime of a PTES when assessing its effect on the surrounding soil and groundwater temperatures.

3.4. PTES zone of influence

In order to determine the dimensions of the soil domain that was affected by the operation of a PTES, a zone of influence was established. This zone was determined by calculating the soil temperature on a horizontal and a vertical line, starting at the bottom of the PTES and extending to the end of the soil domain (see Fig. 9).

A low and a high soil conductivity scenario were investigated to investigate the possible effect of soil conductivity on the size of the zone of influence. For the high conductivity scenario, a thermal conductivity of 3 W/(m K), a specific heat capacity of 1400 J/(kg K), and a bulk density of 2300 kg/m^3 was used. In contrast, for the low conductivity scenario, a thermal conductivity of 0.3 W/(m K), a specific heat capacity of 700 J/(kg K), and a bulk density of 1800 kg/m^3 was used. These values were the extremes for each parameter from Table 1. The ground temperatures are illustrated in Fig. 9 for both scenarios. It should be noted that Fig. 9 shows the temperature in the soil domain at the start of July (i.e., both storage types were fully charged) after 25 years of PTES operation.

As expected, the ground around the short-term PTES reached higher temperatures than the seasonal PTES. Additionally, the high-conductivity soil domain reached higher temperatures than the low-conductivity domain at the same depth. Nonetheless, the soil temperature was unaffected outside of a 100 m radius from the storage, regardless of the operation type or the thermal properties of the soil.

3.5. PTES and groundwater

The effect of groundwater on the soil temperature is illustrated in Fig. 10 after 25 years of PTES operation. In the previous sections of this paper, it was proven that the short-term operation of a PTES results in higher soil temperatures; thus, the results presented in Fig. 10 are only for short-term operation for space-saving purposes.

Fig. 10 presents calculated soil temperature contour plots for three groundwater scenarios; scenario (A) has no groundwater, (B) has a static groundwater layer, and (C) has a moving groundwater layer. The groundwater layer modeling was done as described in Section 2.4. The depth of the groundwater layer was 5 m below the ground surface (average depth for Denmark [46]), resulting in the bottom half of the PTES being within the groundwater layer.

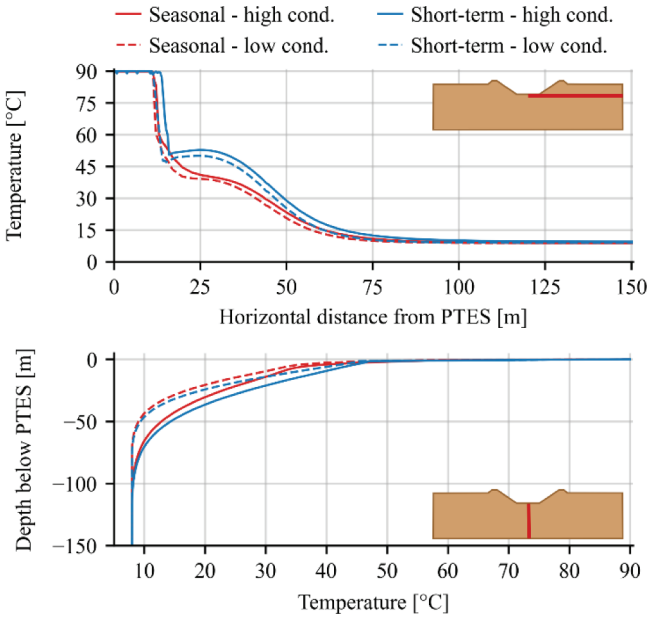

Fig. 9. Ground temperature profile after 25 years of operation for a high and low conductivity (cond.) soil domain. The soil temperature was calculated on a horizontal line and a vertical line. Both lines started at the bottom center of the PTES and extended to the end of the soil domain.

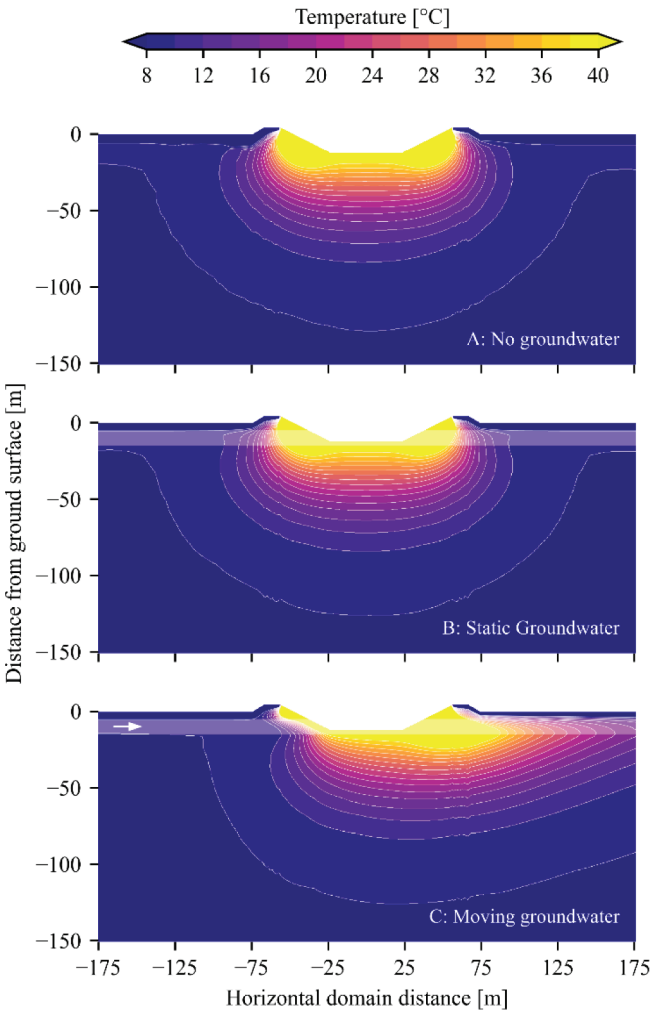

Fig. 10. Soil temperature contours for short-term PTES operation where there is no groundwater (A), one static groundwater layer (B), and one moving groundwater layer (C). The semi-transparent horizontal white bar in the bottom two subplots illustrates the groundwater layer.

It may be observed that the contours in (A) and (B) are very similar. However, in case (B), the soil temperatures are somewhat higher due to the presence of groundwater and, thus, higher thermal conductivity in this layer. As expected, the largest difference can be spotted in sub-figure (C), where, due to the moving groundwater, the temperature contours are shifted in the direction of the moving groundwater.

Apart from the differences in the soil temperature profiles, groundwater also impacted the heat losses. Table 3 presents each case's average yearly heat loss for the 25 years of operation for seasonal and short-term

Table 3
Yearly average heat losses toward the ground of the seasonal and short-term PTES operation for different groundwater conditions. Values are in MWh.

Scenario	Seasonal	Short-term
No groundwater	715	820
Static groundwater	820	927
Moving groundwater	1118	1333

VI

PTES operations. It may be observed that both PTES operations are affected similarly, having approximately 14% higher heat losses for static groundwater (B) and approximately 60% higher heat losses for moving groundwater (C) compared to the case without groundwater (A).

It should be noted that the results in Table 3 are for a case where the groundwater is located 5 m below the ground surface (thus, the lower half of the PTES is surrounded by groundwater). Consequently, the next step was to investigate the impact of the depth of the groundwater layer. Since the highest heat losses occurred for the scenario with moving groundwater (15 m/year), this case was selected for investigating different depths. These results are presented in Fig. 11.

Fig. 11 presents the heat losses from a PTES operating in seasonal or short-term mode with different depths of the groundwater layer. As expected, the closer the groundwater layer is to the PTES bottom, the higher the heat loss. Specifically, the heat losses were approximately 40% higher when the groundwater was 5 m below the ground surface compared to when the groundwater layer was at 25 m.

It may be observed that the PTES heat losses were unaffected by the presence of groundwater at a depth of 25 m below the ground surface (or 13 m below the bottom of the PTES). This was true for both seasonal and short-term PTES operations.

Fig. 12 and Fig. 13 show the corresponding temperature profile for the seasonal and short-term PTES operation, respectively. The groundwater depth ranged from 5 m below the surface (A) to 30 m below the surface (F). It may be observed that the temperature contours are skewed toward the moving direction of the groundwater in both figures. In Fig. 12, the highest temperature contours (greater than 25 °C) are located only close to the PTES sides since the heat pump operation cools the bottom to lower temperatures. However, in Fig. 13, the highest temperature contour is located around all sides of the PTES. Generally,

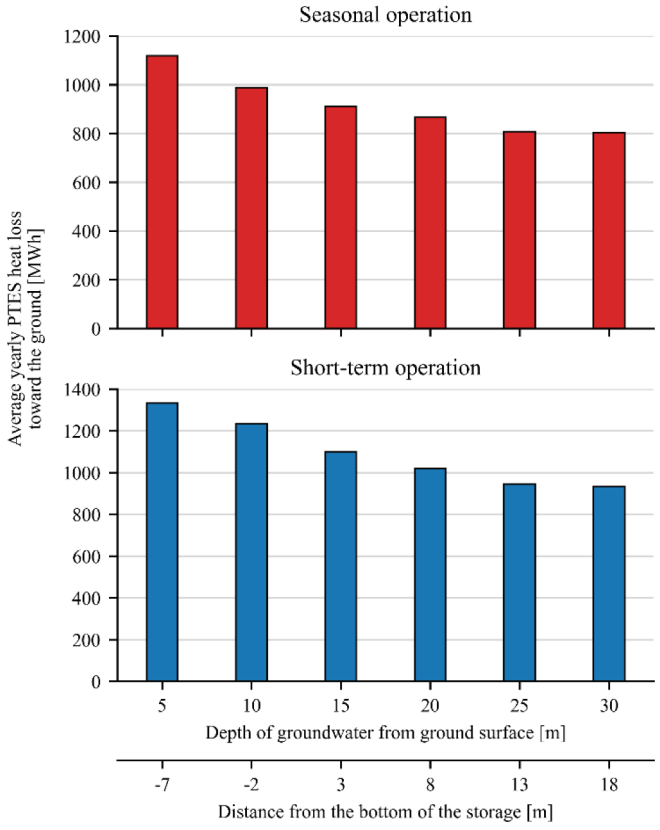

Fig. 11. Average yearly heat losses toward the ground for seasonal and short-term PTES operations at different groundwater depths for a moving groundwater layer.

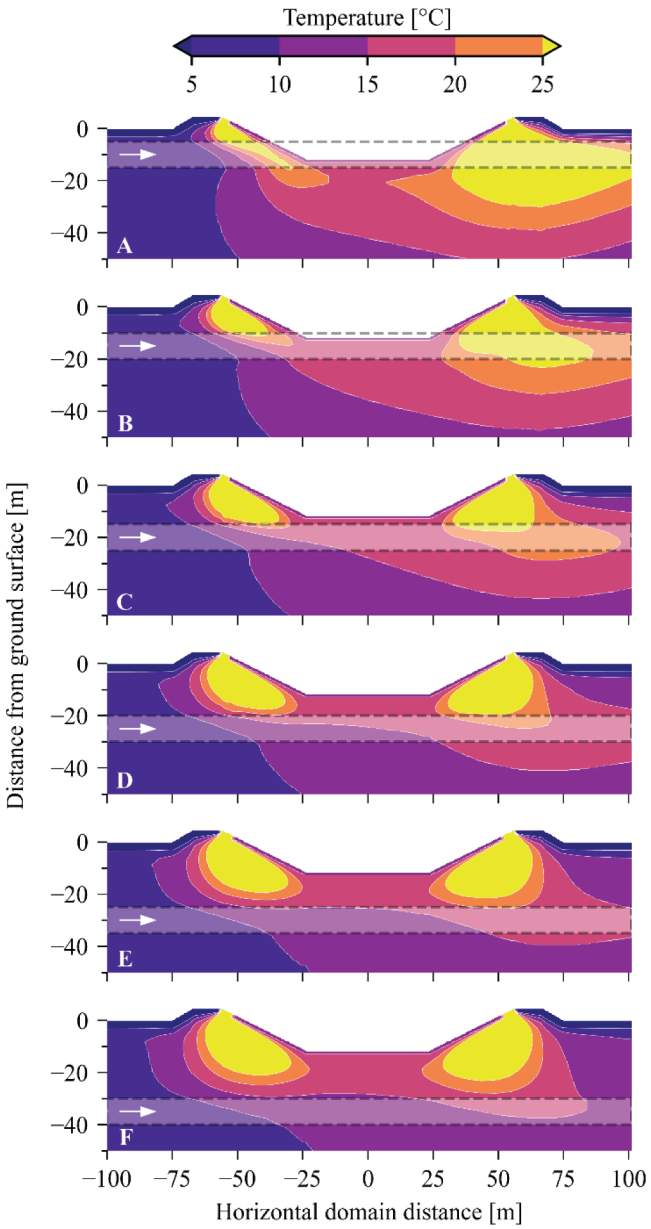

Fig. 12. Ground temperature contour plots for seasonal PTES operation for different depths of moving groundwater. The semi-transparent horizontal white bar illustrates the groundwater layer.

the soil temperature profile changes from the depth of the groundwater downwards.

According to the regulations mentioned in Section 1, the groundwater temperature should not exceed 20 – 25 °C (depending on the country). Thus, it can be observed that the temperature of the groundwater layer remains lower than 25 °C for depths below 20 m for the seasonal operation and below 30 m for short-term operation. In fact, the groundwater temperature was below 20 °C at a groundwater depth of 25 m for the seasonal operation, whereas it was not achievable for short-term operation.

Nevertheless, under no circumstances was it possible to limit the change of the groundwater temperature to ± 6 K, which is required in some countries. Thus, it can be concluded that, in countries where this is required, groundwater should not be present in the selected location. Alternatively, it may be advisable to increase the allowable heating of groundwater within a specified radius of heat storage systems and require documentation that local groundwater wells remain unaffected.

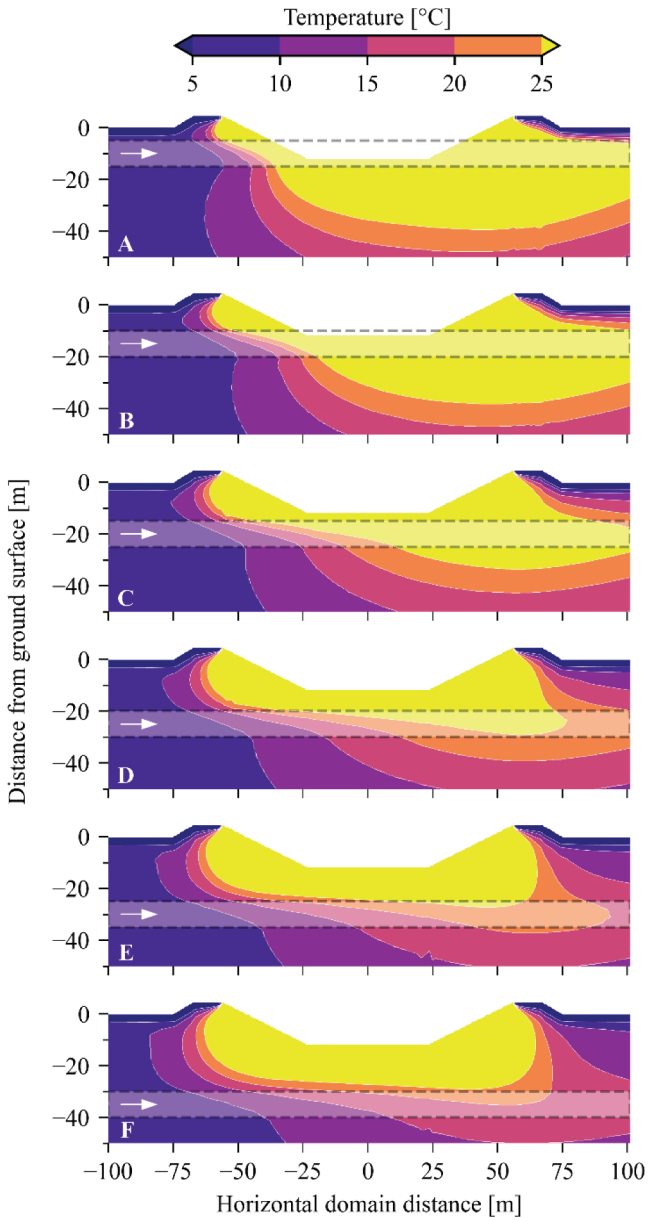

Fig. 13. Ground temperature contour plots for short-term PTES operation for different depths of moving groundwater. The semi-transparent horizontal white bar illustrates the groundwater layer.

4. Conclusions

This study investigated the effect of groundwater on PTES heat losses as well as the effect of PTES operation on the groundwater temperature. A simulation model was developed using ANSYS Fluent and was validated using operation data from the Marstal PTES. The model was modified to be able to simulate seasonal and short-term PTES operations and account for groundwater at different depths. The main conclusions from this study were the following:

- The soil temperature was unaffected at a 100 m radius around the PTES regardless of its operation or the soil's thermal properties.
- The heat losses of a short-term PTES stabilized after eight years of operation, while the heat losses of a seasonal PTES stabilized after 12 years.
- The short-term PTES had, on average, 15% higher heat losses than the seasonal PTES due to higher storage temperatures.
- Static groundwater increased the PTES heat losses by 14%, and for moving groundwater, the heat losses were increased by 60% compared to a case without groundwater.
- PTES heat losses were unaffected by the presence of groundwater when the groundwater table was 13 m below the bottom of the PTES.
- The groundwater layer could maintain a temperature lower than 25 °C at a depth of 20 m for seasonal PTES operation while at 30 m for short-term operation.
- The groundwater temperature was maintained below 20 °C for the seasonal operation at a groundwater depth of 25 m, whereas this was not possible for the short-term operation.

These conclusions can be used primarily in the planning stage of a PTES for choosing a construction location based on geological conditions. Accurate prediction of a storage performance is of major importance for securing financing and delivering the promised results to the DH system. Additionally, since environmental permits are required in most countries, it is important to be able to document that the PTES operation will not affect the groundwater or any cultivation in the vicinity.

Future work could include investigating different groundwater flow rates at different depths. Additionally, with the wider adoption of low-temperature district heating, it could be relevant to investigate different temperature operation ranges for seasonal and short-term operation. It is expected that with low-temperature district heating, the PTES heat losses would be lower, resulting in lower groundwater temperature.

VI

CRediT authorship contribution statement

Ioannis Sifnaios: Conceptualization, Methodology, Visualization, Investigation, Writing – original draft. **Adam R. Jensen:** Methodology, Visualization, Writing – review & editing. **Simon Furbo:** Writing – review & editing, Supervision, Funding acquisition. **Jianhua Fan:** Supervision, Funding acquisition.

Declaration of Competing Interest

The authors declare that they have no known competing financial interests or personal relationships that could have appeared to influence the work reported in this paper.

Data availability

The authors do not have permission to share data.

Acknowledgments

This study was funded by the Danish Energy Agency through EUDP grant no. 64020-2036 (IEA Task 39: Large Thermal Energy Storages for District Heating) and by the Sino-Danish Center for Education and Research (SDC) Ph.D. program.

References

[1] D. Sveinbjörnsson, L. Laurberg Jensen, D. Trier, I. Ben Hassine, X. Jobard, Large Storage Systems for DHC, Networks (2017).
[2] T. Pauschinger, T. Schmidt, P. Alex Soerensen, D. Aart Snijders, R. Djebbar, R. Boulter, C. Jeff Thornton, Integrated Cost-effective Large-scale Thermal Energy Storage for Smart District Heating and Cooling - Design Aspects for Large-Scale Aquifer and Pit Thermal Energy Storage for District Heating and Cooling, Int. Energy Agency Technol. Collab. Program. Dist. Heat. Cool. Incl. Comb. Heat Power. (2018 (2018).).
[3] M. Reuss, The use of borehole thermal energy storage systems, in: L.F. Cabeza (Ed.), Adv. Therm. Energy Storage Syst. Methods Appl, 2nd ed., 2020, pp. 139–171, https://doi.org/10.1016/C2019-0-00061-1.
[4] L. Gao, J. Zhao, Q. An, X. Liu, Y. Du, Thermal performance of medium-to-high-temperature aquifer thermal energy storage systems, Appl. Therm. Eng. 146 (2019) 898–909, https://doi.org/10.1016/j.applthermaleng.2018.09.104.

[5] K. Narula, F.D.O. Filho, J. Chambers, M.K. Patel, Simulation and comparative assessment of heating systems with tank thermal energy storage – A Swiss case study, J. Energy Storage. 32 (2020), 101810, https://doi.org/10.1016/j.est.2020.101810.
[6] M.V. Jensen, Seasonal pit heat storages - Guidelines for materials & construction IEA-SHC Tech Sheet 45.B.3.2, 2014. http://task45.iea-shc.org/fact-sheets.
[7] A. Gabrielsson, U. Bergdahl, L. Moritz, Thermal energy storage in soils at temperatures reaching 90°c, J. Sol. Energy Eng. Trans. ASME. 122 (2000) 3–8, https://doi.org/10.1115/1.556272.
[8] Y. Dong, J.S. McCartney, N. Lu, Critical Review of Thermal Conductivity Models for Unsaturated Soils, Geotech. Geol. Eng. 33 (2015) 207–221, https://doi.org/10.1007/s10706-015-9843-2.
[9] N.H. Abu-Hamdeh, Thermal properties of soils as affected by density and water content, Biosyst. Eng. 86 (2003) 97–102, https://doi.org/10.1016/S1537-5110(03)00112-0.
[10] H.F. Zhang, X.S. Ge, H. Ye, D.S. Jiao, Heat conduction and heat storage characteristics of soils, Appl. Therm. Eng. 27 (2007) 369–373, https://doi.org/10.1016/j.applthermaleng.2006.07.024.
[11] N. Zhang, Z. Wang, Review of soil thermal conductivity and predictive models, Int. J. Therm. Sci. 117 (2017) 172–183, https://doi.org/10.1016/j.ijthermalsci.2017.03.013.
[12] G.J. van den Brink, C.J. Hoogendoorn, Ground water flow heat losses for seasonal heat storage in the soil, Sol. Energy 30 (1983) 367–371, https://doi.org/10.1016/0038-092X(83)90190-1.
[13] M. Bloemendal, N. Hartog, Analysis of the impact of storage conditions on the thermal recovery efficiency of low-temperature ATES systems, Geothermics 71 (2018) 306–319, https://doi.org/10.1016/j.geothermics.2017.10.009.
[14] H.J.G. Diersch, D. Bauer, Analysis, modeling, and simulation of underground thermal energy storage systems, LTD (2020), https://doi.org/10.1016/B978-0-12-819885-8.00007-3.
[15] A. Dahash, M. Bianchi Janetti, F. Ochs, Numerical Analysis and Evaluation of Large-Scale Hot Water Tanks and Pits in District Heating Systems, Build. Simul. Conf. Proc. (2019) 1692–1699, https://doi.org/10.26868/25222708.2019.210566.
[16] A. Dahash, F. Ochs, G. Giuliani, A. Tosatto, Understanding the Interaction between Groundwater and Large-Scale Underground Hot-Water Tanks and Pits, Sustain. Cities Soc. 71 (2021), 102928, https://doi.org/10.1016/j.scs.2021.102928.
[17] C. Suárez, J. Pino, F. Rosa, J. Guerra, Analytical approach to ground heat losses for high temperature thermal storage systems, Int. J. Energy Res. 43 (2019) 439–454, https://doi.org/10.1002/er.4278.
[18] K.S. Lee, Simulation on the cyclic operation of an open borehole thermal energy storage system under regional groundwater flow, Geosci. J. 14 (2010) 217–224, https://doi.org/10.1007/s12303-010-0020-6.
[19] T. Schmidt, T. Pauschinger, P.A. Sørensen, A. Snijders, R. Djebbar, R. Boulter, J. Thornton, Design Aspects for Large-scale Pit and Aquifer Thermal Energy Storage for District Heating and Cooling, Energy Procedia 149 (2018) 585–594, https://doi.org/10.1016/j.egypro.2018.08.223.
[20] World Water Assessment Programme, The United Nations World Water Development Report 3: Water in a Changing World., Paris: UNESCO, and London: Earthscan, 2009.
[21] C. Griebler, H. Brielmann, C.M. Haberer, S. Kaschuba, C. Kellermann, C. Stumpp, F. Hegler, D. Kuntz, S. Walker-Hertkorn, T. Lueders, Potential impacts of geothermal energy use and storage of heat on groundwater quality, biodiversity, and ecosystem processes, Environ. Earth Sci. 75 (2016), https://doi.org/10.1007/s12665-016-6207-z.
[22] T. Riedel, Temperature-associated changes in groundwater quality, J. Hydrol. 572 (2019) 206–212, https://doi.org/10.1016/j.jhydrol.2019.02.059.
[23] S. Haehnlein, P. Bayer, P. Blum, International legal status of the use of shallow geothermal energy, Renew. Sustain. Energy Rev. 14 (2010) 2611–2625, https://doi.org/10.1016/j.rser.2010.07.069.
[24] F. Stauffer, P. Bayer, P. Blum, N. Molina-Giraldo, W. Kinzelbach, Thermal use of shallow groundwater, Taylor & Francis Group, New York, 2014.
[25] C.O. Popiel, J. Wojtkowiak, B. Biernacka, Measurements of temperature distribution in ground, Exp. Therm Fluid Sci. 25 (2001) 301–309, https://doi.org/10.1016/S0894-1777(01)00078-4.
[26] A. Dahash, M.B. Janetti, F. Ochs, Detailed 3-D models of a large-scale underground thermal energy storage with consideration of groundwater conditions, in: Int. Sustain. Energy Conf., 2018: pp. 597–604.
[27] COMSOL, COMSOL Multiphysics software, (n.d.). https://www.comsol.com/ (accessed July 12, 2023).
[28] H.M.K.U. Haq, E. Hiltunen, An inquiry of ground heat storage: Analysis of experimental measurements and optimization of system's performance, Appl. Therm. Eng. 148 (2019) 10–21, https://doi.org/10.1016/j.applthermaleng.2018.11.029.
[29] G. Hellström Ground heat storage: Thermal analyses of duct storage systems 1991.
[30] VEKS, Høje Taastrup fjernvarme, Heat pit storage optimizes district heating, (2022). https://planenergi.eu/wp-content/uploads/2022/07/Heat-pit-storage_folder-2022_uk.pdf (accessed January 19, 2023).
[31] I. Sifnaios, A.R. Jensen, S. Furbo, J. Fan, Performance comparison of two water pit thermal energy storage (PTES) systems using energy, exergy, and stratification indicators, J. Energy Storage. 52 (2022), 104947, https://doi.org/10.1016/j.est.2022.104947.
[32] I. Sifnaios, G. Gauthier, D. Trier, J. Fan, A.R. Jensen, Dronninglund water pit thermal energy storage dataset, Sol. Energy 251 (2023) 68–76, https://doi.org/10.1016/j.solener.2022.12.046.
[33] Dansk Fjernvarme, Inspirations-katalog om solvarme, (2017). https://docplayer.dk/47760153-Solvarme-inspirationskatalog-inspirationskatalog-om-solvarme-inspiration-og-erfaringer-fra-solvarmeanlaeg-i-kombination-med-fjernvarme-i-danmark.html (accessed August 16, 2023).
[34] PlanEnergi, Design of the pit heat storage of the demonstration plant at Marstal Fjernvarme, 2013. https://docplayer.net/40878119-Sunstore-4-deliverable-d-2-2-version-3-design-of-the-pit-heat-storage-of-the-demonstration-plant-at-marstal-fjernvarme.html.
[35] GEO, Marstal damvarmelager geoteknisk undersøgelse, 2010.
[36] M. Nygren, M. Giese, B. Kløve, E. Haaf, P.M. Rossi, R. Barthel, Changes in seasonality of groundwater level fluctuations in a temperate-cold climate transition zone, J. Hydrol. X. 8 (2020), 100062, https://doi.org/10.1016/j.hydroa.2020.100062.
[37] I. Møller, N. Balling, C. Ditlefsen, Shallow subsurface thermal structure onshore Denmark: temperature, thermal conductivity and heat flow, (2018). https://2dgf.dk/xpdf/bull67-29-52.pdf (accessed July 13, 2023).
[38] Verein Deutscher Ingenieure (VDI), Thermische Nutzung des Untergrunds - Grundlagen, Genehmigungen, Umweltaspekte (2010). https://www.vdi.de/richtlinien/details/vdi-4640-blatt-1-thermische-nutzung-des-untergrunds-grundlagen-genehmigungen-umweltaspekte.
[39] ANSYS, ANSYS Fluent, (n.d.). https://www.ansys.com/products/fluids/ansys-fluent (accessed July 12, 2023).
[40] L. Laloui, A.F. Rotta Loria, Heat and mass transfers in the context of energy geostructures, in: Anal. Des. Energy Geostructures, Academic Press, 2020: pp. 69–135. 10.1016/b978-0-12-816223-1.00003-5.
[41] Høje Taastrup fjernvarme, Returtemperatur-tarif, (2022). https://www.htf.dk/returtemperatur-tarif (accessed February 27, 2023).
[42] Aalborg University, Climate Data, (n.d.). https://build.dk/bsim/Pages/Climate-data.aspx (accessed February 27, 2023).
[43] H. Li, J.J. Jiao, Analytical studies of groundwater-head fluctuation in a coastal confined aquifer overlain by a semi-permeable layer with storage, Adv. Water Resour. 24 (2001) 565–573, https://doi.org/10.1016/S0309-1708(00)00074-9.
[44] GEO, Dronninglund. Lunderbjerg 8A Damvarmelager - Vurdering af varmelagerets påvirkning af grundvand, 2012.
[45] A. Atangana, Principle of Groundwater Flow, in: Fract. Oper. With Constant Var. Order With Appl. to Geo-Hydrology, Elsevier, 2018, pp. 15–47, https://doi.org/10.1016/B978-0-12-809670-3.00002-3.
[46] J. Koch, J. Gotfredsen, R. Schneider, L. Troldborg, S. Stisen, H.J. Henriksen, High Resolution Water Table Modeling of the Shallow Groundwater Using a Knowledge-Guided Gradient Boosting Decision Tree Model, Front, Water. 3 (2021) 1–14, https://doi.org/10.3389/frwa.2021.701726.

VII. Integration of a pit thermal energy storage in a district heating network

Ioannis Sifnaios

In preparation

VII

Integration of a pit thermal energy storage in a district heating system

Ioannis Sifnaios[1,2]

[1] Department of Civil and Mechanical Engineering, Technical University of Denmark, Koppels Allé 404, 2800, Kgs. Lyngby, Denmark

[2]Sino-Danish College (SDC), University of Chinese Academy of Sciences, Beijing, China

Keywords: TRNSYS, PTES, LCOH, heat pump, control strategy

1. Introduction

District heating (DH) is a system that provides thermal energy to multiple buildings from a central energy plant [1]. Existing DH systems supply steam or hot water using insulated underground pipes. DH systems have been proven an efficient heating technology for countries with a cold climate and a high space heating demand. For example, 64% of residential heat consumers in Denmark are supplied by DH to cover their heating needs [2].

Since thermal energy is produced in central energy plants, there is no need for traditional boilers in each building that operate using electricity or fossil fuels. Due to the distributed nature and large-scale benefits, DH systems have the flexibility of utilizing various heat sources and can accommodate a high share of renewables. However, to increase the share of renewables in DH systems, thermal energy storage (TES) is required to cover the mismatch between heat demand and production created due to the intermittent nature of renewables [3].

TES systems have been shown to be able to reduce primary energy consumption by 12% by reducing the use of peak boiler units [4] and increasing the potential for using power-to-heat technologies and waste heat [5]. Additionally, they can potentially reduce CO_2 emissions since they limit the use of peak heat production units that usually rely on natural gas [6].

TES systems can be operated as seasonal or short-term storage. Seasonal TES systems are usually combined with a solar collector field, which charges the storage in the summer in order to be discharged in winter. For example, in a small town in Austria, solar collectors and a seasonal TES were added to the existing DH system (based on biomass and natural gas), which resulted in an 11% decrease in the use of natural gas [7]. Additionally, seasonal TES can lower the DH system's cost of heat by allowing for the utilization of cheaper heat sources (e.g., waste heat) [8].

Regarding the DH system economy, the results obtained for TES systems vary a lot depending on the boundaries of the investigation. For example, it is reported in the literature that cost savings can range from 5% (for a university campus and a neighborhood) [4,9] to 23% (at a city level) [10].

Although it is well-known that implementing TES systems in DH grids can be beneficial, choosing the optimal storage dimensions can be challenging. The main reason is that there are many differences between DH grids (e.g., heat sources, production units, seasonal variations in production and consumption, and fuel costs), which play a role in determining the optimal storage size [11]. In a study investigating solar DH systems in Switzerland, the most important identified parameter was the storage volume relative to the solar collector area [12]. Similar conclusions were drawn for a solar DH system in the UK, where proper sizing of the seasonal storage had a positive impact on the solar fraction and the economy of the system [13]. For this reason, researchers have suggested dynamic optimization methods for choosing the optimal TES size [14].

Apart from the proper component sizing, the system's control strategy greatly impacts its performance. In a case study for a DH grid in Northern Italy, optimizing the operation of the generation units benefited the technical (e.g., heat losses) and the economic (e.g., fuel costs) characteristics of the system [15]. On the contrary, a non-efficient control strategy was found to increase the fossil fuel share of a DH system by 1.2% [16]. Last, the importance of including forecasts of the weather and heat demand in the control strategy has been highlighted in the literature [17].

So far, four main types of TES have been utilized in combination with DH systems, namely, tanks (TTES), boreholes (BTES), aquifers (ATES), and pit thermal energy storages (PTES) [18]. In recent years, there has been a particular interest in PTES technology due to its low cost, high efficiency, and high charge/discharge capacity; thus, this

study focused on PTES. A PTES is a large water reservoir dug into the ground, lined with a watertight polymer liner (to prevent water from leaking to the ground), and covered with a floating insulating lid (to reduce heat losses) [19]. The primary advantage of PTES compared to other technologies is their low specific investment cost (< 27 €/m^3 [20]). In comparison, TTES, which are used in nearly all Danish DH systems, have a specific investment cost between 150-320 €/m^3 [21].

The existing PTES systems have been demonstrated in Denmark as seasonal heat storages in combination with large-scale solar collector fields [22]. In a feasibility study for the city of Graz in Austria, PTES combined with a solar thermal field achieved solar fractions of up to 26% [23]. However, some studies found the combination of solar collectors and PTES unprofitable and combined a heat pump with a seasonal PTES to achieve the lowest costs [24]. Moreover, combining PTES with heat pumps can increase storage efficiency by 16% [25].

In 2023, the first PTES was constructed for short-term storage with a volume of 70 000 m^3 in Høje Taastrup, Denmark [26]. The control strategy is the largest difference between seasonal and short-term PTES. Seasonal PTES are operated based on the availability of solar irradiation (i.e., charged in spring/summer, discharged in autumn/winter). In contrast, short-term PTES operation is more dynamic and based on forecasts of the available generation units' heat prices and heat demand. Consequently, a more advanced control strategy must be developed to achieve optimal operation of a short-term PTES.

Short-term PTES are particularly advantageous for DH plants that interact with the electricity market as consumers or producers. As efforts are being made to phase out fossil fuels, more and more DH plants are becoming electricity consumers, whereas they traditionally were only electricity producers. For example, the DH operator in the Danish town of Viborg has planned to phase out traditional natural gas units. Instead, several heat pumps and electric boilers are planned to be installed. This makes the DH grid more dependent on the electricity market; however, adding a short-term PTES can decouple this and allow for economic savings, i.e., shifting heat production to periods when the electricity price is low. This potential financial benefit has yet to be investigated in the literature, as PTES systems have only recently been used for seasonal storage. In the present study, we aim to elucidate the impact of adding PTES as short-term TES in DH grids that mainly rely on electricity-based generation capacity.

Several different software exist for simulating the interaction between heat demand, production units, prices, and storage. Typically, software that simulate a high level of detail (e.g., storage temperatures, resolved heat losses, and stratification) are used for single DH systems, as in [27]. The software used for these types of simulations are usually TRNSYS [28] or Modelica [29].

In the present study, a simulation model of a DH system was developed in TRNSYS. The main reason for choosing TRNSYS was the large number of PTES components available. A list of the available TRNSYS components for simulating PTES systems is presented below [30]:

- The XST component (TRNSYS Type 342) models the PTES as a cylinder, using a 1-D approach for the water domain and a 2-D approach for the soil (assuming rotational symmetry).
- The ICEPIT component (TRNSYS Type 343) was developed for simulating water/gravel heat storages or ice reservoirs of cylindrical shape, using a 1-D approach for the water domain and a 2-D approach for the soil (assuming rotational symmetry).
- The truncated cone components (TRNSYS Types 1535 + 1301). Type 1535 models the water domain as 1-D, and the soil domain is modeled by Type 1301 as 2-D, assuming rotational symmetry. These components are newer than XST and ICEPIT and enable more accurate modeling of the water-soil interaction.

The present study investigated the impact of short-term PTES operation on the economy of a city-scale DH system that relies on heat pumps and electric boilers to cover the entire heat demand. A model of the DH system was created in TRNSYS, and Types 1535+1301 were used for modeling the PTES. The PTES components were validated against measurement data from the PTES in Dronninglund. Furthermore, in order to determine the periods when the PTES should be charged/discharged, a control strategy based on the electricity price was developed. Consequently, a control strategy was implemented using linear programming in Python to optimize the short-term PTES operation, i.e., minimize operation cost.

The present study aimed to answer the following research questions:

- What is the optimal combination of heat pump and electric boiler capacity?
- Can PTES be used to lower the cost of heat of the heat pump-based DH systems?
- How does the size of the main components influence the LCOH (PTES, heat pump, and boiler capacity)?
- What is the impact of the PTES charge temperature?

The investigated DH grid is presented in Section 2.1, followed by a description of the developed TRNSYS model in Section 2.2. Information on the PTES used for the validation is presented in Section 2.3, specifications of the heat pump in Section 2.4, and the implemented control strategy in Section 2.5. The validation procedure for the PTES component is described in Section 2.6. This is followed by an introduction to the key performance indicators used in the study and the economic assumptions in Sections 2.7 and 2.8, respectively. Last, Section 3 presents the results of the study, and Section 4 the conclusions.

2. Methods

2.1. The district heating grid

The data used for the district heating grid were actual operation data from the city of Viborg from 2021. Viborg is a city in central Jutland, Denmark, with a population of 41 000 people. An overview of the mean daily heat demand, supply/return temperatures, ambient temperature, and electricity price is presented in Figure 1.

It may be observed that Viborg has a typical heat demand profile, with a low demand in the summer deriving primarily from domestic hot water use and a high demand in winter due to space heating requirements. The annual heat demand for 2021 was 342 GWh, with a peak load of 107 MW. The supply temperature in the summer was approximately constant at 65 °C, while in the winter, it reached up to 80 °C, depending on the ambient temperature. The return temperature was approximately 45 °C in the summer and 40 °C in the winter.

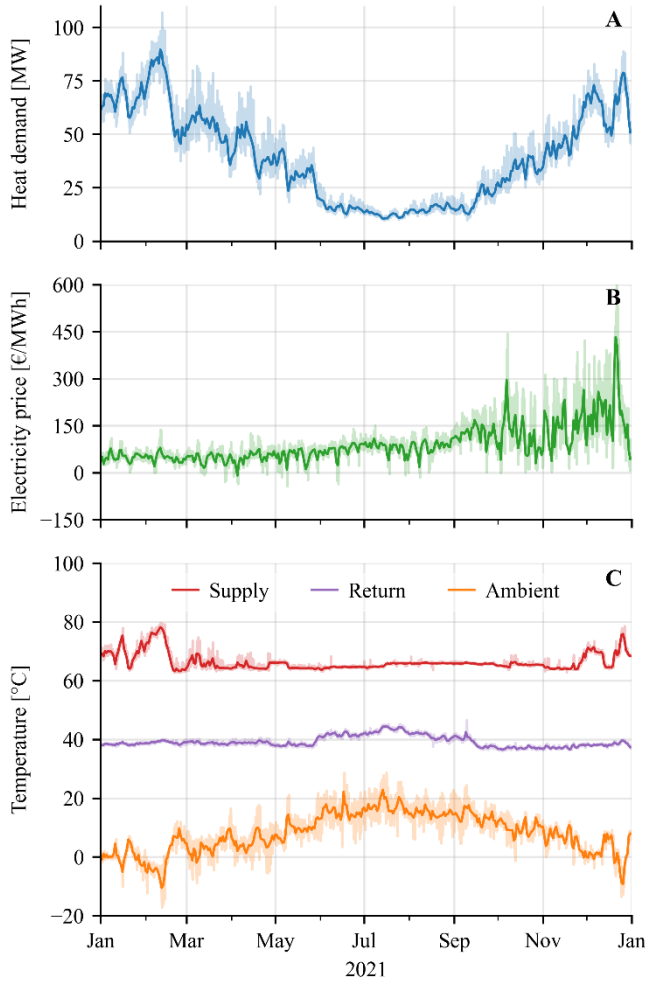

Figure 1: Viborg's (A) heat demand, (B) electricity prices, and (C) supply/return and ambient temperature for 2021. The thick lines indicate mean daily values, while the faded lines indicate hourly values.

The electricity prices in Figure 1B were the hourly spot prices for western Denmark (where Viborg is located) for 2021. The increase in electricity prices toward the end of the year was due to a rise in natural gas prices that directly affected electricity prices across Europe. Historical data for electricity prices can be downloaded freely from the Northern European electricity market Nord Pool [31].

Until 2022, the district heating operator in Viborg relied mainly on a natural gas combined heat power (CHP) plant and peak boiler units to cover the entire heat demand. However, in 2023, a plan to phase out the use of natural gas was initiated. After the summer of 2023, electricity-based technologies will primarily cover the heat demand. Specifically, they plan to install two 7 MW air-to-water heat pumps, a 50 MW electric boiler, a 6 MW groundwater heat pump, and a 7 MW lake water heat pump. Eventually, natural gas technologies will be entirely abandoned by 2025.

2.2. TRNSYS simulation model

In order to investigate the Viborg DH grid and the impact of various heat production units, a model of the DH grid was created in TRNSYS. TRNSYS is a component-based software that can simulate and analyze the performance of transient energy systems [32].

Since the plant operator plans to eliminate the use of natural gas in the near future, only electricity-based generation units were considered in this analysis. A system that covered the entire heat demand using heat pumps and electric boilers was used as a reference system.

To investigate the impact of a short-term PTES on this system, a DH system with a heat pump, an electric boiler, and a PTES was created in TRNSYS (see Figure 2). The components used in the TRNSYS model are reported in Table 1.

Table 1: Components used in the TRNSYS model.

Component	Type number	Description
PTES (water domain)	1535	Inverted truncated conical storage tank
PTES (soil domain)	1301	Ground coupling for a buried truncated cone storage tank
Heat pump	-	Custom equations
Electric boiler	659	Hot water boiler
Mixing valve	649	Mixing valve
Flow diverter	647	Diverting valve
Python LP	3157	Calling Python (CFFI)
Load	682	Heating and cooling loads imposed on a flow stream

The investigated system was simulated using a timestep of 1 hour. As seen in Figure 1, there is a large difference between the mean daily values and the hourly values for heat demand, electricity price, and ambient temperature. Thus, using a high temporal resolution ensured that the volatility of these parameters was sufficiently captured.

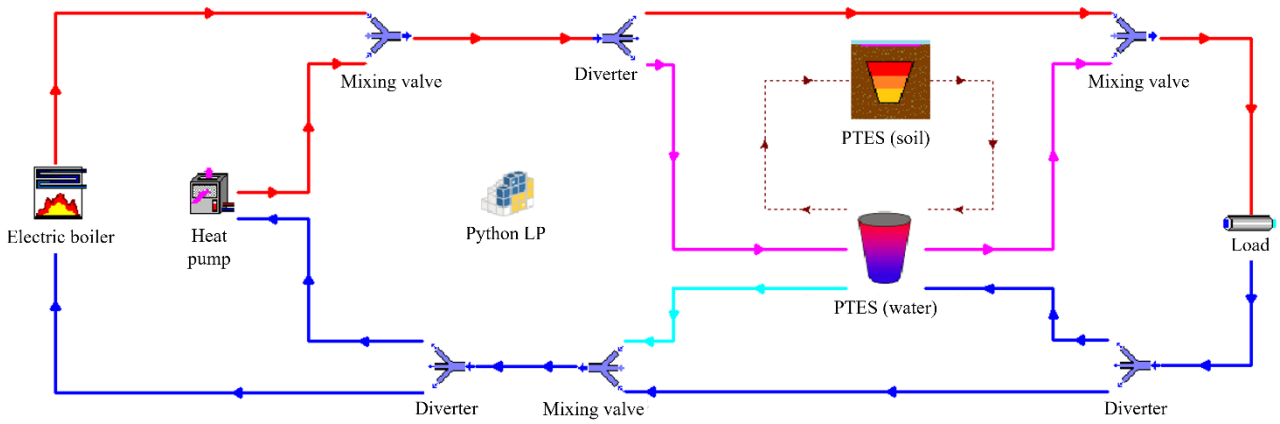

Figure 2: The simulated DH system in TRNSYS.

2.3. PTES

The design of the PTES in Dronninglund was used as a reference for the simulated PTES in this study. This storage was chosen mainly because multiple years of data were publicly available. A schematic of the PTES in Dronninglund, along with photos from different construction stages, is shown in Figure 3.

The PTES in Dronninglund was shaped like an inverted truncated pyramid, with a height of 16 m and an approximate volume of 60 000 m^3 [33]. The reader is referred to [19] for an extensive description and operation data for the PTES in Dronninglund.

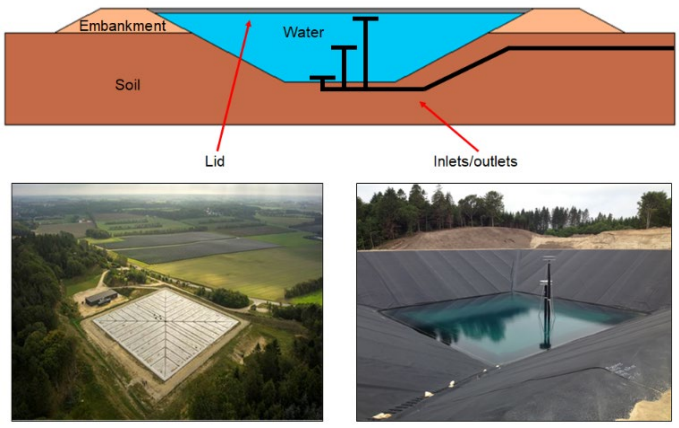

Figure 3: Schematic and construction photos for the PTES in Dronninglund [34].

An important parameter in the PTES operation is the charge/discharge rate. Most existing systems have a charge/discharge rate between 30 – 40 MW [35]. This value is usually adequate for seasonal systems since they discharge slowly over a long period of time. However, short-term PTES need to be able to respond to quick changes in the heat demand and store large amounts of heat when the electricity price is low. Thus, higher values of charge/discharge rate might be necessary, depending on the DH grid. To put this into perspective, the short-term PTES in Høje Taastrup (70 000 m^3) has a charge/discharge rate of 30 MW, while the planned PTES in Fyn (500 000 m^3) will have a charge/discharge rate of 150 MW, and the PTES in Aalborg (1 000 000 m^3) was planned to have a charge/discharge rate of 300 MW. However, it should be noted that the heat demand of each network plays a major role in selecting these charge/discharge rates.

2.4. Heat pump

In recent years, several district heating companies in Denmark have installed air-to-water heat pumps to cover part of their heat demand (e.g., Solrød [36], Saltum [37], and Dronninglund [38]). Air-sourced heat pumps are often chosen over alternatives despite having a lower seasonal coefficient of performance (COP) (e.g., compared to groundwater, lake water, and seawater heat pumps). Their lower seasonal COP occurs due to the inverse correlation of the heat source temperature with the demand (i.e., there is a low ambient temperature in the winter when the heat demand is highest). However, the main benefit of air-to-water heat pumps is that no permits are required for their installation, and they can be installed in almost any location (since they do not depend on the presence of a specific heat source, e.g., groundwater or nearby lakes). Thus, in the present study, air-to-water heat pumps were used as the main heat source for the DH grid, as these are universally applicable. The specifications of the HP operation were based on data supplied by the Danish Heat Pump Handbook [39] and by a heat pump manufacturer. The nominal heat capacity of the heat pump used in the simulations was 7 MW, and the heat pump performance map is presented in Figure 4.

It may be observed that the COP and the heat output of the HP are directly affected by the ambient temperature and the supply temperature. Performance penalty due to part-load operation was assumed negligible due to the large heat pump capacity, which would require several heat pumps.

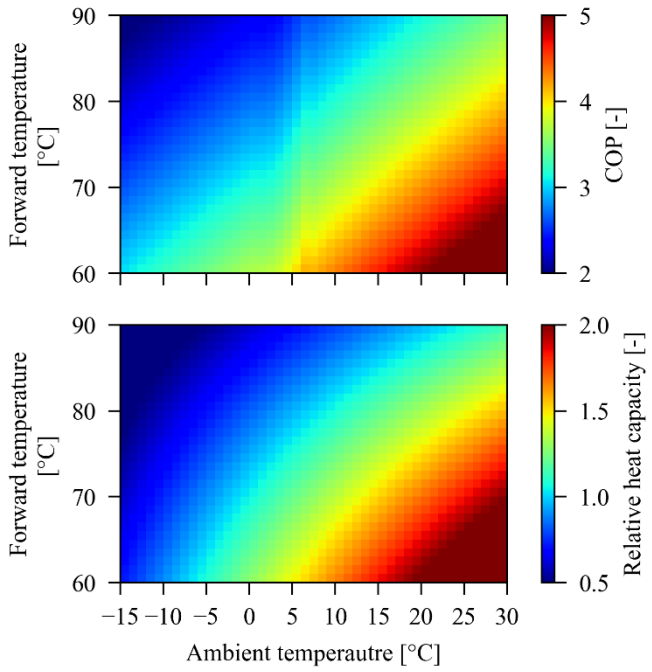

Figure 4: Heat pump performance plots. The relative heat capacity is the heat capacity at specific conditions relative to the nominal capacity. The nominal heat capacity of the heat pump was 7 MW.

2.5. Control strategy

A control strategy was developed in order to determine the dispatch of the generation units and the PTES, i.e., the generation and storage charge/discharge at each time step. A linear programming (LP) model was developed to identify the optimal dispatch strategy based on the system constraints and the load and electricity price 14 days ahead.

The linear programming equations solved are presented below. Equations (1) – (4) define the upper and lower boundaries of the problem variables. Equation (5) specifies the system energy balance, and Equation (6) defines the storage constraints. Last, Equation (7) specifies the objective function to be minimized, which is simply the operation cost.

$$0 \leq Q_{HP}(t) \leq Q_{HP,max} \quad (1)$$

$$0 \leq Q_{Boiler}(t) \leq Q_{Boiler,max} \quad (2)$$

$$Q_{PTES,discharge,max} \leq Q_{PTES}(t) \leq Q_{PTES,charge,max} \quad (3)$$

$$0 \leq E_{PTES}(t) \leq E_{PTES,max} \quad (4)$$

$$Q_{load}(t) = Q_{HP}(t) + Q_{Boiler}(t) - Q_{PTES}(t) \quad (5)$$

$$Q_{PTES}(t) = E_{PTES}(t) - \eta_E \cdot E_{PTES}(t-1) \quad (6)$$

$$Obj = \sum_{t=1}^{T} El_{price}(t) \cdot \left(\frac{Q_{HP}(t)}{COP(t)} + Q_{Boiler}(t)\right) \quad (7)$$

where $Q_{HP}(t)$ is the heat generated by the heat pump, $Q_{Boiler}(t)$ is the heat generated by the boiler, $Q_{PTES}(t)$ is the heat charged (positive) or discharged (negative) from the PTES, $E_{PTES}(t)$ is the energy content of the PTES, η_E is the energy efficiency of the PTES, $El_{price}(t)$ is the electricity price, $COP(t)$ is the heat pump's coefficient of performance, $Q_{load}(t)$ is the heat load, t is the timestep, and T is the system's lifetime in years.

At each timestep, the charge level of the PTES and the maximum HP output (dictated by the ambient temperature) were passed into a Python program using TRNSYS Type 3157. The program solved the linear problem described above and returned the dispatch strategy for the generation units and the PTES. This routine was carried out at each time step.

It should be noted that the PTES was only allowed to discharge if the outlet temperature was greater than or equal to the supply temperature of the DH grid. Thus, the $E_{PTES}(t)$ in Equation (4) should be calculated as the usable energy content of the storage, i.e., only layers with a temperature greater than or equal to the supply temperature should be considered as containing energy.

The control strategy assumed perfect knowledge of the future heat demand and electricity prices. In practice, this is, of course, not possible, and the uncertainty drastically increases with the length of the optimization period. However, the impact of using actual forecasts and introducing uncertainty is considered out of the scope of this study.

2.6. Validation of the PTES component

The TRNSYS component 1535/1301 had not been validated in the past, so it was decided to validate it against operation data from the PTES in Dronninglund. The validation period was two years, namely 2018 and 2019.

The PTES in Dronninglund was a truncated pyramid, whereas the PTES shape for the 1535/1301 TRNSYS components was a truncated cone; thus, some approximation had to be done in the simulated PTES dimensions. The simulated model had the same lid and bottom area, height, and volume. Essentially, the only parameter that differed between the actual PTES in Dronninglund and the simulated one was the slope of the side walls and the area of the side walls.

The thermal properties of the soil were taken as an average value of the reported values for the PTES in Dronninglund, as reported in [19]. This was because the TRNSYS soil component could only accept uniform soil thermal conditions, and having two different soil layers was not possible. An overview of the parameters used in the simulation is presented in Table 2.

Table 2: Parameters used in the PTES TRNSYS component.

Parameter	Value	Unit
Volume	60 000	m^3
Height	16	m
Lid area	8281	m^2
Bottom area	676	m^2
Charge/discharge rate	30	MW
Lid heat loss coefficient	0.196	W/m^2 K
Sides and bottom heat loss coefficient	90	W/m^2 K
Soil thermal conductivity	0.7	W/m K
Soil density	1935	kg/m^3
Soil specific heat	1216	J/kg K
Number of nodes in the water domain	50	-

2.7. Key Performance Indicators

Economic key performance indicators (KPIs) were used to investigate the impact of adding a PTES to a DH grid: the levelized cost of heat (LCOH) and the payback period (PP). LCOH corresponds to the average net present cost of supplying 1 MWh of heat by the heating system. The PP corresponds to the time needed for the investigated system's annual savings to cover the investment cost increase compared to the reference system.

Equation (8) was used to calculate the LCOH, and Equation (9) to find the PP. Both expressions were recommended by the International Energy Agency – Solar Heating & Cooling Programme – Task 60 [40].

$$LCOH = \frac{I_0 + \sum_{t=1}^{T} OM(t) \cdot (1+r)^{-t}}{\sum_{t=1}^{T} Q_H(t) \cdot (1+r)^{-t}} \quad (8)$$

$$I_0 - I_{0,ref} = \sum_{t=1}^{PP} (OM(t)_{ref} - OM(t)) \quad (9)$$

where I_0 is the investment cost, $OM(t)$ is the yearly operation and maintenance cost, and r is the annual discount rate. Parameters of the reference system are denoted with the subscript *ref*.

2.8. Economic assumptions

A 4% annual discount rate was used in the simulations as recommended by the Danish Energy Agency [41]. The operation and maintenance (OM) cost is typically assumed to be 1-2% of the total investment cost [42] plus the fuel cost of the generation units. In this study, the OM cost was taken as 1% of the investment cost plus the electricity consumption of the heat pump and the boiler. The investment costs of this study's generation and storage technologies depended on the installed capacities. The equations used for calculating them are presented in Table 3.

Table 3: Investment costs for the generation and storage technologies.

Type	Cost [million €]	Source
Heat pump	$0.67744 \cdot Q_{HP,nominal} + 0.18831$	[43]
Electric boiler	$0.17 \cdot Q_{Boiler,max}$	[44]
PTES	$1744.6 \cdot (V_{PTES})^{0.659} / 10^6$	[45]

3. Results

3.1. Reference DH system

The first step of this study was to dimension the reference system in order to achieve the lowest LCOH. Since the reference system consisted of a heat pump and an electric boiler (without heat storage), these two units need to be able to cover the entire heat demand at any given time.

Figure 6 illustrates the possible combinations of boiler and heat pump capacities for covering the heat load of the Viborg DH grid. This figure also demonstrates that electric boilers have a low capital cost (CAPEX) but a high operation cost (OPEX), while the opposite holds true for heat pumps. Thus, the OPEX decreased for increasing heat pump capacities, but the CAPEX increased.

Consequently, choosing a combination of the two technologies is economically optimal, as choosing only boilers or heat pumps led to high LCOH. It should also be noted that in case the load should be covered using only heat pumps, an approximately 2.5 times higher heat pump capacity should be installed compared to boilers. This is because the peak load periods correspond to low ambient temperatures, where air-to-water heat pumps have their lowest heat production and COP.

The combination that achieved the lowest LCOH was 68 MW heat pump capacity and 53 MW electric boiler capacity. The corresponding LCOH was 44.4 €/MWh.

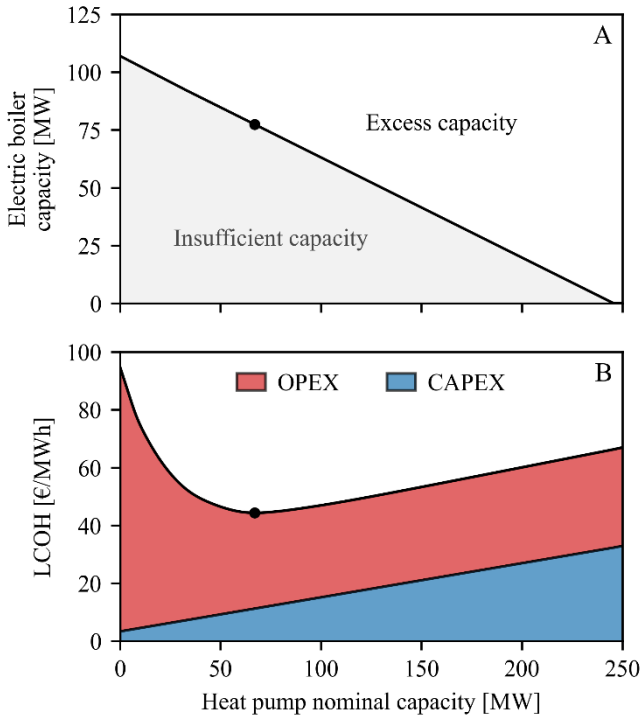

Figure 5: (A) Electric boiler vs. heat pump capacity and (B) LCOH vs. heat pump capacity. The operation expenditures (OPEX) and the capital expenditures (CAPEX) are also indicated in the figure.

It should be noted that the calculated heat pump capacity is higher than the one planned to be installed in Viborg since the actual DH operator intends to use a larger variety of heat sources to cover the demand. However, Viborg's current electric boiler capacity is 50 MW, indicating that the calculated values are realistic.

3.2. PTES component validation

The TRNSYS PTES components 1535+1301 were first validated in order to be added to the reference DH system. Validation was done using operation data from the PTES in Dronninglund for 2018 and 2019. The monthly charged and discharged energy calculated by the TRNSYS components is compared to the measured ones in Figure 5. Overall, it can be seen that there are very small differences between the calculated and measured monthly energy values.

The bias deviation was calculated for the simulated and measured parameters (i.e., charged/discharged energy, heat loss, storage efficiency, and discharge temperature). The storage efficiency was calculated as described by Sifnaios et al. [33]. The results for each year and the mean bias for the entire validation period are presented in Table 4.

In general, it can be seen that for the investigated parameters, there was a bias of less than 5% between the measured and calculated data. Thus, the accuracy of the results was considered acceptable for the present study.

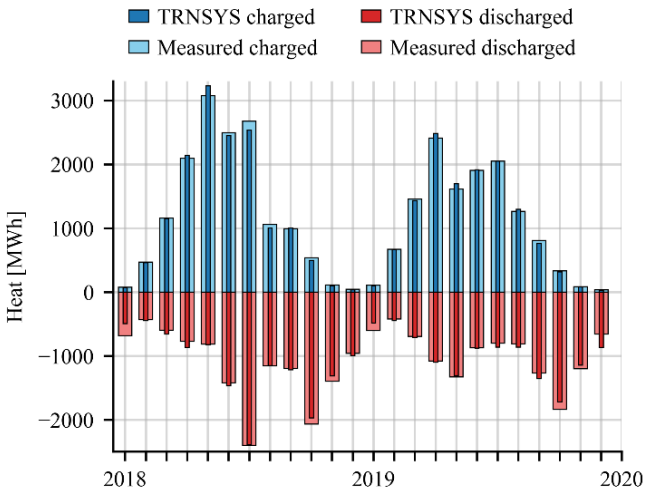

Figure 6: Comparison of monthly charged and discharged energy for the TRNSYS and the Dronninglund PTES.

Table 4: Mean bias deviation in % of the TRNSYS simulation results compared to measurements.

Parameter	2018	2019
Charged energy	-4.7	-2.1
Discharged energy	-0.4	4.5
Heat loss	-3.4	2.1
Efficiency	0.6	0
Discharged temperature	-0.5	0.6

3.3. PTES integration in the DH grid

This section presents the TRNSYS simulation results of integrating a PTES in the reference DH grid. The simulated system was the one introduced in Figure 2, having a PTES volume of 60 000 m^3, a 77 MW heat pump capacity, and a 90 MW electric boiler capacity. The reason for increasing the heat pump and boiler capacity compared to the reference system was to ensure enough generation capacity to cover the load and charge the PTES. The charge/discharge capacity of the PTES in this scenario was 45 MW.

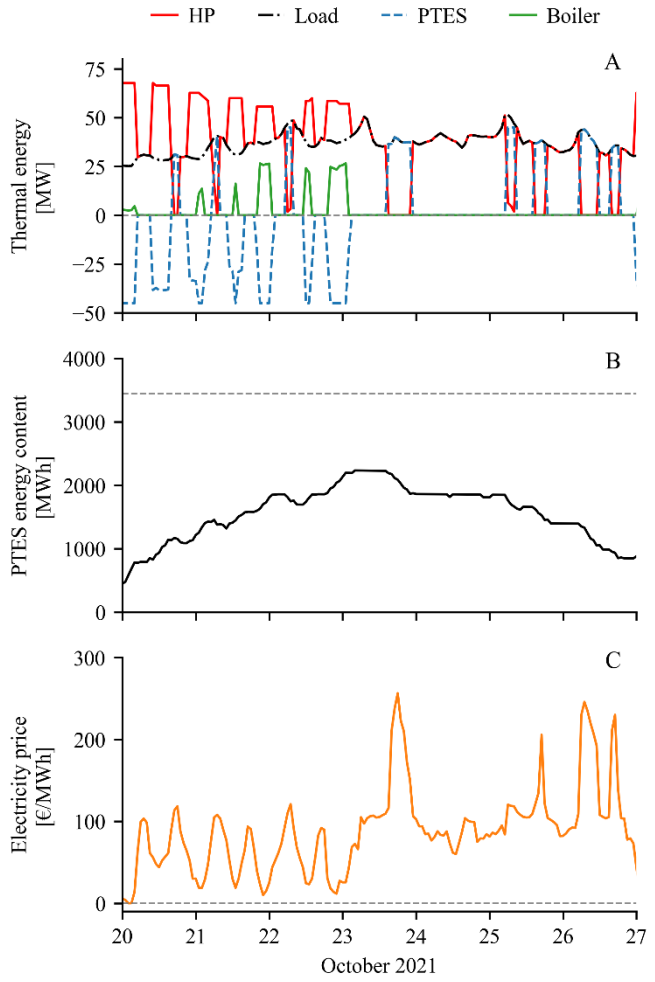

Figure 7: (A) Thermal energy produced by the heat pump, electric boiler, and PTES for a week in October and the corresponding heat load. (B) The energy content of the PTES during the same period as well as (C) the electricity price. The dotted line for the PTES energy content denotes the maximum PTES capacity.

Figure 7 shows the operation of the DH grid for a week in October. It should be noted that the periods where the PTES supplied heat to the grid are denoted as positive PTES thermal energy. In contrast, the periods where the PTES was charged were indicated as negative PTES thermal energy. Additionally, the boiler was only used to charge the PTES when electricity prices were low or to cover the load when the heat pump capacity was insufficient.

The corresponding LCOH of this system was 39.9 €/MWh, which is already 10% lower than the reference system. This system's payback period (PP) was 5.1 years. However, it should be noted that there is potential for the LCOH and the PP to be even lower since this system is not optimized in terms of PTES charge/discharge capacity and volume.

3.4. Impact of PTES volume on the DH system

In order to investigate the impact of the PTES volume on the DH system, three different PTES sizes were investigated: 60 000 m^3, 120 000 m^3, and 200 000 m^3. The results of this investigation are presented in Table 5.

It may be observed that the LCOH and PP increase for increasing PTES volumes, indicating that the investigated volumes were too large for the Viborg DH grid. The increase derived primarily from the higher investment cost for the PTES.

Table 5: Percentage of heat production, CAPEX, OPEX, LCOH, and PP for the investigated PTES volumes.

		Storage size [m^3]		
		60 000	**120 000**	**200 000**
CAPEX [€/MWh]	**HP**	6.9	6.9	6.9
	Boiler	22.0	21.6	21.4
	PTES	2.4	3.9	5.1
OPEX [€/MWh]	**HP**	25.7	25.7	25.7
	Boiler	32.2	34.0	34.0
	PTES	0.6	1.0	1.3
LCOH [€/MWh]	-	39.9	40.6	40.7
PP [years]	-	5.1	6.1	6.6

3.5. Impact of PTES charge temperature

As previously noted, air-to-water heat pumps have their least efficient COP and heat capacity when operating in low ambient and high supply temperature conditions. However, it is common practice to set the charge temperature of the PTES to approximately 90°C, as a higher charge temperature leads to an increased heat storage capacity. Consequently, the use of air-to-water heat pumps for charging the PTES can lead to suboptimal performance, marked by a reduced COP and higher electricity consumption, particularly during winter months. Because of this, the economic implications of varying PTES charge temperatures were evaluated in relation to the district heating system. The findings of this investigation are presented in Table 6.

Table 6: Effect of the PTES charge temperature on LCOH and PP for a 60 000 m^3 PTES.

	PTES charge temperature [°C]		
	80	**85**	**90**
LCOH [€/MWh]	38.5	39.8	39.9
PP [years]	4.2	5	5.1

The findings reveal that charging the PTES at 80°C reduced the LCOH by 4% and the PP by 18% despite having a 20% smaller storage capacity. Consequently, when heat pumps serve as the primary heat generation source in a DH network, it is advisable to consider a lower PTES charge temperature. In addition to the financial advantages, opting for a lower PTES charge temperature would benefit the lifetime of the PTES since one of the biggest challenges is finding polymer liners that can withstand temperatures close to 90°C for a long time.

PTES charge temperatures lower than 80°C were not investigated because this temperature represented the highest supply temperature for the Viborg DH grid during winter. To enable the PTES to be charged with lower temperatures, a

corresponding decrease in the supply temperature of the DH grid would be necessary. Alternatively, varying charging temperatures could be employed across different seasons.

4. Conclusions

This study investigated the impact of adding a short-term PTES to the district heating (DH) grid of the Danish city Viborg. Specifically, TRNSYS was used to model the DH grid, and the investigated parameters were the levelized cost of heat (LCOH) and the payback period (PP). Since electricity-based generation units are expected to dominate future DH grids, this study utilized a reference scenario based on air-to-water heat pumps and electric boilers. Thus, a reference system was determined that could cover the entire heat load using heat pumps and electric boilers without any heat storage and was compared to a system that included a PTES. The main findings of this study were the following:

- Without storage, the lowest achievable LCOH was 44.4 €/MWh for a system with a 68 MW air-to-water heat pump capacity and 53 MW electric boiler capacity.
- Adding a PTES to the reference system decreased the LCOH by 10%. Moreover, the additional investment cost for the PTES installation was paid off in 5.1 years, which is rather short compared to the PTES lifetime (i.e., 25 years).
- Lowering the PTES charge temperature from 90 to 80 °C resulted in a 4% lower LCOH and an 18% shorter payback period.

Overall, this investigation revealed the economic benefit of using PTES in DH grids, elucidating their potential as short-term heat storages, contrary to traditional seasonal storage systems.

References

[1] International District Energy Association, District Heating, (2023). https://www.districtenergy.org/topics/district-heating (accessed July 23, 2023).

[2] Danish District Heating Association, Facts about district heating in Denmark, (2021). https://web.archive.org/web/20220331213035/https://www.danskfjernvarme.dk/sitetools/english/about-us (accessed May 4, 2022).

[3] S.H. Li, Y.X. Zhang, Y. Li, X.S. Zhang, Experimental study of inlet structure on the discharging performance of a solar water storage tank, Energy Build. 70 (2014) 490–496. https://doi.org/10.1016/j.enbuild.2013.11.086.

[4] V. Verda, F. Colella, Primary energy savings through thermal storage in district heating networks, Energy. 36 (2011) 4278–4286. https://doi.org/10.1016/j.energy.2011.04.015.

[5] G. Schweiger, J. Rantzer, K. Ericsson, P. Lauenburg, The potential of power-to-heat in Swedish district heating systems, Energy. 137 (2017) 661–669. https://doi.org/10.1016/j.energy.2017.02.075.

[6] L. Fu, Y. Li, Y. Wu, X. Wang, Y. Jiang, Low carbon district heating in China in 2025- a district heating mode with low grade waste heat as heat source, Energy. 230 (2021). https://doi.org/10.1016/j.energy.2021.120765.

[7] K. O'Donovan, B. Falay, I. Leusbrock, Renewables, storage, intelligent control: how to address complexity and dynamics in smart district heating systems?, Energy Procedia. 149 (2018) 529–538. https://doi.org/10.1016/j.egypro.2018.08.217.

[8] B. Doracic, M. Grozdek, T. Puksec, N. Duic, Excess Heat Utilisation Combined With Thermal Storage Integration in District Heating Systems Using Renewables, Therm. Sci. 24 (2020) 3673–3684. https://doi.org/10.2298/TSCI200409286D.

[9] H. Li, J. Hou, Y. Ding, N. Nord, Techno-economic analysis of implementing thermal storage for peak load shaving in a campus district heating system with waste heat from the data centre, E3S Web Conf. 246 (2021). https://doi.org/10.1051/e3sconf/202124609003.

[10] J. Reynolds, M.W. Ahmad, Y. Rezgui, District Heating Energy Generation Optimisation Considering Thermal Storage, 2018 6th IEEE Int. Conf. Smart Energy Grid Eng. SEGE 2018. (2018) 330–335. https://doi.org/10.1109/SEGE.2018.8499509.

[11] E. Guelpa, V. Verda, Thermal energy storage in district heating and cooling systems: A review, Appl. Energy. 252 (2019) 113474. https://doi.org/10.1016/j.apenergy.2019.113474.

[12] D. Wang, J. Carmeliet, K. Orehounig, Design and assessment of district heating systems with solar thermal prosumers and thermal storage, Energies. 14 (2021) 1–27. https://doi.org/10.3390/en14041184.

[13] R. Renaldi, D. Friedrich, Techno-economic analysis of a solar district heating system with seasonal thermal storage in the UK, Appl. Energy. 236 (2019) 388–400. https://doi.org/10.1016/j.apenergy.2018.11.030.

[14] B. Talebi, F. Haghighat, P. Tuohy, P.A. Mirzaei, Optimization of a hybrid community district heating system integrated with thermal energy storage system, J. Energy Storage. 23 (2019) 128–137. https://doi.org/10.1016/j.est.2019.03.006.

[15] A. Pini Prato, F. Strobino, M. Broccardo, L. Parodi Giusino, Integrated management of cogeneration plants and district heating networks, Appl. Energy. 97 (2012) 590–600. https://doi.org/10.1016/j.apenergy.2012.02.038.

[16] M. Veyron, A. Voirand, N. Mion, C. Maragna, D.

Mugnier, M. Clausse, Dynamic exergy and economic assessment of the implementation of seasonal underground thermal energy storage in existing solar district heating, Energy. 261 (2022). https://doi.org/10.1016/j.energy.2022.124917.

[17] M.N. Descamps, G. Leoncini, M. Vallée, C. Paulus, Performance assessment of a multi-source heat production system with storage for district heating, Energy Procedia. 149 (2018) 390–399. https://doi.org/10.1016/j.egypro.2018.08.203.

[18] T. Pauschinger, T. Schmidt, P. Alex Soerensen, D. Aart Snijders, R. Djebbar, R. Boulter, C. Jeff Thornton, Integrated Cost-effective Large-scale Thermal Energy Storage for Smart District Heating and Cooling - Design Aspects for Large-Scale Aquifer and Pit Thermal Energy Storage for District Heating and Cooling, Int. Energy Agency Technol. Collab. Program. Dist. Heat. Cool. Incl. Comb. Heat Power. 2018 (2018).

[19] I. Sifnaios, G. Gauthier, D. Trier, J. Fan, A.R. Jensen, Dronninglund water pit thermal energy storage dataset, Sol. Energy. 251 (2023) 68–76. https://doi.org/10.1016/j.solener.2022.12.046.

[20] T. Schmidt, T. Pauschinger, P.A. Sørensen, A. Snijders, R. Djebbar, R. Boulter, J. Thornton, Design Aspects for Large-scale Pit and Aquifer Thermal Energy Storage for District Heating and Cooling, Energy Procedia. 149 (2018) 585–594. https://doi.org/10.1016/j.egypro.2018.08.223.

[21] A.J. Kallesøe, T. Vangkilde-Pedersen, Underground Thermal Energy Storage (UTES) – state-of-the-art, example cases and lessons learned., 2019. https://www.heatstore.eu/documents/HEATSTORE_UTES State of the Art_WP1_D1.1_Final_2019.04.26.pdf.

[22] P.A. Soerensen, N. From, High solar fraction with pit heat storages, in: 30th ISES Bienn. Sol. World Congr. 2011, SWC 2011, 2011: pp. 3020–3030. https://doi.org/10.18086/swc.2011.21.07.

[23] P. Reiter, H. Poier, C. Holter, BIG Solar Graz: Solar District Heating in Graz - 500,000 m2 for 20% Solar Fraction, Energy Procedia. 91 (2016) 578–584. https://doi.org/10.1016/j.egypro.2016.06.204.

[24] A. Hast, S. Rinne, S. Syri, J. Kiviluoma, The role of heat storages in facilitating the adaptation of district heating systems to large amount of variable renewable electricity, Energy. 137 (2017) 775–788. https://doi.org/10.1016/j.energy.2017.05.113.

[25] A. Tosatto, A. Dahash, F. Ochs, Simulation-based performance evaluation of large-scale thermal energy storage coupled with heat pump in district heating systems, J. Energy Storage. 61 (2023) 106721. https://doi.org/10.1016/j.est.2023.106721.

[26] EA Energianalyse, Varmelagre i hovedstadsområdet. En vurdering af placeringsmulighederne for varmelagre i hovedstadsområdet . Udbygning med varmelagre i hovedstadsområ- det Indhold, (2018). https://www.gate21.dk/wp-content/uploads/2018/05/Varmelagre_hovedstadsområdet_EPT.pdf.

[27] Y. Bai, Z. Wang, J. Fan, M. Yang, X. Li, L. Chen, G. Yuan, J. Yang, Numerical and experimental study of an underground water pit for seasonal heat storage, Renew. Energy. 150 (2020) 487–508. https://doi.org/10.1016/j.renene.2019.12.080.

[28] Z. Xie, Y. Xiang, D. Wang, O. Kusyy, W. Kong, S. Furbo, J. Fan, Numerical investigations of long-term thermal performance of a large water pit heat storage, Sol. Energy. 224 (2021) 808–822. https://doi.org/10.1016/j.solener.2021.06.027.

[29] Modelica - The Modelica Association, (n.d.). https://www.modelica.org/ (accessed August 11, 2020).

[30] G. Gauthier, Benchmarking, and improving models of subsurface heat storage dynamics. Comparison of Danish PTES and BTES installation measurements with their corresponding TRNSYS models. GEOTHERMICA – ERA NET Cofund Geothermal, (2020). https://www.heatstore.eu/documents/HEATSTORE_WP2_D2.3-Danish PTES and BTES installations_Final_2020.11.02.pdf.

[31] Nordpool, Elspot Prices, (n.d.). https://www.energidataservice.dk/tso-electricity/Elspotprices (accessed July 22, 2023).

[32] S.A. et al Klein, TRNSYS 18: A Transient System Simulation Program, (2017). http://sel.me.wisc.edu/trnsys.

[33] I. Sifnaios, A.R. Jensen, S. Furbo, J. Fan, Performance comparison of two water pit thermal energy storage (PTES) systems using energy, exergy, and stratification indicators, J. Energy Storage. 52 (2022) 104947. https://doi.org/10.1016/j.est.2022.104947.

[34] PlanEnergi, Sunstore 3 - Phase 2: Implementation, 2015. https://planenergi.dk/wp-content/uploads/2018/05/26-Sunstore-3-Final-report.pdf (accessed January 15, 2022).

[35] I. Sifnaios, Investigations of pit thermal energy storages in district heating systems, Technical university of Denmark, 2023. https://doi.org/10.11581/DTU.00000291.

[36] Renewable Energy magazine, Aalborg CSP hands over CO2 heat pump system to Danish district heating plant, (2023). https://www.renewableenergymagazine.com/thermal/aalborg-csp-hands-over-co2-heat-pump-20230503 (accessed July 24, 2023).

[37] State of Green, Aalborg CSP receives order for integrated heat pump system for district heating plant

in Denmark, (2020). https://stateofgreen.com/en/news/aalborg-csp-receives-order-for-integrated-heat-pump-system-for-district-heating-plant-in-denmark/ (accessed July 24, 2023).

[38] European Heat Pump association, Dronninglund District heating, (2023). https://hpa.ehpa.org/dronninglund-district-heating-6-mw-heatpump-with-air-and-thermal-storage/ (accessed July 24, 2023).

[39] PlanEnergi, Drejebog til store varmepumpeprojekter i fjernvarmesystemet, (2017). https://planenergi.eu/arbejdsomraader/fjernvarme/varmepumper/drejebog-til-store-varmepumpeprojekter-i-fjernvarmesystemet/ (accessed August 11, 2023).

[40] D. Zenhäusern, Key Performance Indicators for PVT Systems, 2020. https://doi.org/10.18777/ieashc-task60-2020-0007.

[41] Danish Energy Agency, Technology data for Energy storage, (2018) 1–18.

[42] IEA Task 54, LCOH for solar thermal applications, (2018). http://task54.iea-shc.org/Data/Sites/1/publications/A01-Info-Sheet--LCOH-for-Solar-Thermal-Applications.pdf (accessed October 1, 2021).

[43] H. Pieper, T. Ommen, F. Buhler, B.L. Paaske, B. Elmegaard, W.B. Markussen, Allocation of investment costs for large-scale heat pumps supplying district heating, Energy Procedia. 147 (2018) 358–367. https://doi.org/10.1016/j.egypro.2018.07.104.

[44] M. Marsidi, Technology factsheet - Electric Industrial Boiler, Netherlands Organ. Appl. Sci. Res. (2018). https://energy.nl/wp-content/uploads/electric-industrial-boiler-7.pdf (accessed July 22, 2023).

[45] I. Sifnaios, D.M. Sneum, A.R. Jensen, J. Fan, R. Bramstoft, The impact of large-scale thermal energy storage in the energy system, Appl. Energy. 349 (2023) 121663. https://doi.org/10.1016/j.apenergy.2023.121663.

VII

VIII. The impact of large-scale thermal energy storage in the energy system

Ioannis Sifnaios, Daniel Møller Sneum, Adam R. Jensen, Jianhua Fan, and Rasmus Bramstoft

Applied Energy, 349, 121663 (2023)

VIII

Applied Energy 349 (2023) 121663

Contents lists available at ScienceDirect

Applied Energy

journal homepage: www.elsevier.com/locate/apenergy

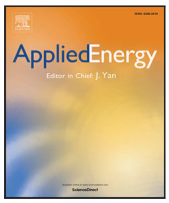

The impact of large-scale thermal energy storage in the energy system

Ioannis Sifnaios [a,b,*], Daniel Møller Sneum [c], Adam R. Jensen [a], Jianhua Fan [a], Rasmus Bramstoft [c]

[a] Department of Civil and Mechanical Engineering, Technical University of Denmark, Koppels Allé 404, Kgs. Lyngby, 2800, Denmark
[b] Sino-Danish College (SDC), University of Chinese Academy of Sciences, Huairou District, Beijing, 101408, China
[c] Department of Technology, Management and Economics, Technical University of Denmark, Produktionstorvet 358, Kgs. Lyngby, 2800, Denmark

ARTICLE INFO

Keywords:
Heat storage
Pit thermal energy storage (PTES)
Integration
District heating
Sector coupling

ABSTRACT

In the last decade, pit thermal energy storage (PTES) systems have been used as a large-scale heat storage solution in district heating systems due to their low specific investment cost and high storage efficiency. Despite the existing knowledge on thermal energy storage (TES) technologies, their economic and environmental impacts have not been quantified in the literature, and very few studies have studied PTES as part of the energy system. For this reason, the energy system model Balmorel was used to quantify the impact of TES on the energy system, particularly PTES, and compare it to the tank thermal energy storage (TTES) alternative. The investigation was focused on Denmark and its neighboring countries. It was found that it was only the energy systems using TES that could achieve carbon neutrality by 2050. The main reason was the added flexibility due to the energy storage that allowed the system to have a 35% higher PV capacity, 10% higher wind capacity, and lower levels of curtailment. Additionally, systems with TES had 2.4 €/MWh lower average heat price (with 24% lower peak price). When comparing PTES with TTES, it was found that PTES systems were more advantageous, achieving a 1.5 €/MWh lower average price of heat.

1. Introduction

Storage as a concept can be defined according to physical and financial optimization. In physical terms, storage can decouple production and consumption within a feasible timeframe. In financial terms, arbitrage through storage allows for buying low and selling high. In the case of heating, the physical abundance of, e.g., excess heat from an electrolyzer may not be matched by an equivalently high heat demand in a given hour. Here, storage can decouple heat sources and sinks, potentially within hours, days, or even months [1]. Financially, such decoupling can enable the utilization of the least-cost heat sources. For instance, low-cost electricity at nighttime can be used to produce heat with a heat pump, which can then be stored in a thermal energy storage (TES) system and used during the day when electricity prices are high.

Large-scale TES used for heating are generally characterized as sensible heat storage, i.e., the storage energy content is raised by increasing the temperature of the storage material [2]. Still, large-scale TES systems merit a further definition since the term can be applied to at least three different technologies: High-temperature storages for electricity production through liquid salt, thermal oils, or similar, typically based on concentrated solar power [3]; high-temperature storages for electricity and heat production in a low-cost medium like rocks [4]; and lower temperature thermal storage in a low-cost medium like water, with heat supply as the sole purpose [5]. Our study applies the latter definition of the term TES.

The simulation of energy systems with TES is highly affected by the selection of the system's boundaries and the trade-off between computational requirements and accurate system representation. Single systems are usually simulated with a high level of detail, e.g., modeling of the TES temperature, stratification, and detailed heat losses, as in [6]. Usually, these simulations use software like TRNSYS [7], Modelica [8], etc. On the contrary, if the energy system boundary is at the city or country level, simplified modeling of TES needs to be done using only techno-economic characteristics (e.g., cost, lifetime, and efficiency, as in [9]). For these analyses, energy system models like Balmorel, EnergyPLAN, GENESYS, PyPSA, etc., can be used [10,11]. Multiple iterations are required (and usually high computational time) to determine the optimal system configuration. Such analyses typically require further system simplifications; thus, temporal and spatial aggregation is applied in the modeling. In temporal aggregations, models use a selection of representative hours/periods (e.g., four weeks using every third hour, as in [12]). In contrast, for spatial aggregation, models use a selection of consumption/production characteristics (e.g., 30

* Corresponding author.
E-mail address: iosif@dtu.dk (I. Sifnaios).

https://doi.org/10.1016/j.apenergy.2023.121663
Received 27 December 2022; Received in revised form 19 July 2023; Accepted 24 July 2023
Available online 7 August 2023

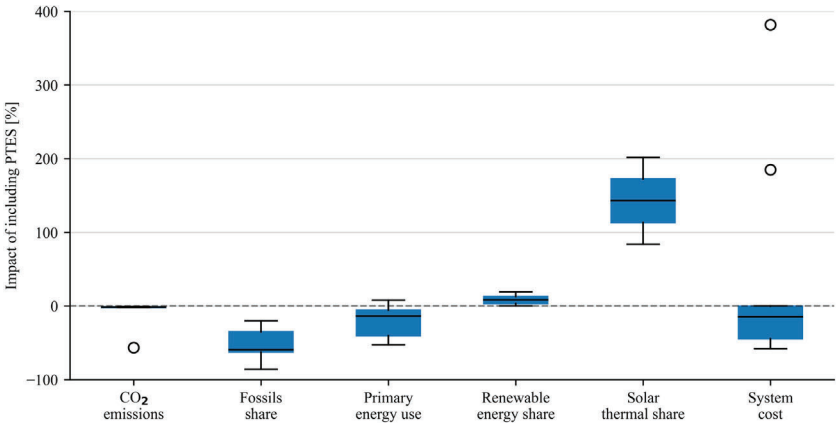

Fig. 1. Comparison of the impact of utilizing PTES on a local energy system. Values denote the percentage increase of systems with PTES compared to systems without PTES (e.g., 150% solar thermal share means that systems with PTES feature 2.5 times higher solar thermal generation compared to systems without TES). Based on the screening of 307 papers, data was reduced to six relevant studies [5,13–17] containing 16 analyses in total. The white circles denote outliers.

nodes, each representing demand and supply from a single European country, as in [9]). Consequently, there are many ways of simulating TES systems based on the modeling approach, boundaries of the energy system, and assumptions.

The two main TES technologies in the Danish district heating sector are water tank thermal energy storage (TTES) systems and water pit thermal energy storage (PTES) systems. While TTES is a well-known technology, PTES is a relatively new technology, with the first large-scale system starting operation in 2012. A PTES is constructed by excavating a pit in the ground, which is lined with a watertight polymer liner and is then filled with water and covered with an insulated floating lid. PTES have become popular in recent years due to their low cost compared to other TES technologies [18]. Since PTES is not yet a mature technology, the efficiencies of the existing pilot PTES systems for long-term storage range from 60% to 70%, being affected by the ground conditions, insulation lid performance, etc. [19]. However, storage efficiencies greater than 90% have been achieved in the PTES in Dronninglund, creating a paradigm for future PTES systems [19].

Often, TES is characterized according to the storage duration: short-term (hours-week) and long-term (months) [20]. Short-term TES are generally used for peak shaving, while long-term TES are used for transferring energy across seasons. In Denmark, TTES systems are typically used for short-term storage, while PTES systems have primarily been used for long-term storage. However, for PTES, this distinction in terms of time may no longer be appropriate. This is due to the possible utilization of a PTES as a very large but short-term storage system (e.g., like the short-term PTES currently under construction in Høje Taastrup, Denmark [21]).

TES for heating is well-described in literature as a part of large-scale energy system analyses (e.g., [22]), in combination with solar heating [23] and in terms of optimizing the production of district heating plants [24]. The usefulness of TTES has been demonstrated in several studies of district heating (DH) systems [25] (storages resulted in lower levelized cost of heat) and in the daily production optimization in the many commercially operating, real-world deployments. The sector coupling relevance of both PTES and TTES has been demonstrated by the large, modeled deployment in energy system studies of Europe by Sneum et al. [22] (229 GWh intraseasonal heat storage by 2035 in Denmark) and Gea-Bermúdez et al. [26] (20 TWh long-term heat storage in Northern-Central Europe by 2035). For comparison, the deployment of Danish TES in 2017 was 50 GWh [27].

Several studies [13,28–30] have reviewed the general traits of PTES and TTES. We extended this work with a meta-review of small and large energy systems with and without PTES. This review shows a slightly mixed picture (see Fig. 1). Literature directly analyzing the impacts of PTES is limited. With a caveat for the small sample size (see Appendix B), we see that PTES generally results in lower system costs, although with a large spread. CO_2 emissions decrease by only 1%–2%, while reductions in fossil use and primary energy use are more pronounced. Conversely, renewables shares are increased. The increase in solar thermal is noteworthy and aligns well with the general practice of co-locating solar thermal plants with PTES. Common for the screened studies is that they investigate single plants, not large-scale energy systems on a national or international level (except [14] that investigates the German energy system).

Recently, there has been a high interest in PTES systems, and many studies have been published. For example, numerical PTES simulations were conducted, assessing the storage performance [31]. Additionally, phenomena related to the operation of PTES (e.g., natural convection) have been numerically investigated [32]. Last, various control strategies regarding the seasonal operation of PTES have been numerically investigated [33]. Nevertheless, all these studies focus on individual plants, not their integration with the energy system.

In summary, PTES systems have been analyzed in theory, demonstrated, and deployed in practice. Despite this, a research gap remains as few studies on PTES' specific impact exist. Borri et al. [34] have reviewed the scientific literature on TES and similarly identified a lack of economic and environmental aspects concerning TES. Finally, neither of the studies analyzed the particular impact of PTES in large-scale energy system analyses.

Thus, the aim of this study was to answer the following research questions:

1. What is the impact of TES in an energy system on a national and international level?
2. What is the impact of PTES in an energy system compared to the TTES alternative?
3. Which PTES characteristics have the largest effect on future deployment and development?

In line with similar large-scale energy system studies on other technological options (e.g., low specific power wind turbines [35] or energy efficiency [36]), we explore the potential deployment and use of PTES in the current and future energy systems. PTES, like other technologies under development, have faced technological challenges (e.g., lid and liner durability). To illustrate the potential of PTES, we assume these teething troubles are solved in the analysis. And in the same vein as the studies mentioned above, we do so not to advocate for the technology but to explore PTES' potential impact.

In the present study, we applied the comprehensive energy system model, Balmorel [37], to answer the research questions. Balmorel has been applied to assess different energy transition scenarios and was developed to enable holistic energy system analyses. Additionally,

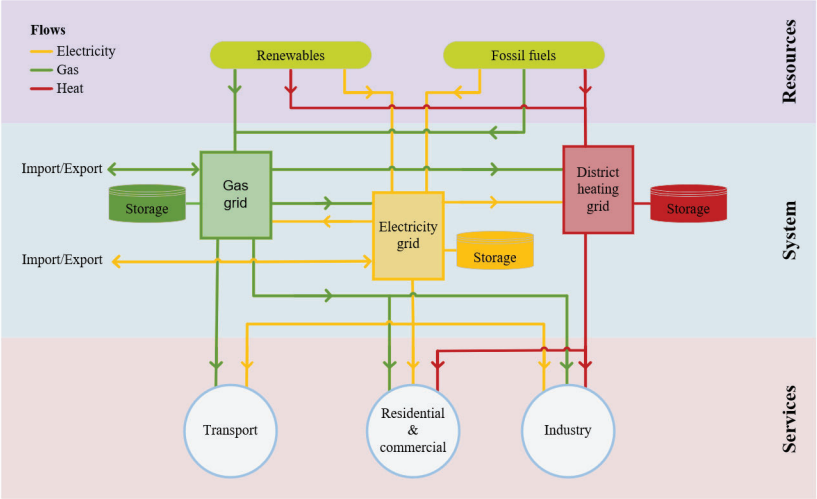

Fig. 2. Schematic of energy sector modeling in Balmorel (adapted from [44]).

it has been used to conduct deep-dive analyses of specific parts of the energy system at different geographical scales and with different scopes. It has, for example, been applied for analyzing the decarbonization of the Northern European integrated power and district heating system [38,39], the role of district heating in a national context [40], and the transition of local heating systems [41]. It has also been used for analyzing the integrated energy system with sector coupling [26] and focusing on producing renewable transport fuels, including Power-to-X (PtX) and sector coupling opportunities [42,43], as well as many other studies.

An overview of the Balmorel model and the applied modeling approach is provided in Section 2. The simulated scenarios, along with the data assumptions, are presented in Section 3, followed by the results of the study in Section 4, and conclusions in Section 5.

2. Method: Energy system model, balmorel

2.1. General description of balmorel

Balmorel [45] is an open-source, deterministic, partial equilibrium model for optimizing energy systems assuming perfect markets and economic rationality [37]. Similar to other energy system models, it builds upon a bottom-up approach and computes the least-cost solution for the energy system (minimizing the investment and operation costs)to satisfy the energy demands. The mathematical formulation and results have recently been compared against four other well-known open-source energy system models [11,46], with conclusions emphasizing the model's validity.

Furthermore, Balmorel is a technology-rich energy system model with a comprehensive representation of energy technologies and infrastructures. The model converts the energy sources to energy vectors, which can then be transmitted to demands or conversion technologies in different energy sectors. In parallel, it optimizes both investment and operational dispatch.

2.2. Spatial and temporal dimensions

The spatial representation in Balmorel consists of countries, regions, and areas. Each country can have multiple regions, and each region can have multiple areas. The division of each country into regions and areas can be facilitated using different measures, for example, geography, market bidding zones, or the size of energy demand. The regions are used to define a country's electricity demand and maintain the electricity balance, while the areas specify the characteristics inside a region (e.g., wind and solar potential) and define heat demands. The areas can also be used for any other categorization of the heat sector, for example, the split between the industrial and residential sectors, temperature levels, etc.

The temporal resolution in Balmorel consists of three levels: years, seasons, and terms. Years are divided into seasons, and seasons are divided into terms. In this way, the temporal resolution in Balmorel is flexible and can be designed to capture the main features depending on the research question and required accuracy while potentially reducing the computation time. For example, instead of simulating all hours of the year, it is possible to select some periods that are representative of the entire simulation period. It is also possible to simulate all time steps at high resolution considering all hours. Overall, the choice is a trade-off between computation time and temporal resolution.

2.3. Energy system coupling and coverage in balmorel

Balmorel covers the main energy sectors (i.e., power, heat, gas, and transport) and vectors (i.e., electricity, gas, and heat transfer fluids), thereby allowing for holistic analysis of the current and future sector-coupled energy system. Balmorel is built upon a modular structure, which enables the user to include energy sectors in the modeling scope and more detailed features within each sector. Fig. 2 illustrates the representation of energy sectors and interactions between energy vectors in the Balmorel model.

2.3.1. Coupling between the heat, power, and transport sectors

In most countries, energy sectors are already coupled to some extent and are expected to become even more interlinked in the future [47]. One way of facilitating the linkage across energy sectors is by employing energy conversion technologies. Examples of conversion technologies that couple the heating sector with the power sector are heat pumps, boilers, and combined heat and power (CHP) plants. Furthermore, linkages between electricity, heating, and fuel production for the hard-to-abate transport and industrial sector are expected to be more widespread in the future. For example, Power-to-X (PtX) fuels could supply the heavy long-haul transport sector and also decarbonize the industrial sector.

Electricity is supplied to cover the demand of the power sector, while the transport sector demand is supplied either through electrification or the production of liquid fuels, e.g., PtX. Last, the heating sector is supplied with electricity, district heating, or fuels. This way, Balmorel can optimize the system, including different conversion pathways and efficient utilization of sources.

Furthermore, as the future power system is expected to be dominated by high penetrations of variable renewable energy sources,

system flexibility becomes prominent and urgently needed. The flexibility can be provided through four main options, i.e., flexible generation, increased transmission capacity, demand side management, and storage (electricity, heat, and hydrogen). Consequently, internal competition across the flexibility providers appears, even with cross-sectoral benefits. These cross-sectoral effects are assessed in the present study, where Power-to-Heat technologies combined with district heating and TES might be the least-cost opportunity to provide the needed flexibility to the power system, compared to, e.g., batteries.

2.3.2. Heating sector

The simulation of the non-industrial heat consumption in Balmorel is done without accounting for temperature levels. For example, while the district heating supply temperature differs in each country, in Balmorel, only the heating demand is considered (details for each country are presented in Appendix C). Additionally, the utilization of excess heat (e.g., from electrolyzers) is included in the model, and it is assumed that it can be supplied directly to the district heating grid (without the need for heat pumps to increase its temperature).

District heating networks transfer heat from large-scale production technologies (e.g., boilers, CHP plants, heat pumps, electrolyzers, solar heating, and storage technologies) to consumers. The DH demands were included in the modeling framework, and conversion from individual heating solutions to DH was allowed for different heating sectors, e.g., residential, tertiary, and industry. District heating areas were aggregated to reduce the simulations' computation time. Aggregation was done according to the size of the demands to account for the effects of economies of scale of some technologies (e.g., heat storage), land availability, costs, etc. Since the aggregation was according to demand size and not geography (as in [42,43,48]), heat transfer was not allowed between the DH areas. The resulting scales for the DH areas were: small, medium, and large.

The heat demand of the industry sector was modeled based on the temperature level required by each industry type. This way, the industry sector was divided into high-temperature (HT), requiring temperatures higher than 500 °C; medium-temperature (MT), requiring temperatures between 100 - 500 °C; and low-temperature (LT), requiring temperatures lower than 100 °C. A more detailed explanation of the temperature split is described in [26,49].

Apart from the temperature division, the heat consumption of the industrial consumers was further divided into whether or not they were connected to the DH grid and, if so, which DH grid scale they belonged to. The industry not connected to DH could be connected to the large DH areas as long as the model found it economical to invest in heat transmission capacity. Additionally, it was also possible for the LT industry to supply excess heat to the DH grid if they were connected. Similarly, the MT industry could supply excess heat to the LT industry.

Similar to the industry sector, the remaining heat load (encompassing the residential and tertiary sectors) was divided into two categories for each region: already connected to the DH network and not connected. This load was implemented by assigning an inflexible demand for domestic hot water and space heating to the population of each country. The heat load not connected to the DH network was called "individual users" and corresponded to a different percentage of the total demand depending on the country (see [50]). The reader is referred to [39] for more details on this.

Furthermore, the individual users connected to the DH grid were divided into groups depending on which scale of DH they belonged and were not allowed to use other technologies to cover their heat demand. On the contrary, individual users not connected to the DH grid had to cover their heat demand using technologies such as solar heating, heat pumps, boilers, and small-scale heat storage. In case it was considered profitable by the model, these users had the option to be connected to DH-large areas.

It should be noted that this study focused only on the optimization of the supply side. Thus, the effect of flexible demand and small-scale storage in individual buildings was not investigated. The reader is referred to [51,52] if more information is desired on this topic.

2.3.3. Modeling heat storage

Balmorel only simulates energy flows; thus, aspects like thermal stratification, efficiency based on storage duration, etc., are not accounted for. These simplifications reduce the computation time, which is essential when doing country-level simulations.

Two types of heat storage can be used, namely short-term and seasonal heat storage. Short-term heat storage (intra-seasonal) is defined as having a storage duration of less or equal to one week. In comparison, seasonal heat storage (inter-seasonal) is defined as having a storage duration longer than one week and up to one year. The modeling of TES in Balmorel is facilitated using five equations that account for different aspects of the storage operation, namely the system heat balance (1), storage dynamics (2), storage charge and discharge limit (3)–(4), and storage capacity (5). The mathematical formulations in Eqs. (1)–(5) are generalized to represent both inter- and intra-seasonal heat storages. More information on the modeling of TES in Balmorel can be found in Appendix D.

The heat balance (Eq. (1)) ensures that heat demand, $d^{heat}_{y,a,s,t}$, is satisfied in all areas a, at all timesteps s,t, and for every year y. The heat generated by the various generation technologies, $p^{gen\_heat}_{y,a,g,s,t}$ can be stored by charging the TES $p^{TES,charge}_{y,a,g,s,t}$, and discharged at a later timestep $p^{TES,discharge}_{y,a,g,s,t}$.

Eq. (2) represents the dynamic equation for heat storage modeling, i.e., the heat storage content at the next time step, $v^{TES}_{y,a,g,((s,t)+1)}$, is equal to the heat storage content at the beginning of the time segment, $v^{TES}_{y,a,g,s,t}$, plus the difference between charging the TES, $p^{TES,charge}_{y,a,g,s,t}$, and discharging, $p^{TES,discharge}_{y,a,g,s,t}$, while also considering the storage efficiency, $\epsilon^{TES,eff}_{g}$. The difference is multiplied by the length of the time segment, $\gamma_{s,t}$, in order to account for time aggregation. Note that heat losses from the storage are accounted for during discharging.

Eq. (3) sets the upper limit for the charging rate of the heat storage, $\lambda^{TES,charge}_{g\in\mathcal{G}^{TES}}$. Similarly, Eq. (4) defines the upper limit for the discharging rate of the TES, $\omega^{TES,discharge}_{g\in\mathcal{G}^{TES}}$.

Finally, in Eq. (5), the capacity of the TES, $v^{TES}_{y,a,g,s,t}$, should be less or equal to the sum of the existing capacity, $k^{TES,ex\_CAP}_{y,a,g}$, and new investment $k^{TES,new\_CAP}_{y,a,g}$, also considering decommissioning of capacity, $k^{TES,decom\_CAP}_{y,a,g}$.

System heat balance equation (heat supply equals demand):

$$\sum_{g\in\mathcal{G}^{heat}} p^{gen\_heat}_{y,a,g,s,t} - \sum_{g\in\mathcal{G}^{TES}} p^{TES,charge}_{y,a,g,s,t} + \sum_{g\in\mathcal{G}^{TES}} p^{TES,discharge}_{y,a,g,s,t} = d^{heat}_{y,a,s,t} \quad \forall y\in\mathcal{Y},\ a\in\mathcal{A},\ g\in\mathcal{G},\ s\in\mathcal{S},\ t\in\mathcal{T} \tag{1}$$

See Eqs. (2)–(5) given in Box I.

3. Data assumptions and scenarios

3.1. Geographical and temporal scope

The present study assesses the impact of large-scale thermal storage in energy systems focusing on Denmark as a part of the Northern European energy system. As elucidated in the methods section, energy systems are becoming increasingly interconnected in terms of energy sectors and across countries. Therefore, as the Danish power system is connected to surrounding countries, a larger geographical scope is needed to capture system effects on the power system and, thereby, power prices. Therefore, this study's geographical scope includes Denmark, Norway, Sweden, and Germany, whose power systems are connected through transmission lines. The electricity system is divided into market bidding zones, as defined by Nord Pool power market [53] and illustrated in Fig. 3A.

Unlike electricity distribution, heat distribution can only happen locally, i.e., through district heating. As described in Section 2.3.2, district heating networks can supply part of each country's heat demand. All simulated countries can have all grid scales (i.e., large,

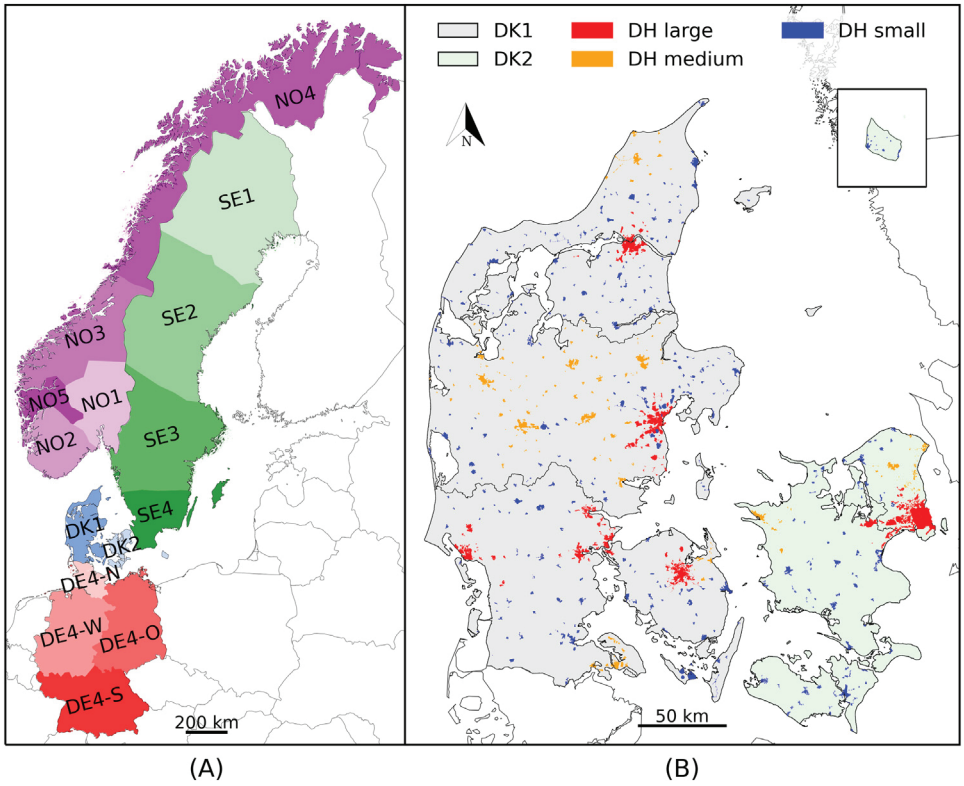

Fig. 3. Map of countries and regions (colored) (A), and aggregation of district heating areas in Denmark in Balmorel (B).

VIII

TES dynamic equation:

$$v^{TES}_{y,a,g,s+1,t+1} = v^{TES}_{y,a,g,s,t} + \gamma_{s,t}\left[p^{TES,charge}_{y,a,g,s,t} - \frac{p^{TES,discharge}_{y,a,g,s,t}}{\epsilon^{TES,eff}_{g}}\right] \quad (2)$$

TES charge capacity limit:

$$p^{TES,charge}_{y,a,g,s,t} \leq \frac{k^{TES,ex\_CAP}_{y,a,g} - k^{TES,decom\_CAP}_{y,a,g} + k^{TES,new\_CAP}_{y,a,g}}{\lambda^{TES,charge}_{g}} \quad (3)$$

TES discharge capacity limit:

$$p^{TES,discharge}_{y,a,g,s,t} \leq \frac{k^{TES,ex\_CAP}_{y,a,g} - k^{TES,decom\_CAP}_{y,a,g} + k^{TES,new\_CAP}_{y,a,g}}{\omega^{TES,discharge}_{g}} \quad (4)$$

TES capacity:

$$v^{TES}_{y,a,g,s,t} \leq k^{TES,ex\_CAP}_{y,a,g} - k^{TES,decom\_CAP}_{y,a,g} + k^{TES,new\_CAP}_{y,a,g} \quad (5)$$

$\forall y \in \mathcal{Y}, a \in \mathcal{A}, g \in \mathcal{G}^{TES}, s \in \mathcal{S}, t \in \mathcal{T}$

Box I.

medium, small) in every region; however, this is not always the case (e.g., Norway only has medium-sized DH areas, while Germany only has large ones).

Specifically, Denmark has six large central district heating networks and around 400 small- and medium-sized district heating networks [54]. Five of the large DH areas are located in DK1 (Aarhus, Aalborg, Odense, TVIS [55], Esbjerg), and the sixth is in DK2 (Greater Copenhagen area). The DH areas are aggregated into three main categories, i.e., DH-large, DH-medium, and DH-small, for each of the DK1 and DK2 regions. For example, all small DH areas of one region are modeled as one area, having a demand equal to the sum of the individual areas. Thus, the heating networks are not modeled individually. The criterion by which the DH grids were divided into the three categories was their size/demand. With this division, it could also be ensured that different technologies could be built in different areas

(e.g., a large CHP plant was not allowed to be installed in a DH-small area to consider economy-of-scale effects). More details on the division of DH grids by size can be found in [56]. An example of the Danish DH areas in Balmorel is illustrated in Fig. 3B.

In this study, Balmorel is computing the least-cost solution for the energy transition toward 2050, with 10-year intermediate steps. Each year of the simulation is represented by 8 seasons and 12 terms. Each season corresponds to one week of the year, i.e., weeks 1, 8, 15, 22, 29, 36, 43, and 50. Furthermore, each of these weeks is represented by 12 hourly time steps selected from one day. Each timestep is repeated until the next modeled timestep arrives, thus, simulating an entire year. Although the temporal resolution is rather coarse, the simulation still accounts for seasonal trends (e.g., ambient temperature, energy demand, prices, seasonal storage charge level). It should be noted that, despite the time aggregation, the computational time of the model was 2.5 days. Therefore, it was not considered feasible to investigate the effect of higher temporal resolutions on the results.

3.2. Techno-economic parameters for heat storage systems

In general, Balmorel uses TTES for short-term heat storage (storage duration of less than a week) and PTES for seasonal heat storage (storage duration of more than a week and up to one year). Although it is common practice to use the term seasonal storage when heat is transferred across seasons (i.e., from summer to winter), seasonal storage does not have a fixed storage duration in Balmorel. Therefore, the efficiency for the PTES (80%) was taken as an average between 70%, which is expected for PTES seasonal storage without a heat pump [57], and 90%, which is expected for PTES used for short-term storage (Table 1). It should be noted that this is a simplistic modeling approach since, in reality, the storage efficiency depends on the cycle duration.

It should also be noted that the existing seasonal TES systems have primarily utilized solar thermal as the heat source. However, PTES can be coupled to any heating source and is thus considered flexible in Balmorel. This is for example the recent PTES in Høje Taastrup (Denmark), which is charged from various heating sources including waste incineration, biomass combustion, and heat pumps.

Regarding the charge/discharge capacity, PTES and TTES were assumed to have the same limits since they were connected to the same network. Similarly, since all the investigated thermal energy storage systems were directly connected to the district heating network, the storage capacities were calculated assuming that TES operated with an upper temperature of 90 °C (forward temperature) and a lower temperature of 40 °C (return temperature). These temperatures are typical for PTES in Danish district heating networks when a heat pump is not used to cool down the storage [58]. Nonetheless, Balmorel does not simulate temperatures but energy flows. The temperature difference is used for calculating the specific storage cost, i.e., determining the relationship between m^3 and MWh. Thus, the effect of different operating temperatures can be elucidated from the sensitivity analysis graphs of the investment costs (see Section 4.3). For example, half the temperature difference corresponds to twice the investment cost.

The economy data for TTES are based on tank installations in Danish DH plants and were taken from Sveinbjørnsson [27]. Fig. 4 illustrates the specific investment cost for PTES and TTES with respect to their storage volumes. Each dot represents the data for one heat storage system. It may be observed that PTES and TTES are technologies of scale since their specific cost decreases significantly with an increase in volume. Despite the similar trend of the investment cost for the two technologies, it must be noted that the specific cost for PTES is much lower than TTES (the y-axes differ by a factor of 4). The main reasons are the differences in materials and construction approaches. The individual data points from actual systems were fitted to a power function, which was later used to calculate the cost of storage systems of various sizes.

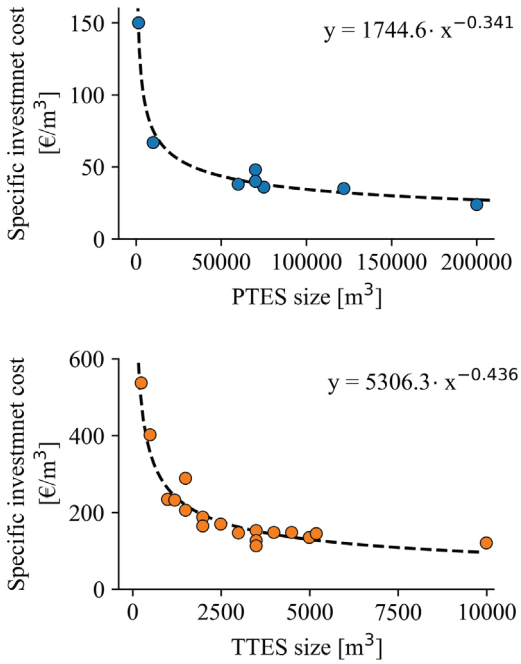

Fig. 4. Specific investment cost for PTES and TTES as a function of their size in m^3. Each dot corresponds to an actual system. The dashed curve is the corresponding trend line.

As it may be seen in Fig. 4, most TTES systems have volumes of 500 - 5 000 m^3, with an average size of approximately 3 000 m^3. TTES systems are generally considered more cost-effective than PTES for small volumes (i.e., smaller than 10 000 m^3) [57]. For this reason, for the simulated TTES systems, a volume of 3 000 m^3, which is common in Denmark, was selected (Table 1).

Regarding the Danish PTES, the volumes of the operational storage systems range from 60 000 - 200 000 m^3. However, at the moment of writing, two serially connected PTES systems with volumes of 750 000 m^3 and 250 000 m^3 are planned to be constructed in the town of Odense, Denmark. Thus, it is evident that the sizes of the future constructed PTES might be much larger than the existing ones.

It has to be noted that, in Balmorel, due to the aggregation of DH areas, the installed TES capacity does not correspond to one storage system but to many smaller ones (depending on the number of aggregated areas). For this reason, the chosen sizes for the simulated PTES were not selected as the largest possible, but sizes were chosen based on the installed storage capacity during the simulation. PTES of 250 000 m^3 were only allowed to be installed in large DH areas, 100 000 m^3 in medium DH areas, and 50 000 m^3 in small DH areas (Table 1). Choosing larger storage volumes would lead to a lower specific investment cost that would give a financial advantage to the technology; however, suitable land availability is often an obstacle, especially in large cities, and consequently, large storage systems may not be practically feasible. Thus, choosing smaller PTES sizes was an attempt to have more realistic scenarios and representative costs for the actual systems.

The land cost was also included in the investment cost for PTES. For the TTES, due to their smaller size and construction style, the cost of land was not found to affect the final price significantly. The land price used was based on data for Denmark (2015 - 2019) and was taken equal to 1.8 €/m^2 [59]. Last, it should be noted that all investment costs were discounted using a 4% annual discount rate, as recommended by the Danish Energy Agency [57]. The techno-economic parameters used for simulating PTES and TTES are summarized in Table 1. The characteristics of the remaining generation and storage technologies included in the simulations were based on data from the Danish Energy Agency's Technology Catalogs [60].

Table 1
Data used for PTES and TTES simulation in Balmorel. The investment cost for PTES is assumed to decrease in the future as the technology matures, and there is a linear decrease from 2020 to 2050.

Type	Size [m^3]	Investment year	Investment cost [k€/MWh]	Efficiency [%]	Charge/Discharge capacity rate [MW]	Lifetime [years]
PTES large	250 000	2020 2050	0.35 0.28	80	40	20 25
PTES medium	100 000	2020 2050	0.49 0.40	80	40	20 25
PTES small	50 000	2020 2050	0.64 0.52	80	40	20 25
TTES	3 000	–	2.90	98	40	40

Table 2
Fuel prices [€/GJ] and CO_2 costs [€/tCO_2] in Balmorel for simulated years.

Fuel [€/GJ]	2020	2030	2040	2050
Coal	2.31	2.67	2.74	2.81
Lignite	0.75	1.00	1.00	1.00
Municipality waste	−3.26	−3.26	−3.26	−3.26
Natural gas	5.64	8.32	9.29	10.26
Nuclear	0.76	0.76	0.76	0.76
Wood chips	6.20	6.20	6.20	6.20
CO_2 costs [€/tCO_2]	5.93	75.16	105.22	127.77

Table 3
Renewable potential by region.

Region	Solar PV [GW]	Onshore wind [GW]	Offshore wind [GW]
DK1	15.6	6.1	70.2
DK2	9.4	1.9	15.2
DE4-O	119.5	32.7	16.6
DE4-N	39.8	4.8	–
DE4-S	119.5	29.1	–
DE4-W	119.5	32.1	58.8
NO1	4.7	3.5	–
NO2	4.7	2.5	18.4
NO3	4.7	1.9	34.1
NO4	4.7	5.6	30.7
NO5	4.7	0.5	7.0
SE1	14.7	8.9	10.8
SE2	14.7	11.0	10.8
SE3	14.7	11.0	10.8
SE4	14.7	4.0	10.8

3.3. Fuel and carbon emission costs and renewable potential

Fuel and carbon emission costs are presented in Table 2. The fuel price projections are adopted from [61]. The municipality waste has a negative fuel price to represent the value that the waste incineration plant receives. From a modeling perspective, it also ensures that this fuel is used for baseload production.

It may be observed that, apart from nuclear, there is an increase in fuel prices toward 2050. The increase in fossil-fuel prices is in line with future plans for carbon neutrality. Furthermore, the decarbonization pathway of the entire energy system is driven by a carbon emission cost, which is also taken from [61], to ensure a coherent transition.

The potentials of onshore wind and solar PV are often constraining the solution space for the optimal energy system configuration. Therefore, Table 3 presents the implemented availability potentials for wind and solar PV in the two Danish electricity market regions. The onshore wind and solar PV potentials are further divided into different resource grades to account for differences in full load hours (capacity factor) inside a region and to illustrate that the most prominent locations are explored first.

3.4. Simulated scenarios

Various scenarios were simulated to elucidate the effect of TES on the complete energy system. First, the No TES scenario was compared to the TES scenario to shed light on the value of thermal storage for the energy system. Afterward, scenarios with either PTES or TTES were compared to reveal the benefit of installing one heat storage technology over the other. The simulated scenarios were:

- No TES: A No TES scenario was created in which Balmorel was not allowed to install thermal energy storage systems.
- TES: The TES scenario allowed investments in both TTES and PTES heat storage systems.
- PTES: In the PTES scenario, Balmorel was allowed to invest only in PTES systems as a heat storage technology (for both short-term and seasonal storage).
- TTES: In the TTES scenario, Balmorel was allowed to invest only in TTES systems as a heat storage technology (for both short-term and seasonal storage).

4. Results

First, the effect of heat storage systems on the energy system is investigated in Section 4.1. Later, a system using PTES as a heat storage technology is compared to a system using TTES in Section 4.2. The PTES characteristics were investigated with an aim to quantify their effect on the utilization of this technology in Section 4.3. Last, the influence of the electricity transmission capacity on the energy system (in particular the TES systems) is presented in Section 4.4.

4.1. Comparison between the No TES and TES scenario

The No TES and the TES scenarios were compared to identify the effect of heat storage systems on a country level (Section 4.1.1) and on all the simulated countries (Section 4.1.2).

4.1.1. Effect on a country level (Denmark)

From Fig. 5A, it may be seen that the TES scenario enables wider utilization of renewable energy sources like solar and wind. Although both TES and No TES install the maximum capacity for onshore wind in Denmark, the TES scenario installs over the entire simulated period 35% more PV capacity and 10% more offshore wind capacity than the No TES scenario. On the contrary, the No TES scenario features a larger capacity of dispatchable technologies like boilers (electric and biomass), CHP, and heat pump units to cover the electricity and heat demand.

It should be noted that the No TES scenario has a larger share of technologies with high-capacity factors (e.g., CHP and heat pumps). In contrast, the TES scenario features a larger share of low-capacity factor technologies (e.g., PV and wind). This means that the TES scenario has to install higher generation capacities, as a higher capacity would be required in order to generate the same amount of energy.

Due to the mismatch between electricity production from renewables and electricity demand, generation technologies can be curtailed. Renewables can be shut down (curtailed) in high-production and low-demand periods. Curtailment is calculated as the difference between the unconstrained generation and the actual supplied power. Balmorel

can curtail generation if it is more profitable than expanding the energy infrastructure (e.g., electricity transmission grid, Power-to-Heat technologies, storage). Due to the lack of thermal storage in the No TES scenario (and thus flexibility), the curtailment levels are much higher than in the TES scenario. In Fig. 5B, curtailment is compared between the two scenarios as an absolute value (in TWh). It may be observed that the TES scenario has, on average, 53% lower curtailment than the No TES scenario.

The higher curtailment level of the No TES scenario can also be depicted in the hourly cost of heat (Fig. 5C). In periods when the electricity price reaches zero, it was observed that the heating price was negative when there was an absence of heat storage (No TES scenario). From late Spring to early Autumn, hours of negative heat prices were present in the No TES scenario (mainly during daytime), while in the summer, there were entire days of negative heat prices.

Two steps explain the negative prices: firstly, negative prices derive from the choice of modeling method, and second, they derive from the simulation scenario conditions (see list below). As mentioned, Balmorel is a partial equilibrium model optimizing toward a societal optimum across different markets — electricity and heat. Prices can be high, low, or even negative in these markets. Negative prices arise when non-storable supply exceeds demand (e.g., when profits from electricity generation from a CHP plant exceed losses from heat generation). This reflects the real world, where we also see negative prices in the electricity and heat markets. The scenario-specific reasons for the negative prices were a combination of the following:

1. Low heat demand in the summer period.
2. Forced operation of CHP back-pressure plants producing both heat and electricity from burning municipality waste.
3. High renewable energy production (especially PV).
4. Insufficient heat storage capacity.

The presence of TES also affects the peak price of heat. Discharging the storage in periods of high heat demand instead of using more costly alternatives (e.g., natural gas boilers) ensures lower peak heat prices. Consequently, on average, the TES scenario had a 24% lower peak price for heat compared to the No-TES scenario. For all the simulated years, the No TES scenario had an average price for heat 2.4 €/MWh higher than the TES scenario.

It has to be mentioned that during the timesteps when the model invests in new technologies, high price spikes occur for heat and/or electricity (depending on whether the technology produces heat or electricity). For this reason, outliers are not shown in the box plots in Fig. 5C, and 99% of the data is presented.

The corresponding electricity cost for Denmark for the TES and No TES scenarios are presented in Appendix E. It was found that the weighted mean electricity price is almost the same for the TES and No TES scenarios (on average, the No TES scenario had an approximately 1% higher mean electricity price).

In order to get a better understanding of the energy flows in the heat sector, a Sankey diagram for the Denmark 2050 TES scenario is presented in Fig. 6. It may be observed that heat pumps produce most of the required heat. Moreover, the heat storage systems supplied 20% of the total demand (19% and 1% for long-term and short-term, respectively).

It should be noted that Balmorel produces each commodity (e.g., hydrogen) in the country that has the lowest cost and then transports it to neighboring countries. For this reason, in the situation where only Denmark, Norway, Sweden, and Germany are investigated, Denmark is chosen to produce the majority of PtG and export electricity instead of just covering its own energy needs due to its good offshore wind conditions (see Table 3). Consequently, since the excess heat is primarily produced by hydrogen production, the high PtG production in Denmark increases the installation of TES systems for utilizing the excess heat. However, this would not necessarily be the case if other countries were included in the simulation (e.g., Southern European countries with higher solar energy potential).

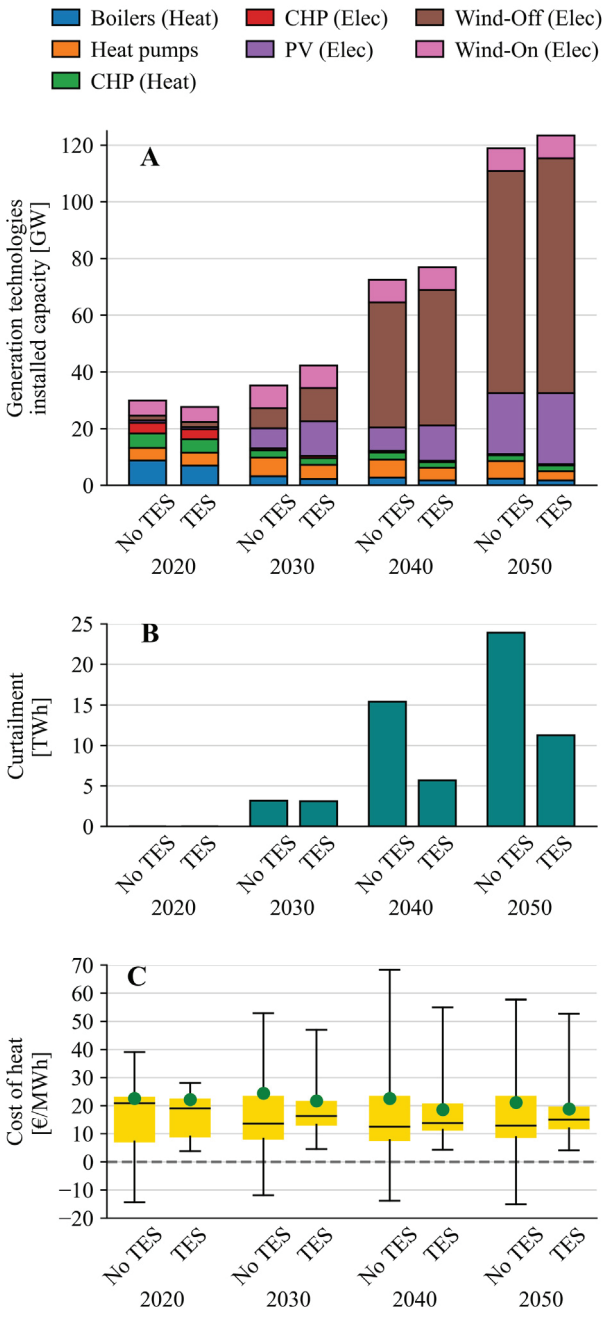

Fig. 5. Comparison between the No TES and TES scenarios for Denmark regarding the installed capacities (A), curtailment (B), and cost of heat (C). The weighted mean yearly heat prices are indicated with a green circle.

It should be noted that hydrogen is used in the model to cover the energy demand in the transport and industrial sectors. However, it could also be used for peak production through fuel cells, but this was not considered profitable by the model for most countries.

Regarding heat storage, it should be mentioned that the actual installed TES capacity in Denmark in 2017 was 50 GWh, mainly consisting of TTES systems [27]. However, in Balmorel, in the TES scenario, the TES capacity for Denmark in 2050 was 3 858 GWh (66 GWh of TTES and 3 792 GWh of PTES). To put this into perspective, it corresponds to approximately 390 TTES systems, each having a volume of 3 000 m^3,

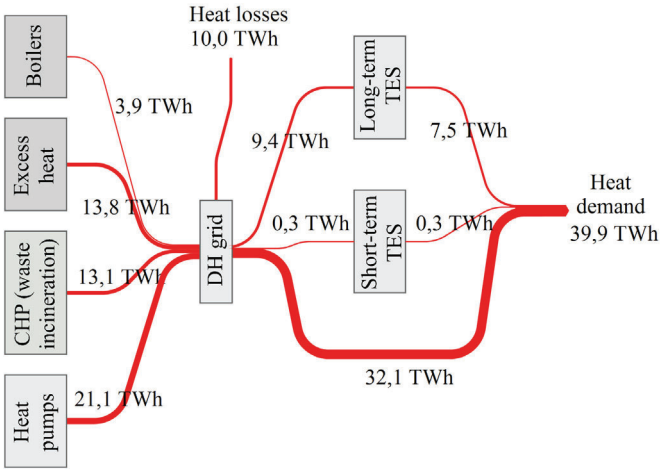

Fig. 6. Sankey diagram showing the energy flows for Denmark's heat sector in the 2050 TES scenario. Excess heat is produced primarily from hydrogen production.

and 240 PTES systems, each having a volume of 250 000 m^3, with a charge/discharge capacity of 40 MW.

However, the aggregation of district heating networks in Balmorel is inflating the use of TES, so the actual optimal values are expected to be somewhat lower. Nonetheless, it is clear that the number of installed TES in Denmark has to increase dramatically in the near future to reach cost-optimal carbon neutrality by 2050.

Last, for Denmark, the costs of TES (capital, operation, and maintenance (O&M)) corresponded to approximately 6% of the total costs of the energy system for the entire simulation period.

4.1.2. Effect on the entire simulated area (multiple countries)

It should be mentioned that the main reason for including Denmark's neighboring countries is to obtain realistic energy trading (electricity and fuels). Since electricity and fuel trading is permitted among neighboring countries, the model can find it more beneficial to have higher emissions, costs, or fuel use in one specific area. Thus, by including the entire simulation area, it was possible to have a more holistic view of the results. Consequently, in order to assess the effect of heat storage on the primary fuel consumption, CO_2 emissions, and total annual costs, it was considered necessary to include the results for all simulated countries.

Fig. 7A presents the primary fuel consumption for all the simulated countries. It may be observed that the No TES scenario uses coal and lignite in 2020 and 2030, while the TES scenario only uses them in 2020. Similarly, the No TES scenario uses natural gas as fuel until 2040, while the TES scenario has a lower usage and only utilizes them until 2030. As expected, the TES scenario uses more solar and wind power as fuel, while the No TES scenario compensates for that by using more wood chips (biomass). Both scenarios use similar amounts of hydropower, municipal waste (for waste incineration), and nuclear.

Based on the primary fuel used, it is evident that the TES scenario limits the use of fossil fuels after 2030 and goes entirely carbon-free by 2050. This may also be seen in Fig. 7B, where the CO_2 emissions for the two scenarios are presented. Notice that the No TES scenario still has CO_2 emissions in 2050 (around 10 kt). When looking at the total emissions over the entire simulation period, the quicker decarbonization of the TES scenario led to 5% lower CO_2 emissions, corresponding to approximately 26 Mt, thus providing also a more environmentally friendly solution.

Regarding the total costs, the TES scenario had, on average, 4% lower costs than the No TES scenario, corresponding to approximately 10 billion €. As it may be observed in Fig. 7C, the No TES scenario had higher capital, fixed, and fuel costs due to the different technologies,

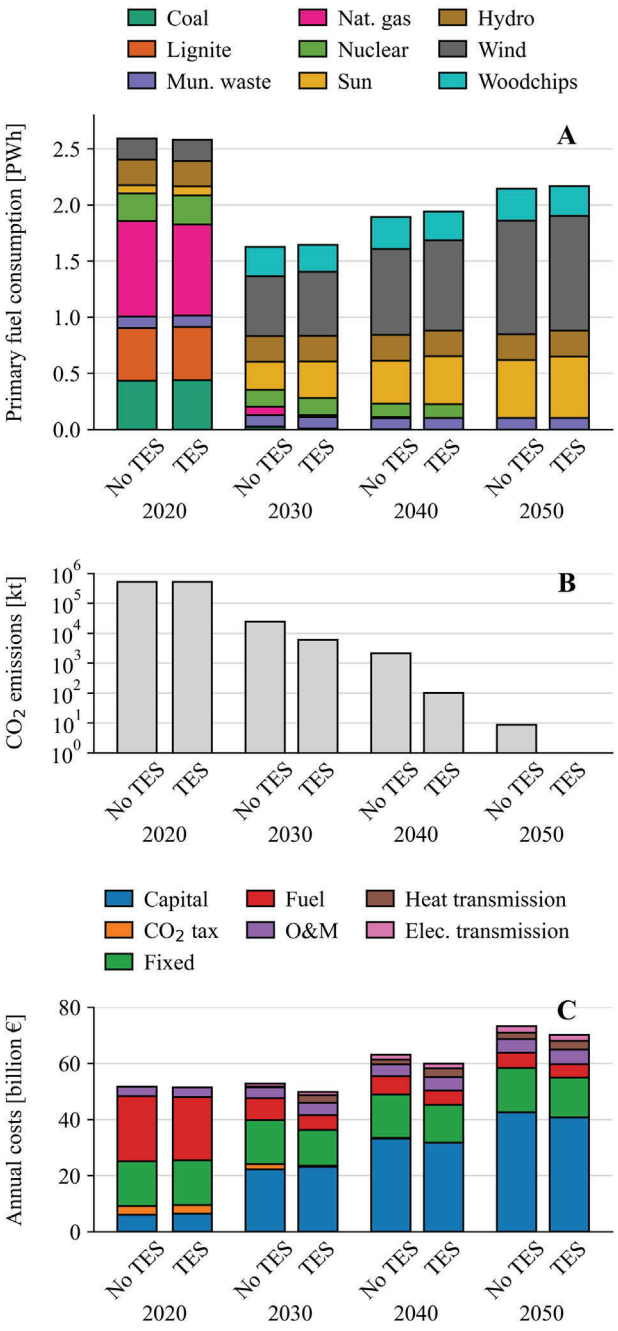

Fig. 7. Comparison between the No TES and TES scenarios for all investigated countries regarding the primary fuel consumption (A), CO_2 emissions (B), and annual costs (C).

fuels, and amount of energy trading, as well as a higher CO_2 tax burden than the TES scenario. The higher capital costs were due to the greater installed capacity of the more expensive technologies (e.g., heat pumps, boilers, and CHP). On the contrary, the TES scenario had higher O&M and transmission costs.

It should be noted that although the study focused on Denmark and its neighboring countries, the obtained results could potentially be applied to other countries with district heating grids. The main difference in the Danish district heating network compared to other countries is the low supply/return temperatures. However, this study investigated future scenarios, and future generations of district heating feature low supply/return temperatures [62]. Overall, this study presents a possible

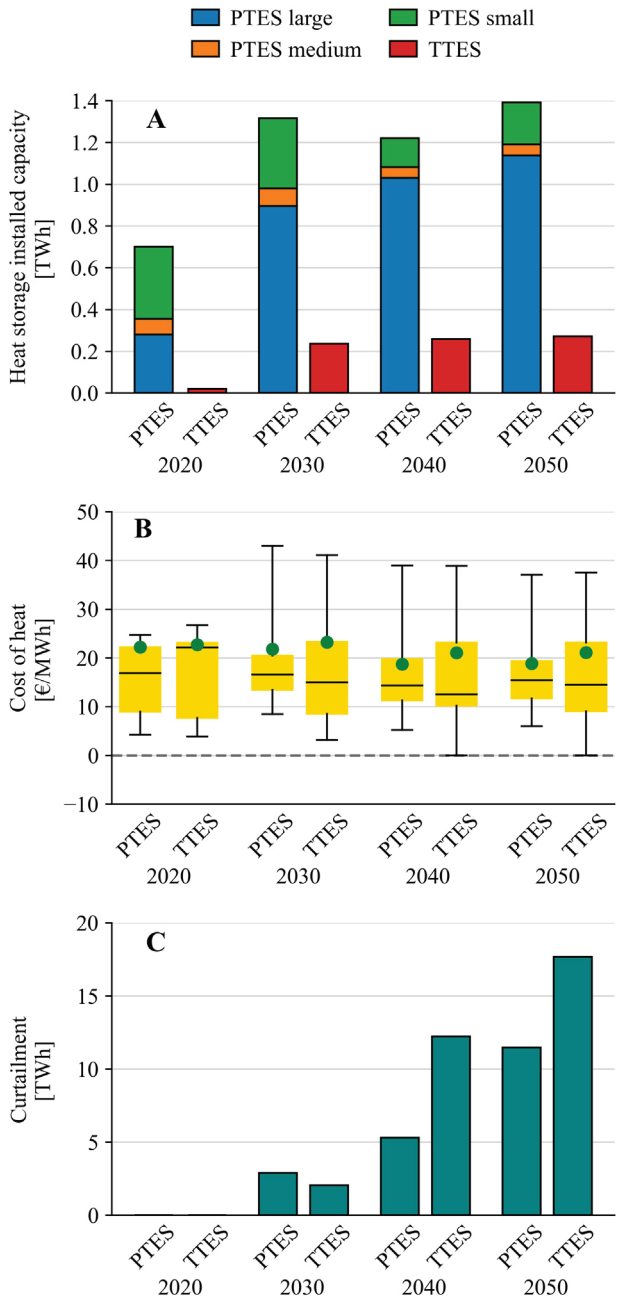

Fig. 8. Comparison between the PTES and TTES scenarios for Denmark regarding the installed heat storage capacity (A), the hourly cost of heat (B), and curtailment (C). The weighted mean yearly heat prices are indicated with a green circle.

future alternative to conventional heating technologies (e.g., natural gas boilers) with the implementation of sector coupling.

4.2. Comparison between PTES and TTES

In this section, the impact of PTES and TTES technologies was investigated on a country level (Denmark) in order to identify differences between the use of the two TES technologies. Information about the installed capacities in Denmark's neighboring countries can be found in Appendix F.

In Fig. 8A, it may be observed that the installed capacity for PTES is, on average, approximately five times higher than TTES. The main reason is the much lower cost of PTES compared to TTES (the specific cost for PTES is approximately 24 €/m^3 while for TTES, it is 121 €/m^3). This results in a much larger heat storage capacity for the PTES scenario, enabling higher use of renewables. In the PTES scenario, the optimal system has 6% higher PV capacity and 6% higher wind capacity than the TTES scenario. On the contrary, in the TTES scenario, investments favor dispatchable technologies, with 8% higher boiler capacity, 6% higher CHP capacity, and 19% higher heat pump capacity. As a result, the PTES scenario features more sun and wind as primary fuel, while the TTES scenario utilizes more wood chips. The higher share of renewables in the PTES scenario enables a larger production and export of hydrogen and electricity.

It should be noted that the installed TES capacity depends on many factors (including the heat demand and the characteristics of each technology), but also on whether the model finds more profitable alternative flexibility options (e.g., electricity transmission), as described in Section 2.3.1. Thus, very different results can be obtained for each TES technology.

The effect of cheaper storage leads to an increase in heat storage capacity, resulting in a lower heat price as illustrated in Fig. 8B. Although the peak heat prices for each year are similar for the two scenarios, the TTES scenario has a higher mean price for heat (22.1 vs. 20.6 €/MWh). The high heat storage capacity in the PTES scenario enables large amounts of heat to be transferred from summer to winter but also enables arbitrage, i.e., charging with cheap energy when there is an energy surplus. This leads to a lower average price of heat and a lower level of curtailment, as seen in Fig. 8C. In general, PTES seems more favorable to TTES regarding costs and performance at a system level, especially considering that it is not yet a mature technology and there is still a margin for improving the technology.

The validity of the obtained results from Sections 4.1 and 4.2 was compared with results from existing studies in the literature, where it was found that they were in good agreement. Details of this comparison can be found in Appendix G.

As it may be seen in Fig. 8A, most of the installed PTES are "large", meaning that they are built in large DH areas (i.e., large cities) where large plots of land might not be available. The construction of PTES on the outskirts of cities could be a solution; however, this often requires costly extensions of the existing network. For this reason, research is ongoing to find ways of exploiting the PTES surface for other uses, e.g., like the ones described in [63].

Unlike TTES, which can be built on the ground and has a small footprint, PTES is an underground storage technology; thus, stable ground conditions are required for its construction. Additionally, sites with shallow groundwater tables should be avoided since this could increase heat losses from the storage and complicate its construction.

Last, due to the usage of steel and concrete, TTES can store temperatures up to 100 °C (even a bit higher if pressurized), while PTES is limited up to 90 °C due to the polymer liner. Thus, PTES might not be a viable option in countries with high DH supply temperatures. However, this is considered a minor issue since lower DH supply temperatures are expected to be adopted in the future (supply temperatures lower than 70 °C [23]).

Overall, with adequate planning, PTES systems can be considered a highly effective solution for most future heat storage projects since they outperform TTES systems in terms of increasing renewables' utilization, minimizing heat price, etc.

4.3. Effect of PTES characteristics

A sensitivity analysis was conducted to investigate the PTES characteristics' effect on implementing this technology in the energy system. The four main parameters of PTES were investigated: charge/discharge capacity, lifetime, investment cost, and efficiency. It has to be mentioned that although these parameters can be interconnected (e.g., cost and lifetime), this has not been quantified in the literature for PTES. Additionally, there are situations where this might not be applicable

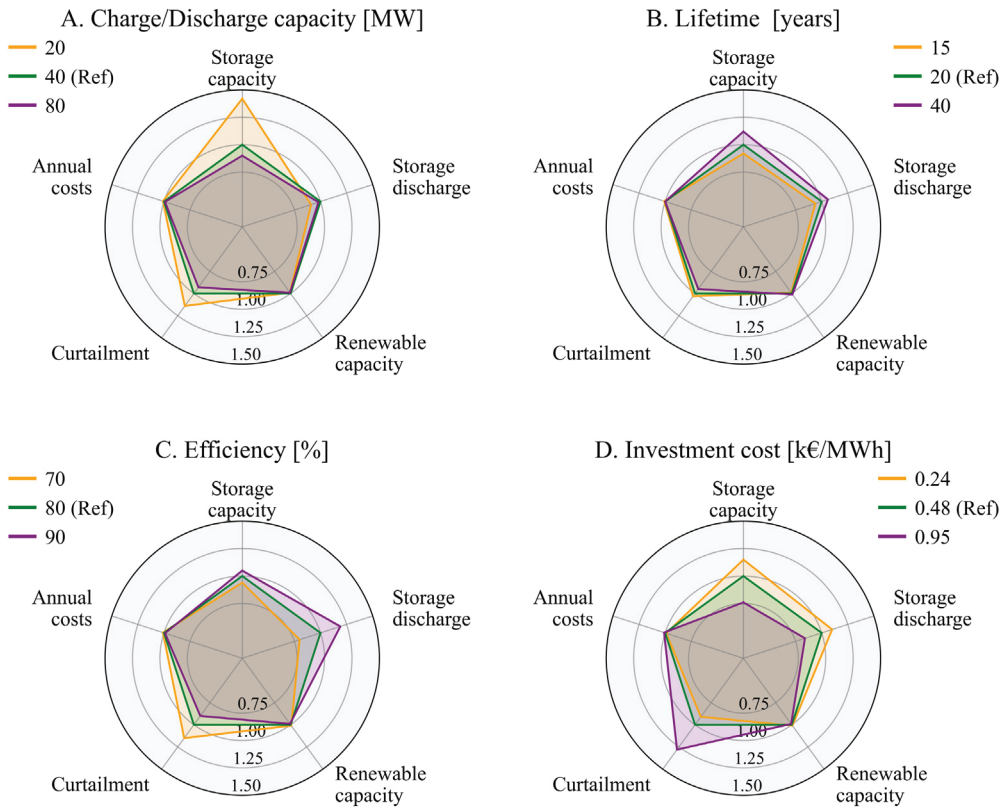

Fig. 9. Sensitivity analysis on the main technical PTES parameters. Values denote the increase of each parameter compared to the reference scenario (e.g., 1.5 storage capacity means that this scenario features a 1.5 increase in the storage capacity compared to the reference scenario).

Table 4
PTES parameter values used in the sensitivity analysis.

Parameter	Low extreme	Reference	High extreme
Charge/discharge capacity [MW]	20	40	80
Lifetime [years]	15	20	40
Investment cost [k€/MWh]	0.24	0.48	0.96
Efficiency [%]	70	80	90

(e.g., additional expenses due to non-ideal ground conditions). For this reason, these parameters were investigated individually.

Three scenarios were simulated for each parameter: a reference scenario (i.e., the PTES scenario from Section 4.2) and two extreme scenarios. The average parameter values used in the sensitivity analysis are presented in Table 4.

Five system parameters were assessed to identify the sensitivity of the investigated parameters on the energy system: optimal installed heat storage capacity, heat storage discharged energy, installed renewable capacity, curtailed energy, and annual costs. Storage discharged energy refers to the amount of energy discharged by the short- and long-term TES to the district heating grid. Renewable capacity refers to the installed capacity of PV and wind installed in the energy system. The sensitivity analysis results are presented as four spider charts in Fig. 9.

It has to be noted that since the reference system already had a high implementation of renewable technologies, only marginal differences were observed regarding the installed renewable energy capacity and annual costs among the different scenarios. This observation was true for all the investigated parameters.

Fig. 9A illustrates that a lower charge/discharge capacity would increase the installed storage capacity but simultaneously reduce the energy discharge from the storage and increase curtailment. This indicates the importance of this parameter, as it dictates how fast the storage can respond to either a surplus of energy or a peak in demand. A high charge capacity enables the PTES to store a large amount of excess energy in a short time, thus limiting the need for curtailment. Similarly, heat storage systems with a high discharge capacity can supply heat in a short time to cover a demand peak, thus reducing the peak load. Balmorel tried to offset this limitation by installing a 40% higher PTES capacity for the case with low charge/discharge capacity, but even so, the heat discharged by the PTES was marginally lower compared to the reference scenario. However, it must be noted that little benefit was observed from increasing the charge/discharge capacity of the Reference case.

The lifetime of the PTES affects the implementation of the technology through the Levelized Cost Of Energy (LCOE). A shorter lifetime leads to higher LCOE, thus making the technology less financially attractive. This can be seen in Fig. 9B, where a longer life led to a higher installed capacity for PTES and, as a result, lower curtailment; however, the differences from the reference case were small compared to other parameters tested.

The effect of storage efficiency may be observed in Fig. 9C. Compared to the reference case, a PTES efficiency of 70% would reduce the installed storage capacity by 6% and the storage discharge by 20% (due to higher heat losses), also leading to 15% higher curtailment. As expected, a higher PTES efficiency positively affects the storage and overall system operation.

Last, for the investment cost, by reducing the price of the PTES by 50%, there was a 15% increase in the installed heat storage capacity, 10% higher storage discharge, and a 10% reduction in curtailment.

It is evident that improving all the investigated PTES parameters would improve both the PTES and the overall energy system performance, increasing the technology's implementation at the same time. However, this investigation identified the investment cost and the efficiency of the PTES as the two parameters having the largest impact on the future utilization of the technology. Perhaps most importantly,

the sensitivity analysis confirms the robustness of the study in terms of deployment of PTES: This deployment remains large, even under less favorable conditions.

4.4. Flexibility options

As was mentioned in Section 2.3.1, flexibility in an energy system can be achieved through generation, transmission, demand side management, and storage (electrical, heat, and hydrogen). These four options are utilized in order to cover the electricity and heat demand in the least-cost way.

Since storage is the main focus of this study, it was decided to investigate another flexibility option to identify its effect on the energy system (and possibly on storage). It was decided to investigate electricity transmission since a lot of countries could be facing transmission bottlenecks and might have the aim to become more self-sufficient. Additionally, planning transmission capacity between countries is time-consuming and could be subject to political decisions. It has to be noted that this is only one of many flexibility options that could be investigated. Other relevant options include load shifting, smart charging of electric vehicles, etc.

The electricity transmission scenarios that were investigated were, apart from the reference scenario (PTES scenario also used in Section 4.3), Denmark in island mode (i.e., not being able to trade energy with any of its neighboring countries) and Denmark without being allowed to install new transmission capacity (i.e., only using the existing transmission capacity in 2020 and able to trade fuels).

In order to investigate the effect of electricity transmission capacity on the energy system, the total installed heat storage, PV, wind, hydrogen storage, and dispatch capacities, along with the average electricity and heat price, were plotted for the entire simulation period (2020–2050), as presented in Fig. 10.

In island mode, the model invested 25% less in PV and 70% less in wind capacity and tried to cover the heat and electricity demand by investing 50% more in dispatchable capacity and 25% more in heat storage capacity. The use of conventional generation technologies had a major impact on the average electricity price, which was 20% higher. However, the increase in heat storage capacity was able to maintain the average heating price at approximately the same level. In parallel, since electricity and hydrogen exports were impossible, there was 80% lower hydrogen storage capacity.

Using the existing transmission capacity in 2020, it may be observed that the heat storage, dispatchable, and PV capacity, as well as the average heat and electricity prices, remain approximately constant. However, since there are limitations in electricity exports, there is 25% less wind capacity installed, which in turn equally reduces the hydrogen storage capacity due to fewer periods of cheap electricity for hydrogen production.

Last, it should be noted that although Balmorel could invest in different flexibility providers (e.g., storage, flexible generation, transmission interconnectors) in all scenarios, batteries were not used in Denmark. This indicates the high relevance of sector coupling as an alternative to installing battery storage. It should be noted that the cost of batteries was based on [64].

Overall it is obvious that additional electricity transmission capacity adds a high degree of flexibility to the energy system. Nonetheless, it was also revealed that heat storage could offset the absence of transmission capacity in order to maintain a similar average price of heat.

5. Conclusions

This paper investigated the effect of thermal energy storage (TES), particularly pit thermal energy storage (PTES), on an energy system. The study focused on Denmark and its neighboring countries and quantified the impacts of PTES on their future energy systems. The analysis was done using the energy system model Balmorel, which was used to calculate the least-cost solution for the energy transition toward 2050. As PTES is not a mature technology, sensitivity analyses were also performed on its technical and economic characteristics. The main findings from this investigation were the following:

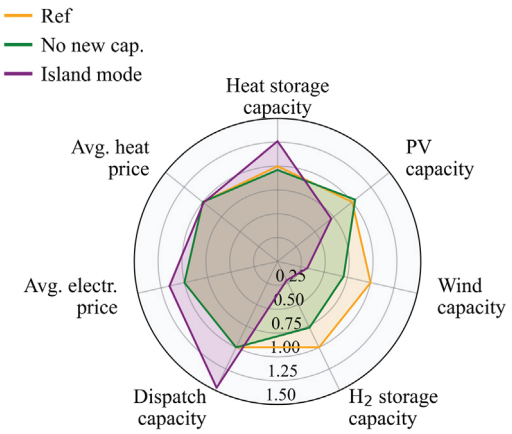

Fig. 10. Investigation on transmission capacity flexibility for Denmark.

- Energy systems using TES could achieve carbon neutrality by 2050, unlike systems without TES, where CO_2 emissions existed even in 2050. TES systems accelerate decarbonization through increased cost efficiency.
- TES systems utilized 35% higher PV capacity and 10% higher wind capacity. In parallel, TES systems had a 53% lower level of curtailment and ultimately 2.4 €/MWh lower average heat price (with 24% lower peak price).
- In the absence of electricity transmission capacity with neighboring countries, a larger deployment of TES capacity could ensure an almost constant average heat price.
- PTES systems were found to reduce system costs, enabling higher utilization of renewables (both wind and solar) compared to TTES due to the lower cost of PTES systems and, thus, greater deployment (approximately five times).
- PTES systems led to a 1.5 €/MWh lower average heat price than TTES.
- The combination of PV, wind, heat pumps, and new energy infrastructure will have an important role in future energy systems. Particularly in Denmark, they are expected to cover approximately half of the heat demand. When large volumes of TES are available (e.g., PTES), the installed PV and wind capacity is increased, while for smaller TES volumes (e.g., TTES), greater heat pump capacities are used to cover the demand.

It has to be mentioned that since Balmorel simulates only energy flows, similar results can be expected when substituting PTES with other heat storage systems that have similar characteristics, i.e., high efficiency and low cost.

CRediT authorship contribution statement

Ioannis Sifnaios: Writing – original draft, Visualization, Software, Methodology, Formal analysis, Data curation, Conceptualization. **Daniel Møller Sneum:** Writing – original draft, Conceptualization. **Adam R. Jensen:** Writing – review & editing, Visualization. **Jianhua Fan:** Writing – review & editing, Supervision, Funding acquisition. **Rasmus Bramstoft:** Writing – original draft, Methodology, Conceptualization.

Declaration of competing interest

The authors declare that they have no known competing financial interests or personal relationships that could have appeared to influence the work reported in this paper.

Data availability

No data was used for the research described in the article.

Acknowledgments

Part of this research was funded by the Danish Energy Agency through EUDP grant no. 64018-0134 (FLEX-TES) and 134223-495989 (IEA ES Task 41 - Economics of Energy Storage) and by the Sino-Danish Center for Education and Research (SDC) Ph.D. program.

Daniel Sneum's contribution to this study was under the auspices of two projects. Firstly, the FlexSUS project: Flexibility for Smart Urban Energy Systems (Project nbr. 91352). FlexSUS has received funding in the framework of the joint programming initiative ERA-Net Smart Energy Systems' focus initiative Integrated, Regional Energy Systems, with support from the European Union's Horizon 2020 research and innovation program under grant agreement No 775970. Second, the EMB3Rs project which has received funding from the European Union's Horizon 2020 research and innovation programme under grant agreement 847121.

Appendix A. Nomenclature

Nomenclature

Sets

$\mathcal{A}$	Areas
$\mathcal{G}$	Technologies
$\mathcal{G}^{TES}$	Subset of storage technologies
$\mathcal{S}$	Seasons
$\mathcal{T}$	Time periods in a season
$\mathcal{Y}$	Years

Variables

$k^{TES,new\_CAP}_{y,a,g}$	new installed capacity of heat storage technology $g \in \mathcal{G}^{TES}$, in year, y, and area a
$p^{gen\_heat}_{y,a,g,s,t}$	heat generation in year, y, area a of technology g in the time period s,t
$p^{TES,charge}_{y,a,g,s,t}$	heat for charging the heat storage technology $g \in \mathcal{G}^{TES}$ in year, y, area a, and time period s,t
$p^{TES,discharge}_{y,a,g,s,t}$	heat from discharging of heat storage technology $g \in \mathcal{G}^{TES}$ in year, y, area a, and time period s,t
$v^{TES}_{y,a,g,s,t}$	heat storage content of the heat storage $g \in \mathcal{G}^{TES}$ in year, y, area a, and time period s,t

Parameters

$\epsilon^{TES,eff}_{g}$	efficiency of heat storage technology $g \in \mathcal{G}^{TES}$
$\gamma_{s,t}$	length of chronological time segment s,t
$\lambda^{TES,charge}_{g}$	charging time for heat storage technology $g \in \mathcal{G}^{TES}$
$\omega^{TES,discharge}_{g}$	discharging time for heat storage technology $g \in \mathcal{G}^{TES}$
$d^{heat}_{y,a,s,t}$	heat demand in year, y, for area a in the time period s,t
$k^{TES,decom\_CAP}_{y,a,g}$	decommissioning capacity of heat storage technology $g \in \mathcal{G}^{TES}$, in year, y, and area a
$k^{TES,ex\_CAP}_{y,a,g}$	existing capacity of heat storage technology $g \in \mathcal{G}^{TES}$, in year, y, and area a

Table 5
Electricity and heat demand for investigated countries from 2020–2050.

Country	Year	Heat [TWh]		Electricity [TWh]	
		Total	Peak	Total	Peak
DK	2020	74	1.5	30	0.5
	2030	50	1	36	0.5
	2040	50	1	42	0.6
	2050	50	1	43	0.6
DE	2020	1304	29.1	446	6.5
	2030	880	19.6	449	6.5
	2040	880	19.6	473	6.9
	2050	880	19.6	497	7.2
NO	2020	58	1.2	97	1.4
	2030	39	0.8	98	1.4
	2040	39	0.8	99	1.4
	2050	39	0.8	100	1.5
SE	2020	171	3.4	101	1.5
	2030	115	2.3	102	1.5
	2040	115	2.3	106	1.5
	2050	115	2.3	111	1.6

Appendix B. Methodology – literature review

The query (interseasonal OR inter-seasonal OR large-scale OR "large scale" OR seasonal OR long-term OR long-duration) AND ("heat storage" OR "thermal storage" OR "thermal energy storage") AND ("district heating" OR "district energy") brought 307 results, whereof 121 was found relevant in the initial screening. A large portion (68) of these primarily dealt with solar thermal. Borri et al. [34] have similarly noted the large body of research linking TES and solar. Along with irrelevant studies, the solar studies were sorted out since the scope of the present study is PTES in energy systems with a diversity of sectors and producers. Solar thermal is still represented in the remaining studies but as one source among others. This left the review with a final set of 92 relevant references. Numbers on 15 scenarios were extracted out of five studies to perform the analysis in and around Fig. 1.

Appendix C. Electricity and heat demand for investigated countries

The heat and electricity consumption for the investigated countries is presented in Table 5. It may be observed that from 2030 onward, there is a reduction in the heat demand for all countries. This reduction is based on the European Union regulation regarding energy efficiency targets for 2030, which states that consumption should be decreased by 32.5% compared to 2020 [65]. The increase in energy efficiency is not obvious in the electricity demand, as there is added demand due to electrification. Thus, overall there is a small increase in electricity demand for all countries. The peak demand for heat and electricity is also presented in Table 5 for each country and year.

It should be noted that the magnitude of the heat demand is proportional to the population of each country, while the electricity demand also depends on other factors (e.g., industry, degree of electrification in transport and heating sectors). The allocation of the heat demand to the different regions of each country was based on the electricity demand of each region.

The data for the heat demand were taken from [37,49,66,67]. Electricity demand and distribution losses were obtained by Eurostat [67]. Since Balmorel is open-source, all data can be accessed and downloaded freely from [45].

The seasonal variation of the electricity and heat demand for Denmark in 2050 is presented in Fig. 11. It should be noted that only the 8 simulated weeks and 12 h (every other hour for one day) for each week are presented in the figure. The profile of the heat demand was based on the methodology presented in [49]. For obtaining the final yearly results, temporal aggregation of the values was performed. Similar profiles were used for all simulated countries and all simulated years.

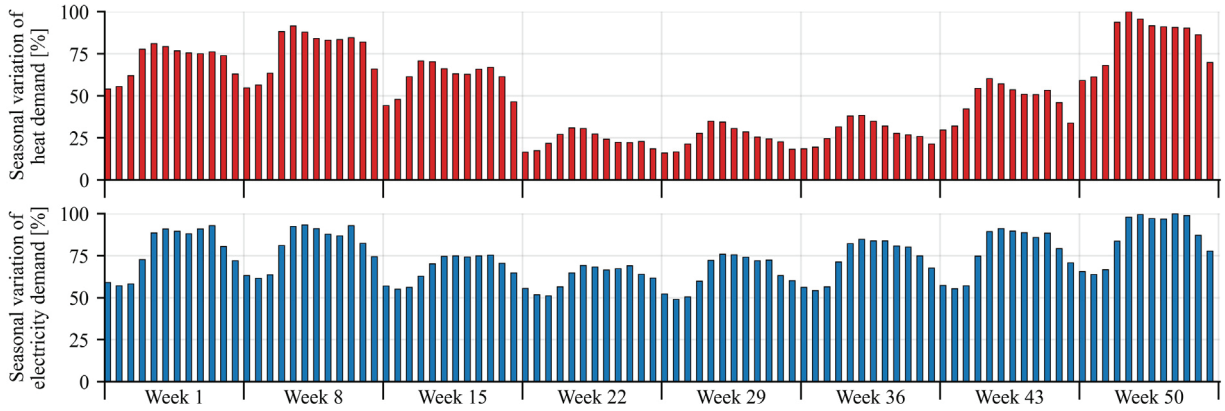

Fig. 11. Seasonal heat and electricity demand variation for Denmark in 2050. The simulated hours and weeks were repeated in order to represent one full year. A similar trend was followed in all simulated countries for all simulated years.

Table 6
Total installed generation and storage capacities for simulated countries.

		Dispatch [GW]	Wind [GW]	PV [GW]	Hydro [GW]	Fuel cells [GW]	Short-term TES [GWh]	Long-term TES [GWh]	Batteries [GWh]	H_2 storage [GWh]
DK	PTES	46	174	50	0	0	305	4626	0	114
	TTES	50	166	48	0	0	72	715	0	101
DE	PTES	1039	458	1007	36	17	4227	75874	34	693
	TTES	1044	460	949	36	21	786	21493	20	682
NO	PTES	35	36	30	128	0	0.6	2950	0	17
	TTES	39	36	25	124	0	36	749	0	15
SE	PTES	125	58	70	65	0	170	8706	0	57
	TTES	134	56	60	65	0	122	1830	0	51

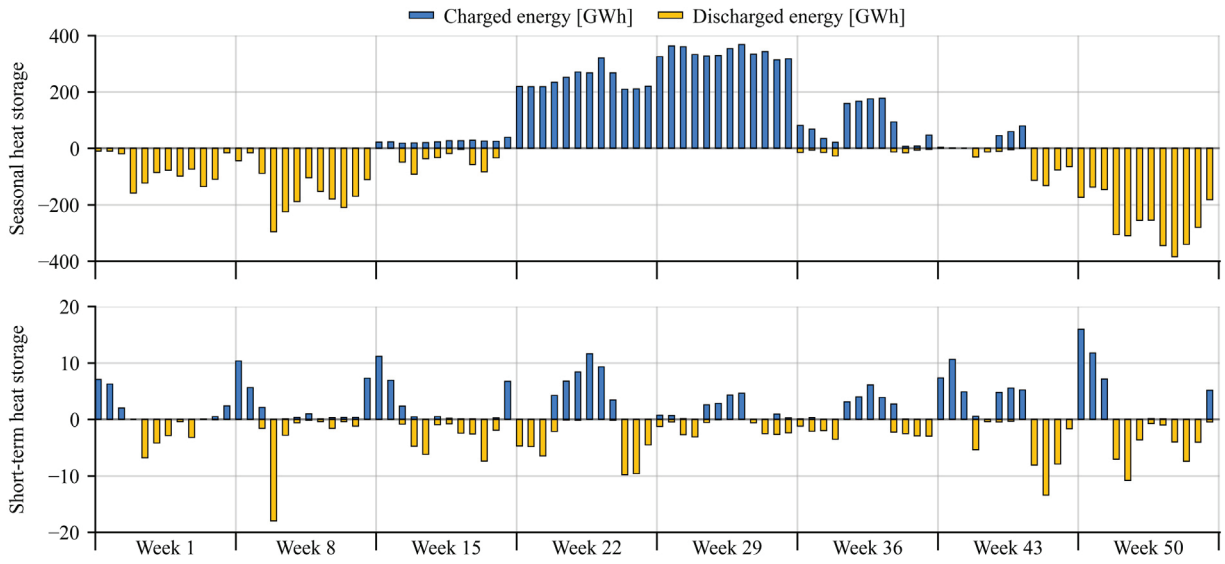

Fig. 12. Seasonal and short-term TES operation for Denmark in 2030.

Appendix D. Heat storage operation

The modeling of TES in Balmorel is done using the following assumptions.

- The short-term TES needs to have the same energy content at the start and end of each season. However, its energy content can vary from time step to time step.
- The seasonal TES needs to have the same energy content at the beginning and end of each year. However, its energy content can vary across seasons and time steps.
- An aggregation factor representing the length of the time segment (denoted with $\gamma_{s,t}$ in Eq. (2)) should be used to calculate the yearly charged and discharged energy from TES.
- Balmorel is free to decide the charge level of the storage at the start of the simulation (both for seasonal and short-term TES).

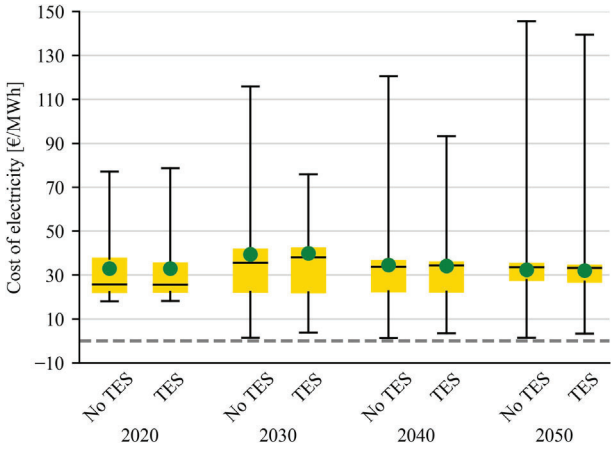

Fig. 13. Comparison between the No TES and TES scenarios for Denmark regarding the electricity cost. The weighted mean yearly electricity prices are indicated with a green circle. The grey dashed line denotes an electricity price of zero.

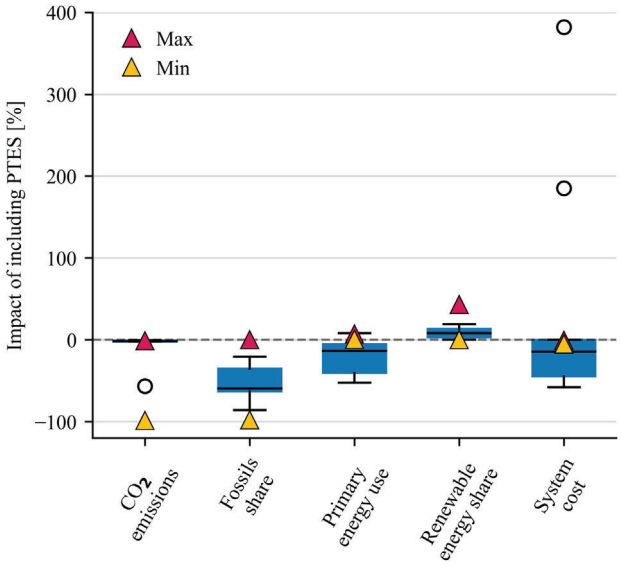

Fig. 14. Comparison between the obtained results from this study (triangles) with the results of similar studies from the literature (boxplots). The two triangles indicate the maximum and minimum obtained values.

A visualization of the seasonal and short-term operation is presented in Fig. 12. It can be observed that the seasonal storage is charged primarily during the summer and discharged during winter. On the other hand, the short-term TES performs one storage cycle per week. In the winter, the short-term TES is primarily charged during nighttime and discharged during the day, whereas, in the summer, it is charged during daytime and discharged at night.

Appendix E. Electricity cost in Denmark

The electricity cost in Denmark for the simulated years is presented in Fig. 13. It may be observed that the TES scenario has, in general, lower peak electricity prices compared to the No TES. The main reason is that the TES scenario can use the stored heat to cover the heat demand when the electricity price is high (instead of operating, e.g., a heat pump using expensive electricity). However, the weighted mean electricity price is almost the same for the TES and No TES scenarios (on average, the No TES scenario had an approximately 1% higher mean electricity price).

Appendix F. Installed capacities

The total generation and storage capacities installed in the simulated countries are presented in Table 6. The term "dispatch generation capacity" denotes the sum of heat pumps, boilers, and CHP plants installed in a country. In general, in all simulated countries, it may be observed that the PTES scenario installs more PV, TES, and H_2 storage, while the TTES scenario installs more dispatchable generation technologies. Of course, some countries do not follow the same trend due to their different energy systems. For example, in Norway, a very small capacity of short-term TES is installed in the PTES scenario, and the model invests more in hydropower compared to TTES.

Last, as mentioned in Section 4.4, batteries were not used in Denmark, although they have the potential to be used. In Table 6, it can be observed that batteries and fuel cells are only installed in Germany.

Appendix G. Comparison of the literature with the results of this study

As mentioned in the introduction of the present paper, the existing studies concerning the impact of PTES are few in number and varied in assumptions. Only one study found in the literature is based on analyses of a whole country (Germany) [14], while the remaining studies are analyses of single district heating systems [5,13,15–17]. In terms of the time period studied, the range is 1 to 30 years.

Keeping this in mind, we carried out a meta-study comparing results from the literature against the difference between the present study's No TES and PTES scenarios. The study included all the simulated countries (DK, DE, NO, SE) and the entire simulated period (2020–2050). Fig. 14 presents this comparison, and it may be observed that, in general, the results of this study are comparable to the literature results. The biggest difference was found for the CO_2 emissions and the fossil share since, in the present study, decarbonization was achieved by 2050 for the PTES scenario.

As a summary of the figure, when including PTES in the energy system, the present study reported on average 5% lower CO_2 emissions, 8% less use of fossil fuels, 4% higher primary energy use, 13% higher renewable energy share, and 4% lower system costs, compared to systems without having TES.

Appendix H. Supplementary data

Supplementary material related to this article can be found online at https://doi.org/10.1016/j.apenergy.2023.121663.

References

[1] Lund H, Østergaard PA, Connolly D, Ridjan I, Mathiesen BV, Hvelplund F, et al. Energy storage and smart energy systems. Int J Sustain Energy Plan Manag 2016;3–14. http://dx.doi.org/10.5278/IJSEPM.2016.11.2.
[2] Cabeza L, Martorell I, Miró L, Fernández A, Barreneche C. Introduction to thermal energy storage (TES) systems. In: Advances in thermal energy storage systems. Elsevier; 2015, p. 1–28. http://dx.doi.org/10.1533/9781782420965.1.
[3] Madaeni SH, Sioshansi R, Denholm P. How thermal energy storage enhances the economic viability of concentrating solar power. Proc IEEE 2012;100(2):335–47. http://dx.doi.org/10.1109/JPROC.2011.2144950.
[4] Soprani S, Marongiu F, Christensen L, Alm O, Petersen KD, Ulrich T, et al. Design and testing of a horizontal rock bed for high temperature thermal energy storage. Appl Energy 2019;251:113345. http://dx.doi.org/10.1016/j.apenergy.2019.113345.
[5] Hast A, Rinne S, Syri S, Kiviluoma J. The role of heat storages in facilitating the adaptation of district heating systems to large amount of variable renewable electricity. Energy 2017;137:775–88. http://dx.doi.org/10.1016/j.energy.2017.05.113.
[6] Bai Y, Wang Z, Fan J, Yang M, Li X, Chen L, et al. Numerical and experimental study of an underground water pit for seasonal heat storage. Renew Energy 2020;150:487–508. http://dx.doi.org/10.1016/j.renene.2019.12.080.

[7] Xie Z, Xiang Y, Wang D, Kusyy O, Kong W, Furbo S, et al. Numerical investigations of long-term thermal performance of a large water pit heat storage. Sol Energy 2021;224(February):808–22. http://dx.doi.org/10.1016/j.solener.2021.06.027.
[8] Modelica Association. Modelica® - A unified object-oriented language for physical systems modeling. Tutorial. 1.4 ed. Modelica Association; 2000, URL http://www.modelica.org/documents/ModelicaTutorial14.pdf.
[9] Victoria M, Zhu K, Brown T, Andresen GB, Greiner M. The role of storage technologies throughout the decarbonisation of the sector-coupled European energy system. Energy Convers Manage 2019;201(June):111977. http://dx.doi.org/10.1016/j.enconman.2019.111977.
[10] Connolly D, Lund H, Mathiesen BV, Leahy M. A review of computer tools for analysing the integration of renewable energy into various energy systems. Appl Energy 2010;87(4):1059–82. http://dx.doi.org/10.1016/j.apenergy.2009.09.026.
[11] van Ouwerkerk J, Hainsch K, Candas S, Muschner C, Buchholz S, Günther S, et al. Comparing open source power system models - A case study focusing on fundamental modeling parameters for the German energy transition. Renew Sustain Energy Rev 2022;161. http://dx.doi.org/10.1016/j.rser.2022.112331.
[12] Sneum DM, González MG, Gea-Bermúdez J. Increased heat-electricity sector coupling by constraining biomass use? Energy 2021;222. http://dx.doi.org/10.1016/j.energy.2021.119986.
[13] Sveinbjörnsson D, From N, Sørensen PA, Schmidt T, Klöck M, Pauschinger T. Pit thermal energy storage for smart district heating and cooling. Technical report, Skørping, Denmark: IEA DHC CHP; 2020, Annex XII.
[14] Sveinbjörnsson D, Trier D, Hansen K, Vad Mathiesen B. Technical and economic potential of distributed energy storages for the integration of renewable energy. Technical report, Copenhagen: IEA ECES; 2018, p. 218, Annex 28.
[15] PlanEnergi, Danish Technological Institute, GEO, Energi G. Udredning vedrørende varmelagringsteknologier og store varmepumper til brug i fjernvarmesystemet. Technical report, Danish Energy Agency; 2013.
[16] Dominković DF, Wahlroos M, Syri S, Pedersen AS. Influence of different technologies on dynamic pricing in district heating systems: Comparative case studies. Energy 2018-06;153:136–48. http://dx.doi.org/10.1016/j.energy.2018.04.028.
[17] Tosatto A, Dahash A, Ochs F. Simulation-based performance evaluation of large-scale thermal energy storage coupled with heat pump in district heating systems. J Energy Storage 2023;61:106721. http://dx.doi.org/10.1016/j.est.2023.106721.
[18] Sifnaios I, Jensen AR, Furbo S, Fan J. Performance comparison of two water pit thermal energy storage (PTES) systems using energy, exergy, and stratification indicators. J Energy Storage 2022;52(PB):104947. http://dx.doi.org/10.1016/j.est.2022.104947.
[19] Sifnaios I, Gauthier G, Trier D, Fan J, Jensen AR. Dronninglund water pit thermal energy storage dataset. Sol Energy 2023;251:68–76. http://dx.doi.org/10.1016/j.solener.2022.12.046.
[20] Gadd H, Werner S. Thermal energy storage systems for district heating and cooling. In: Advances in thermal energy storage systems. Elsevier; 2015, p. 467–78. http://dx.doi.org/10.1533/9781782420965.4.467.
[21] Ea Energianalyse. Varmelagre i hovedstadsområdet. 2018, https://www.gate21.dk/wp-content/uploads/2018/05/Varmelagre_hovedstadsomr%C3%A5det_EPT.pdf.
[22] Sneum DM, González MG, Gea-Bermúdez J. Increased heat-electricity sector coupling by constraining biomass use? Energy 2021-05;222:119986. http://dx.doi.org/10.1016/j.energy.2021.119986.
[23] Lund H, Werner S, Wiltshire R, Svendsen S, Thorsen JE, Hvelplund F, et al. 4th generation district heating (4GDH). Energy 2014-04;68:1–11. http://dx.doi.org/10.1016/j.energy.2014.02.089.
[24] Sala J. Thermal energy storage (TES) systems for cogeneration and trigeneration systems. In: Advances in thermal energy storage systems. Elsevier; 2015, p. 493–509. http://dx.doi.org/10.1533/9781782420965.4.493.
[25] Sneum DM, Sandberg E. Economic incentives for flexible district heating in the nordic countries. Int J Sustain Energy Plan Manag 2018-05-22;27–44. http://dx.doi.org/10.5278/IJSEPM.2018.16.3.
[26] Gea-Bermúdez J, Jensen IG, Münster M, Koivisto M, Kirkerud JG, kuang Chen Y, et al. The role of sector coupling in the green transition: A least-cost energy system development in Northern-central Europe towards 2050. Appl Energy 2021;289(March). http://dx.doi.org/10.1016/j.apenergy.2021.116685.
[27] Sveinbjörnsson D, Laurberg Jensen L, Trier D, Ben Hassine I, Jobard X. Large storage systems for DHC networks. 2017, p. 85.
[28] Guelpa E, Verda V. Thermal energy storage in district heating and cooling systems: A review. Appl Energy 2019-10;252:113474. http://dx.doi.org/10.1016/j.apenergy.2019.113474.
[29] IRENA. Innovation outlook: Thermal energy storage. Abu Dhabi: International Renewable Energy Agency; 2020.
[30] Sarbu I, Sebarchievici C. A comprehensive review of thermal energy storage. Sustainability 2018-01-14;10(1):191. http://dx.doi.org/10.3390/su10010191.
[31] Dahash A, Ochs F, Tosatto A, Streicher W. Toward efficient numerical modeling and analysis of large-scale thermal energy storage for renewable district heating. Appl Energy 2020;279:115840. http://dx.doi.org/10.1016/j.apenergy.2020.115840.
[32] Chang C, Wu Z, Navarro H, Li C, Leng G, Li X, et al. Comparative study of the transient natural convection in an underground water pit thermal storage. Appl Energy 2017;208:1162–73. http://dx.doi.org/10.1016/j.apenergy.2017.09.036.
[33] Li X, Wang Z, Li J, Yang M, Yuan G, Bai Y, et al. Comparison of control strategies for a solar heating system with underground pit seasonal storage in the non-heating season. J Energy Storage 2019;26:100963. http://dx.doi.org/10.1016/j.est.2019.100963.
[34] Borri E, Zsembinszki G, Cabeza LF. Recent developments of thermal energy storage applications in the built environment: A bibliometric analysis and systematic review. Appl Therm Eng 2021-05;189:116666. http://dx.doi.org/10.1016/j.applthermaleng.2021.116666.
[35] Swisher P, Leon JPM, Gea-Bermúdez J, Koivisto M, Madsen HA, Münster M. Competitiveness of a low specific power, low cut-out wind speed wind turbine in North and Central Europe towards 2050. Appl Energy 2022;306:118043. http://dx.doi.org/10.1016/j.apenergy.2021.118043.
[36] Hansen K, Connolly D, Lund H, Drysdale D, Thellufsen JZ. Heat roadmap Europe: Identifying the balance between saving heat and supplying heat. Energy 2016;115:1663–71. http://dx.doi.org/10.1016/j.energy.2016.06.033.
[37] Wiese F, Bramstoft R, Koduvere H, Pizarro Alonso A, Balyk O, Kirkerud JG, et al. Balmorel open source energy system model. Energy Strategy Rev 2018;20:26–34. http://dx.doi.org/10.1016/j.esr.2018.01.003.
[38] Jensen IG, Wiese F, Bramstoft R, Münster M. Potential role of renewable gas in the transition of electricity and district heating systems. Energy Strategy Rev 2020;27(November 2019):100446. http://dx.doi.org/10.1016/j.esr.2019.100446.
[39] kuang Chen Y, Jensen IG, Kirkerud JG, Bolkesjø TF. Impact of fossil-free decentralized heating on northern European renewable energy deployment and the power system. Energy 2021;219. http://dx.doi.org/10.1016/j.energy.2020.119576.
[40] Münster M, Morthorst PE, Bregnbæk HVLL, Werling J, Lindboe HH, Ravn H. The role of district heating in the future danish energy system. Energy 2012;48. http://dx.doi.org/10.1016/j.energy.2012.06.011.
[41] Amer SB, Bramstoft R, Balyk O, Nielsen PS. Modelling the future low-carbon energy systems - case study of Greater Copenhagen, Denmark. Int J Sustain Energy Plan Manag 2019;24. http://dx.doi.org/10.5278/ijsepm.3356.
[42] Bramstoft R, Alonso A, Jensen I, Ravn H, Munster M. Modelling of renewable gas and fuels in future integrated energy systems. Appl Energy 2020;268. http://dx.doi.org/10.1016/j.apenergy.2020.114869.
[43] Lester MS, Bramstoft R, Münster M. Analysis on electrofuels in future energy systems: A 2050 case study. Energy 2020;199:117408. http://dx.doi.org/10.1016/j.energy.2020.117408.
[44] Münster M, Møller Sneum D, Bramstoft R, Bühler F, Elmegaard B, Giannelos S, et al. Sector coupling: Concepts, state-of-the-art and perspectives. In: ETIP SNET. 2020, https://smart-networks-energy-transition.ec.europa.eu/sites/default/files/documents/workinggroups/ETIP-SNEP-Sector-Coupling-Concepts-state-of-the-art-and-perspectives-WG1.pdf.
[45] Balmorel community. Balmorel source code. 2022, URL https://github.com/balmorelcommunity/Balmorel.
[46] Candas S, Muschner C, Buchholz S, Bramstoft R, van Ouwerkerk J, Hainsch K, et al. Code exposed: Review of five open-source frameworks for modeling renewable energy systems. Renew Sustain Energy Rev 2022;161. http://dx.doi.org/10.1016/j.rser.2022.112272.
[47] Munster M, Sneum DM, Bramstoft R, Elmegaard B, Buhler F, Losa I, et al. Sector coupling: Concepts, potentials and barriers. In: 12th AEIT international annual conference. AEIT 2020, 2020, http://dx.doi.org/10.23919/AEIT50178.2020.9241201.
[48] Pizarro Alonso AR, Cimpan C, Ljunggren Söderman M, Ravn HV, Münster M. The economic value of imports of combustible waste in systems with high shares of district heating and variable renewable energy. Waste Manag 2018;79:324–38. http://dx.doi.org/10.1016/j.wasman.2018.07.031,.
[49] Rehfeldt M, Fleiter T, Toro F. A bottom-up estimation of the heating and cooling demand in European industry. Energy Effic 2018;11(5):1057–82. http://dx.doi.org/10.1007/s12053-017-9571-y.
[50] WE District. Interactive map: share of district heating and cooling across Europe. 2023, https://www.wedistrict.eu/interactive-map-share-of-district-heating-and-cooling-across-europe/.
[51] Hedegaard K, Balyk O. Energy system investment model incorporating heat pumps with thermal storage in buildings and buffer tanks. Energy 2013;63:356–65. http://dx.doi.org/10.1016/j.energy.2013.09.061.
[52] Egging-Bratseth R, Kauko H, Knudsen BR, Bakke SA, Ettayebi A, Haufe IR. Seasonal storage and demand side management in district heating systems with demand uncertainty. Appl Energy 2021;285:116392. http://dx.doi.org/10.1016/j.apenergy.2020.116392.
[53] Pool N. Day-ahead overview. 2022, URL https://www.nordpoolgroup.com/en/maps/#/nordic.
[54] Danish Energy Agency. Regulation and planning of district heating in Denmark. 2017, https://ens.dk/sites/ens.dk/files/Globalcooperation/regulation_and_planning_of_district_heating_in_denmark.pdf.
[55] TVIS. District heating companies (TVIS). 2022, URL https://www.tvis.net/gron-omstilling/fjernvarmeselskaber/.
[56] Danish Energy Agency. Fjernvarmens rolle i den fremtidige energiforsyning. 2014, p. 62, URL https://ens.dk/sites/ens.dk/files/Vindenergi/fjernvarme_-_analyse_2014_web.pdf.

VIII

[57] Danish Energy Agency. Technology data for energy storage. 2018, p. 1–18, August.
[58] Tschopp D, Tian Z, Berberich M, Fan J, Perers B, Furbo S. Large-scale solar thermal systems in leading countries: A review and comparative study of Denmark, China, Germany and Austria. Appl Energy 2020;270:114997. http://dx.doi.org/10.1016/j.apenergy.2020.114997.
[59] Statistics Denmark. Prices for agricultural land and tenancy by region, product and unit. 2022, URL https://www.statbank.dk/statbank5a/SelectVarVal/Define.asp?Maintable=LPRIS37&PLanguage=1.
[60] Danish Energy Agency. Technology data. 2023, URL https://ens.dk/en/our-services/projections-and-models/technology-data.
[61] Nordic Energy Research and International Energy Agency. Nordic energy technology perspectives 2016. 2016, URL http://www.nordicenergy.org/project/nordic-energy-technology-perspectives/.
[62] Lund H, Werner S, Wiltshire R, Svendsen S, Thorsen JE, Hvelplund F, et al. 4Th generation district heating (4GDH). Integrating smart thermal grids into future sustainable energy systems. Energy 2014;68:1–11. http://dx.doi.org/10.1016/j.energy.2014.02.089.
[63] van Helden W. Giga-scale thermal energy storage for renewable districts. 2021, p. 74, URL https://www.gigates.at/images/Appendix16_publishable_report_graphically_designed_EN.pdf.
[64] Lazard. Lazard's levelized cost of storage analysis - version 3.0. 2017, p. 49, URL https://www.lazard.com/media/450338/lazard-levelized-cost-of-storage-version-30.pdf.
[65] European Union. Amending directive 2012/27/EU on energy efficiency. 2018, p. 210–30, Official Journal L328 URL https://eur-lex.europa.eu/legal-content/EN/TXT/PDF/?uri=CELEX:32018L2002&from=EN.
[66] Skytte K, Bergaentzlé C, Fausto FJ, Gunkel PA. Flex4RES - flexible nordic energy systems. 2019, p. 120, URL https://www.nordicenergy.org/wp-content/uploads/2019/07/Flex4RES_final_summary_report_aug2019.pdf.
[67] Eurostat. Eurostat database URL https://ec.europa.eu/eurostat/data/database.

In recent years, there has been a growing interest in utilizing large-scale heat storage in combination with district heating systems. This thesis investigated water pit thermal energy storage (PTES) as a cheap and efficient heat storage technology for district heating. The main focus was the performance assessment of PTES and their techno-economic impact. The effect of PTES geometries on performance was investigated, and energy and exergy indicators were suggested for comparing PTES performance with different operations (seasonal or short-term). On a country scale, it was found that PTES can increase the flexibility of the overall energy system, thus increasing the utilization of renewables while reducing curtailment. Additionally, PTES can benefit the economy of a single district heating system by reducing the cost of heat as they can shift production from times when the electricity prices are high to periods with low electricity prices. Overall, this study elucidated the need to increase the number of PTES to reach cost-optimal carbon neutrality by 2050.

DTU Construct

Section of Energy and Services
Koppels Allé 404
2800 Kgs. Lyngby

www.construct.dtu.dk

ISBN: 978-87-7475-767-2
DCAMM: S340